The Fire Performance of Steel-faced Insulation Panels with Stone Wool or Polymer Cores – A Scaling and Heat Transfer Study Based on Full-scale and Scaled Experiments

Leisted, Rolff Ripke

Publication date:
2018

Document Version
Publisher's PDF, also known as Version of record

The Fire Performance of Steel-faced Insulation Panels with Stone Wool or Polymer Cores - A scaling and Heat Transfer Study Based on Full-scale and Scaled Experiments

Rolff Ripke Leisted

PhD Thesis

Department of Civil Engineering
2018

DTU Civil Engineering Report 392

DTU Civil Engineering
Department of Civil Engineering

The Fire Performance of Steel-faced Insulation Panels with Stone Wool or Polymer Cores

A Scaling and Heat Transfer Study Based on Full-scale and Scaled Experiments

Rolff Ripke Leisted

Ph.D. Thesis

Technical University of Denmark

Department of Civil Engineering

December 2018

Preface

This thesis is submitted as part for the degree as Doctor of Philosophy at the Technical University of Denmark, Denmark. The Ph.D. study was initiated in September 2014, concluded in December 2017 and successfully defended in April 2018 under the supervision of:

Professor Grunde Jomaas, principal supervisor, Department of Civil Engineering, Technical University of Denmark, Denmark and BRE Centre for Fire Safety Engineering, Institute of Infrastructure and Environment, School of Engineering, University of Edinburgh, United Kingdom.
Professor José Luis Torero, co-supervisor, School of Civil Engineering, The University of Queensland, St. Lucia, QLD 4072, Australia, now at the Department of Fire Protection Engineering, University of Maryland, College Park, MD, United States.

The use of "*experiment*" throughout this thesis is reserved for a non-standard setups, such as all the experiments performed in this thesis. The use of "*studied*" also refers to an experimental context. The use of the words: "*test"*, "*tests*" and "tested" are reserved for use in a classification and standardised context such as a classification test setup.

The use of "non-combustible", "*reaction-to-fire*" and "*resistance-to-fire*" are exclusively used in context regarding standardised test classification or tests whereas "*performance*" is used in an experimental context.

The use of "sandwich panel" exclusively refers to steel faced sandwich panels used in the building industry. For other materials or industries "*composite panel*" is used.

The following journal publications have been a part of the Ph.D.:

- **R. R. Leisted**, M. X. Sørensen and G. Jomaas; "Experimental Study on the Influence of Different Thermal Insulation Materials on the Fire Dynamics in a Reduced-scale Enclosure", Fire Safety Journal, Vol 93, pp 114-125, 2017.
  The full-scale experiment presented herein is part of the heat transfer analysis, as presented in Section 3.3 - Detailed Results.

- **R. R. Leisted**, J. P. Hidalgo and G. Jomaas; "Heat Transfer Analysis of Fires in Geometrically Scaled Compartments", 2017, *submitted to Applied Thermal Engineering.*
  The methodology and results presented in this paper can be found as part of Section 2.3 - *Heat Transfer Analysis and Section* 3.3 - *Detailed Results, respectively.*

- **R. R. Leisted** and G. Jomaas; "An experimental study of assemblies incorporating different thermal insulating building materials in a 1 to 5 scale modified ISO 13784-1 fire test", 2017 (in preparation).
  The results presented in this paper are part of the first series of thee 1:5 scale and presented in Section 2.1 - *Scaling Analysis.*

The following journal publications have been a part of the Ph.D. education, but will not be referred to herein:

- S. Chernyy, S. Ullah, G. Jomaas, **R.R. Leisted**, P. A. Mindykowski, J. B. Ravnsbæk, S. W. Tordrup, K. Almdal; "Modification of poly(styrene-block-butadiene-block-styrene) [SBS] with phosphorus containing fire retardants", European Polymer Journal, Vol 70, pp. 136-146, 2015.

- Saif Ullah, Pierrick Anthony Mindykowski, Rolff Ripke Leisted, Sergey Chernyy, Sie Woldum Tordrup, Grunde Jomaas, Kristoffer Almdal; "Synergistic fire-retardancy properties of melamine coated ammonium poly(phosphate) in combination with rod-like mineral filler attapulgite for polymer-modified bitumen roofing membranes", *submitted to Polymer Degradation and Stability.*

- P. A. Mindykowski, V. Karatzas, **R. R. Leisted**, M. Rezaei, C. Berggreen, G. Jomaas; "A new thermal approach to facilitate the Heat-Transfer Rate Inducing System usage for composite materials", 2017, (in preparation).

Abstract

The heat transfer and fire dynamics of enclosure fires in compartments made from steel-faced sandwich panels were studied experimentally in order to determine the feasibility of down-scaling the enclosure size of the ISO 13784-1 test compartment. The different scales used for the experiments were 1:5, 2:5, 1:2 and 1:1. For all scales, experiments were conducted with two types of steel-faced sandwich panels, one with a core of stone wool (SW) and the other with a core of a polymeric product (Polyisocyanurate (PIR) or Polyurethane (PUR)). The parameters studied were the heat release rate (HRR), the temperatures of the air and smoke layer inside the compartment, the temperatures at and in the walls, the pressure differences and temperatures in the doorway of the compartment and the time to flashover. For the smallest scale that was studied (a 1:5 ratio relative to the ISO 13784-1), the mass loss as a function of time was also measured.

The majority of the experiments was conducted at 1:5 the scale of the ISO 13784-1 test compartment. The 1:5 scaled compartment measured 0.48 m x 0.72 m x 0.48 m internally in width, length and height, respectively, with a 0.40 m tall by 0.16 m wide doorway in the middle of one of the short walls. A gas burner was located at the wall in one of the corners opposite the doorway. Rather than a section of the compartment the scaling of the entire compartment was hypothesised to reflect the full sized compartment test better than the current standard test, thus making it a more robust test method. By scaling the whole geometry of the compartment on top of the energy provided by the gas burner the boundary conditions seen at full scale would be represented better. This is unlike the current open corner configuration where smoke is immediately extracted and removed from the specimen which is a part of the current way of determining the performance of the panels in Europe. The experiments followed the methodology presented in the ISO 13784-1 with a two-step fire scenario with 100 kW and 300 kW for 10 min of duration each but also other variants of fire scenarios were studied.

The two polymeric cored panels studied, PIR and PUR, were class B with respect to contribution to flashover by EN 13501-1 which is the European classification standard for reaction to fire. Despite the PUR showing a lower calorific energy content than the PIR at component level, it performed significantly worse in the scaled compartment. Exposed to the same fire scenario, the compartment of PUR panels lost 85% of its mass in 10 minutes, all while releasing 220 kW at its peak which was more than 30 times the energy output from the burner. As such, the PUR panel did not have

characteristic trade of a class B product such as a limited contribution to flashover and was deemed unsafe to use at larger scales. The PIR core contributed about 15 times the energy output from the gas burner and lost about 60% of its initial mass over a period of 10 minutes. The remaining 40% of the mass consisted of both char, various degrees of decomposed foam and virgin material. The mass of the char, compared to the virgin material, was much less and much of the remaining mass is attributed to virgin material being effectively protected by the char. The stone wool panels were studied under more challenging conditions at 1:5 scale where the input of the burner was sufficient to cause external flaming emanating through the doorway. Despite the average temperature of the compartment being more than 600 °C, the measured HRR was simply following the energy output from the burner. At larger scales the smoke production increased, which suggested a decomposition of the core rather than just a decomposition of the steel-face finish. Across all the scales the thermocouples embedded in the walls showed signs of minor exothermic reactions identified as an increase in the temperature 2 cm in-depth after the passing of the thermal wave.

A newly developed one-dimensional heat transfer model with the thermal properties of the SW core lumped together as an effective parameter was used to analyse and compare the experiments across the scales. The model together with the measured temperature of the boundaries in combination with flow measurements quantified the total energy distribution in the compartment during the experiments. The model was able to predict the thermal wave within 5% for the first 20 mm of the in-depth measured temperature and was therefore able to inversely provide the net heat flux transferred through the internal compartment boundaries. The measurements of hot gases were used to calculate and analyse the convective energy flowing out of the compartments and the fraction of the total heat transfer it accounted for. The nature of the heat transfer model allowed for the quantification of the net heat transfer for the experiments with SW panels. The goal to combine the model with the measured data to show that down-scaling the compartment geometrically was done by scaling the size of the fire based on the Froude number with respect to the geometry of the compartment. The calculated steady state heat flux between the 1:2 scale and 2:5 scale experiments were matching making meaning reducing the size by 25% was possible. Furthermore, the temperature in the compartments for the 2:5, 1:2 and a full scale experiment from literature matched for the first two burning periods. The third burning period was much warmer in the full scale than the 2:5 and 1:2 indicating a limit for the scaling with respect to the size of the fire. The successful reduction in the size of the compartment has many advantages such as work safety, product development, classification and cost.

The data herein presents the use of micro scale and macroscale to understand critical temperatures and incident heat flux where the core material pose a potential risk. In the 1:5 scale compartments both the temperature and the rate of temperature change over time were lower than for the other scales and the temperature did not reach steady or even quasi-steady state. The temperature in the 1:2, 2:5 and full scale (1:1) compartments reached a quasi-steady state during the first 10 minutes burning periods. Meaning the 1:2 and 2:5 scale compartments behaved in the same manner as the full scale. The compartments with stone wool had the same ratios of global heat transfer, consisting of 60% - 80% convective losses through the doorway and 20% - 40% conductive losses through the compartment boundaries for all scales. The 60% is just after the increase in the burner intensity where the gradient between the boundaries and the gas phase is greatest. As time passes and the walls heat up and less heat is lost via conduction and more through the doorway as convective energy increasing its proportion of the total energy to 80%. It was not possible for the heat transfer model to account of 100% of the energy dispensation throughout the duration of the experiments. However, taking the uncertainties of the measurements into consideration, the global heat transfer presented the same energy distribution across all four scales towards the end of the experiments, where steady state was approximated. The experiments therefore show that the energy distribution in compartment with the fire scaled using the Froude number is the same when approaching steady- or quasi steady state.

The successful downscaling of the size of the compartment was limited to 1:2 and potentially 2:5, whereas the 1:5 scale compartments were not able to mimic the exact behaviour seen at larger scales. This is based on the compartment temperatures and non-dimensional HRR prior to failures differed too much. This was evident from the fact that the compartment and walls during the first and second burner step stabilised for the 1:5 scale, whereas failure occurred immediately after the initiation of the second burner step at both 1:2 and 1:1 scale. The heat transfer through the walls of the compartments with SW panels determined that the third burner step where the HRR was additionally doubled compared to the second step was not successfully scaled as the heat flux was much greater in the full scale experiment compared to the other scales. The experiments with the 1:2 sized compartments had matching compartment temperatures and net heat fluxes across the solid boundaries as the full scale experiment. The net heat flux for the SW compartments showed that the first burner step for the 1:2 and 1:1 scale from literature was matching while the second step had matching net heat fluxes in the near and far field from the burner. The HRR development and time to failure for the 1:2 and two 1:1 scale (of which one is from literature) experiments with

PIR panels matched very well and all the compartments failed at the initiation of the second burner step

The fact that the results from the experiments with the 1:2 scale compartments matched the results from the full scale experiments provides; 1) data for successfully conducting research on compartment fires at smaller scale, which greatly benefits intuitions with smaller laboratories, 2) classifying and regulatory bodies data arguing for smaller compartments tests, which are easier to handle, and 3) the manufactures with data showing how reduced scale testing can predict large scale failures for research and development at a reduced expense.

Table of Content

Acknowledgements

For the past three years I have been on a fantastic journey both academically and personally! A journey I could never have dreamed of and that would not have been possible or as interesting without the support of numerous people, universities, companies and colleagues. I have had interactions with so many fantastic people that in one way or another, who knowingly or unknowingly, helped me grow, develop and ultimately helped me to accomplish my goals. I would like to thank each and every single one of those people for their influence on me and my project, and in particular the following:

Rockwool International A/S for sponsoring my project. Birgitte Messerschmidt, at the time from Rockwool International A/S, now at the NFPA, for trusting in my abilities and always being ready to assist me.

Grunde Jomaas, my supervisor, for his inspiring work mentality, endless support, motivation and guidance throughout these three years. I am truly grateful for his supervision and willingness to include me on side-projects, teaching obligations and allowing me to co-supervise students alongside him in order to help me develop my academic competences.

José Luis Torero, my co-supervisor, for his guidance and enabling my research stay at the University of Queensland, Australia.

Juan Hidalgo Medina, for his willingness to take his time to assist me and share some of all his knowledge and data with me especially during my stay at the University of Queensland.

Bjørn Skjønning Andersen, Laurens van Gelderen and Pierrick Mindykowski, for being such fantastic colleagues for these past three years - without them it would not have been nearly as fun. I have initiated my fair share of discussions with the two latter ones on a wide range of topics and always emerged, at least a little bit, wiser than initially.

Claude Feige from ROCKWOOL FRANCE, for his patience with me and persistency to push suppliers in order to acquiring the panels required for my Ph.D. project.
Martin X. Sørensen from If P&C Insurance, previously at the Technical University of Denmark, for sharing his data, his knowledge and laying some of the ground work for my research.

The Building Research Establishment and especially Phil Clark, Tom Lennon and Octavian Lalu who had a huge influence and without whom it would not have been possible to get the half and full scale experiments conducted and especially on such a short notice.

Jonas Tolstrup and Maria Hedegaard Brok from the Technical University of Denmark for conducting the vast majority of the scaled experiments with me.

All the students involved in the fire laboratory at the Technical University of Denmark for generating a positive and great atmosphere and making the daily work more interesting and at times challenging in the good way.

To the entire fire group at the University of Queensland for being so welcoming and making me feel like a part of your group during my exchange.

The BRE Centre for Fire Safety Engineering, University of Edinburgh, Scotland, for allowing me to borrow some of their thermocouples and for assisting in establishing the contact with BRE.

Maxime Perrin and Thibault Maunoury from the University of Angers, France, for helping me with the intermediate scale experiments conducted at BRE.

Ulises Alva Rojas, Jens Steemann Kristensen, Zafiris Triantafyllidis and Russell Wallace from the BRE Centre for Fire Safety Engineering, the University of Edinburgh, Scotland, for setting aside their own project to provide their invaluable assistance with the experiments conducted at BRE.

Tom Abildgaard from Scandi Supply A/S and Scandi Supply A/S for supplying their FireFree® ScandiBoards to facilitate my research.

My lovely girlfriend, Matilde, who always supported, believed in- and picked me up during these past years, especially the last half year, where the work was overwhelming. For supporting my decisions and traveling across the world with me to Brisbane, Australia, to study while I was on exchange.

Nomenclature

A	Conduction term for gases	(W/m·K)
A	Area of the burner	(m^2)
B	Conduction term for solids	($W \cdot m^2/K \cdot kg$)
Bi	Biot number	(-)
c_p	Specific heat capacity	(J/kg·K)
C	Conduction term for the radiation	($W \cdot kg/K \cdot m^4$)
C	Calibrated vessel conversion coefficient	(kJ/K)
C	Burner location factor	(-)
CO	Carbonmonoxide	(-)
CO_2	Carbon dioxide	(-)
D	Length scale	(m)
E	Energy content per kg of oxygen consumed	(MJ/kg)
E_{CO}	Energy content per kg of CO produced	(MJ/kg)
Fr	Froude number	(-)
g	Gravitational constant	(m/s^2)
$\dot{g}'''$	Energy generation	(W/m^3)
h	Convective heat transfer coefficient	($W/m^2 \cdot K$)
k	Conductivity	(W/m·K)
k_0	Conductivity at ambient	(W/m·K)
k_1	Linear conductivity term	($W/m \cdot K^2$)
m	Mass	(kg)
$\dot{m}$	Mass flow	(kg/s)
M	Molecular mass	(kg/mol)
Nu	Nusselt number	(-)
P	Pressure	(Pa)
Q	Energy	(J)
$\dot{Q}$	Heat release rate	(W)
$\dot{Q}^*$	Non-dimensional heat release rate	(-)
$\dot{q}''$	Heat flux	(W/m^2)
R	Universal gas constant	(J/mol·K)
Re	Reynolds number	(-)
T	Temperature	(°C) /(K)
t	Time/thickness	(s)/(m)
v	Velocity	(m/s)

Nomenclature

V	Volume	(m^3)
X	Mole fraction	(-)
X	Compartment height and width	(m)
x, y, z	Direction coordinates	(m)
ΔH	Heat of combustion	(MJ/kg)

Subscripts

0	Temperature independent coefficient
1	First element / coefficient linearly dependent of temperature
2	Second element
Air	of the air
$Burner$	of the burner
c	Complete / Core
CO	Carbon monoxide
CO_2	Carbon dioxide
$cond$	Conduction
$conv$	Convection
eff	Effective
F	Full scale
gas	of the gas
ig	ignition
in	Entering
int	Internal
M	Model scale
n	n^{th} element
N	Last element
net	net
out	Exiting
$panel$	of the panel
rad	Radiation
s	of the steel
∞	ambient

Superscripts

j	Current step
$j+1$	Next step
0	Initial value
A	Actual/measured value

Greek Letters

α	Diffusivity / absorptivity	(m^2/s) / (-)
δ	Differential	(-)
Δ	Increment	(-)
ϵ	Emissivity	(-)
ρ	Density	(kg/m^3)
σ	Stefan-Boltzmann constant	(W/m^2K^4)
ϕ	Depletion coefficient	(-)
χ	Combustion efficiency	(-)

Abbreviations

$ASTM$	American Society for Testing and Materials	
BRE	The Building Research Establishment	
CHF	Critical Heat Flux	(kW/m^2)
CEN	Comité Européen de Normalisation	
CFD	Computational Fluid Dynamic	
DTU	Technical University of Denmark	
DSC	Differential Scanning Calorimetry	(W/g)
E	Integrity	(min)
EN	European Norm (standard)	
EPS	Expanded Polystyrene	
$FIGRA$	FIre Growth RAte	(kW/s^2)
FM	Factory Mutual Global	
GW	Glass Wool	
HRR	Heat Release Rate	(kW)
I	Insulation	(min)
ISO	International Standardization Organization	
LFS	Lateral Flame Spread	
LPS	Loss Prevention Standard	
MDI	Methylene di-phenyl di-isocyanate	
MLR	Mass Loss Rate	(g/s)
MW	Mineral Wool	
$NFPA$	National Fire Protection Association	
pHRR	Peak Heat Release Rate	(kW)
PF	Phenolic Foam	
PIR	Polyisocyanurate	
PP	Pressure Probe	
PUR	Polyurethane	
SBI	Single Burning Item test	
$SMOGRA$	SMOke Growth Rate	(m^2/s^2)
R	Resistance	(min)
STA	Simultaneous Thermographic Analysis	(%/min)
SW	Stone Wool	
TC	Thermocouple	
TCT	Thermocouple Tree	
UL	Underwriters Laboratories	
XPS	Extruded Polystyrene	

List of Figures

Appendix Figures

List of Tables

1 Introduction

The population of the world is projected to continue to increase [1] and the population density is prone to follow. As a result, the need for housing is increasing and is projected to continue [2], and this requires careful planning [3]. There is a realisation among citizens and developers alike that living a more responsible life is required from a sustainability perspective. At the same time, reducing emissions and the carbon dioxide levels in the atmosphere [4] is equally important. An increasing global population will increase the stress on the earth [5] which is a big concern and several initiatives have been launched [4] and others are planned [6] to relive the stress. Energy consumption is a big contributor to the health of the planet, and the burning of fossil fuels in the generation of said energy used by e.g. the transportation or construction sector is a concern which has caused innovation in the energy sector [7]. A way to reduce emissions is for consumers to reduce their consumption, buy efficient products or for manufactures to optimise their products in an efficient way. Furthermore, a driver for innovation in the construction industry specifically can also be forced by politically influenced, e.g. by restrictive regulations, as pointed out by Domingues-Rosado et al. [8] and Modesti and Lorenzetti [9]. However, political decisions can also influence the industry positively by promoting energy efficient building, e.g. the Energy Performance of Buildings Directive from 2010 and the Kyoto protocol [4] seeking to reduce the greenhouse emissions.

Since the 1970s there has been a development in some European countries towards increasing the insulation thickness of buildings in order to decrease their energy consumption [10] and save money. This is reflected in the growth of the insulation industry [11, 12], as the growth is stronger than the population growth alone. Due to their cold climate, the Scandinavian countries have been increasing their requirement for the thermal resistance, R-value, for buildings in comparison to the rest of Europe, as seen in Figure 1.1. If all European countries would adapt the same level of thermal resistance as the Swedish standards (10 m^2K/W for ceilings and 6.67 m^2K/W for walls), it has been estimated that Europe would save 50% of its energy consumed by buildings (2001 numbers) [13]. The thermal resistance of a material is a function of its conductivity and thickness, so if the conductivity is high, this has to be compensated for by an increase in the thickness. The total thermal resistance of a building element is the sum the thermal resistances of all the individual materials in, for example, a composite material or product such as steel-faced sandwich panels. The thermal resistance depends on a materials thermal conductivity and thickness, which are desired to be as low and thin, respectively, as possible. Polymer-based insulation materials commonly have a

low thermal conductivity and therefore require a smaller thickness than glass wool to obtain a certain thermal resistance, as seen in Figure 1.2.

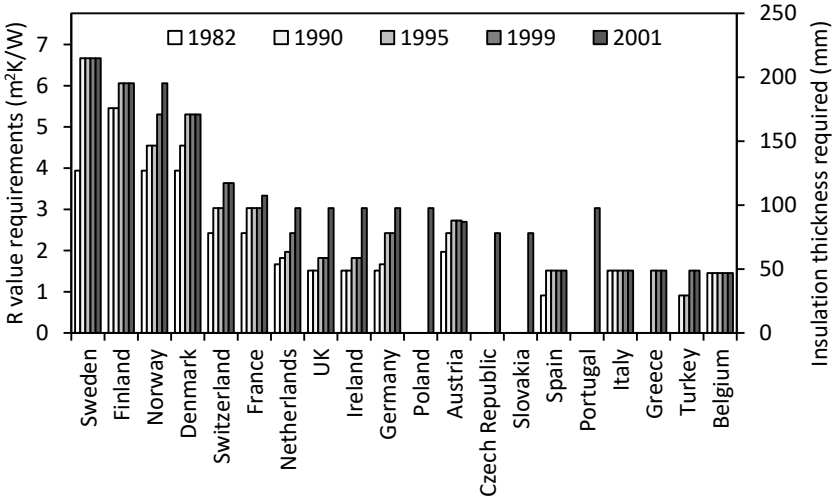

Figure 1.1: The development of national thermal resistance requirements for 20 European countries from 1982 to 2001 and the required thermal insulation thickness based on a thermal conductivity of 0.033 W/m·K, from [13].

As the data in Figure 1.1 is from 2001, the *Energy Performance of Buildings Directive* from 2010 [2] was not yet in effect, and national regulations have therefore improved since then. This directive requires European member states to draw up national plans to increase the number of *nearly-zero* energy buildings and all new buildings must be *nearly-zero* energy prior to 2021. However, 39% of the housing stock in Europe is from before 1960, where building regulations were scarce, and 44% are from between 1961 to 1990 [10]. Thus, more than 80% of the housing stock in Europe was erected under pre-1990 regulations. As buildings currently represent close to 40% of the final energy consumption in Europe, the reduction of their energy consumption is critical to reduce the overall energy consumption [10]. However, as the majority of the buildings in Europe were built under older regulations, prior to the boost of environmental awareness and political motivation, it can be difficult to fit the required amount of insulation into the existing walls and ceilings. Furthermore, those 40% include the energy consumed in the phases prior to completion such as material manufacturing, transportation and the reduction of energy requires a multidisciplinary focus to be successful.

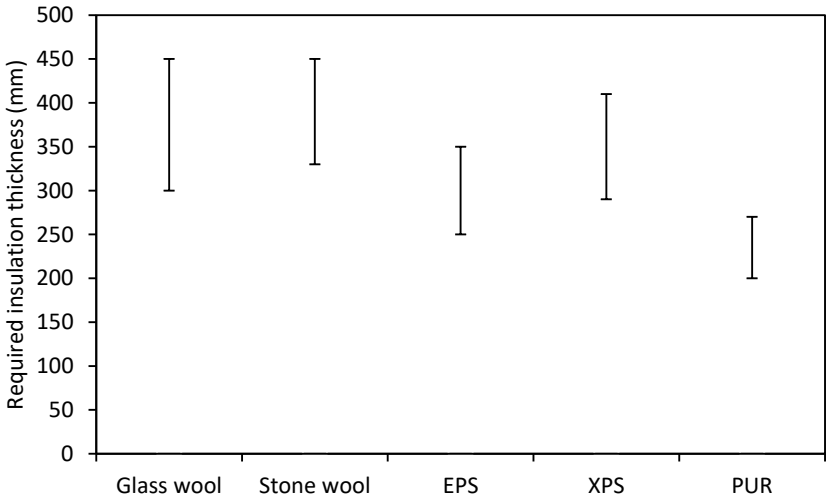

Figure 1.2: The required insulation thickness range needed to obtain a thermal resistance equal to 10 m²K/W (as in Sweden) for common insulation materials, from [13].

1.1 Insulation Requirements and Materials

Not all insulation manufactures choose the same solution when overcoming the mutual restrictions, as their products inherently can be very different. The insulation market is therefore very diverse with very different products available that offer a variety of solutions addressing the same performance objectives. Logically manufactures with a product superior in one aspect are inclined to improve other aspects, such as reducing the conductivity of a product with low energy content or increase the fire safety properties of a product with low thermal conductivity. Additionally, some manufactures are expected to focus solely on minimising or maximising certain material characteristics such as yield strength, weight, conductivity and moisture diffusion, while others focus on a combination of properties. However, generally speaking, the building insulation industry is dominated by two major product groups of insulation products which are; 1) inorganic fibrous materials, e.g. glass and stone wool (GW and SW, respectively), or 2) organic foam materials, e.g. extruded or expanded polystyrene (XPS and EPS, respectively), phenolic, polyurethane or polyisocyanurate (PF, PUR and PIR, respectively). Still, it should be mentioned that other alternatives such as paper wool, wood wool and phase changing materials are available [14]. The majority of the exterior walls, roofs and floors in modern buildings in developed countries are multi-layered and of at least one insulation layer. The seemingly most important physical property of an insulation material, its thermal conductivity, has not seen significant improvement much in the last decade. Rather, other aspects such as reaction to fire, moisture or mechanical strength has been improved in an optimisation process driven by market demands [14].

The *Energy Performance of Buildings Directive* will be a driver to reduce the energy consumption in EU from buildings over the next decade. There are several methods architects, engineers or the owners have at their disposal for reducing the energy consumption of their building. Equipment and appliances as well as the choice of construction materials can be chosen with care so they consume less in use or during the manufacturing. In the design phase a higher thermal resistance can be incorporated reducing the energy consumption further and be a key aspect in the design. However, existing buildings would need a total renovation with a change of all the facades at a much higher cost and is undesired. A way to achieve these energy goals for existing buildings is to refurbish buildings, as proposed in the directive. A better thermal resistance of existing walls can be achieved by injecting an insulation material into a wall cavity such as cellulose, mineral wool or spray foam. Not all buildings, however, have cavities in the walls and therefore are not suited for this solution. External Thermal Insulation Composite System(s) (ETICS) are multi-layered and contain an insulating layer as well as a finish which can be installed externally on existing walls, as seen in Figure 1.3. This provides existing buildings with additional thermal resistance as well as a new appearance which can contribute with additional protection from the weather and provide a modern look. Increasing the thermal resistance of an existing building with the same benefits as an ETICS solution is metal faced composites, commonly called “sandwich panels”. Sandwich panels consist of a core of thermal insulation sandwiched between two thin faces often made of metals such as steel, cobber or aluminium but many combinations of core and faces exist. Unlike ETICS systems, sandwich panel systems are not fitted directly to the existing wall. Rather, sandwich panel systems are fitted to a metal frame which can then be externally attached to existing buildings or as part of new buildings. Like the ETICS system it can have varying thicknesses to provide any required thermal resistance. Typical applications for sandwich panels are industrial buildings, sports halls and warehouses [15]. Other systems such as structural insulated panels and insulating concrete formwork are also available on the market with their own benefits and restrictions, as highlighted by Hidalgo [16], and will not be covered further herein.

Façades with more traditional materials, such as brick, concrete and light-weight concrete, can often be replaced by a sandwich panel with the same thermal resistance at a lower weight and reduced thickness. The weight of sandwich panels can be lower than traditional wall elements as the density of the core range from 15 kg/m^3 [17] to 120 kg/m^3 [18] for lightweight EPS and dense stone wool, respectively. Such low weight solutions are very attractive for many buildings. As an example, for taller buildings the lower weight of the panels can in turn lead to a reduced thickness of the load-

carrying elements as sandwich panels are usually not load-carrying. The lightest sandwich panels are with aluminium facings but stainless steel is also common.

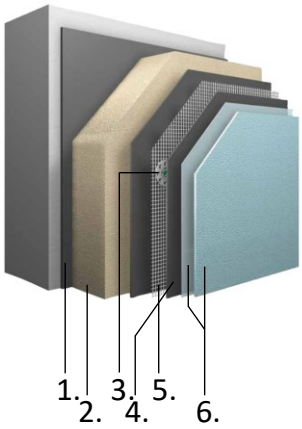

1. Adhesive
2. Thermal Insulation Material
3. Anchors
4. Base coat
5. Reinforcement
6. Finishing layer

Figure 1.3: A typical ETICS solution attached with adhesive to an existing façade to improve the thermal resistance and efficiency of the existing building through a renovation or retrofit, from [19].

Sandwich panels are not exclusive to industrial, commercial buildings or dwellings. For maritime vessels composite panels are usually solid or when of a multilayer structure it is either honeycomb, corrugated and made of all-metal, hybrid metal or composites. The composite is usually filled with either a polymer foam or balsa [20], but will not be further discussed as they are used under different conditions and are regulated differently compared to the sandwich panels intended for the building industry.

New industrial and commercial buildings, such as office buildings, retail outlets, storage units and sandwich buildings are often constructed with steel or aluminium faced sandwich panels. In Europe, a traditional alternative to this would be an insulating material between any combination of brick and concrete. The steel faced sandwich panels, however, are lighter than the traditional external and internal facades, and they are therefore often a cheaper and more attractive solution. An ever growing trend in the building industry is to construct as fast as possible to profit as much as possible and materials and products that are easy to handle and allow for quick construction are desired [21]. This makes products that are lighter and easier to handle and work with preferred. The thermal conductivity is not the only key parameter in terms of keeping a building well insulated, as thermal bridges and lack of integrity can increase the heat flow significantly. Thermal bridges can occur as a result of poor craftsmanship, but also for non-façade elements such as doors, windows and window

frames. It is therefore not enough to keep adding insulation to the building envelope. It is, however, an effective initial step to reduce the heat losses from a building to a minimum. It is a full building analysis and not just a single component analysis that is needed to obtain the optimal solution with considerations e.g. towards acoustics and natural light. Many manufactures provides wall, ceiling and corner-joints as a system-solution. This way builders and contractors can assemble the façade with prefabricated elements that fit together which reduce the risk of thermal bridges as well as the influence of craftsmen. However, as all panels are limited in width by the production line they are manufactures with joints and seals which do require attention to ensure optimal system performance. A political, corporate and societal focus on sustainability, carbon emissions [22], environmental impact and life-cycle analyses [23] [24] is starting to emerge as key parameters in the building planning process [25]. These analyses, however, are not an easy task to begin with as the international standards on the subject are vague in its execution [26]. Buildings consist of a wide range of materials and products, use electricity, heating and water, equipment and requires maintenance which all influences the performance of the building. As a result, building material ratings are emerging to indicate the limited environmental impact of products, such as biodegradability, CO_2 foot print, payback times for energy and greenhouse gases, disposal or toxicity. Such requirements often put newer products such as sandwich panels in front of the traditional products, as they are designed to optimize the mentioned parameters [27] originally from [28]. However, ratings can also be misused as they are trademarked and can be the property of a single company where the rating have no scientific, standardised meaning or limiting factors preventing it from being applied to all the products of that company.

Plastic insulation materials have many of the properties desired by the building industry: low conductivity is ideal for high thermal resistance, the low density makes them easier to work with and requires slimmer load-carrying elements, compressive strength for flat roofs and the low permeability prevents moisture transport and high airtightness to minimise convective heat losses. However, as all plastic insulations inherently are made out of hydrocarbons, it is a combustible insulation type. For this reason is it common for manufactures to add flame retardants during the transformation of the raw material to the finished product in order to meet mandatory fire safety regulations. Many of the first generations of plastic insulation cores contained Chlorofluorocarbons (CFC) as they reduced the density, improved the thermal conductivity [29] and worked as a flame retardant. The CFC worked as a fire retardant was by quenching the fire and reducing the conversion of CO to CO_2 [30] which reduce the heat released, temperature and therefore also the heat feedback

to the fuel which is required to sustain its flaming conditions [31]. However, after the realisation of the ozone depleting potential of CFCs the Montreal Protocol [32] bound the world to phasing out all CFC products, with a few irreplaceable exceptions, the industry had to adapt and change. The obvious replacement, Hydro chlorofluorocarbons (HCFCs), have always been considered a temporary replacement as these are also in the process of being phased out also under the Montreal Protocol due to their high Global Warming Potential (GWP). Currently the foam industry in the developed world is not using CFCs or HCFCs but instead water to form CO_2 and hydrocarbon fuels such as pentane or hydrofluorocarbons (HFCs) [9] as the blowing agents in order to achieve the desired density and thermal property [33] [34]. For reference, water and CO_2 has a GWP of 1, Pentane about 11 and some HFC such as -245a and -134a has a GWP of 1030 and 1430, respectively. In the US these should be banned by the end of 2017 [35]. In the EU the HFCs with a GWP higher than 150 will be banned in XPS and all other insulating foams from 2020 and 2023, respectively [36].

1.2 Fire Performance of Insulation Materials

The classification of sandwich panel products with respect to fire safety, moisture transport, mechanical strength, conductivity, global warming potential, allows for engineers, architects and contractors to navigate through a diverse market to find the optimal product fitting their needs. However, prescriptive fire safety is not presented in the same way as a quantification of a single important parameter, merely as a pass/fail or an underlying level of accepted risk (not to be confused with the classical risk analysis where the risk is the product of the probability and the consequence [37]). Most parameters of importance are directly measured or inferred values such as mechanically strength and conductivity, respectively, are usually determined by an appropriate classification. Furthermore, fire is a complex phenomenon and can be influenced by numerous factors such as ambient temperature, nearby materials, wind flows, oxygen availability, just to mention some, which makes it unlikely for two fires to be identical. This makes the market for fire safe products difficult to navigate for an outsider having to consider multiple aspect in the building process and determining which parameters are important while choosing the product with the desired level of safety.

Currently, in the EU, the reaction to fire test standard for a steel-faced sandwich panels is the EN 13823:2010+A1:2014 [38] (Single Burning Item, SBI) and is thereafter classified according to the EN 13501-1+A1:2009 [39]. The test standard is an intermediate-scale corner configuration measuring 0.5 m x 1.0 m x 1.5 m in L x W x H, respectively, without any horizontal restriction. The products are

subjected to flame impingement by the corner located triangular gas burner. The standard was development in several iterations and 30 materials deemed *commonly* used in the construction industry were tested as part of the first round robin. The test standard successfully correlated the fire growth at its intermediate-scale to behaviours seen in full scale compartment tests (ISO 9705). This held true for about 87% of the materials [40]. A sandwich panel with a classified combustible material was however, among the 13% of the tested material types that did not show a strong correlation [40]. Other types that failed to be correlated accurately were pipe insulation and cables which are linear products and they were instantly recognised as unfit for extrapolation between the smaller corner configuration and the compartment. A polycarbonate panel where the classification test overestimated its fire growth compared to what was seen in the compartment test was also among those 13% with worse. Other standards were later developed specifically for these types of linear products. The classification test for sandwich panels, however, remained the SBI, despite the fact that the SBI test determined the sandwich panel to be safer than its actual performance when tested in the compartment. The end result is problematic, as the test and classification standard, which is still used, knowingly under-predicts the risks of certain products. Nevertheless, EN 13823:2010+A1:2014 is the current standard for testing the performance and risk of a sandwich panels in an enclosure.

There is a societal perception that all buildings are up to code and therefore safe in case of a fire. This is however not always the case as seen; during the apartment block fire in *Lakanal House*, England, that killed 6 people in 2009 due to unsafe renovation work and failure to inspect the building [41]; A day-care centre fire in *Hermosillo*, Mexico, that killed 49 also in 2009 because of lack of emergency exits and improper compartmentation [42] [43]; One of several garment factory fires in Gazipur, India, where 7 died fighting the fire in 2013 due to an improper fire hydrant system [44]; An apartment building fire in London (Grenfell Tower), England, where 71 occupants died in 2017, caused by a combination of poor and/or defect fire safety solutions resulting in an internal fire spreading vertically on the outside while smoke was filling the inside [45, 46], just to mention a few from a very long list of failures. It should be noted that there is a clear difference between following a poor code and ignoring all together or cutting corners with regulations, respectively. It is not feasible for the code to require designs capable of preventing all damage in case of a fire but merely be able to mediate the risks and prevent consequences not deemed acceptable. Furthermore, the codes cannot always expect designs to predict and be protected from any and all fires which can cause great losses, or even worse, fatalities. Standards often specify the Heat Release Rate(s) (HRRs)

or a temperature, such as the design fires in the NFPA 286, EN 13823 [38] (Single Burning Item - SBI), ISO 13784-1 [47] and the ISO 834 [48] respectively, as seen in Figure 1.4 to the left and right, respectively, to represent a fire scenario which needs to be passed for compliance and access to the market. The ISO 834 standard used to classify building elements with respect to their resistance to fire is a test that subject a complete product such as a door, wall or ceiling to a fixed predefined temperature-time correlation. It is not possible for this thermal attack to represent all possible fires and actual performance of materials and products in a fire is fundamentally unpredictable [49].

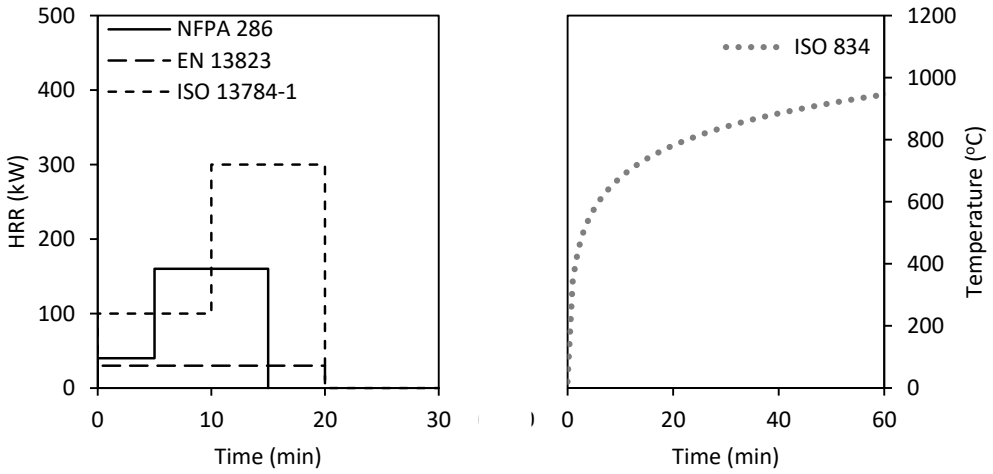

Figure 1.4: The designed thermal load for various test standards.

Designing a building that is compliant with the building code can be done in several ways where the simple one is to simply follow the solution(s) prescribed in the building regulations to the letter. Another way is to meet the underlying objective of the prescribed solution e.g. ensure the life safety of occupants. This way is referred to as a performance-based design where the objective is more important than the solution used to ensure it. This offers many possibilities for architects, designers and engineers to make innovative designs while still following the, usually, stringent building regulations with respect to fire safety. Using a performance-based design approach is based on the design being “as-good-as” the prescribed solution in the building regulations. Performance-based building designs can be an essential part of novel buildings, which does not fit into the rigid prescriptive code system, to obtain building permits. The Performance-Based Fire Designs (PBFD) can be quite complex and often include computational fluid dynamic (CFD) simulations and pedestrian flow calculations to assess whether the design is as-safe-as a prescriptive design where occupants is deemed to have sufficient time to evacuate safely. The PBFD can be used in countries

where the building regulations allow it and while it is capable of providing a solution to any problem a higher level of knowledge is required compared to the prescriptive code. The design is only as good as the knowledge of the engineers and their understanding of the materials and the risks they present. Therefore a lot of underlying assumptions with respect to the assumed or prescribed final fuel load in the building, material properties such as calorific energy content, ΔH, ignition temperature, T_{ig}, Critical incident Heat Flux (CHF) as well as the human behaviour of the occupants in an event of a fire can play a vital role. Furthermore, the PBFD methodology allows for fire safety engineers to conduct a desktop studies justifying why their choice of materials should be considered "*just-as-safe"* as a permitted prescriptive design would be [50, 51]. In order to allow for desktop studies in a regulatory framework, the building code is often formulated as an objective merely with examples that are compliant but not mandatory. In England, the Approved Document B furthermore allows for accredited domestic fire laboratories to make an expert statement regarding a material choice if the test documentation is not available or appropriate for a specific design [52]. This could, as an example, be a desktop study arguing that a certain material with insufficient documentation behaves as a material with sufficient test documentation and this way could be approved for the studied project.

From a design purpose, fire safety engineers have often used the discrete fire growth values, α, from the NFPA 204M [53]. The standard contains a list with single fuel sources and their growth rates. Furthermore, four typical values are proposed for materials without a known growth rate: *ultra-fast*, *fast*, *medium* and *slow*, representing 75 s, 150 s, 300 s and 600 s growth time to reach 1055 kW (1000 BTU/h). These values cover a large range of commodities such as wool pallets, mail bags and various plastic items. Growth rates can be extracted from journals and reports and with caution be applied to any design if the effects of the experimental setup are understood such as if they were performed in an enclosure, under a suspended ceiling or with any nearby walls. If the data obtained is from a free burning fire under a hood, which can be the case [54] [55](from [56]), or in a compartment [57, 58] as the only fuel the results should be used with care as the dynamics and burning behaviour might be different in another enclosure or even position.

A major difference between a HRR controlled fire scenarios vs a temperature controlled is the actual heat input to the test set-up. The HRR controlled tests are defined by their input value and the temperature controlled tests are adjusted based on the output temperature and both have their advantages. The HRR is therefore fixed prior to the initiation of the test via a flow meter whereas the

temperature is continuously monitored during the test and adjusted. A product contributing with more energy to the test system would have a disadvantage over a product contributing less in any scenario with a fixed HRR whereas a temperature controlled test its contribution would be countered by a lower input from the testing setup. In Figure 1.5 “Panel #A.1” refers to the first test with a class B stone wool panel type and “Panel #B.3” refers to the third test for a class B PIR panel. Figure 1.5 presents the data for fuel consumed and both panels consumed less propane than an inert concrete wall did and that panel type *B* even less than panel type *A* to maintain the prescribed furnace temperature. There are two reasons for this; the panels provide some energy to the system or they have higher thermal resistance and less heat is lost through the boundary. A similar and opposite problem arise if a product release an oxygen replacing gas or a gas phase flame retardant and therefore reduce the completeness of the combustion and HRR for tests where the HRR is pre-defined.

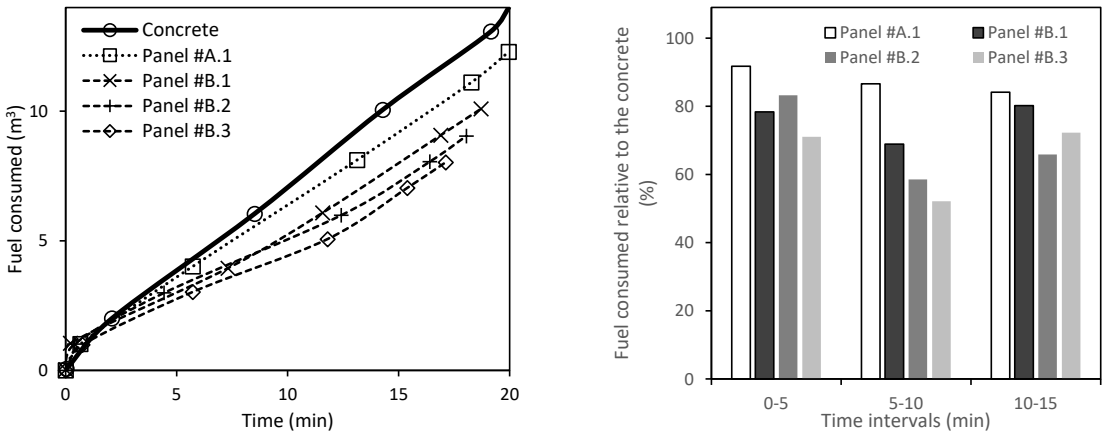

Figure 1.5: The fuel consumption during an EN 1364:1 fire resistance furnace test for two types of sandwich panels compared to the fuel consumption of an aerated concrete reference wall; a) as a function of time and b) as a function of 5 min increments (all three #B panels failed between 15 min and 20 min), extracted from [59].

Smaller scale tests can and are being used as a screening tool to evaluate if a material is likely to pass a large scale classification tests or replace them all together. To be successful, however, this requires that the failure mode or modes are transferrable across scales, such as material properties like the density, critical heat flux (CHF) and ignition temperature (T_{ig}), are. The cone calorimeter (ISO 5660-1 [60], BS 476-15 [61]) is often used in scientific research as it provide researchers with valuable fire safety properties of a material such as the time to ignition, HRRPUA and CHF [62, 63]. This makes it possible to evaluate the samples and compare them across studies. In Japan it is even

used as a classification tool itself. The cone calorimeter can also be very useful for PBFD as CFD models require input data which it can provide. However, for non-combustible faced sandwich panels with a combustible core the cone calorimeter did not identify the risks when compared to a scaled compartment fire, as Yosiaka et al. [64] pointed out. The lack of correlation between tests across different scales was also recognised by Johansson and Van Hees [65] and Axelsson and Van Hees [66] that compared the results of sandwich panels with various core types tested in the SBI test apparatus with a free standing compartment on fire. They found the SBI to underestimate the contribution from the panels with a combustible core to the fire growth in all three tested products [66]. When assessing compartment boundaries with high energy content that is either exposed or partially covered, fire safety engineers and regulators have to be aware of the potentially changed fire dynamics associated with such design choices. For example, sandwich panels provide a cheap, light and relatively high thermal resistance, while timber is deemed carbon neutral and as a construction material preferred over CO_2 heavy alternatives, but both also provide additional fire load in certain compartment fire scenarios. Research is however being conducted with the focus of studying sandwich panels and cross-laminated timber in enclosures under fire conditions [64, 67, 68, 69] trying to understand when they contribute and when they do not, with the goal to improve building fire safety.

There are several ways to improve the fire safety properties of a material. Five common methods using flame retardants are, but not limited to; 1) avoid using materials with a high energy content, 2) dilution of pyrolysis gases usually by the release of inert gases such as H_2O and CO_2, 3) formation of a protective layer e.g. by charring or intumescence, 4) surface cooling by endothermic reactions, 5) radical quenching slowing the combustion process down [70]. For thermoplastic materials such as EPS and XPS charring and intumescence effects are not possible as the materials becomes soft and eventually liquid when heat is applied. Thermoset plastics such as PF, PUR and PIR are capable of having the four latter of the mentioned positive effects but predominately a char layer which protects the underlying virgin material from any direct flames is used [8]. If the char is cellular it has a low conductivity which lowers the heat transfer and if solid it reduces the oxygen diffusion [9] both are beneficial from a fire safety perspective. In reality it is a transition from a solid layer towards more cellular and will therefore change its fundamental method of providing protection. While the reduction of materials flammability is most desirable it can also have adverse effects such as increased toxic smoke production, as pointed out by Molyneux et al. [71]. Ultimately it is a trade-off between desired and unwanted affects and the cost. It should be noted that the smoke from fire

tests are currently not analysed for toxic compounds. However, the *color* [72], the *smoke production rate* [38], the *smoke obscuration* [73] or the *smoke growth rate* (SMOGRA) [38], just to mention some, are reported. This missing measure is also explicitly recognised in the National Fire Protection Agency (NFPA) 286 "*The method of test does not provide the following: (1) Full information concerning toxicity of combustible gases…*" [74]. The lack of regulative restrictions on the toxic products make products that release toxic compounds while reducing the fire advantageous over products with a less toxic release but with a higher release of energy.

1.3 Mineral Wool and Polymeric Foams

This section describes various commercially available sandwich insulation products in more detail, with a focus on the two core types studied herein, i.e. mineral and polymeric cores. Herein, the panels with a core of mineral wool were all of the stone wool core type. The Stone Wool (SW) was processed at temperatures as high as 1500 °C, making the core ingredients basalt rock and slag liquid enough to be whipped into thin strands of stone wool before being cured and packed. In a typical SW product the vast majority by mass is the wool itself combined with an organic binder and very little oil usually about 2% [75], [76]. Densities range from 40 kg/m^3 to 180 kg/m^3 with the denser types for applications that require a high level of passive fire protection [77] [16] [18]. The typical core also has a melting temperature above 1000 °C [78] according to the DIN 4102-17 [79]. The thermal conductivity in a mineral wool at ambient temperature is well understood as this is the main operational temperature range of with respect to the orientation of the fibres, modes of heat transfer and density, as seen in Figure 1.6, Figure 1.7 and Figure 1.8, respectively.

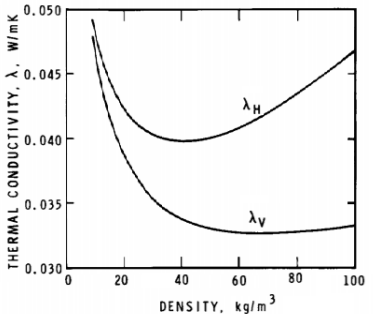

Figure 1.6: Thermal conductivity for a mineral wool as a function of the orientation where λ_V and λ_H is parallel and perpendicular, respectively, to the surface. Extracted from [80] with modifications and originally from [81].

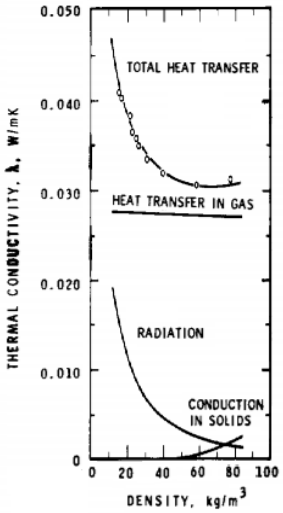

Figure 1.7: The contribution of three major modes of heat transfer to the total thermal conductivity at 20 °C as a function of the density, from [80] with modifications and originally from [82].

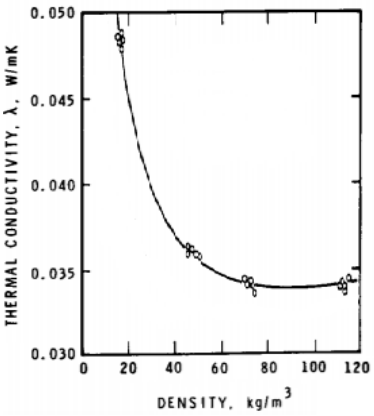

Figure 1.8: Representative thermal conductivity for a mineral wool at 24 °C as a function to the density. Extracted from [80] with modifications and originally from [83].

These relationships between conductivity and density at ambient help understand the internal heat transfer as they illustrate three distinctive trends as the density will decrease as first the binder and later when the minerals start to decompose :

- The importance of the fibre orientation as at high densities the thermal conductivity can increase by 33% for horizontally compared to vertical oriented fibres.
- The increased density means more fibres which is important as the mean free distance in the core will decrease and the radiation contribution likewise, at ambient temperature at least.
- The reduced mean free distance will also increase the conductive contribution which means the core material heats up faster.
- A decrease in density will generally increase the thermal conductivity if between 20 kg/m^3 and 100 kg/m^3

Ultimately this means as the temperature in the core increase and any binder is combusted the thermal conductivity will increase as the density will decrease and the radiation term will dominate due to its power relationship over the other terms linear relationship with respect to temperature.

This resulted in a proposed linear relationship for the thermal conductivity at ambient temperatures by Klarsfeld [84], as a function of the density of the mineral wool, as seen in Eq. 1.1

$$k_0 = A + B \cdot \rho + \frac{C}{\rho} \qquad \textbf{1.1}$$

Where k_0 is the global conductivity of the mineral wool at ambient temperature, A, B and C are the internal convective, conductive and radiation terms, respectively, and ρ is the density of the fibrous material. Even though these correlations are based on studies with glass wool the similarity between gas and rock fibres, as seen in Figure 1.9, are noticeably and the theoretical approach is believed to be valid for stone wool as well, as presented by Dyrbøl [85] and Hidalgo [16]. However, differences as a function of the materials can be expected, as also pointed out by Dyrbøl [85], stating that "*minor variations in the constants will exist when comparing with the work of other authors"*.

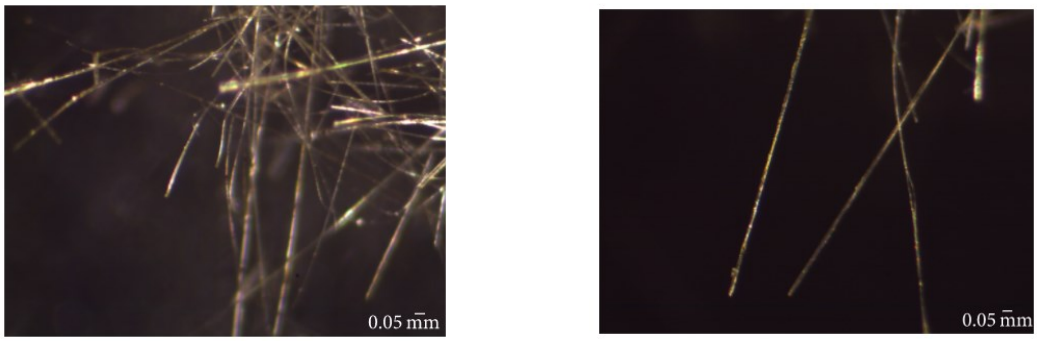

a) **b)**

Figure 1.9: Cleaned glass wool and rock wool seen through a microscope in a) and b), respectively, from [86].

De Dianous et al. [87] studied the thermal conductivity using a bi-guarded hot plate and a spectrophotometer on rock wool batts with 38.5 wt% slag at ambient and higher temperatures and determined that the spherical shaped slag increased the radiation. Additionally, De Dianous et al. noted that in high-density board the fibres are more prone to be parallel to the face of the board as they get more compressed (for them heavy was 100 kg/m^3). For boards with densities of 50 kg/m^3 and 100 kg/m^3 the conductivity was increased from 0.037 W/m·K and 0.035 W/m·K to 0.138 W/m·K and 0.092 W/m·K, respectively, when the temperature was increased 24 °C to 400 °C (values

extracted from their “FIG. 7” in [87]). Livkiss et al. [88] measured an increase from 0.027 W/m·K to 0.176 W/m·K in the thermal conductivity for a 105 kg/m^3 stone wool batt from 24 °C to 400 °C (values extracted from their “Figure 1” in [88]). However, as the slag content was not known and is suggested to be the dominant mode of heat transfer at high temperatures quantitative predictions are impossible to make a priori. Nevertheless, the conductivity of mineral wool panels can be expected to increase at higher temperatures e.g. during a fire. The use of the heat transfer model, for Stone Wool (SW) will be presented in Section 2.3 - *Heat Transfer Analysis* coupled with a least-square solver that provides the temperature dependent conductivity term, k_1. The least-square solver is based on minimising the difference between the temperatures provided by the model compared to those measured throughout the duration of the experiments.

1.3.1 Stone Wool Panels

The type of steel-faced panel with a core of mineral wool used in this work consisted of a core of ~100 mm stone wool with two 0.5 mm steel facings with a matt off-white finish. The panel is not a *self-standing* sandwich panel but a *building material* and is classified accordingly under the EN 13501-1 +A1:2009 [39]. However, in Europe, compliance with EN 14509 [89] also dictates compliance with the EN 13501-1 classification system, even for self-supporting metal faced panels. These panels are furthermore classified by the Loss Prevention Standard (LPS) 1181, the LPS 1208 and by the International American Society for Testing and Materials (ASTM) E119-12 [90] from Underwriters Laboratories (UL) and as *Class 1* according to the 4880 [91] and 4882 [73] standard from the Factory Mutual Insurance Company (FM) [18]. The SW core (outside of sandwich panel use) itself is classified as a non-combustible material following the EN 13501-1 which correspond to either *A1* or *A2* [18]. The SW is, however, bound together by a binder within the core material as well as some glue binding the steel facings to the core. As a composite it is therefore not possible for the SW sandwich panel to reach one of the two *non-combustible* classifications. There is therefore a potential for this classified as non-combustible core to release energy when used as a sandwich panel core material. The panels were symmetrical around the horizontal centreline, as seen in Figure 1.10, with the same steel-sheet thickness and coating the panels could not be installed incorrectly. There was no gaskets, film or other means providing protection to the core at the joints or ends. While the design of the joints were simple, they were often not filled with insulation, as seen in Figure 1.10, and thus reducing its thermal resistance at every joint.

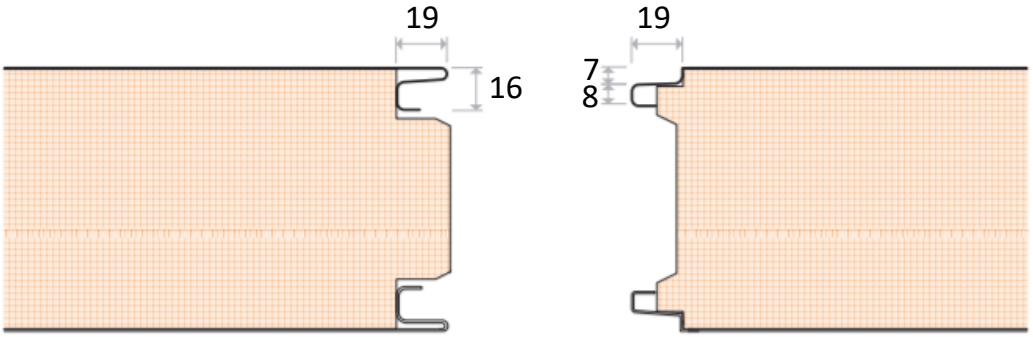

Figure 1.10: Cross-section of the joint of the panel with SW core with measurements in mm, from [18].

1.3.2 Polymeric Panels

Polymeric foam products includes, but are not limited to, polyurethane (PUR) and polyisocyanurate (PIR) foams and from an building insulation perspective always of the rigid type whereas the flexible type is more commonly used in the furniture industry. The two types, PUR and PIR, are also similar with respect to their chemical composition to the extent that they are never exclusively one or the other but a bland of the two. Their main component is the methylene di-phenyl di-isocyanate (MDI) and a reactive polyol. Together with toluene di-isocyanate (TDI) MDI is accounting for 90% of the global industrial PU production [92]. However, TDI is more commonly used in flexible PU and MDI in rigid PU. The main difference between PUR and PIR is not the chemical composition but the way the molecules are bound together. The PIR foam is formed using a higher MDI to polyol ratio together with a catalyst to promote the creation of isocyanurate rings, as seen in Figure 1.11, [92, 93] and a blowing agent to decrease the density [94] as well as other, usually proprietary, additives such as flame retardants. PUR is made in the same way as PIR, but with a lower MDI to polyol ratio and the generation of isocyanurate rings is therefore less frequent. Generally, for PUR, the polyol is reacting with the isocyanurates to produce a urethane, as seen in Figure 1.12, which can then again react to form another group. There are several other reaction schemes for PUR/PIR production and they are presented in greater detail by Avar et al. [92] and McKenna et al. [93] .

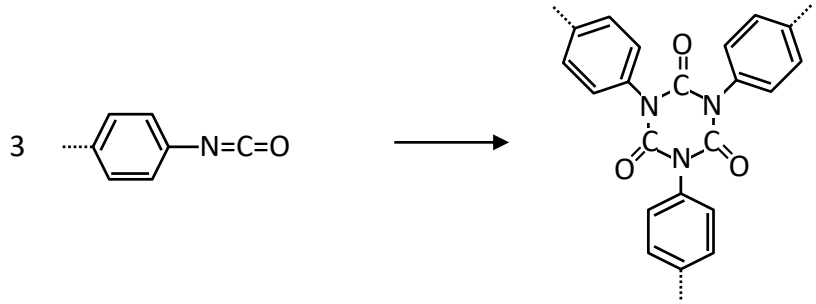

Figure 1.11: Three isocyanurates reacting to produce an isocyanurate ring, adapted by [93].

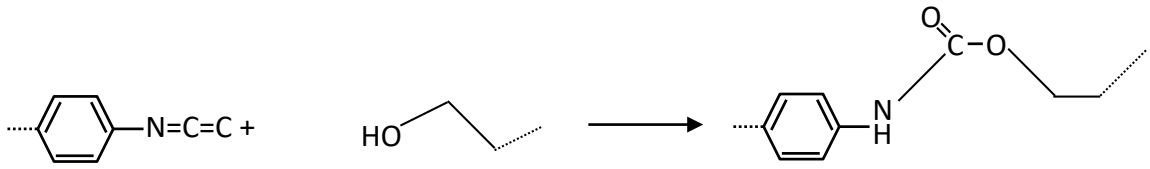

Figure 1.12: An isocyanurate reacting with an alcohol to produce an urethane, adapted by [93].

The advantage of the isocyanurate rings is their ability to maintain their stability at higher temperatures compared to the urethane bond, 270 °C to 300 °C and 180 °C to 200 °C, respectively [95].If the foam, however, is manufactured with too many isocyanurate rings it becomes too brittle and with too few it loses it bond strength and therefore its stability at higher temperatures. A combination of isocyanurate rings and urethane are therefore desired [96]. The two major types of polyols used are polyester and polyether and, as shown by Dominguez-Rosado et al. [8], can the right amount of polyether can give the foam the same or better thermal stability than foam with polyester.

Generally speaking, consensus has been reached among the insulation industry, fire safety engineers, construction industry and regulatory bodies that *PIR* foam behave better under elevated temperatures than *PUR* foam [97]. This is attributed to the aforementioned increased amount of isocyanurate rings over urethane as their bonds remain stable at higher temperatures, and as seen by the classifications obtained by various products [98, 99, 100, 101]. The ratio between MDI and the polyol can vary between each PIR and PUR formulations based solely on their desired properties decided by the manufacture without an industry specified standard, ISO, EN or ASTM in place to guide the naming. Also, the type of polyol can also vary independent of the PUR or PIR name label. The differentiating ratio between MDI and the polyol from calling it PIR and PUR is not a fixed value which can mean that a *PUR* product can behave equal or better with respect to fire as a product named *PIR*, as seen in Table 1.1. The added Fire Retardant (FR) additive can additionally influence

the thermal behaviour to make the reaction in case of a fire completely independent of the PIR/PUR name.

Table 1.1: Example of how naming does not correspond to a better reaction to fire classification.

Naming	Classification (EN 13501-1+A1:2009)	
PUR	B-s3, d0	[101]
PIR	B-s3, d0	[102]
PUR	B-s2, d0	[103]
PIR	B-s2, d0	[100]
PIR	B-s1, d0	[99]

B-classifications are obtained under the EN 13501-1 [39] framework. The guidelines for mounting and fixation products to be followed by the accredited testing laboratory limits the influence by the operator, and thus improves the repeatability of the test results. The mounting shall be as close to the end-use as possible, and it is specified by the manufacturer or supplier providing the product for testing. Specifications can include the type of substrate, air gap or method of fixation. As the standard tests the product as a whole and under specific conditions it means the *reaction to fire* of the product is limited to the exact circumstances at which the classification was obtained. Researchers and engineers will have a hard time to extrapolate the obtained classification to other circumstances where, for example, the mounting, substrate or the fire differs even slightly and new tests can be needed. This will be further elaborated in Section *1.4 Classification*. The standard does, however, allow for expert judgments to extend the use of the classification test results.

1.3.2.1 Polyurethane

The panels with a core of PUR was classified as B-s3.d0 [101] indicating the highest SMoke Growth RAte with a limited contribution to the FIre GRowth RAte, SMOGA and FIGRA, respectively, without forming burning droplets. Plastic products classified as d0 are thermoset and a formation of char is often expected. The PUR panels were not additionally classified with respect to fire safety properties such as insurance tests e.g. Loss Prevention certification Board (LPS 1181) or FM 4880. The panels were asymmetrical with an external 0.45 mm thick wave formed steel sheet and a 0.6 mm thick internal steel sheet with a gasket to seal the joint at one end, as seen in Figure 1.13.

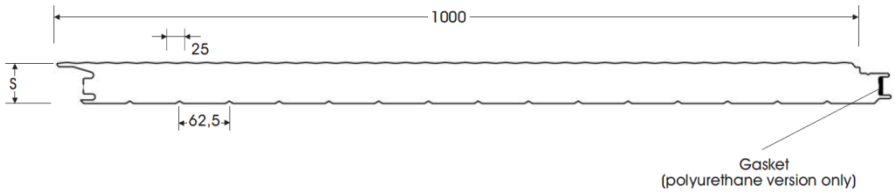

Figure 1.13: Cross-section of the PUR panel in mm, from [101].

1.3.2.2 Polyisocyanurate

The PIR panels were classified as B-s1,d0 as per EN 13501-1 with the additional fire safety classifications: LPS 1181 and FM global 4880 & 4881 Class 1 fire classification for unlimited height [99]. The additional fire safety relevant certificates are not necessary for access to the European market but the additional voluntary scrutiny the panels have been subjected presents the product as resilient with good performance against more than a single fire scenario just as the panels with SW. Like the PUR panels the PIR panel were asymmetrical, differently shaped and gasket placement, as seen in Figure 1.14. The steel thickness was 0.63 mm and 0.40 mm with a matt white and matt grey finish internally and externally, respectively.

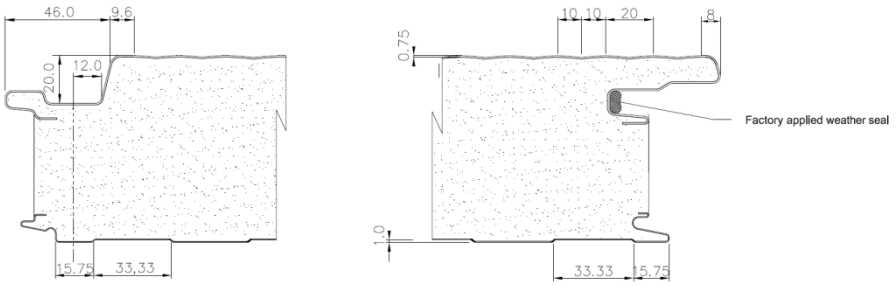

Figure 1.14: Cross-section of the joint of the PIR panel in mm, from [104].

The classifications obtained by the products, such as FM 4880 and EN 13501, are depending on the mounting and the conditions at which the panels were tested under. This means that any discrepancies between the test set-up and the experimental set-up can potentially change the behaviour of the panel and a different contribution or reaction to fire depending on the robustness of the panel can be found.

1.3.3 Material Properties

The material properties for the three steel-faced sandwich panels studied in a compartment setup, as seen in Table 1.2, show how minor details are approximately the same such as the thickness of the steel, coating colour and the European classification with respect to fire growth. The specific heat capacity was taken from literature as 1450 J/kg·K [105, 106] and 840 J/kg·K [107, 108] for PIR, PUR and SW, respectively, while the rest was taken from the technical data sheet provided by the manufactures or experiments conducted.

Table 1.2: Summary of material properties for the four studied sandwich panes from the techical documentation if not otherwise stated.

		PIR [99]	PIR [99]	PUR [101]	SW [18]
Thickness	(m)	0.10	0.06	0.06	0.10
ΔH_c	(MJ/kg)	29.1 ±0.5	29.1 ±0.5	23.1 ±0.5	2.1 ±0.1
ρ_c	(kg/m^3)	40.0 ± 1	40.0 ± 1	40 ± 3	120 ± 3
steel to core ratio	(kg/kg)	0.31	0.31	0.20	0.59
ρ_{panel}	(kg/m^3)	128	187	180	200
m	(kg/m^2)	12.8	11.2	11.8	21.8
c_p	(J/kg·K)	1450	1450	1450	840
k_0	(W/m·K)	0.021	0.035	0.024	0.038
$k_0\rho c$	(W^{2}s/m^4·K^2)	1218	1218	1392	3830
Internal coating		Matt white[1]	Matt white[1]	White[1]	Matt white
Internal thickness	(mm)	0.40	0.40	0.45	0.50
External coating		Matt grey[2]	Matt grey[2]	White[1]	RAL9010
External thickness	(mm)	0.63	0.63	0.60	0.50
Organic content	(%)	99.61[3]	99.61[3]	*	9.99[3]
Internal face type		Mini box[1]	Mini box[1]	Box[2]	Flat[1]
External face type		Micro[1]	Micro[1]	Mini box[2]	Flat[1]
EN 13501-1 classification		B-s1,d0[4]	B-s1,d0[4]	B-s3-d0[4]	B-s1,d0[4]
FM 4881 classification		Class 1[4]	Class 1[4]		Class 1[4]

[1] as described by invoice **[2] as per visual observation**

[3] as found by STA analysis, see Section 3.1.1. **[4] with prescribed mounting as done when classified**

*** Only experiments with N_2**

1.4 Classification

Generally speaking there are two major types of fire classifications, namely *resistance to fire* and *reaction to fire*. The mandatory tests, such as the r*eaction to fire tests* are required for access to the European marked whereas there are also voluntary tests. These voluntary tests can be from the insurance industry where their own additional tests needs to be passed to qualify for certain insurances. Other tests can include aspects such as sustainability and acoustic performance. In Europe, for sandwich panels, various standards are used to regulate sandwich panels such as the general EN 14509 [89] for steel-faced sandwich panels. The fire-section prescribes compliance with EN 13501-1+A1:2009 [39] with respect to the *reaction to fire* and in general the EN 1363 [109] for *resistance to fire*. The fire classifications help e.g. architects or engineers making design decisions as the data is presented in an orderly manner with a simple letter and number system indicating the performance of all the products available in Europe.

In Europe, internally mounted self-supporting sandwich panels are regulated under the EN 14509 [89] and for fire safety compliance with the Euroclass system (EN 13501-1) which also goes for non-self-supporting sandwich panel for internal cover. With respect to fire growth, under American regulations, the NPFA 286 applies to any internal and ceiling finishes which include steel-faced sandwich panels. The Euroclass system is separated into several classes ranging from best (class A1) to the worst (Class F) based on one or two tests which dependents on the class. The NFPA 286 is a simple pass/fail test where the flame spread, flashover, smoke production and peak Heat Release Rate (pHRR) are reported. An additional test is required if the panels are in need of classification for load bearing, R, insulating, I, or integrity, E. For European classification these are determined by measuring their resistance against the ISO 834 [48] also known as the "*temperature-time curve*" while the American equivalent is the ASTM E119 [90], however these are outside the scope of this project. Other test methods, also outside the scope of this project, are the British Standard (BS) 8414 -1 [110] and -2 [111], the Swedish SP-105 [112] which includes the assessment of the panel to withstand external fire spread. For external fires, FM 4881 [113] is considered one of the most stringent tests and recognised internationally as a stamp of limited external fire spread, but is voluntary.

The chosen summarised standards are important to the overall understanding of the standards that determines the classifications of sandwich panels with respect to fire. Table 1.4 lists the positive and negative aspects identified by the author, e.g. fundamental failure mechanisms. The important

classification with respect to sandwich panels will be presented in the following paragraphs focusing on the key aspects. These descriptions should not be taken as the summary of the full standard as the standards contain a lot of information as well as notes on minor but potentially important aspects to consider when classifying. The summarised standards does not include façade testing, as it is outside the bounds of this project. Supplementary classification relevant to sandwich panels but not specifically relevant to this project can be found in *Appendix – Supplementary Standard Tests Relevant for Sandwich Panels*.

1.4.1 EN 13501-1+A1:2009

The EN 13501-1+A1:2009 – Fire classification of construction and building elements – Part 1: classification using data from reaction to fire tests [39] is one of the key classifications in Europe when assessing the reaction to fires of a construction or building element. The EN 13501-1 standard works as an umbrella covering many other standards ranging from micro to macro scale testing. The classification provides a letter from the best (A1) to worst (E) with an additional class F for products without a performance determined or failed to obtain class E or higher. An overview, as seen in Table 1.3, illustrates all of the classifications from a European context for construction and building elements (excluding floorings, which are tested differently).

The EN/ISO 1182 [114] is known as the *non-combustibility* test where a sample in lowered into a 700 °C furnace and is not allowed to have a temperature exceeding the temperature of the oven by 30 °C, have a mass loss greater than 50% or any sustained flaming during the 30 minutes test period in order to pass. The EN/ISO 1716 [115] is the *gross calorific value* test and the theoretical energy content for all individual components is determined by testing just a few grams. These two tests are only used for the A1 and A2 classes which are non- and nearly non-combustible, respectively, due to their low energy content and are believed to have no contribution to the fire growth. Materials in the A1 class are usually of the concrete, steel, stone and ceramic type of materials [116]. For any composite and sandwich panel the non-combustibility classes are unlikely to achieve as they at the very least require a type of glue to combine the various layers. For non-homogeneous products and building elements such as a sandwich panel the A2 classification is also obtainable by passing the EN 13823:2010+A1:2014 [38], known as the *Single Burning Item test* (SBI) and the EN/ISO 1716. However, the glue is an *internal non-substantial component* and usually of organic nature and will therefore struggle to have a complete heat of combustion of less than 4 MJ/kg as required to obtain the A2 classification, as seen in footnote *b* in Table 1.3. The B classification is therefore the highest

classification a sandwich panel with an organic component and a glue can realistically obtain as the panel will be tested as a system rather on its individual components.

Table 1.3: The underlying test standards under the EN 13501-1 classification standard, extracted from [39].

Class	Test method(s)	Classification criteria	Additional classification	
A1	EN ISO 1182 [1], and	$\Delta T \leq 30°C$, and $\Delta m \leq 50\%$, and $T_f = 0$ (no sustained flaming)		
	EN ISO 1716	$\Delta H_c \leq 2.0$ MJ/kg [1], and $\Delta H_c \leq 2.0$ MJ/kg [2, 2a], and $\Delta H_c \leq 1.4$ MJ/kg [3], and $\Delta H_c \leq 2.0$ MJ/kg [4]		
A2	EN ISO 1182 [1], or	$\Delta T \leq 30°C$, and $\Delta m \leq 50\%$, and $T_f = 20$	s_1 = SMOGRA $\leq 30 m^2/s^2$ and $TSP_{600s} \leq 50 m^2$, s_2 = SMOGRA $\leq 180 m^2/s^2$ and $TSP_{600s} \leq 200 m^2$, $s_3 \geq s_2$	d_0 = No flaming droplets/particles within 600 s, d_1 = No flaming droplets/particles persisting longer than 10 s within 600 s, d_2 = not d_0 or d_1,
	EN ISO 1716, and	$\Delta H_c \leq 3.0$ MJ/kg [1], and $\Delta H_c \leq 4.0$ MJ/kg [2], and $\Delta H_c \leq 4.0$ MJ/kg [3], and $\Delta H_c \leq 3.0$ MJ/kg [4]		
	EN 13823 (SBI)	FIGRA ≤ 120 W/s^2 LFS < edge of specimen $THR_{600s} \leq 7.5$ MJ		
B	EN 13823 (SBI), and	FIGRA ≤ 120 W/s^2 , and LFS < edge of specimen, and $THR_{600s} \leq 7.5$ MJ		
	EN ISO 11925-2[8] Exposure = 30s	Fs ≤ 150 mm within 60s		
C	EN 13823 (SBI), and	FIGRA ≤ 250 W/s^2 , and LFS < edge of specimen, and $THR_{600s} \leq 15$ MJ		
	EN ISO 11925-2[8] Exposure = 30s	Fs ≤ 150 mm within 60s		
D	EN 13823 (SBI), and	FIGRA ≤ 750 W/s^2 , and $THR_{600s} \leq 15$ MJ		
	EN ISO 11925-2[8] Exposure = 30s	Fs ≤ 150 mm within 60s		
E	EN ISO 11925-2[8] Exposure = 15s	Fs ≤ 150 mm within 20s		
F	Performance not determined			

[1] For homogenous products and substantial components of non-homogenous products.

[2] For any external non-substantial components of non-homogenous products.

[2a] Alternatively, any external non-substantial component having a PCS ≤ 2.0 MJ/m^2, provided that the product satisfies FIGRA ≤ 20 W/s^2 and LFS <edge of specimen and $THR_{600s} \leq 4.0$ MJ and s_1 and d_0 according to the EN 13823

[3] For any internal non-substantial component of non-homogenous products.

[4] For the product as a whole

[7] Pass = no ignition of the paper (no classification), Fail = ignition of the paper (d_2 classification)

[8] Under conditions of surface flame attack and, if appropriate to the end-use application of the product, edge flame attack

1.4.2 EN 13823:2010+A1:2014

Figure 1.15 shows the test configuration for *EN 13823:2010+A1:2014 - Reaction to fire tests for building products – Building products excluding floorings exposed to the thermal attack by a Single Burning Item.* It can be seen that the mounted building element is impinged by a fire from the corner located triangular shaped gas burner which is fuelled by propane and releases 30.7 ±2 kW. The fire impinges on the face of the building elements and the Fire Growth Rate (FIGRA), Total Heat Released (THR_{600s}) and Smoke Growth Rate (SMOGRA) are calculated based on the collected and analysed combustion gases and the Linear Flame Spread (LFS) is visually determined. The surface flame spread must not reach end of the 1 m long wall in any of the three required repetitions. However, if the flame reaches the edge, three new tests can be conducted with the length of the wall being 1 m + *t*, where *t* is the thickness of the panel. This configuration is also acceptable for obtaining the classification. Based on the limit values expressed in EN 13501-1+A1:2009 an A2, B, C and D classification can be obtained in combination with one other test. For A2 that other test is the EN/ISO 1716 known as the *gross calorific value test* while for the classes: B, C and D that test is the EN/ISO 11925-2:2010 [117] known as the *single-flame source test*.

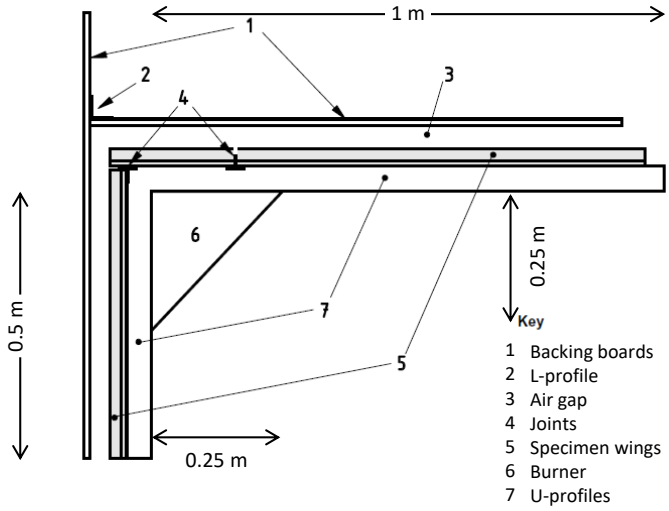

Figure 1.15: Top view of the EN 13823:2010+A1:2014 SBI test setup. The test specimen is placed in the U-profiles marked with a *7* in the figure, from [38] with modifications.

1.4.3 ISO 13784-1

The ISO 13784-1:2014 [47] is a compartment fire similar to the ISO 9705 [118] where a 0.17 m x 0.17 m sandbox gas burner is located either near a corner in the wall opposite of the door opening or in the middle at wall opposite the door opening at a joint between two panels. The internal dimensions of the compartment measures 2.4 m x 3.6 m x 2.4 m in width, length and height, respectively, with a

door measuring 0.8 m x 2.0 m in width and height, respectively, as seen in Figure 1.16. Unlike the ISO 9705 the compartment boundaries in the ISO 13784-1 are completely build-up of the sandwich panel elements desired to test fastened onto the internal frame and not onto a non-combustible enclosure as in the ISO 9705.

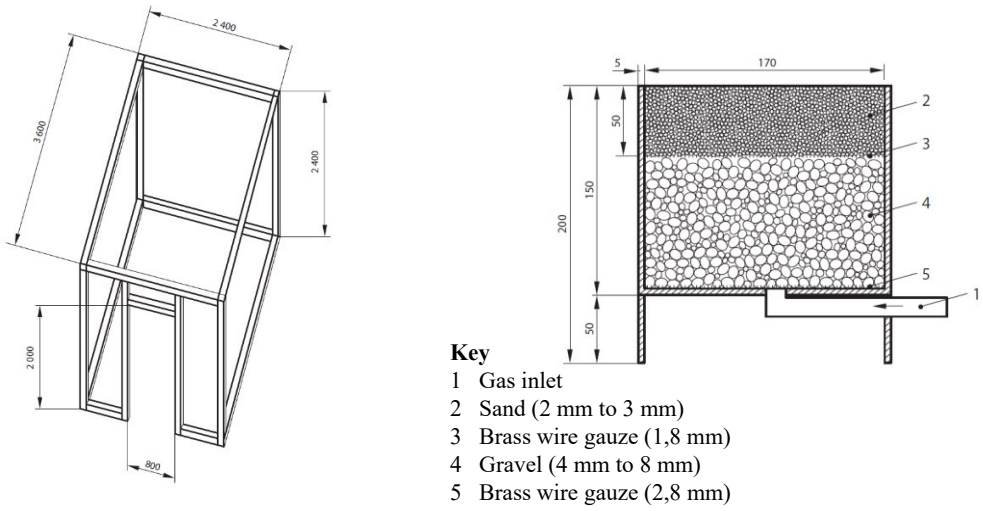

Key
1 Gas inlet
2 Sand (2 mm to 3 mm)
3 Brass wire gauze (1,8 mm)
4 Gravel (4 mm to 8 mm)
5 Brass wire gauze (2,8 mm)

Figure 1.16: The internal test frame for the ISO 13784-1 to the left and a cross-section of the gas burner to the right, from [47].

There is not a fixed failure definition and a report of the test reporting various times such as time to flashover, temperature development at specified locations as a function of time is produced. The ISO 13784-1 and the ISO 9705 are HRR regulated standards which are fixated to pre-determined values, as seen in Figure 1.4 on page 9. The fire exposure in these tests is 100 kW and 300 kW for 10 min each, provided by the 0.17 m x 0.17 m sandbox burner with its opening 20 cm above the floor. For the ISO 9705 the burner is fixated in the corner as the lining materials are nailed or otherwise attached to the compartment. However, as the compartment in the ISO 13784-1 is potentially constructed with the sandwich panels attached to an internal frame the burner can be prevented from impinging the internal corner as the scope of the standard otherwise state is the purpose of the test. If an internal frame is used and a column is in the corner the burner must be moved to the nearest joint on the back wall (relative to the doorway) while being “not less than 300 mm” or “≤ 300 mm” from the corner depending on the contradicting paragraphs in the standard. For all the experiments conducted herein, except the full scale, this was not a concern, as the panels were supported externally and not internally. The only two experiments with different burner locations than the corner were E15 and E16, see Table 2.12 on page 65, where the burner was placed in the middle of the compartment at the back wall and in the centre of the compartment, respectively.

Table 1.4: A Summarising pro and con list for the standards applicable to sandwich panels.

EN 13501-1+A1:2009 [39]	Pro	All materials and products can be fitted under this umbrella of sub classifications and provides a unified classification system from A to F which is useful for e.g. engineers, architects and designers.
	Con	All materials and products inherently vary and an arbitrary scaling system ranging from A to F has difficulties capturing differences between products as they are lumped together in letters determined by different classification masking the measured quantities.
EN ISO 1182 [114]	Pro	Provides a direct measure of the thermal degradation of a material at 700 °C exposure for 30 min. Five replications are prescribed adding robustness to the result.
	Con	The 700 °C is produced by heating coils and is just as much a reaction to ~51 kW/m^{2*} of radiation on all the surfaces than an actual direct temperature exposure. A multi-component product might shield a specific material from the direct radiation and as such the heat transfer will be conduction rather than radiation. Alternatively an air gap can be part of the end-use. Such design features will not be recognised as components are tested individually.
EN ISO 1716 [115]	Pro	Provides a direct measure of the gross calorific value of the component useful for determining the total fuel load in a compartment for e.g. design purposes and risk assessments.
	Con	The gross calorific value assumes the H_2O in the combustion is in its liquid phase, which it rarely is in a fire giving an overly-conservatively measure. A multi-component product with a design preventing either oxygen or high temperature from reaching a component with high gross energy content (>4 MJ/kg) is not recognised as all components are tested individually.
EN 13823 [38]	Pro	The flame spread across the surface in a corner configuration, which is considered to be the worst, is estimated by a direct impinging flame from a 31 kW fire which is a realistic scenario as single burning items are capable of releasing such energy. The products are tested as in their “end-use” application which provides a product rather than a component measure. Three repetitions provide some robustness of the obtained results.
	Con	This configuration is believed to capture the dominant mode of fire growth in a compartment. Multi-layered products with a non-combustible outer layer have a critical failure mode different than surface spread which is not recognised by this configuration. The configuration has no horizontal restriction like the ceiling in a compartment and both the build-up of hot gases and flame impingement which could happen in a compartment.
EN ISO 11925-2 [117]	Pro	The lowest possible threshold for the European market is defines by a restriction of vertical flame spread by a lighter sized flame which is a likely initial source.
	Con	For class B, C and D classifications the exposure is 30 s and monitored until 60 s have passed. For the class E requirement is the

		product exposed to 15 s of exposure and the experiment is stopped after 20 s and potentially not all spread is measured. For multi-layered products the burner is moved inwards to impinge the centre of the product if applicable and the vertical surface flame spread is no longer measured.
FM 4880 (the part about fire) [91]	Pro	The classification involves four tests; a 50 kW/m^2 radiation exposure to the face of the product which is the part that will be exposed during a fire, large corner mock up with the products installed as in their "end-use", an even larger corner mock-up similar to the other corner test, and a compartment fire with the product mounted as an internal lining. All represents realistic fire scenarios and the products are tested as specified in their end-use providing an accurate expected performance during a fire. Two of the three tests are full scale.
	Con	The main mode of fire spread in three of the four tests are surface flame spread and in the corner mock-ups the hot gases and smoke are able to exit the system after heating the un-confined ceiling. For products with a non-combustible face this will not be the dominant mode of fire- spread or growth. The compartment fires to choose from are not the same design fire or failure criteria which one is less severe which can make it a preferred choice and thus give a less conservative estimate of the ability of the product tested. Two of three tests are large and therefore expensive to conduct.
ISO 13784-1 [47]	Pro	Provides a test report for the product in a compartment setup for a 20 min specific fire scenario. Full scale experiment with end-use configuration
	Con	The fire scenario is partially testing the surface flame spread of the product. The test is not required under the European regulatory framework and is considered large and therefore expensive to conduct. No failure is defined in the standard, only tick boxes for flashover and integrity failure
LPS 1181-2 [119]	Pro	A compartment fire test with a 34 kg wood crib as fuel elevated from the floor to ensure the flames are impinging onto the ceiling is a realistic fire scenario. Full scale compartment fire scenario with end-use configuration.
	Con	The fire source can be considered relative small compared to the size of the compartment with a short burning duration. The test is considered large and therefore expensive to conduct.
		* Based on blackbody radiation, $q'' = \epsilon \cdot \sigma \cdot T^4$, where ϵ is 1 for a black body, σ is the Stefan-Boltzmann constant ($5.67 \cdot 10^{-8}$ W·m^{-2}·K^{-4}) and T is the temperature of the heating coil.

The FM test does include ceilings in order to reflect the horizontal restriction and the hot gases from the wood crib or panels themselves are free to leave the control volume of the test setup, as described in Table 1.4 and in *Appendix A - FM 4880 and FM 4881* on page 154, but also in order to

be a compartment test. As the FM and LPS tests are from an insurance perspective their focus is on the protection of the property, which is optional in the national prescriptive standards known to the author. However, as the insurance industry stands to lose money if a fire develops beyond their estimate, their requirements are often more stringent than the mandatory national regulations. This is possible as insurers potentially have less interest groups advocating for certain choices and are less influenced by outside forces, beneficiaries or lobbyists than the international standards committees are. In addition to considering inputs from manufactures and interest groups advocating their cases, national regulators also have an interest in the labour heavy construction industry to erect buildings without imposing too much bureaucracy and over-regulation [120]. This has to do with avoiding imposing unnecessary regulations which does not directly benefit the general public. An argument can be that it is not the role of the state to dictate the expected lifetime of the constructions build by private companies or investors. The state does however have a responsibility to keep the public safe and such an objective can be regulated and is what often is written into the respective building codes worldwide. At the same time collapsing buildings will be a risk for the health of the general public making it balance for any regulator to consider.

1.5 Knowledge Gap

The problem with tests arises when it does not address fundamental or intrinsic properties where the outcome is independent of the input and in fire testing this is often the case. Fires are dynamic and influenced by many factors such as combustion kinetics and boundary conditions and material and product diversity is a challenge for standardised tests. Some products containing a lot of fire retardants can be effective at resisting a single burning item or the first item burning. A growing fire, however, might be too developed for the same fire retardants to have their desired effect and at higher combustion temperatures they can even have an adverse effect increasing the lethality of the smoke [121]. One of the fundamental problem with these kind of fire safety tests is the success solely depends on the ability of the classification test to predict the exposure of real-life fires to the elements. Furthermore, there is often no requirement in any of the ISO, EN or ASTM test standards that indicate the robustness of a material. Robustness could include a lot of things, e.g. the ability of the element to reproduce results (some small scale test standards do require up to 5 samples), how a 10% fire load/temperature/mechanical stress increase or how deviations from optimal instalment affects the performance. Combined with the rules of extrapolating classification based on the passing of similar materials can lead to a transferred classification based on a single passed test out perhaps several attempts. Olsson reported temperatures even within the same furnace were far

from homogenous [122], albeit for resistance-to-fire tests. This indicates a lack of reproducibility in test procedures where local deviations can determine the performance of the whole element and possibly future similar products responsible. The consequence of this is that a product passing its 11^{th} test but failing the first 10 will be classified differently the 11^{th} time and sold as such. Depending on the test, this could be from a *C* to a *B* classification or from REI 30 to REI 60. Although this is a hypothetical scenario, the unintentional deviations occurring across test setups and materials makes this scenario possible as consecutive similar results are not a requirement.

There are an abundance of standards to choose from when the time comes to classifying your product, and while some are mandatory others remain voluntary. National building codes are always concerned with the *life safety* aspect of a fire safety design solution and mandated classifications such as the EN 13501-1, in Europe, is required. The interest of a manufacturer can be different from the buyer and the user. A manufacturer is obliged to pass any required classification tests before it can be sold and anything voluntary can be considered as a loss as it is not necessary, such as prolonging a standard test till failure occurs. Furthermore, passing a test with a large margin can also be costly if the cause of this is an expensive ingredient or feature and is undesirable [123]. In the EN 13501-1 and the underlying standards materials not tested for *non-combustibility* is conducted on the product as a whole and not its individual components and is considered appropriate from an end-use perspective.

The cost of the room corner test lead to research into other smaller scale tests and the Single Burning Item (SBI) test was found sufficiently successful in predicting the behaviour observed in a compartment. The assumption is the behaviour seen in a corner configuration at smaller scale could be extrapolated to the behaviour in compartments. However, this premise is primarily based on the main mode of fire growth is flame spread across the surface of the tested samples. Providing products with a surface layer not prone to surface spread proved this method of scaling unable to extrapolate result [40]. Furthermore, steel-faced sandwich panels are used either as wall or ceiling in a compartment and never as free standing wall without a ceiling or a horizontal restriction of some kind. The SBI test therefore fails to consider the effect of the enclosure as that part of the end-use feature and is a poor test for identifying the behaviour of steel-faced sandwich panels [66, 124, 40]. The SBI test is however great at extrapolating the behaviour of materials where the surface flame spread is the dominating method of fire growth. Materials with a combustible surface, which the

majority of construction materials have, had a strong correlation between the SBI and the room corner test [40], which is the reason the standard was implemented in the first place.

Making informed decisions regarding the choice of the fitting sandwich panel, or any product in general, to use for specific applications requires information. Fire tests do not truly indicate how a material will behave in an actual fire [125]. Fire tests are at best meant for comparative studies between products or elements and at times it does not even do that [126]. Building elements and products can fulfil the same objective in different ways and can be optimised to pass the exact impacts prescribed in tests. The rate of flame spread across a surface, which is the assumed failure mode in the EN 13823, can be reduced by the addition of sufficient flame retardants, having a non-combustible surface layer or have a non-combustible homogenous product. All three materials have the potential to surpass the requirements posed in any pass/fail test which only focuses on the flame spread. However, the indebt temperature gradient and penetration could be of importance, and so could the boundary conditions, just to mention some. This means two identically classified materials based on fundamental different methods of passing that test can behave differently when the test set-up and boundary conditions are changed, which was supported by Maluk [127] with respect to the boundary condition, albeit for structural members under the EN 13501-2 frame work. If the parameter causing the failure is not the same as the one it was tested for, but only a side effect of the test, then extrapolation of the data and/or the classification of the tested product or material will often be poor. This means there can be a discrepancy in the interpreted classification of a product and the reaction, resistance or performance during an actual fire. All providers of steel-faced sandwich panels are required by regulation to show their product can pass classification tests appropriate for its use before access to the market is granted. This ensures the product has a minimum level of safety. One test can, as noted, be a poor indication of the actual level of fire safety for certain products, which is more probable if the basis of the test standard is the wrong type of failure mode to such extent that the actual performance will remain unknown.

The data sheet for any sandwich panel is often available online or at the very least available upon request from the manufacture/distributor. The data sheet has to contain the legally required information such as the fire classification obtained. Much of the underlying information is hidden and not required to be disclosed as limit values are inferred by the provided classification. These could include the actual mass loss percentage or gross calorific energy content from a non-combustibility test behind the non-combustible product class or the exact smoke growth rate

calculated based on the SBI test, both part of the EN 13501-1 classification standard. Conducting experiments with the intention to acquire additional information not disclosed by manufactures are essential for understanding the materials and identifying risks of exothermal reactions, phase change, mass loss or loss of integrity can be of great value for research and development and scientists. Eventually this knowledge can also be useful for the decisions makers determining acceptable the societal fire safety level and the design of test standards intended to classify accordingly or engineers and architects dimensioning and designing buildings.

If the price, difficulty and time restraints of conducting full scale experiments is believed to outweigh the benefit of an accurate classification then an alternative test that is cheaper, easier and faster, which also provide an inaccurate identification of the risk of a product would seemingly be preferred. However, identifying the dominating behaviour of the fire growth at full scale and designing a simpler alternative test would be ideal and the appropriate scaling method would be selected and the ability to extrapolate the data back to large scale would increase. A free burning fire is different from an enclosure fire as the heat feedback from the enclosure and the formation of a hot gas layer can play a role in the fire dynamics. Determining the potential for a compartment to fail by either flashover (a change to an oxygen controlled fire) or integrity failure for wall covers, products or materials tested in a compartment would be preferred. This also goes for steel-faced products the choice of scaling the whole compartment rather than an open corner test setup is preferred. By conducting more complex experiments, as a compartment fire compared to a surface flame spread test is, several key aspects have to be considered:

- The size of the compartment.
- The fuel and appropriate fire scenario.
- The scaling theory deployed.

Which all add additional questions such as: how to assemble, what to measure, what to measure and what, if at all, should be the failure criterion. These aspects will be covered in section 2 - *Analysis Methods and Experimental Setups* and specifically in 2.1 *Scaling Analysis* and 2.2.5 - *Detailed Description of the Scaled Compartment Experiments*.

Fire experiments are valuable as it allows for the acquisition and addition of non-regulatory knowledge such as failure modes, important parameters and key operational parameters. By changing the boundary conditions and geometrical factors additional knowledge can be acquired

which will help develop the understanding of the behaviour of any materials over a wider range of scenarios assisting making an informed decision with respect to fire safety uses.

1.6 Research Overview

This section provides an overview of the important parameters necessary to determine the appropriate experimental setup and scale required to fulfil the research objective. The steel-faced insulating panels were studied at a component level and at product level to determine parameters important from a fire safety perspective.

1.6.1 Geometrical Scaling

An appropriate method to determine the performance of steel-faced insulation panels builds on the understanding of the behaviours of the products at a detailed and fundamental level. Fire is a complex phenomenon relying on transient physical properties, chemical reactions and ambient conditions where the extrapolation of the knowledge across scales is often a necessity. The scale at which the products are studied at has to be sufficiently detached from the boundary conditions and the experimental setting to be useful outside the experimental environment. The reliance of the extrapolation from the surface flame spread in the current open corner configuration to a compartment is not believed to be the appropriate way of testing sandwich panels with an inert surface material. By employing a geometrical scaling methodology the entire geometry, boundary conditions and fire scenario of the full scale compartment is all be maintained at a reduced size. This is thought to be a more robust and appropriate way of conducting the test as the failure mode will be the heating up of all the boundaries by direct flame impingement and by enclosing the hot gases in the compartment from the burner, just as in a full scale compartment fire.

1.6.2 Micro Scale Experiments

The microscale experiments are designed to determine fundamental intrinsic material properties. The thermographic analysis (TGA) conducted under inert or reactive atmosphere is a simple experiment for which the sample size needs to be sufficiently large in order to ensure a measureable mass loss as well as a ratio between porosity and the heating rate of analyser. Ensuring heating rate independence will provide useful information, such as reactivity as a function of the temperature of the sample. The data can be used for modelling purposes, for example to determine the

temperature of a compartment with the material internally mounted, as Marquis et al. [128] successfully did using Fire Dynamic Simulator.

Energy content is a key material property that can provide a quantitative measure of a products material compositions and often is not provided by manufacturers leaving the engineer to assume a value often based on generic literature values. Energy content is determined under extremely favourable combustion conditions and will therefore provide results considered conservative compared to the expected energy release during conditions common in fires. The total energy available is, however, a key parameter for fire safety engineers when determining the thermal load for a compartment with parametric fire curves, i.e. the curves for structural design by Magnusson and Thelandersson [129] or Pettersson et al. [130]. The results of the microscale experiments are presented in Section 3.1 - *Small Scale Experiments* with a holistic perspective with respect to fire safety and enclosure fire dynamics.

1.6.3 Macro Scale Experiments

At the macro scale the dissection of the products in parametric studies were conducted to determine under which conditions the products are posing a fire risk. Steel-faced insulation panels have been investigated thoroughly under the cone calorimeter and compared to the SBI and ISO 9705 compartment from a standardized test perspective where the focus was on the extrapolation of the results [66, 64, 131]. However, intermediate results are rarely presented in literature as the focus too often lies exclusively in the successful results, relationships and inter- and extrapolation possibilities. By dissecting at what boundary condition the core material behave a certain way it is easier to design an experiment which prevents any negative aspects from becoming a problem also at larger scales. The mass loss calorimeter experiments used to measure the mass loss, thermal penetration and to tract the thermal wave penetrating through the thickness of the samples was performed under various incident heat fluxes. The results and analysis are presented in Section 3.1.2 - *Cone Calorimeter* and discussed with respect to the implications for larger scale experiments and the limitations of the experimental results.

1.6.4 Compartment Setup

The steel-faced insulation panels are designed to be used as compartment walls and it is only natural that the panels are studied in a compartment framework. The compartments are sized as a

"standard" room meaning it is a small compartment prone to flashover fires where the temperature and heat release rate within the compartment is limited by the availability of oxygen rather than the amount of fuel available [132]. In compartments, the fuel is usually placed on the floor and enclosed by the walls preventing the fire from spreading to other adjacent compartments or to any outside façade. The studied compartments, however, contain its fuel within the walls and ceiling and if involved can cause the fire to spread beyond the volume of the compartment. The growth of the fire will then be controlled by the mass loss rate of the fuel as well as the supply of oxygen externally and internally, respectively. The geometrically scaled compartments and scaled HRR from the gas burner was varied in order to determine the validity of the scaling method across several scales by comparing the temperatures and time to failure. The compartment fails if one of three criteria are meet:

- The occurrence of flashover (a change to an oxygen controlled fire),
- Integrity failure with respect to flames,
- Collapse of one of the panel boundaries

The compartment setups are reported in detail in Section 2.2.5 -
Detailed Description of the Scaled Compartment Experiments.

1.6.5 Heat Transfer Analysis

The requirements of conducting large scale experiments are numerous and the ability to conduct reduced scale experiments are of great advantage. Maintaining the appropriate ratios of modes of heat losses and transfer is important for the extrapolation and robustness of the method. The thermodynamics in the compartments were analysed to ensure the quantitative measurements such as temperature and heat flows were also scaled satisfactory. A simple one-dimensional heat transfer model through a solid governed by the heat diffusion equation derived from Fourier's law and the conservation of energy, as described by Hidalgo [16], was used to determine the net heat flux through the solid boundaries of the enclosure. The conductive losses combined with the convective losses determined by doorway measurements enabled a non-dimensional global heat transfer analysis for cross-scale comparison. The heat transfer model is presented in Section 2.3 - *Heat Transfer Analysis* with the subsequent results presented in Chapter 3 alongside a comparison to experimental results from literature provided by Sørensen [133].

1.7 Research Objectives

The focus of this study was to assess the fire dynamics, measure the heat transfer and the fire growth in compartments constructed with steel-faced insulation panels when subjected to various design fires at different scales. In order to quantitatively assess the key parameters important to the fire growth of a compartment, the internal enclosure temperatures, the amount of energy emanating as hot air, heat released, smoke produced, and the heat conducted through the boundaries were measured. Fires are governed by physical relationships, chemical kinetics and heat transfer, therefore, the important and dominating physical relationships while having a simple main fuel source were scaled to examine the possibility of acquiring data at small scale and extrapolate it back up. The dimensions of the compartments and heat release of the fires were scaled rectilinearly and by maintaining the Froude number constant, respectively. The analyses of the important parameters were done to determine the viability of conducting the experiments at a smaller scale to reduce the operational difficulties and burdens that conducting large scale testing and experiments has.

The objective of this research is to determine a suitable experimental setup and size for determining the performance of steel-faced insulation material used as compartment boundaries. This is done by analysing the critical parameters such as boundary and compartment temperatures, heat transfer and heat released. The different sizes of compartments also allowed for a comparison between the fire performance and the size of the compartment with respect to the scaling.

1.8 Outline of the Thesis

The thesis has four chapters, and starts with the Introduction, which includes the background for the thesis and sets up the problem definition, including the classifications used to determine the fire safety properties of sandwich panels by using standardised testing methods. The subsequent sub-sections present the scaling theory behind the scaled compartment experiments and the heat transfer model used to compare the energy distribution in the compartment. The compartments used for the 1:5, 2:5, 1:2 and at full scale are presented in Chapter 2 as well as the smaller scale setups and findings. Chapter 3 presents all the findings of the compartment experiments and discuss the uncertainties and limitation of the methods used, with Section 3.2 presenting the results illustratively for a quick overview of the findings. Chapter 4 presents the conclusions, as well as the recommendations for future work.

2 Analysis Methods and Experimental Setups

This chapter introduces the experimental setups and analysis methods used in order to determine the performance of the core materials, both individually and the products as a whole. The scaling theory behind the majority of the conducted experiments is presented in Section *2.1 Scaling Analysis*, which includes the relationship between compartment size, HRR of the fire, and panel thickness. This chapter also presented the setup for the three small scale experiments in 2.2.1 - *Small Scale Experiments* and the compartment experiment setups which include: 2.2.3 - *Compartment Experiments* where the full scale compartment is presented, and: 2.2.5-
Detailed Description of the Scaled Compartment Experiments with the experimental setup of the compartments scaled as 1:5, 2:5, 1:2 of the full scale compartment. Finally, a versatile non-dimensional heat transfer model used for analysing the distribution of energy to the enclosure boundaries during the compartment fires is presented at the end in Section *2.3 Heat Transfer Analysis*.

2.1 Scaling Analysis

The scaling of any fire, which governed by complex physical- as well as chemical process, is challenging as it is virtually impossible to maintain all material and ratios identical across all scales. While the material properties such as the density and conductivity are easily transferable, the total mass of the panels scales to the power of two while the volume of the compartment to the power of three. The non-dimensional numbers such as the Reynolds and Froude numbers with respect to the flow velocity scale linearly and to the power of two. A fire in a compartment adds to the complexity as other effects such as the boundary layers and the build-up of a hot gas layer can become a factor to consider. The latter will play a dominating role if the gas layer heats up while having a high emissivity caused by a high soot concentrations and as the radiation increase the risk of compartment failure likewise increase. The downscaling of compartment fire tests allows for a safer and faster execution and it is therefore feasible to conduct several and not a single test. Conducting several experiments or tests the applicability, limitations and robustness of a product can be studied and is therefore very attractive and if not for regulatory and classification purposes then surely for research and development. Several scaling laws exist throughout the literature, but the Froude, pressure and analogue scaling methods are commonly used in fire research as they scale the important parameters relevant to fires.

The analogue scaling is, as the Froude scaling, based on preserving the Froude number by using liquids with different densities to simulate the ratio between the hot and cold gases in a fire. The advantage of this method, besides preserving the Froude number, is the ease of likewise preserving the Reynolds number if the flow is high enough to be turbulent. The disadvantage of this method is that the choice of liquids is based on maintaining the ratio between densities across scales, which often means scaling a fully developed fire as the ratio remains constant. This problem can, however, be overcome by changing the gases over time, adjusting for the change in temperature and densities between the mimicked hot and cold gases. However, the scaling method does not involve a fire, which for this research is paramount as the involvement of the panels and fire growth is essential data. The pressure scaling allows for the preservation of both the Froude and Reynolds numbers across all regimes which is important for fires inducing laminar flow fields. The pressure scaling, however, is demanding from an experimental point of view, as the entire compartment would need to be inside a pressurised vessel throughout the duration. If the HRR is to be measured by means of oxygen calorimetry a flow through the analysing equipment is furthermore required and with a reduction in the geometrical length to 0.4 an increase to four times the atmospheric pressure (L^3P^2=constant [134]) is required, and thus making the setup process cumbersome. The Froude scaling is able to maintain the ratio between the inertial and gravitational forces and with high enough fuel mass flows and fire size the Reynolds number should also be preserved as the flow is turbulent.

A partial scaling method was used preserving the Froude number, Fr, and the non-dimensional heat release rate, $\dot{Q}^*$, across all the scales. This method has previously been used for free burning wood crib fires [135] as well as compartment fires [136](cross-reference from [137]) with good results. However, it is also important to acknowledge that this method of scaling downplays the importance of other, potentially important, relationships such as the Reynolds number and radiative contribution. For pre-flashover fires the radiation from the gas layer is of negligible magnitude while exact magnitude of the Reynolds number is not of importance with turbulent flow fields. When radiation becomes important, the fire is so developed that the dynamics causing it already has played its role. Therefore, when radiation is ignored in the Froude Scaling, the duration and potentially the magnitude of the fully developed compartment fire is questionable. The basic non-dimensional heat release rate of the gas burners in the current study was 7.95, making it behave as a pool fire rather than a jet flame. The values were then multiplied with the integers 1, 3, 4 and 6 for various fire scenarios, and for the full scale experiments this translates to 100 kW, 300 kW, 400 kW

and 600 kW, respectively. At full scale each value would be kept for a duration of 10 min, as explained in more detail in Section 2.1 and Table 2.12.

The non-dimensional Froude (Fr) number, which is a measure of the inertial forces with respect to gravity, as pointed out by Drysdale [138], is shown in Eq. 2.1 , where *u* is the velocity of the fluid, this is assumed to always be air, *D* is the length of the source of the flow, i.e. the sides of the square gas burner, and *g* is the gravitational constant.

$$\mathrm{Fr}^2 = \frac{\text{inertia forces}}{\text{gravity forces}} = \frac{u^2}{D \cdot g} \qquad \textbf{2.1}$$

All of the three mentioned scaling methods are a result of rewriting the governing conservation equations (mass, momentum, energy, radiation, species, state, solid energy) into 28 independent and dimensionless groups [139] (from [137]), π_1 to π_{28}. It is not possible to preserve all 28 groups, and a partial scaling is therefore needed. Williams [139] derived all the groups and Heskestad [140] and Quintiere [137] presented key assumptions focusing on fire dynamics such as ignoring the preservation of the Reynolds number, the radiation and conductive groups. The preservation of the Reynolds number is of minor importance as long as the flow is turbulent, the radiative group is ignored as the design fires are not fully developed fire while the conduction in air is very low. Additionally, the Boussinesq approximation is applied for the conservation of momentum equation. This is also done for the ideal (weak) plume theory and the density of the gas only is important with respect to the buoyancy and otherwise can be assumed equal to the ambient environment which increase in validity as the distance to the fire source increases. By keeping the dimensionless group with the Froude number constant, the heat release rate can be transformed to the universal non-dimensional heat release rate, shown in Eq. 2.2.

$$\dot{Q}^* = \frac{\left(\dot{Q}'''\right) \cdot D}{u \cdot \rho_\infty \cdot \mathrm{c_{p,\infty}} \cdot T_\infty} = \frac{\dot{Q}}{D^{5/2} \cdot \rho_\infty \cdot \mathrm{c_{p,\infty}} \cdot T_\infty \cdot \sqrt{g}} \qquad \textbf{2.2}$$

Where the area of the fire source, *A*, is assumed to be a square with the lengths *D,* ρ_∞, $c_{p,\infty}$, and T_∞ are the density, specific heat capacity and temperature of the ambient environment, respectively.

The thickness of the PIR panels differed and the experiments with the 6 cm thick panels were scaled with respect to time, as done by [137, 141, 135] and seen in Eq. 2.3. This means the burning durations were shorter for the 6 cm compared to the 10 cm thick panels by a factor 77.5% corresponding to a reduction from 600 s periods to periods of 465 s.

$$t_2 = t_1 \cdot \left(\frac{t_2}{t_1}\right)^{0.5} \quad \textbf{2.3}$$

Maintaining the same Froude number for the burners across the scales used for the performed experiments will then have the same temperature along their relative vertical centre axis and the non-dimensional HRR will also remain identical for the scales. If the ambient conditions are kept the same, the relationship between Fr_1 and Fr_2 becomes a ratio between the HRR and length, as seen in Eq. 2.4.

$$\frac{\dot{Q}_1}{D_1^{5/2} \cdot \rho \cdot c_p \cdot T \cdot \sqrt{g}} = \frac{\dot{Q}_2}{D_2^{5/2} \cdot \rho \cdot c_p \cdot T \cdot \sqrt{g}} \quad \textbf{2.4}$$

$$\frac{\dot{Q}_1}{D_1^{5/2}} = \frac{\dot{Q}_2}{D_2^{5/2}} \quad \textbf{2.5}$$

This means the scaled HRR will be proportional to its length ratio to the power of 5/2 multiplied by the non-scaled HRR, as all other parameters are close to constant across the two experiments, which was ensured by conducting the experiments under controlled ambient conditions.

2.1.1 Examples of the use of Froude scaling in literature

The relationship between the HRR and the length is also used in the plume correlations proposed by McCaffrey [142] and Heskestad [143] to predict the mass flow of the plume and temperature along the vertical centre axis, respectively, useful for smoke management designs. Both correlate the effect of the fire, $\dot{Q}$, to a height of interest, z, as part of their plume correlations. The temperature correlation by McCaffrey was for a buoyant plume split into three distinctive regions based on the HRR of the fire. The intermittent plume region, and where the tip of the flame ends, was quantified, as expressed in Eq. 2.6, for all three regions shown in Figure 2.1.

$$T(z) = T_\infty \cdot \left(1 + \left(\frac{\kappa}{0.9 \cdot \sqrt{2 \cdot g}}\right)^2 \cdot \left(\frac{z}{\dot{Q}^{2/5}}\right)^{2 \cdot \eta - 1}\right) \qquad \textbf{2.6}$$

Where T(z) is the temperature at height z above the fire source and κ and η are experimentally obtained constants unique to each of the three regions of interest. For the continuous region and intermittent regions the constants κ and η are 0.5, 6.8 $m^{1/2}/s$ and 0, 1.9 $m/(kW^{1/5}s)$, respectively. The plume region is not of interest as the ceiling of the compartment will prevent the plume from rising far enough above the fire.

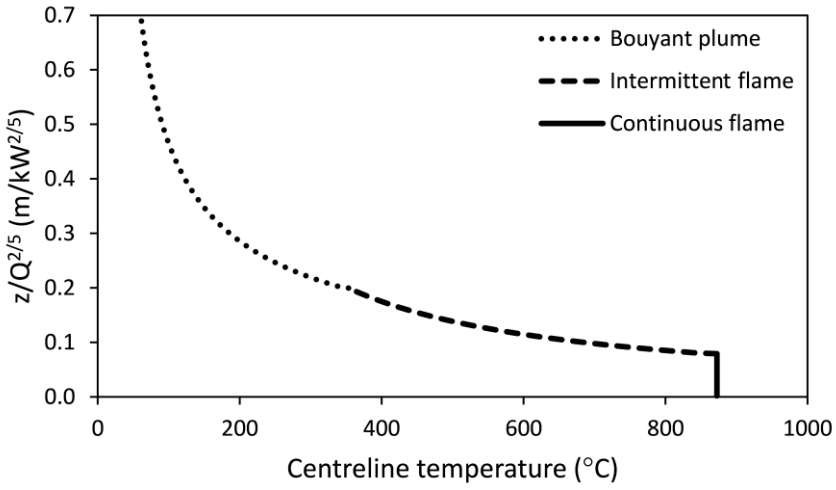

Figure 2.1: The temperature along the centreline of a fire as a function of the distance from the source divided by the HRR to the power of 2/5 according to McCaffrey's plume correlation.

The three regions defined by McCaffrey splits the flame into 0%-21%, 21%-53% and higher than 53% of the height of the compartment for the first burner step, as seen in Table 2.1, whereas the third step would cause the *intermittent* region (flame tip) to impinge the ceiling above the burner.

Table 2.1: The flame height for the intermittent and continuous regions for two scales: 1:1 and 1:5, with a relative height for reference.

	1:1 (m)	1:5 (m)	z/H (%)
Step 1 $\dot{Q}_1^* = 8$			
Intermittent flame	0.50	0.10	21
Continuous flame	1.26	0.25	53
Step 2 $\dot{Q}_2^* = 3 \cdot \dot{Q}_1^*$			
Intermittent flame	0.78	0.16	33
Continuous flame	1.96	0.39	82
Step 3 $\dot{Q}_2^* = 6 \cdot \dot{Q}_1^*$			
Intermittent flame	1.03	0.21	43
Continuous flame	2.58	0.52	108

McCaffrey et al. [144] correlated the compartment temperature over a range of fuels and compartment sizes with a least-square method to the HRR, as seen in Eq. 2.7. Rewriting the equation to solve for the HRR shows how it scales with the geometrical length to the power of 9/4 and not 10/4 as the Froude scaling does. The scaling of this compartment temperature is, however, scaled with respect to the ventilations controlled conditions, e.g. the availability of oxygen, and the compartment openings are therefore also scaled. The compartment temperatures used for the correlations ranged from as low as 20 °C to 550 °C but the upper limit is reported as extendable [145]. However, care should be taken if the compartment becomes ventilation controlled as all the energy is no longer released within the enclosure.

$$T_{\mathrm{g}} = T_{\infty} + C \cdot 6.85 \cdot \left(\frac{\dot{Q}^2}{A_0 \sqrt{H_0} A_T \cdot h_k} \right)^{1/3} \qquad \textbf{2.7}$$

Here C is a correction factor for the locations of the fire (1.7 for corners, 1.3 for walls and 1 if none of above), A_T is the total surface area where heat is conducted through and h_k is the effective heat transfer coefficient and a function of the square-root of the thermal inertia (kpc) divided by the time.

The compartment experiments were constructed out of sandwich panels and geometrically scaled so all the dimensions were therefore a function of a single length, X. Changing the length-related constants in Eq. 2.7 to a function of a single length, X, as seen in Eq. 2.8, simplifies the expression. Isolating the HRR, $\dot{Q}$, provides an estimate of the limiting HRR where the compartments flashes over, and as a result transition from being fuel controlled to being ventilation controlled.

$$\dot{\mathrm{Q}} = C^{-3/2} \cdot 0.07 \cdot \sqrt{X^{9/4} \cdot h_k} \cdot \Delta T^{3/2} \qquad \textbf{2.8}$$

Here ΔT is the increase in temperature ($T_g - T_\infty$) and T_g often assumed to be between 500 °C and 600 °C. Equation 2.8 suggests that an increasing C reduces the required HRR needed to cause the transition. McCaffrey et al. empirically determined C as 1.7 and 1.0 for corner and centre burner locations, respectively, which significantly decreases the limit of $\dot{\mathrm{Q}}$ (by 55%).

2.2 Experimental Methods

2.2.1 Small Scale Experiments

The complete heat of combustion was determined as described in EN ISO 1716 *Gross calorific value test* while the STA experiments were carried out according to ISO 11358-1, *Thermogravimetric (TG) of Polymers – Part 1: General principles* [146].

2.2.1.1 Thermographic Analyses and Differential Scanning Calorimetry

Three different materials were studied in a Jupiter® 449 F3 STA from Netzsch [147], two polymeric cores: one PIR and one PUR, and one stone wool core. A balance between the experimental duration and the sample size is always required when doing experiments where transient heat transfer is involved. Ideally the duration should be as short as possible without compromising the accuracy by

having the heating rate higher than the time for the entire sample to be in thermal equilibrium. The samples were prepared by cutting them with a sterilised scalpel while hold the sample suspended in mid-air and at least 1 mg was removed and loosely packed in an open Al_2O_3 crucible. The exact initial and final mass of each sample can be seen in Table 3.1. The heating rate was fixed at 10 K/min to increase the resolution of the data [148] as a higher heating rate can make the identification of reactions and corresponding temperatures harder. The samples were heated from ambient temperature at 28 °C to 1050 °C in a flow of nitrogen. This temperature range was chosen as previous compartment experiments conducted in full and 1:5 scale had temperatures within this range [149, 150]. The PIR and SW core were studied further in an atmosphere of air in a Perkin Elmer STA 6000 [151], also with a heating rate of 10 K/min, although from 30 °C to 950 °C due to the temperature limitation of the Perkin Elmer STA 6000.

2.2.1.2 Mass loss cone and in-depth temperature measurements

The cone calorimeter, standardised under the ISO 5660:1 [60], NFPA 271 [152] and ASTM E1354 [153], is often used by researchers to investigate the response of a material under a known heat flux [154, 155, 156, 157]. Measurements of the combustion gases (O_2, CO_2, CO) as well as the smoke obscuration and production can enable the calculation of the soot yield of a product when combined with the mass loss rate (MLR). The experiments were conducted in a mass loss cone (shown in Figure 2.2) with five 0.25 mm thick type-K thermocouples inserted into pre-made holes in the sample with one thermocouple placed on the surface in a pre-stressed state that ensured contact throughout the exposure. An ignition source in form of a spark plug was rotated on top of the specimens, as seen in Figure 2.2, to facilitate the ignition of combustible gases released by the specimens during the heating process. The incident heat fluxes of 10 kW/m^2, 20 kW/m^2, 30 kW/m^2, 40 kW/m^2, 50 kW/m^2 and 70 kW/m^2 to the samples was provided by a standard mass loss calorimeter from Fire Testing Technology Ltd. [158]. The studied samples measured 0.105 m x 0.105 m x 0.05 m ±0.002 m in width, length and thickness, respectively, and the cores studied were the PIR and the SW.

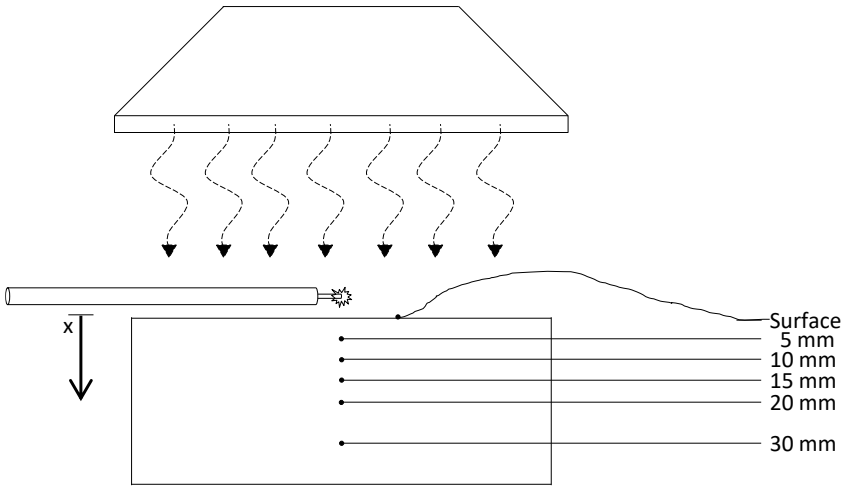

Figure 2.2: Schematic of experimental setup including the conical heater, the spark plug and the location of the thermocouples in a sample in a mass loss cone setup. Inspired by [159, 160].

Extrapolating the cone calorimeter results to compartment experiments is difficult, because some of the assumptions are too crude for sandwich panels [64]. More specifically, this is due to the fact that the results are too closely linked to the conditions of the experimental method and separated from the boundary conditions of the setup. As the experiments, however, are not used to classify products but to understand their behaviour during elevated temperatures the addition of in-depth thermocouples and the load scale provided experimental data of value. On average, the SW and PIR samples had an initial core mass of 90 g and 44 g, respectively, as seen in *Appendix – Additional Mass Loss Cone Graphs*. A rig was built with five straight 5 cm long stainless steel pikes to ensure approximately identical thermocouple location for all the samples.

2.2.1.3 Gross calorific content

The calorific content of building materials, as seen in Eq. 2.9, is a key parameter in the design fire process and three samples of each of the cores: SW, PIR and PUR were studied in an IKA C200 bomb calorimeter apparatus [161]. The temperature increase is used in the following expression to calculate the heat of combustion of the studied material:

$$\Delta H_c = \frac{C \cdot \Delta T - Q}{m} \qquad \textbf{2.9}$$

where ΔH_c is the complete heat of combustion, m is the mass of the sample, C is the calibrated vessel conversion coefficient, ΔT is the change in vessel temperature from ignition to finish and Q is the known added fuel i.e. the ignition thread. Additional fuel, in form of a benzoic tablet with known calorific content, was used to facilitate a continuous combustion in the vessel for the SW samples, as their low calorific value was insufficient to support a combustion and enabling a measurable quantity on its own.

2.2.2 Fire Scenarios and Burner Outputs

A compartment fire normally has an incipient phase followed by a growing phase that generates smoke. If the smoke is produced faster than it is flowing out through openings and leakages a smoke layer builds up within the compartment. Depending on the intensity of the fire the smoke layer increase in temperature and will eventually so hot it causes all other fuels within sight to ignite via radiation. This can lead to a flashover- and often a steady burning phase while the fuel is consumed and eventually decays, as seen in Figure 2.3 for two scenarios. There is, however, also a dependency on the ventilation conditions [162] as large opening in the upper half of the compartment will allow for hot gases to exit, which can prevent a thermal runaway (flashover), while openings in the lower half of the compartment will provide openings for oxygen to sustain any combustion processes taking place.

In order to study the contribution of the core of the panels and the material behaviour, a growing design fire scenario with an incipient and growth phase inspired by the ISO/EN 9705 and ISO 13874-1 and -2 [163] was chosen. The prescribed burner intensities in the ISO/EN 9705 and ISO 13784-1 standards are 100 kW for 10 minutes, followed by 300 kW for another 10 minutes, and for the ISO 13874-2 in durations of 5 min with an additional final step of 600 kW also with a 5 min duration. Herein, the burner settings for the first 20 min served as the baseline intensity and was abbreviated as “1_3” whereas several other experiments, matching previous studied intensities [149, 150, 133], were abbreviated as 1_3_6 indicating an additional burner step of 600 kW for 10 min. The naming is universal across the scales to indicate the fire scenario being scaled and as such “1_3_6”, according to the scaling theory, as seen in 2.1 - *Scaling Analysis* and Eq. 2.5, translates to 1.79 kW for 10 min followed by 5.37 kW for 10 min finished off with 10.74 kW for 10 min for the 1:5 scale experiments.

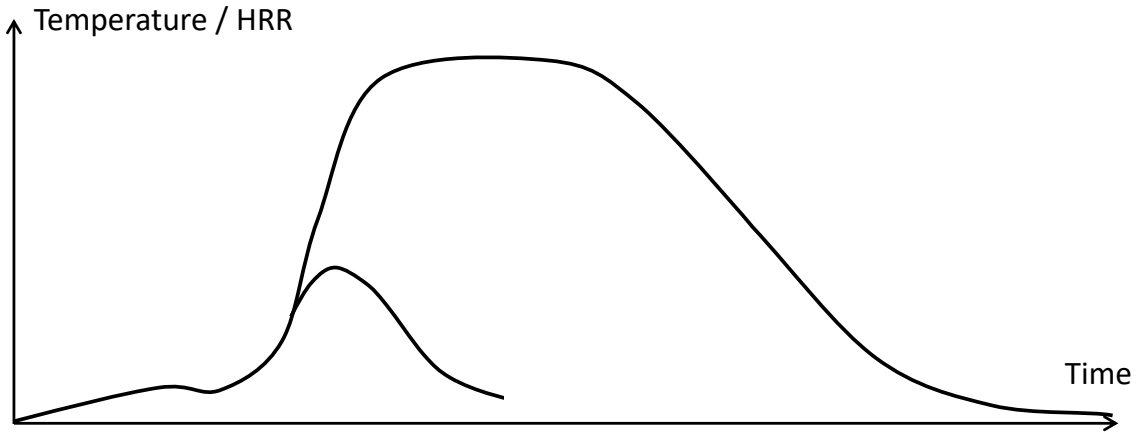

Figure 2.3: Two possible enclosure fire developments with respect to temperature or HRR as a function of time.

The various steps represents various fires and if the studied compartment exhibited signs of a thermal runaway or integrity failure the gas burner was turned off for safety reasons. The terminated burner intensity is, however, still included in the naming to indicate the input required for the failure to occur. The HRR curve for a "1_3_6" fire running its full duration at various scales is presented in Figure 2.4. This fire scenario was used for eight 1:5 scale experiments, one 2:5 scale, one 1:2 scale as well as two full scale from literature [149]. The two experiments from literature were conducted with the same SW and PIR cored panels as used in the work herein, just from a different batch, but with the same classifications.

The geometry and ventilation opening of the compartments in this study favours a change from a fuel-surface-controlled compartment fire to a ventilation controlled fire. There are differences in the fire dynamics between a close to cubical and long or very tall compartments. These differences were great enough for Thomas et al. [164] and Harmathy [165] to separate the dynamics into two distinguished categories. Thomas et al. preferred labelling them as *Regime I* and *Regime II* whereas Harmathy used the terms *ventilation controlled* and *fuel-surface-controlled* but essentially refers to the same concepts. A compartment with sufficiently small openings allowing for the smoke to fill the compartment falls under *Regime I* and the *ventilation controlled* category. The second category, where the smoke can leave the compartment and the combustion is governed by the fuel rather than the availability of oxygen is *Regime II* and *fuel-surface* controlled. The compartments with a fire determined by the fuel-surface was found to be a less severe scenario as the temperature were lower as well as the burning duration shorter, as pointed out by Harmathy [165].This regime can, however, only occur if the panels contribute with a significant amount of energy, because, as

mentioned, the HRR of the gas burner alone was designed to be insufficient to cause the transition to ventilation controlled conditions. Wood cribs are frequently used in fire testing [110, 91, 119] and are able to distribute the energy out over a large surface area. As the compartment tests use a gas burner at full scale this was likewise done for the scaled compartments experiments as would be safer, easier to control and repeatable. The design fires for the experiment was based on the methodology implemented in the standard compartment fire tests i.e. ISO 9705 and EN 13784-1 (100 kW for 10 min followed by 300 kW for 10 min). The HRR from the burners was scaled by using the Froude number which have shown great potential for both free burning wood crib fires [135] and enclosure fires [136](from [137]). The gas burner was turned off once the compartments became ventilation controlled and the fire was only sustained by the combustion of the core material.

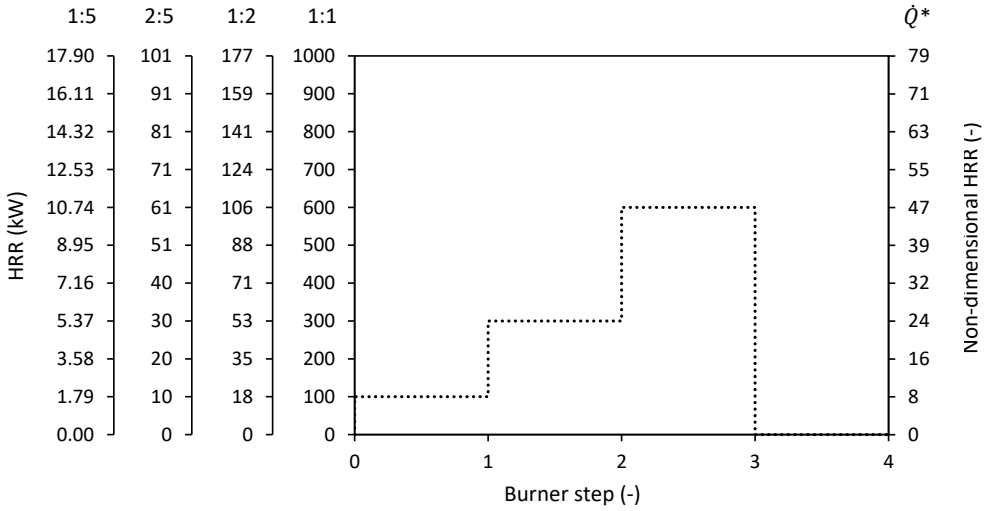

Figure 2.4: The HRR curve for the "1_3_6" fire scenarios for various scales with respect to the burner steps.

Herein, the thermal runaway was identified by either a rapid increase in the measured HRR, uniform compartment temperature or external flames through the doorway indicating under ventilated conditions (external flames often occurred other places than through the doorway but always after the thermal runaway took place).

2.2.3 Compartment Experiments

Compartments in four different sizes were assembled to study the behaviour of compartments constructed with steel-faced sandwich panels with PIR, PUR and SW thermal insulation cores. The

internal geometry of the compartments was scaled linearly in the scales: 1:5, 2:5, 1:2 of the full scale compartment. The full scale compartment measures 2.4 m x 3.6 m x 2.4 m in width, length and height, respectively, with a 2 m high and 0.8 m wide doorway placed in the middle of a short side, as seen in Figure 2.5 and Table 2.2, just as in the ISO 9705 and ISO 13784-1 tests. Rivets could have been used as part of the mounting for the classification of the sandwich panel, but as this was not disclosed in the documentation, it was treated as an unknown. The compartment experiments were conducted without rivets along the joints to provide additional fixation beyond the friction caused by the mounting. As panels in their end-use often have flashings along their edges they were also installed herein by fastening the various 2 mm thick flashings with 25 mm long and 4 mm thick stainless steel screws. L-profiles measuring 2.5 cm by 2.5 cm were fastened internally every X/4 along all ceiling and wall edges. Externally, 15 cm by 5 cm L-profiles were fastened along the ceiling and walls with Y/5 intervals and along the door frame the exposed core was protected by 10 cm by 2.5 cm U-profiles fastened every X/5. The flashings served as a method of keeping the panels in place, as they restricted longitudinal expansion and limited the possibility of panel deflection. As the experimental setup herein is very different from that in the standard tests the behaviour of the panels could be different depending on their robustness.

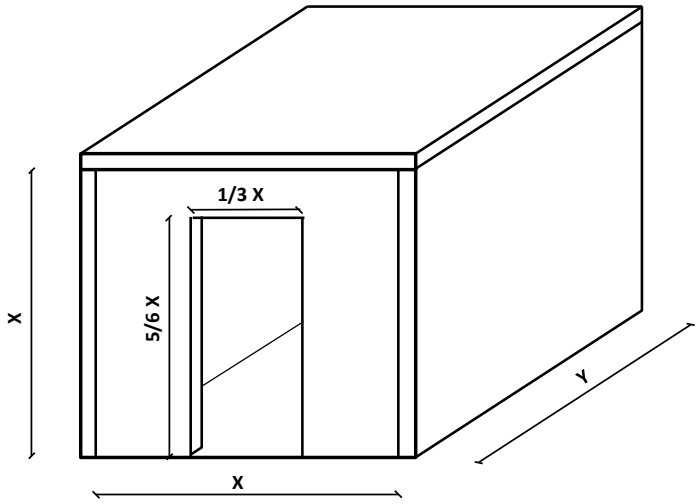

Figure 2.5: Schematic of the constructed compartments without internal- or external flashings or joints.

Table 2.2: X and Y dimension for all the compartment scales.

Scale	X (m)	Y=1.5X (m)
1:1	2.40	3.60
1:2	1.20	1.80
2:5	0.96	1.44
1:5	0.48	0.72

As a natural consequence of the different sized compartments comparisons across scales will be made with respect to relative coordinates and distances, e.g. 80% of the compartment height, but with scalar measurements such as temperature.

For the 1:5 scale compartments, two different instrumentation setups were used:

- The first series was conducted to measure the one-dimensional thermal penetration through the walls, the influence of the thickness of the panels and the effect of having joints mid-span. A total of 14 experiments were conducted: four with SW, 10 with PIR of which six with 10 cm panels and the remaining four with 6 cm panels and summarized in Table 2.11.
- The second series was conducted to determine the net heat flux through the compartment boundaries and the effects of the thickness was re-visited.

Both experimental configurations will be explained in further detail in *Section 2.2.5.3 1:5 compartment setup*. The larger scales, such as the 2:5, 1:2 and 1:1 were mounted with the same thermocouple configuration as the second 1:5 scale series. The panels used were delivered in standard sizes and cut on site in the dimensions required for the specific scales. All the experiments excluding the full scale experiments (E29 and E30, see Section 2.2.3 and Table 2.12) were conducted with panels from the same batches of SW, PIR (both 10 cm and 6 cm), respectively. The full scale experiments with PIR and SW were conducted with the same types of panels as the scaled experiments but with a different production date. The compartments were constructed such that the front and end panels were X by X in width and height, respectively, as seen in Figure 2.5 and Table 2.2, whereas the sides were X in height and Y plus two times the thickness of the panels long to overlap the end and front walls. The ceiling rested on the walls thus overlapping and measured X + 2 · t by Y + 2 · t, where t is the thickness of the panel. This system for assembling the compartments was used for all the 1:5 scale experiments. A 2.20 cm thick non-combustible *FireFree® ScandiBoard 850* [166] calcium silicate board designed for protecting steel members from elevated temperatures was used as the base for all the scaled experiments providing a stable and inert floor for the panels to rest on. In the full scale experiments the plates inside the compartment rested on a concrete floor. The joints in the 1:5 scale experiments were placed so there was one in middle of all the walls and ceiling. These joints were placed in the centre line of the X, Y and Y plane for the front and backsides, long sides, and ceiling, respectively, as seen in Figure 2.13b) on page 60. This was the same way the joints in the other scales were also oriented, however, with more than 1 joint due to the size of the compartments, seen for 2:5, 1:2 and 1:1 in Figure 2.15 b), c) and d) respectively, on page 63. This prevented the joint in the front above the doorway to align with the joint(s) in the ceiling all the way through to the backside wall.

The compartments were equipped with various sized sandbox gas burners linearly scaled with respect to the burner used for the ISO 9705 and 13784-1 compartment tests, which measures 0.17 m x 0.17 m with its opening being 0.20 m from the floor, as seen in Figure 1.16. The internal width of the burners were 0.034 m, 0.064 m, 0.086 m (1 mm excess) for the 1:5, 2:5 and 1:2 scales, respectively, and seen in Figure 2.6 a) for the 1:5 scale and Figure 2.6 b) for the full scale. The design of the burners for the 2:5 and 1:2 scales were scaled linearly in all dimensions with respect to the design of the 1:5 scale burner, except for the thickness of the steel, which was constant. The flanges allowed for the burners to be fitted through the floor plates in their respective 1:5, 2:5 and 1:2 scale compartments. The gas to the full scale burner was flowing in a pipe penetrating the side wall of the compartment, rather than being supplied through the floor as was the case for the scaled compartments. As a result, the full scale gas burner did not have flanges, as it was resting on four legs to ensure the height of the top of the opening of the gas burner was correct.

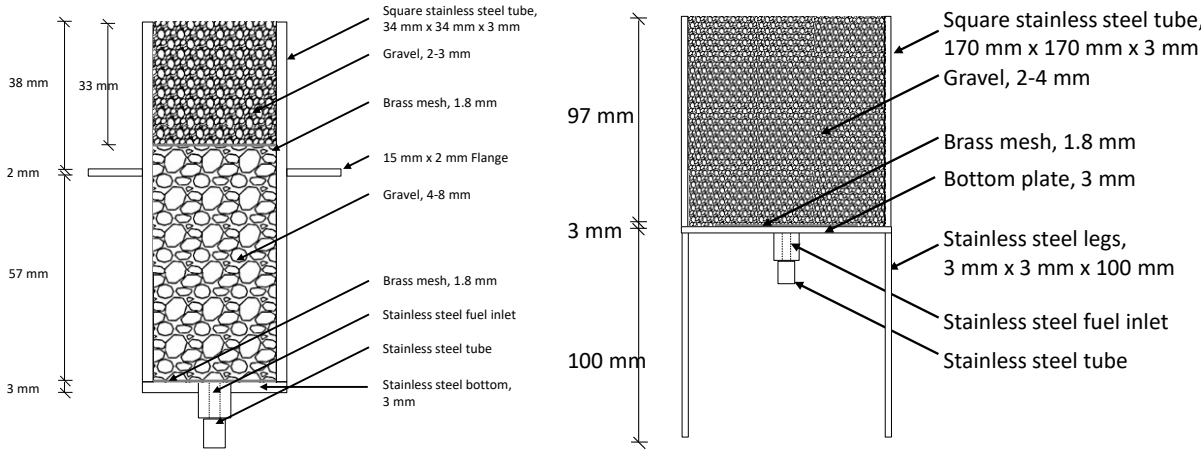

Figure 2.6: Gas burners used for a) the 1:5 scale experiments and b) for the full scale experiments. Note that the two figures have different scales, so see the given size measurements.

The gas burners for the 1:5, 2:5 and 1:2 scale experiments were placed as close to the corner as the flanges of the respective burners allowed to. This resulted in a slight off-set from the walls, which was undesired, but was also the case in the full scale experiments as the column of the internal frame prevented the burner from getting closer to the walls than the thickness of the frame members (5 cm). The flow of gas to the gas burners was regulated and controlled by mass flow meters. The 1:5 and 2:5 scale experiments were conducted with *Kosan Propane* (>90% propane (C_3H_8), <10% butane (C_4H_{10}) and <<1% other) [167] while the fuel for the experiments at 1:2 and full scale was >95% propane. The complete heat of combustion for the fuels is 45.83 MJ/kg and 46.45

MJ/kg, respectively [168]. The differences between these two gases were considered negligible for the comparisons and analysis throughout this work. The fire from the gas burner was a diffusion flame as the fuel was not mixed with air prior to reaching the flame front.

All the compartment experiments were conducted under an exhaust hood O_2, CO_2, CO and gas temperature were measured. The three measured species were used to calculate the HRR, pHRR and time to the thermal runaway in the compartment, which was characterised by a rapid change in the slope of the HRR. The total HRR from the burner and compartment was estimated by oxygen consumption calorimetry using the following expression by Janssens [169], as seen in Eq. 2.10.

$$\dot{Q} = \left[E\phi - (E_{CO} - E) \cdot \frac{1-\phi}{2} \frac{X_{CO}^{A}}{X_{O_2}^{A}}\right] \cdot \frac{\dot{m}_e}{1+\phi(\alpha-1)} \frac{M_{O_2}}{M_a} \left(1 - X_{H_2O}^{o}\right) \cdot X_{O_2}^{o} \qquad \textbf{2.10}$$

where $\dot{Q}$ is the HRR, E is the energy content per kg of oxygen consumed, ϕ is the oxygen depletion factor, E_{CO} is the energy content per kg of CO produced, X_{CO}^{A} is the actual measured CO concentration in the duct, $X_{O_2}^{A}$ is the actual measured O_2 concentration in the duct, $\dot{m}_e$ is the mass flow, α is set for 1.105 as recommended by Janssens for large hoods and flows, $M_{O_2}$is the molar mass of O_2, M_a is the molar mass of the ambient air, $X_{H_2O}^{o}$ is the fraction of water in the ambient air and $X_{O_2}^{o}$ is the fraction of O_2 in the ambient air.

The use of oxygen consumption to determine the heat released for unknown fuels is based on the stoichiometric reaction schemes for liquids and gases [170] and solids [171]. The average value of *E* for these common fuels was found to be 13.1 $\mathrm{MJ/kg_{O_2}}$ with a ± 5% deviation. Nevertheless, it is considered valid for a wide range of hydrocarbon fuels such as e.g. methane (g) or benzene (l), it is, albeit, just an average value.

The full scale experiments were conducted using an internal frame, as also described in the ISO 13784-1 and seen in Figure 1.16. The two compartments studied at full scale were constructed with panels with a core of PIR or with SW, as seen in Table 2.3. The internal steel frame was constructed with U-shaped stainless steel profiles measuring 100 mm x 50 mm x 8 mm in height, width and thickness, respectively, which protected the internal corners and edges. 1.5 mm thick stainless steel L-shaped flashings measuring 150 mm x 50 mm with a white coating were fastened along the

external edges and U-profile flashings were fastened around the edges in the doorway. All the thermocouples used, both the internal and external, were 2 mm thick stainless sheeted steel of the type K. The thermocouples in the centrally located thermocouple tree and the ones placed within the walls measured at the same relative coordinates as for the 1:2 scale experiments, as shown in Figure 2.7 and Figure 2.10 a) and b), respectively. The thermocouples in the walls were placed evenly amongst the walls and ceiling in a 0.6 m x 0.6 m grid (except for the front) and 0.3 m from the internal edges to other walls, ceiling and floor, as seen in Figure 2.8. Additionally, two clusters of six thermocouples were mounted in the middle of the two walls closest to the burner to measure the in-depth temperature to track the thermal penetration. The pressure probes in the doorway with attached thermocouples were placed in the top half of the doorway, as seen in Figure 2.9, to increase the number of measurements of the gas leaving the compartments. This was done to improve the accuracy of the calculation of the energy leaving the compartments.

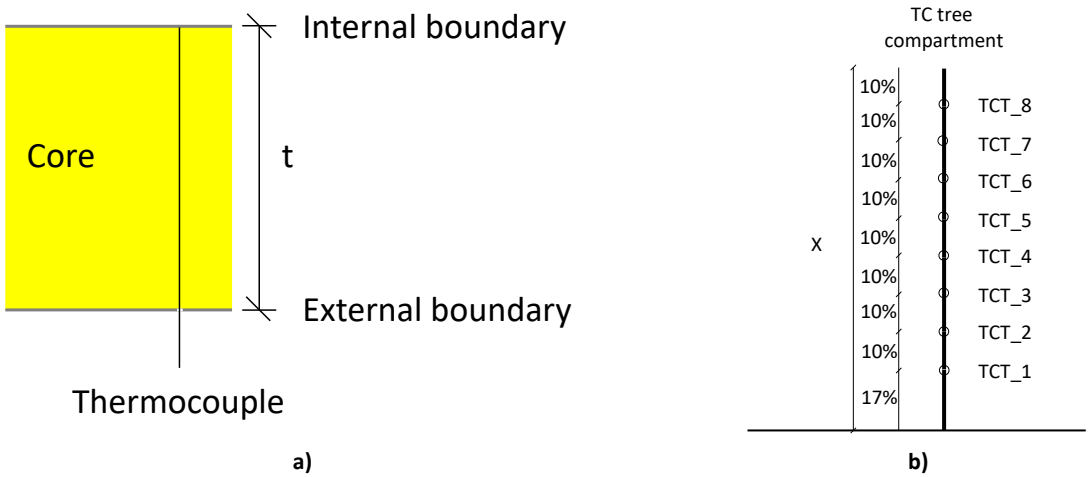

Figure 2.7: a) In-depth thermocouple location in a core sample *t* thick and b) Thermocouple distribution along the height of the compartment.

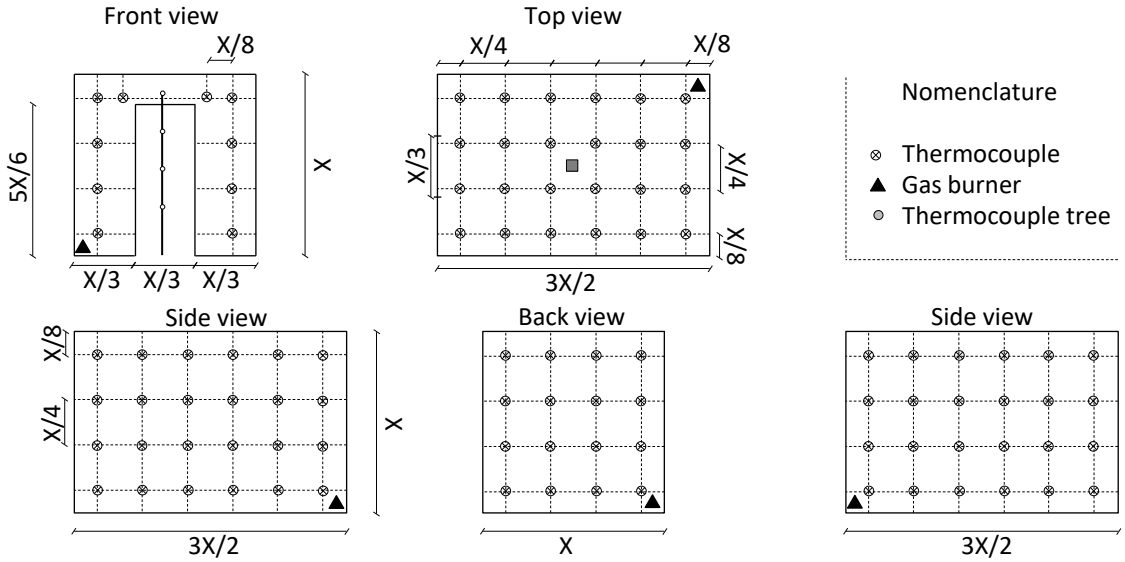

Figure 2.8: The placement of thermocouples measuring the temperature of the internal steel sheet.

Figure 2.9: a) Placement of the pressure probes with thermocouples along the height of the door and b) Picture of the 1:1 scale SW compartment (E30) post experiment with the back wall and ceiling still attached.
***the brigtness and contrast have been changed by +40% and -40 %, respectively.**

Table 2.3: Experimental matrix for the full scale compartment experiments.

Experiment number	Scale	Core type	Thickness	Burner location	Equivalent burner input [a]	Actual rounded burner input [b]	Joints	In-depth TCs
(-)	(-)	(-)	(m)	(-)	(kW)	(kW)	(-)	(-)
E29	1:1	PIR	0.10	Corner	1_3	100_300	Yes	1
E30	1:1	SW	0.10	Corner	½_2_2	50_200_200	Yes	1

a. The "Equivalent burner input" refers to the full scale input in hundreds for segments of 10 min for 10 cm thick panels or 7 min 45 s for 6 cm panels e.g. 1_3_3 refers to 100 kW for 10 min and 300 kW for 20 min at full scale for a 10 cm thick panel.
b. "The actual rounded burner input" is the burner input rounded to the nearest kW in segments of 10 min for 10 cm thick panels or 7 min 45 s for 6 cm panels for the experiment.

2.2.4 Summary of Conducted Experiments

Two polymeric cores and a single stone wool are studied in various experimental set-ups. The experiments are separated into two larger sections, the small scale experiments and the compartment experiments. The three types of insulation material have all been studied under the STA and the SW was on top of all the scales of the compartment experiments studied under the cone calorimeter. The overall experimental matrix can be seen in Table 2.4 and the specific ones for the Cone, STA, bomb and the compartment experiments in Table 2.5 to Table 2.8, respectively.

Table 2.4: Overall experimental matrix for all the studied materials with respect to experimental-setups.

	Small scale experiments			Compartment experiments			
				Scaled compartment			Full scale
	Cone	STA	Bomb	1:5	2:5	1:2	1:1
SW	**X**	**X**	**X**	**X**	**X**	**X**	**X**
PIR	**X**	**X**	**X**	**X**		**X**	**X**
PUR		**X**	**X**	**X**			

Table 2.5: Experimental matrix for the mass loss cone conducted both with and without protective steel sheet.

	10 kW/m^2	20 kW/m^2	30 kW/m^2	40 kW/m^2	50 kW/m^2	70 kW/m^2
PIR	**X**	**X**	**X**	**X**	**X**	**X**
SW	**X**	**X**	**X**	**X**	**X**	**X**

Table 2.6: Experimental matrix for the STA.

	Air	Nitrogen
SW	**X**	**X**
PIR	**X**	**X**
PUR		**X**

Table 2.7: Experimental matrix for the bomb calorimeter.

SW	**X**
PIR	**X**
PUR	**X**

Table 2.8: Experimental matrix for the compartment experiments

	In-depth thermocouples		Surface thermocouples		Surface thermocouples		
	Joint	No joints	Joints	No Joints	Joints	Joints	Joints
	1:5	1:5	1:5	1:5	2:5	1:2	1:1
SW	**X**	**X**	**X**	**X**	**X**	**X**	**X**
PIR	**X**	**X**	**X**	**X**		**X**	**X**
PUR				**X**			

2.2.5 Detailed Description of the Scaled Compartment Experiments

2.2.5.1 1:2 Compartment Setup

The compartments in the 1:2 scale experiments like the 2:5 scale was placed in a top-open frame of aluminium struts resting with partial coverage of flashings supporting the compartment, as seen in Figure 2.10 a) with white solid and dashed circles, respectively. Three experiments were conducted at this scale of which two with PIR and one with SW (E26, E27 and E28, respectively, see Table 2.9). The flashings were covering the edges closes to the burner to provide the maximum strength to resist deflections and rotational movement while the edges in the doorway were completely covered which unfortunately left some edges exposed. The compartment was fitted with a thermocouple tree inside the compartment and in the walls, as seen in Figure 2.10 b) and Figure 2.8, respectively. All the thermocouples used, both the internal and external, were 2 mm thick stainless sheeted steel of the type K. Additionally, two clusters of six thermocouples were mounted in the middle of the two walls closest to the burner to measure the in-depth temperature and to track the thermal penetration.

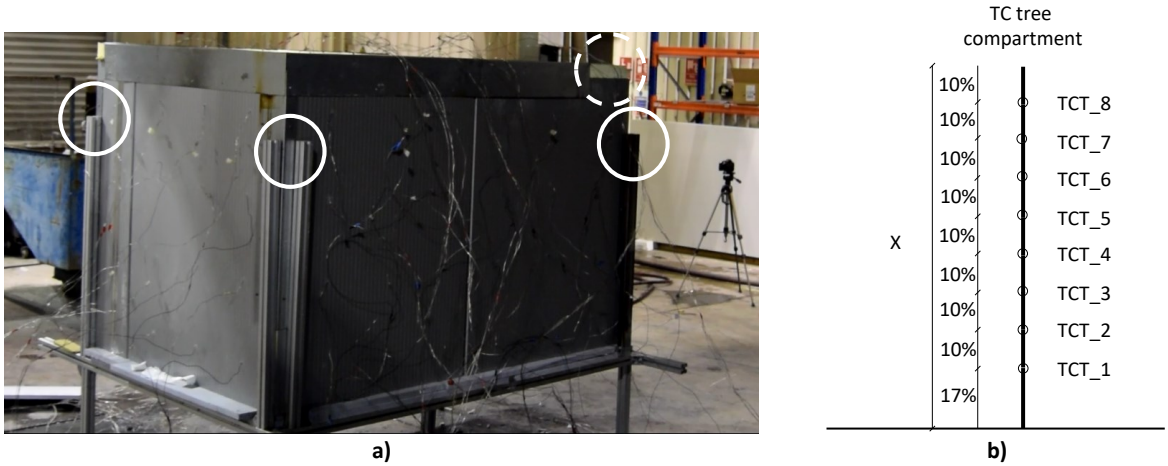

Figure 2.10: a) Picture taken from the backside of the compartment for E27 with 10 cm thick PIR panels prior to the experiment and b) Thermocouple distribution along the height of the compartment.

Table 2.9: Experimental matrix for the 1:2 scale compartment experiments

Experiment number (-)	Scale (-)	Core type (-)	Thickness (m)	Burner location (-)	Equivalent burner input [a] (kW)	Actual rounded burner input [b] (kW)	Joints (-)	In-depth TCs (-)
E26	1:2	PIR	0.06	Corner	1_2	17_34	Yes	1
E27	1:2	PIR	0.10	Corner	3_3	53_53	Yes	1
E28	1:2	SW	0.10	Corner	1_3_6	17_53_106	Yes	1

a. The "Equivalent burner input" refers to the full scale input in hundreds for segments of 10 min for 10 cm thick panels or 7 min 45 s for 6 cm panels e.g. 1_3_3 refers to 100 kW for 10 min and 300 kW for 20 min at full scale for a 10 cm thick panel.

b. "The actual rounded burner input" is the burner input rounded to the nearest kW in segments of 10 min for 10 cm thick panels or 7 min 45 s for 6 cm panels for the experiment.

2.2.5.2 2:5 compartment setup

An intermediate scale between the smallest, half and full sized compartment experiments were conducted at 2:5 scale (E25, Table 2.10). The compartment was constructed with panels with a core of SW with holes drilled to fit the thermocouples measuring the internal temperature of the surface and a thermocouple tree placed in the centre of the compartment measuring at four different heights, as seen in Figure 2.11 a). The compartment was constructed with SW panels and had the same thermocouple configuration for measuring the internal steel boundary and thermocouple three as the second series of the 1:5 scale compartments. The pressure probes and thermocouples in the door opening were skewed towards the top of the opening as the measurements in the smoke layer were prioritised over the air flowing into the compartment, as seen in Figure 2.11 b).

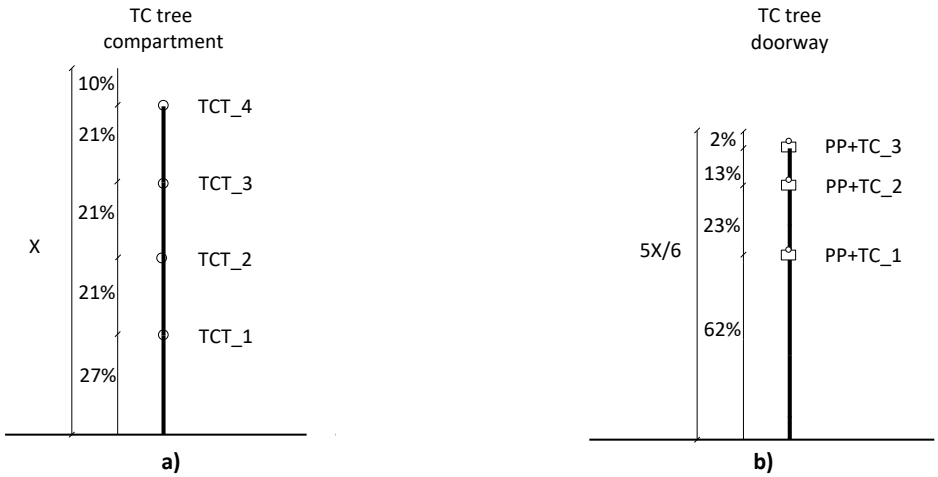

Figure 2.11: a) Thermocouples along the height of the compartment in the centre of the compartment, and b) Pressure probes and thermocouples along the height of the doorway.

The small scale compartments were placed in a stainless steel frame, as seen in Figure 2.13 d), which was not possible for this compartment being twice the size in all dimensions and eightfold the internal volume. It was, therefore, confined in a top-open frame constructed out of 45 mm x 45 mm Bosch Rexroth strut profiles in aluminium similar to the 1:2 scale setup, as seen Figure 2.10 a). Furthermore, all the external edges were covered by 2 mm thick and measuring 150 mm by 50 mm L-shaped galvanized steel flashings including the vertical edges. Internally all non-floor edges were also covered by 2 mm thick and 50 mm x 50 mm L-shaped flashings.

Table 2.10: Experimental matrix for the 2:5 scale compartment experiment.

Experiment number	Scale	Core type	Thickness	Burner location	Equivalent burner input [a]	Actual rounded burner input [b]	Joints	In-depth TCs
(-)	(-)	(-)	(m)	(-)	(kW)	(kW)	(-)	(-)
E25	2:5	SW	0.10	Corner	1_3_6	10_30_60	Yes	1

a. The "Equivalent burner input" refers to the full scale input in hundreds for segments of 10 min for 10 cm thick panels or 7 min 45 s for 6 cm panels e.g. 1_3_3 refers to 100 kW for 10 min and 300 kW for 20 min at full scale for a 10 cm thick panel.
b. "The actual rounded burner input" is the burner input rounded to the nearest kW in segments of 10 min for 10 cm thick panels or 7 min 45 s for 6 cm panels for the experiment.

2.2.5.3 1:5 compartment setup

The 1:5 scale experiments were conducted by using two different sizes of steel frames one for the 10 cm and another for the 6 cm thick panels which were constructed with 3 mm and 2 mm plate thickness, respectively. However, they both served the same purpose of providing confinement in order to avoid a collapse of the compartments. The frame was placed on a Sartorius EA35EDE-L scale with a 60 kg capacity with 0.010 kg readability to measure the mass loss of the panels throughout the duration of the experiments.

For the first series of experiments 0.25 mm thick type-K thermocouples were mounted in clusters of 6 measuring every one-fifth of the thickness of the panel in-depth throughout from the internal steel boundary all the way through to the external steel boundary, as seen Figure 2.12. The thermocouples were inserted to the desired depth from the external side through 5 drilled holes. This prevented the exposure of virgin core material to the higher temperatures in the compartment during the experiments and avoiding the thermocouple wires from being unnecessarily damaged. Five thermocouple clusters were inserted into all the walls except the front, as seen in Figure 2.13 a). A thermocouple tree measuring the gas temperature in the compartment at four different

heights, as seen in Figure 2.13 e), was placed approximately in the centre equipped with four 1.25 mm thick stainless steel sheeted type K thermocouples. For E 16 two thermocouple trees were placed 1/3rd and 2/3^{rds} into the length along the middle of the compartment, respectively, as the burner was placed in the centre of the compartment, as seen in Figure 2.15. Furthermore, four bi-directional pressure probes [172] with thermocouples attached on top were mounted in the centre of the doorway along the vertical axis to measure the air flow and temperature of the gases.

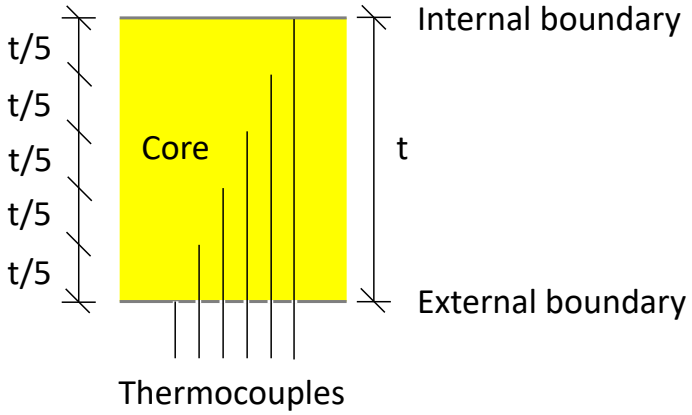

Figure 2.12: In-depth thermocouple location in a core sample with the thickness, *t*.

The six compartments where the influence of joints were studied, as seen in Figure 2.13 b), were assembled in such a way that the sides and ceiling joint aligned as a shorter span would always be preferred in a construction situation to minimise the bending moment as well as deflections. The panels with and without joints were fix along their edges by 2 mm flashings in stainless steel. L-profiles measuring 2.5 cm by 2.5 cm were fastened internally every 0.12 m along all ceiling and wall corners, as seen in Figure 2.13 c). Externally, 15 cm by 5 cm L-profiles were fastened along the ceiling and walls with 15 cm intervals, as seen in Figure 2.13 d). Along the door frame the exposed core was protected by 10 cm by 2.5 cm U-profiles fastened every 8 cm. Furthermore, along the external ceiling-to-wall interface a strip of aluminium tape was applied to limit convective heat loses and allows the compartment to build up a pressure, as seen in Figure 2.13 d). The multiple in-depth inserted thermocouples in this experimental series were used for the LM least-square method to determine the temperature dependent conductivity terms for the heat transfer model for use across all scales.

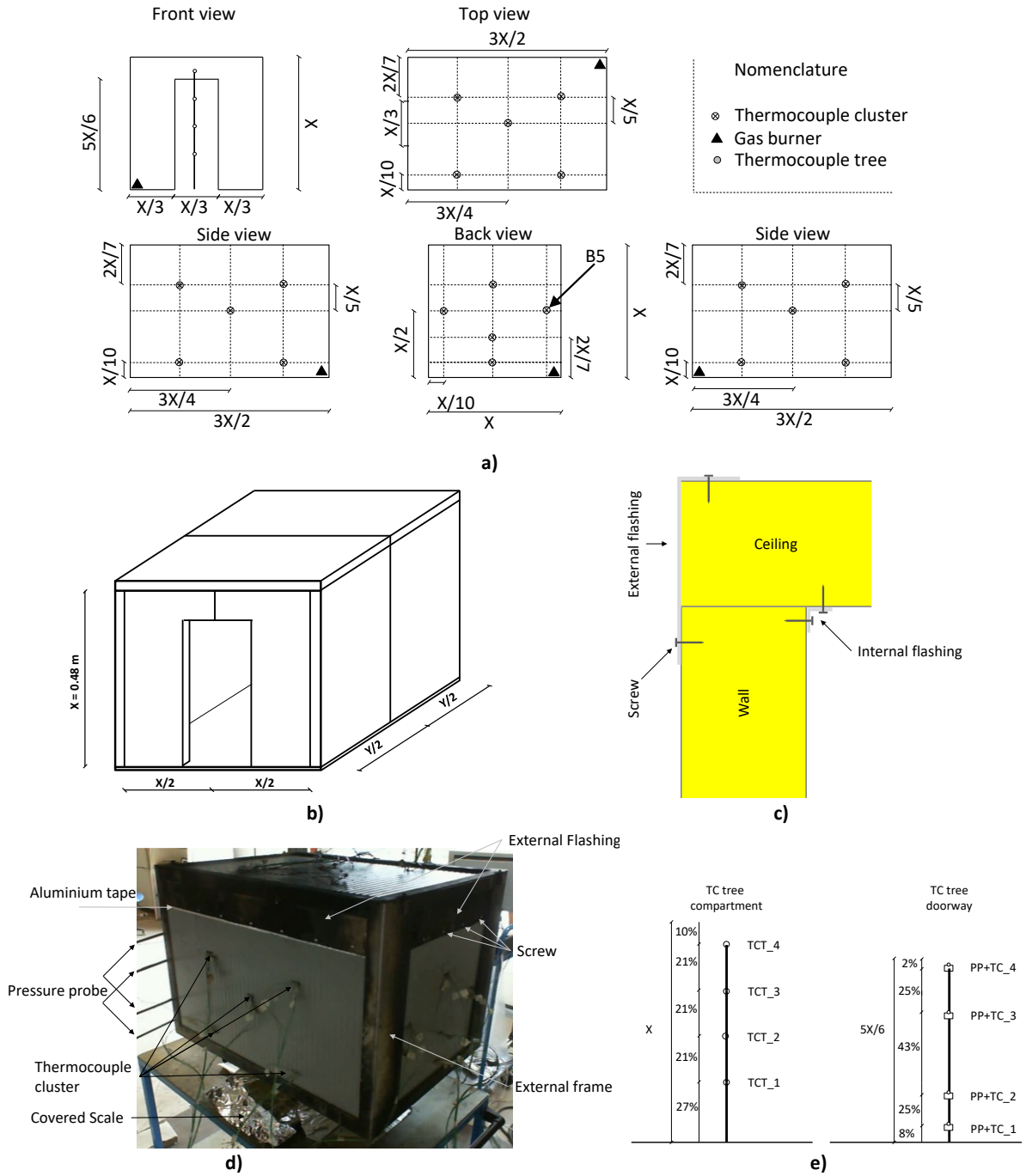

Figure 2.13: a) The thermocouples location of the 1:5 scale compartment, b) without flashings and. c) A sketch of the flashing for a wall-to-ceiling interface, d) experimental setup for E14 (see Table 2.11 and Table 2.12) from the back, e) Thermocouple trees placed inside the compartment and in the doorway, from right to left, respectively.

The second series of 1:5 scale compartment experiments were focused on determining the distribution of heat using the heat transfer model with the temperature dependent conductivity. The results from the first series raised some questions regarding the effect of the thickness of the panels with respect to the time of the thermal runaway which meant different fire scenarios were

used. The thermocouple tree and pressure probe tree placed inside the compartment and in the doorway was identical to the ones placed for the first series, as seen in Figure 2.13 e).

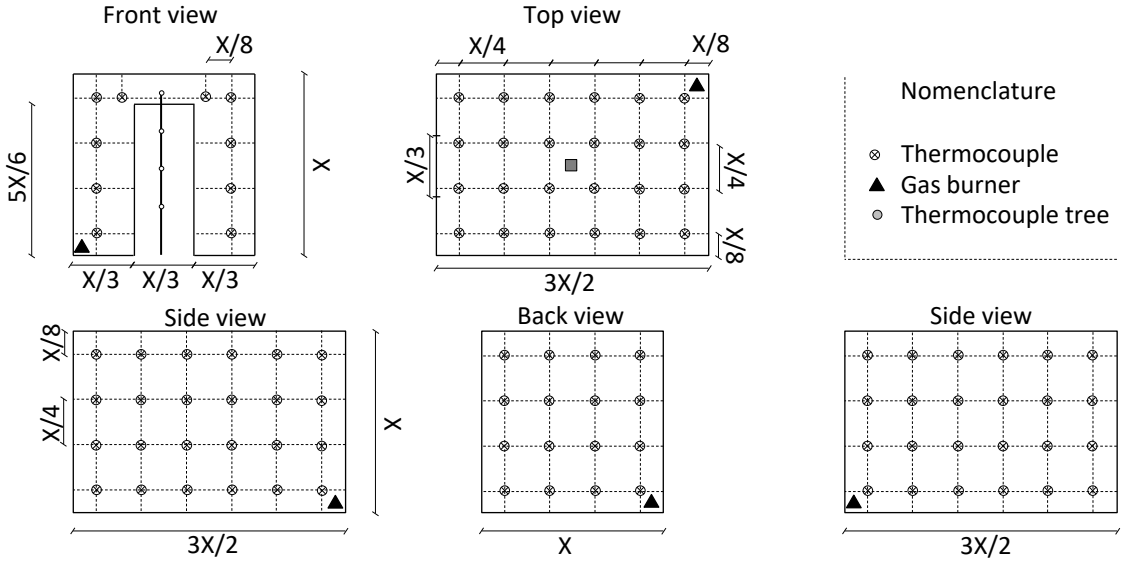

Figure 2.14: The placement of thermocouples measuring the temperature of the internal steel face.

The thermocouples measuring the in-depth temperature through the thickness of the cores were redistributed to the internal surface to increase the number of thermocouples measuring the temperature of the internal steel-face, as seen in Figure 2.14. The two series of 1:5 scale experiments included 23 experiments with various combinations of joints, burner input and panel thickness, as seen in Table 2.11.

Table 2.11: Experimental matrix for the two 1:5 scale compartment experiment series.

Experiment number	Scale	Core type	Thickness	Burner location	Equivalent burner input [a]	Actual rounded burner input [b]	Joints	In-depth TCs
(-)	(-)	(-)	(m)	(-)	(kW)	(kW)	(-)	(-)
E1	1:5	SW	0.10	Corner	1_3	2_5	No	5
E2	1:5	SW	0.10	Corner	1_3_6	2_5_10	No	5
E3	1:5	SW	0.10	Corner	1_3	2_5	Yes	5
E4	1:5	SW	0.10	Corner	1_3_6	2_5_10	Yes	5
E5	1:5	PIR	0.10	Corner	1_3	2_5	No	5
E6	1:5	PIR	0.10	Corner	1_3_6	2_5_10	No	5
E7	1:5	PIR	0.10	Corner	1_3	2_5	Yes	5
E8	1:5	PIR	0.10	Corner	1_3_6	2_5_10	Yes	5
E9	1:5	PIR	0.06	Corner	1_3	2_5	No	5
E10	1:5	PIR	0.06	Corner	1_3_6	2_5_10	No	5
E11	1:5	PIR	0.06	Corner	1_3	2_5	Yes	5
E12	1:5	PIR	0.06	Corner	1_3_6	2_5_10	Yes	5
E13	1:5	PIR	0.10	Corner	1_1_1_1	2_2_2_2	No	5
E14	1:5	PIR	0.10	Corner	3_3	5_5	No	5
E15	1:5	PIR	0.06	Back	1_3_6	2_5_10	No	1
E16	1:5	PIR	0.06	Centre	1_3_6	2_5_10	No	1
E17	1:5	PIR	0.06	Corner	3_3_3_3	5_5_5_5	No	1
E18	1:5	PIR	0.06	Corner	3_3	5_5	No	1
E19	1:5	PIR	0.06	Corner	1_3_3	2_5_5	No	1
E20	1:5	SW	0.10	Corner	1_3_6_6_10_16	2_5_10_10_18_29	No	1
E21	1:5	PIR	0.06	Corner	4_4	7_7	No	1
E22	1:5	PIR	0.10	Corner	4_4	7_7	No	1
E23	1:5	PIR	0.06	Corner	1_3_6[c]	2_5_10	No	1
E24	1:5	PUR	0.06	Corner	4_4	7_7	No	1

a. The "Equivalent burner input" refers to the full scale input in hundreds for segments of 10 min for 10 cm thick panels or 7 min 45 s for 6 cm panels e.g. 1_3_3 refers to 100 kW for 10 min and 300 kW for 20 min at full scale for a 10 cm thick panel.

b. "The actual rounded burner input" is the burner input rounded to the nearest kW in segments of 10 min for 10 cm thick panels or 7 min 45 s for 6 cm panels for the experiment.

c. The burning periods were 10 min for this experiment with 6 cm thick panels.

2.2.5.4 Summary of the compartment setups

The compartment setup for the four different scales and five different series varied as a result of the shifting focus from experiment to experiment as knowledge was gained and unknowns presented themselves. As the delivered panels were long and wide enough to form the enclosures for the 1:5 scale compartments without mid-span joints, constructing with joints was optional. As the compartment size and lengths increased, joints were no longer optional. The number of joints along the walls and ceiling increased as the size of the compartments grew, as shown in Figure 2.15.

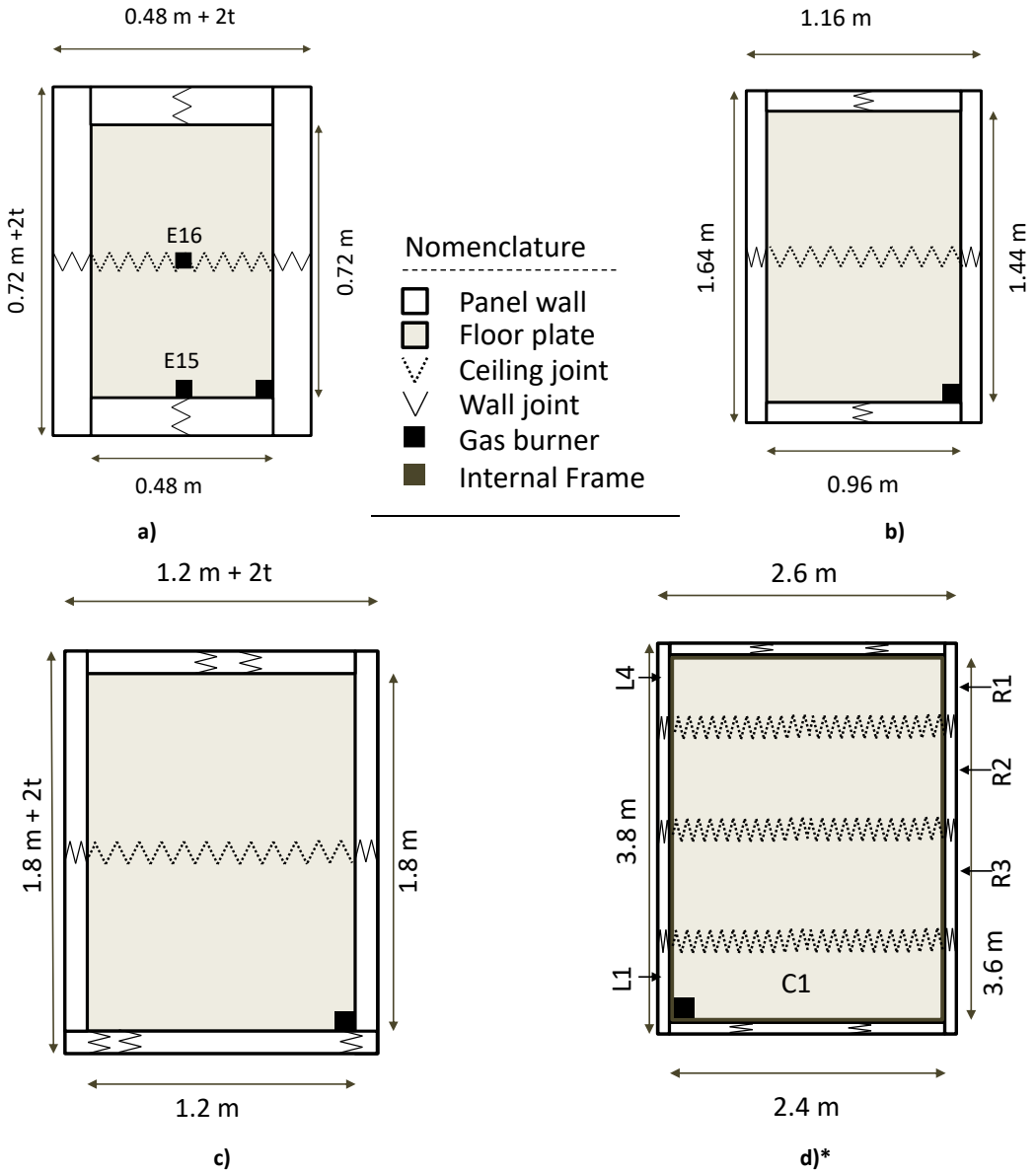

Figure 2.15: Top view including the joints marked and the burner location for a) 1:5 scale, b) 2:5 scale, c) 1:2 scale and d) full scale experimental setups. * The name tags: L1, L4, R1, R2, R3 and C1 refers to the sandwich panels, as seen in Figure 3.33.

A picture from the front of each experimental scale is shown in Figure 2.16 to illustrate the size of the compartments. The summary of the experimental matrixes provided in Table 2.12 provides information on how the various parameters (i.e. fire scenario, panel thickness, joints) were combined.

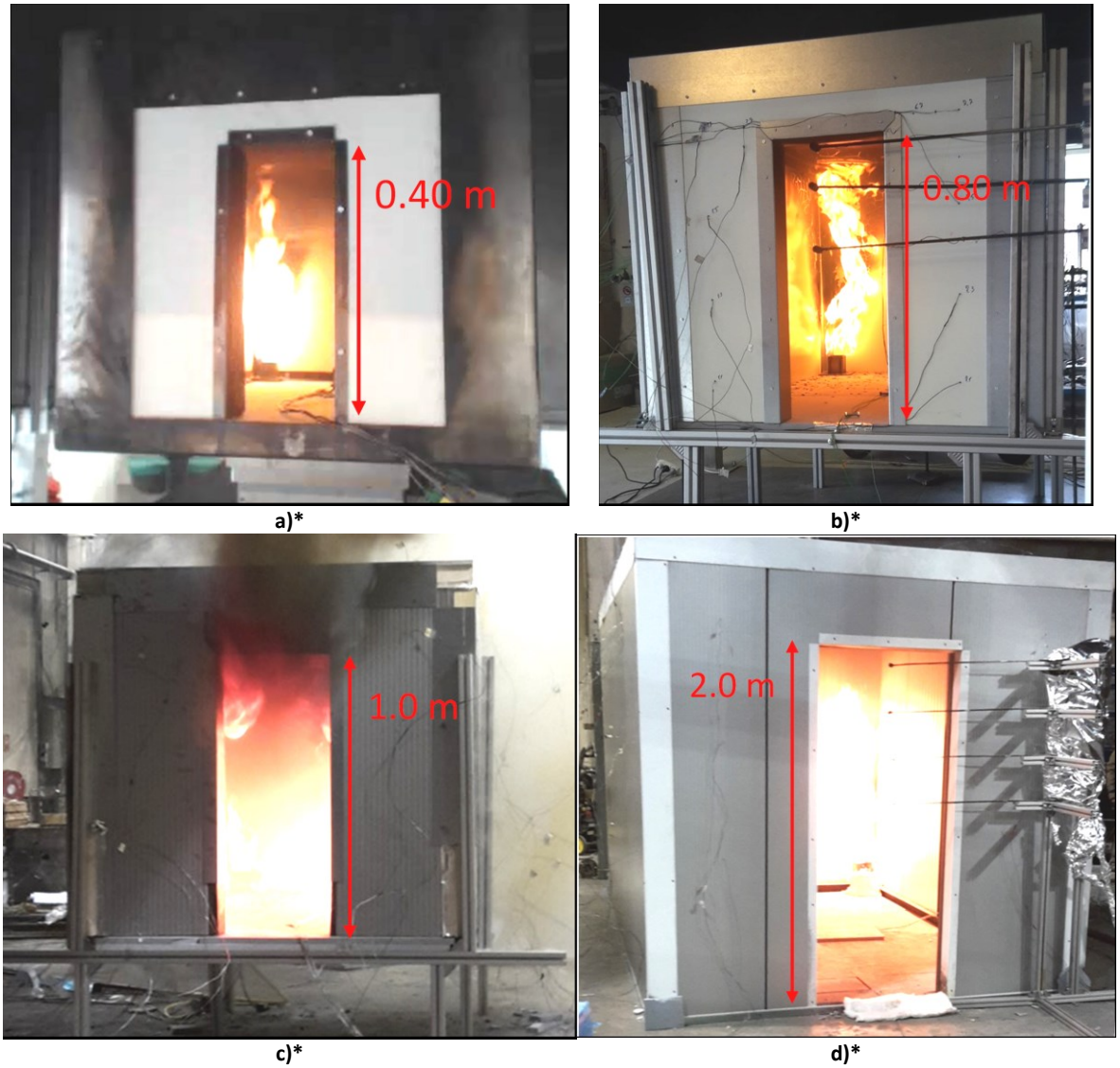

a)* b)*

c)* d)*

Figure 2.16: a) 1:5 scale compartment from the first series, b) 2:5 scale compartment, c) 1:2 scale compartment with 10 cm PIR panels and d) full scale compartment with 10 cm PIR panels.*Brigtness and contrast increased with 20%.

Table 2.12: Experimental matrix for all the compartment experiments conducted as well as two experiments from literature.

Experiment number	Scale	Core type	Thickness	Burner location	Equivalent burner input [a]	Actual rounded burner input [b]	Joints	In-depth TCs
(-)	(-)	(-)	(m)	(-)	(kW)	(kW)	(-)	(-)
E1	1:5	SW	0.10	Corner	1_3	2_5	No	5
E2	1:5	SW	0.10	Corner	1_3_6	2_5_10	No	5
E3	1:5	SW	0.10	Corner	1_3	2_5	Yes	5
E4	1:5	SW	0.10	Corner	1_3_6	2_5_10	Yes	5
E5	1:5	PIR	0.10	Corner	1_3	2_5	No	5
E6	1:5	PIR	0.10	Corner	1_3_6	2_5_10	No	5
E7	1:5	PIR	0.10	Corner	1_3	2_5	Yes	5
E8	1:5	PIR	0.10	Corner	1_3_6	2_5_10	Yes	5
E9	1:5	PIR	0.06	Corner	1_3	2_5	No	5
E10	1:5	PIR	0.06	Corner	1_3_6	2_5_10	No	5
E11	1:5	PIR	0.06	Corner	1_3	2_5	Yes	5
E12	1:5	PIR	0.06	Corner	1_3_6	2_5_10	Yes	5
E13	1:5	PIR	0.10	Corner	1_1_1_1	2_2_2_2	No	5
E14	1:5	PIR	0.10	Corner	3_3	5_5	No	5
E15	1:5	PIR	0.06	Back	1_3_6	2_5_10	No	1
E16	1:5	PIR	0.06	Centre	1_3_6	2_5_10	No	1
E17	1:5	PIR	0.06	Corner	3_3_3_3	5_5_5_5	No	1
E18	1:5	PIR	0.06	Corner	3_3	5_5	No	1
E19	1:5	PIR	0.06	Corner	1_3_3	2_5_5	No	1
E20	1:5	SW	0.10	Corner	1_3_6_6_10_16	2_5_10_10_18_29	No	1
E21	1:5	PIR	0.06	Corner	4_4	7_7	No	1
E22	1:5	PIR	0.10	Corner	4_4	7_7	No	1
E23	1:5	PIR	0.06	Corner	1_3_6 [c]	2_5_10	No	1
E24	1:5	PUR	0.06	Corner	4_4	7_7	No	1
E25	2:5	SW	0.10	Corner	1_3_6	10_30_60	Yes	1
E26	1:2	PIR	0.06	Corner	1_2	17_34	Yes	1
E27	1:2	PIR	0.10	Corner	3_3	53_53	Yes	1
E28	1:2	SW	0.10	Corner	1_3_6	17_53_106	Yes	1
E29	1:1	PIR	0.10	Corner	1_3	100_300	Yes	1
E30	1:1	SW	0.10	Corner	½_2_2	50_200_200	Yes	1
PIR[d]	1:1	PIR	0.10	Corner	1_3_6	100_300_600	Yes	5
SW[d]	1:1	SW	0.10	Corner	1_3_6_6	100_300_600	Yes	5

a. The "Equivalent burner input" refers to the full scale input in hundreds for segments of 10 min for 10 cm thick panels or 7 min 45 s for 6 cm panels e.g. 1_3_3 refers to 100 kW for 10 min and 300 kW for 20 min at full scale for a 10 cm thick panel.

b. "The actual rounded burner input" is the burner input rounded to the nearest kW in segments of 10 min for 10 cm thick panels or 7 min 45 s for 6 cm panels for the experiment.

c. The burning periods were 10 min for this experiment with 6 cm thick panels.

d. From literature [16] used for the comparison across scales and the heat transfer model presented in Section 2.3

2.3 Heat Transfer Analysis

The boundary conditions of any test or experimental setup are essential for determining, replicating and ultimately extrapolating the results onto other conditions. The boundary conditions in experiments are often a feature of the setup itself such as the thermal exposure from a flame but it can also be a feature of the product or material such as the surface or density of the material. The latter is easy to transfer to other setups as it is an intrinsic property, whereas the thermal exposure is an extrinsic property. By transferring extrinsic properties, which is often the case for fire tests, there is a risk of error and the robustness and versatility of the test is relied upon to ensure a correct extrapolation.

Setting up an energy balance with the compartment as the Control Volume (CV), as seen in Figure 2.17, results in Eqns. 2.11 and 2.12. The energy entering the CV is either stored as a change in its internal energy or leaving the CV again.

$$\frac{dQ_{CV}}{dt} = \dot{Q}_{in} - \dot{Q}_{out} \quad \textbf{2.11}$$

$$\dot{Q}_{gas} = \dot{Q}_{burner} + \dot{Q}_{core} + \dot{Q}_{vent,in} - \dot{Q}_{vent,out} - \dot{Q}_{cond} \quad \textbf{2.12}$$

Here Q_{CV} is the energy in the CV that is the volume of the compartment, $\frac{dQ_{CV}}{dt}$ is the change in energy in the $\dot{Q}_{gas}$, $\dot{Q}_{in}$ consists of the heat input from the gas burner, $\dot{Q}_{burner}$, the heat generated by ignition of pyrolysis gases from the core, $\dot{Q}_{core}$, and the heat entering the compartment through the door opening $\dot{Q}_{vent,in}$, while $\dot{Q}_{out}$ is the heat leaving the compartment, which consists of the heat losses by radiation and convection through the door opening, $\dot{Q}_{vent,out}$, and the heat conducted through the compartment boundaries, $\dot{Q}_{cond}$, as seen in Figure 2.17. The heat leaving the compartment through the door opening through radiation has, however, been found to be less than 1% by Häglund [173] and 3% by Haramathy [132] and was considered negligible.

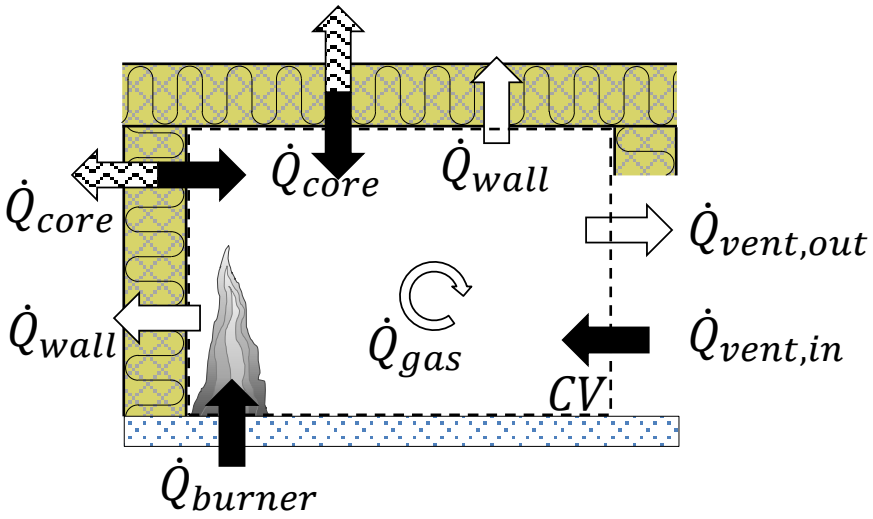

Figure 2.17: A simplistic schematic of the heat transfer in a compartment with a marked Control Volume (CV) warmer than the ambient environment. The arrows indicate the direction of the energy and the wave, white and black arrows indicate the energy not being part of, leaving and entering the CV, respectively. Not to scale.

Ignoring the flow of the fuel (calculated as less than 1% of the total mass flow) from the burner and any pyrolysis gases from the core following the conservation of mass, $\frac{\partial m}{\partial t} = 0$, the mass flow in and out of the compartment must be identical. This means the change in heat entering and leaving the compartment can be calculated as a function of the measured temperature and flow leaving the compartment, as expressed in Eq. 2.13.

$$\dot{Q}_{conv} = \dot{Q}_{vent,out} - \dot{Q}_{vent,in} = C_d \cdot v \cdot A \cdot \rho_g \cdot c_p \cdot \left(T_g - T_\infty\right) \qquad \textbf{2.13}$$

Here $\dot{Q}_{conv}$ is the difference in the energy leaving, $\dot{Q}_{vent,out}$, and entering, $\dot{Q}_{vent,in}$, the compartment and C_d is the flow coefficient. Although the theoretically flow is the highest along the measured centreline and lower at the doorway boundaries, the coefficient is assumed to be 0.8 [145] on average. v is the weighted measured velocity along the height of the smoke layer, *A* is the area where the gases flowing out, ρ is the density, *T* is the temperature where the subscripts *g* and ∞ refers to the gas and ambient air, respectively. The velocity was based on the measured pressure difference by bi-directional pressure probes along the centreline of the door. The pressure was assumed to follow a linear distribution as a function of the change in gas density. The temperature in the compartments was measured by several thermocouples, and the change in the internal energy

in the volume of the compartment was determined as the sum of those changes over time, as seen in Eq. 2.14.

$$\dot{Q}_{gas}^{j} = \sum_{n=1}^{N} V_n \cdot \rho_n^j \cdot c_{p,n}^j \cdot \frac{T_n^j}{\Delta t} \qquad \textbf{2.14}$$

Here V is the volume, ρ is the density, c_p is the specific heat capacity, T is the measured temperature, n runs to N number of thermocouples and j denote the time.

The net heat absorbed by the enclosure boundary exposed to the fire is the balance of the sum of the net convective and radiative fractions of the incident heat, as expressed in Eq. 2.15, and with opposite signs for the boundary between the enclosure and the ambient environment, as seen in Figure 2.18.

$$\dot{q}_{net}'' = \dot{q}_{rad}'' + \dot{q}_{conv}'' = -k_s \cdot \frac{\delta T_s}{\delta t} \qquad \textbf{2.15}$$

Here $\dot{q}_{net}''$ is the net heat exchange, $\dot{q}_{rad}''$ and $\dot{q}_{conv}''$ are the net heat transferred by radiation and convection, respectively, k is the conductivity and s denotes steel. The steel-faced sandwich panels provide the possibility to transform the problem into a purely conductive one, which greatly simplifies it. Because it is a purely conductive problem, time dependent parameters such as the local Reynold's number and the emissive property of the coating, which was prone to cracking and flaking, can be circumvented, and, as a result, the accuracy of this method increases.

The heat transfer through a solid media governed by the heat diffusion exchange between the compartment and the walls and ceiling sandwich panels is derived from Fourier's equation in Eq. 2.16. The interface between the steel and the core has to abide the same rules, as seen in Eq. 2.17.

$$-\frac{\delta \dot{q}''_{cond}}{\delta x} = \dot{q}'''_{int} + \dot{g}''' \quad \textbf{2.16}$$

$$-k_s \cdot \frac{\delta T}{\delta x} = -k_c \cdot \frac{\delta T}{\delta x} \quad \textbf{2.17}$$

Here $\dot{q}''_{cond}$ is the conducted heat, $\dot{q}'''_{int}$ is the internal volumetric heat stored and $\dot{g}'''$ is either an endothermic absorption or exothermic heat generation within the core element. k_s and k_c, are the conductivities for the steel and core material, respectively. Attaching thermocouples to the backside of the steel face at the edge of the CV can, if desired and with calibration, also be used as thin-skin calorimeters [174, 175] to measure the incident heat flux rather than the net heat flux. However, the purpose of the thermocouples in this work was to determine the surface temperature of the panel. This was for determining the boundary condition to eliminate the uncertainties and difficulties related to the boundary layer between the wall and compartment volume and therefore used in these analyses.

An a priori analysis was used to determine whether or not the steel faces of the panels would in fact act as a thermally thin element by estimating the limiting conditions that made the Biot number exceed 0.1 and thus making it act as a thermally thick material. The steel face plates were reported as 0.7 mm in thickness by the manufacturer. Maintaining a Biot number less than 0.1 for the stainless steel plates with an assumed constant conductivity of 15 W/m·K [176] requires the convective heat transfer coefficient to be lower than 2000 W/m^{2}K. The flow in the compartment, for well-ventilated cases, is assumed to be laminar and the convective heat transfer coefficient is very likely to be less than 2000 W/m^{2}K [138]. Veloo and Quintiere [177] reported convective heat transfer coefficients for fully developed compartment fires ranging from 30 to 80 W/m^{2}K. Even conditions resulting in forced convection are unlikely to exceed 2000 W/m^{2}K (typically for a forced flow the convective heat transfer coefficient ranges from 10 to 500 W/m^{2}K [138]). The thermocouples were therefore placed within the walls, and the temperature distribution throughout the thickness of the steel was assumed to be uniform.

The problem formulation for the heat balance is based on the application of an implicit and numerically stable finite difference method to solve the one-dimensional conduction heat equation. An inverse heat transfer model is proposed for the determination of equivalent thermal properties

prior to any thermal degradation. The heat transfer through a solid medium is governed by the heat diffusion equation derived from Fourier's law and the conservation of energy as described by Hidalgo [16] and presented in Eq. 2.18.

$$-\frac{\partial}{\partial x}\left(k(T)\cdot\frac{\partial T}{\partial x}\right)=\rho(T)\cdot c_p(T)\cdot\frac{dT}{dt}+\dot{g}''' \qquad \textbf{2.18}$$

Here $k(T)$, $\rho(T)$, $c_p(T)$ are the temperature, T, dependent thermal conductivity, density and specific heat capacity, respectively, and $\dot{g}'''$ is an endothermic or exothermic heat absorption or generation within the core element. The left-hand-side term represents the spatial variation of the heat conducted through the material and the first right-hand-term represents the heat stored by the core. $\dot{g}'''$ can be either positive or negative for generation or absorption of energy, respectively. The contribution of the core was determined theoretically by measuring the mass loss rate of a 1:5 scale experiment. The gross calorific value of the core was determined as 2.1 MJ/kg and the peak mass loss rate was 0.3 g/s during the modified burner step. The theoretical contribution of the core could be 6% of the input of the burner. Based on this, the $\dot{g}'''$ was assumed to be of a negligible magnitude. The energy balance below the steel facing extracted from Figure 2.18 with Fourier's law and the energy stored in the face was solved for the net heat flux at the surface, as seen in Eq. 2.19 and in its finite difference form in Eq. 2.23. The internal nodes between the steel surfaces and the external boundary condition are expressed in Eq. 2.20 and Eq. 2.21, respectively. The backside temperature was not measured and the boundary condition is therefore formulated as a simple balance between convective and radiative losses or gains between the steel face and the ambient environment.

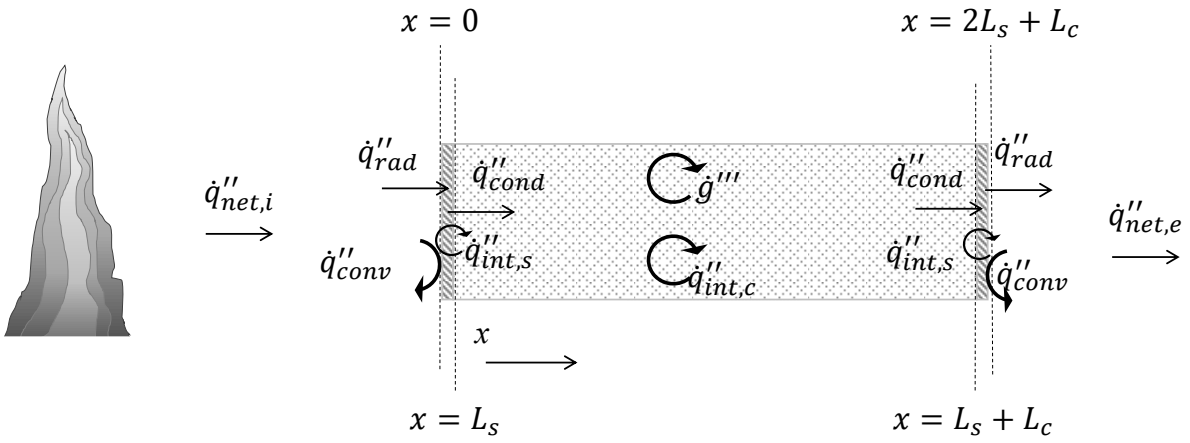

Figure 2.18: Heat transfer model of a cross-section of a wall or ceiling. Not to scale.

$$\dot{q}''_{net,i} = -k\frac{\partial T}{\partial x}\Big|_{x=0} = L_s \cdot \rho_s(T) \cdot c_{p,s}(T) \cdot \frac{dT_s}{dt} + \left(-k_c \frac{\partial T}{\partial x}\Big|_{x=L_s^+}\right) \qquad \text{for } 0 < x < L_s \quad \textbf{2.19}$$

$$\frac{\partial}{\partial x}\left(k_c(T) \cdot \frac{\partial T}{\partial x}\right) = \rho_c(T) \cdot c_{p,c}(T) \cdot \frac{dT}{dt} \qquad \text{for } L_s < x < L_s + L_c \quad \textbf{2.20}$$

$$\dot{q}''_{net,e} = -k\frac{\partial T}{\partial x}\Big|_{x=(2L_s+L_c)} = h \cdot (T_\infty - T_N) + \epsilon \cdot \sigma \cdot (T_\infty^4 - T_N^4) \quad \text{for } x = 2L_s + L_c \quad \textbf{2.21}$$

Here $\dot{q}''_{net_i}$ is the net heat flux at the internal side, *i*, $k(T)$, ρ(T) and $c_p(T)$ is the conductivity, density and heat capacity of the core, respectively, *h* is the convective heat transfer coefficient, ϵ is the emissivity, σ is the Stefan-Boltzmann constant, $\dot{q}''_{net_e}$ is the net heat lost to the ambient environment, and the subscripts *c* and *s* represent the core and steel, respectively. The convective heat transfer coefficient, *h*, was determined using the Nusselt number, *Nu*, for air flowing over a hot plate as function of the temperature of the plate with an assumed emissivity of 0.8. The specific heat capacity and density of the steel is deemed independent of the temperature as the variation ranges between 450 - 650 J/kg·K and 7910-7540 kg/m^3 from 20°C to 870°C [178], respectively, and average values were taken. The density of the SW core material was also deemed independent of the temperature as the Thermogravimetric Analysis (STA) showed less than 4% mass loss for three studied samples in the range between 28 °C and 1050 °C. One-third of the mass loss from the core occurred between 250 °C and 350 °C, as seen in Figure 2.19, which is the region for decomposition of urea-formaldehyde [179] a common binder for stone wool products [180]. The structure of stone wool changes significantly when reaching its glass-transition and crystallisation temperature of

691 °C and 867 °C [181], respectively. However, the specific heat capacity for the core was taken as a standard value for stone wool products as 840 J/kg·K [180] as it is thought to change negligible in the temperature region of these experiments [182]. As stone wool is an insulation material and thermally thick the in-depth temperature is lower than the temperature of the surface and the glass-transition is, furthermore, only assumed to be a surface phenomenon and of negligible magnitude. The materials parameters, except the conductivity for the core material, were therefore assumed to be constant.

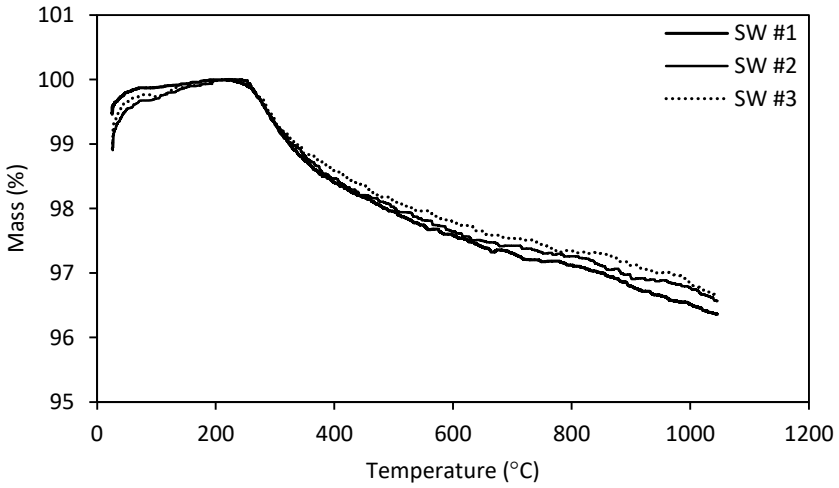

Figure 2.19: STA analysis from 28°C to 1050°C for three mineral wool core samples.

In order to perfectly model the heat transfer problem in a fibrous material such as the stone wool core, computational fluid dynamics and a radiation transfer equation in addition to the diffusive heat transfer would be required [85]. This is to fully account for the nature and behaviour of the core, i.e. the core is heated and the binder pyrolysis and the pores within the core as well as the internal radiation between dark slag particles and the fibres increase. Although this might be preferred for some scenarios such as product development, the goal of this work, however, is to show how a simple model can estimate the net heat transfer across geometrical scales to show the similarities. To further simplify the problem the contact resistance between the steel and core is considered negligible. This assumption implies that the steel does not delaminate from the core causing the mode of heat transfer to change significantly. This is a reasonable assumption in the early stages of the fire (before flashover), where temperatures are lower than the decomposition temperature of the glue and because it is prior to thermal expansion that can cause delamination or

buckling of the steel relative to the core. A cone experiment following the ISO 5660-1 was used to determine when the steel face would delaminate from the core and was found to be at surface temperatures higher than 600 °C. This temperature was only exceeded at the measurement positions closest to the burner and the ceiling measurements directly above the burner. Measurements exceeding 600 °C only occurred during the third and final burner step. This means the model loses some accuracy towards the end of the experiments as up to 20% of the thermocouples would no longer measure the temperature of the steel face directly.

The finite difference method used to solve the heat transfer problem is a Crank-Nicolson scheme [183]. This method uses a second order scheme, implicit in time and numerically stable and the temperature is determined as the temperature at the previous step plus the average growth between two steps, as seen in Eq. 2.22. The formulation is based on a system of N linear equations with N variables, where the thickness of the elements are Δx/2 for the nodes *i=1* and *i=N*, and Δx for all other nodes. The temperature at node *i=1* is known, as noted in the experimental setup section. The net heat flux is unknown and the number of unknowns therefore remains N. The equations in differential form for the two locations namely the internal boundary node and core nodes are expressed in Eq. 2.23 and Eq. 2.24, respectively. As the steel sheets at the boundaries were acting as thermally thin materials they were not included as separate nodes and the model exclusively calculated the heat transfer through the core material with the change of internal energy of the steel added.

$$T_i^{j+1} = T_i^j + \frac{\Delta t}{2} \cdot \left(\left.\frac{\Delta T}{\Delta t}\right|_i^j + \left.\frac{\Delta T}{\Delta t}\right|_i^{j+1} \right) \quad \textbf{2.22}$$

$$\dot{q}''^{\,j+1}_{net_1} = L_s \cdot \rho_s \cdot c_{p,s} \cdot \frac{T_1^{j+1} - T_1^j}{\Delta t} + \frac{\Delta x}{2} \cdot \rho_c\left(T^{j+1}\right) \cdot c_{p,c}\left(T^{j+1}\right) \cdot \frac{T_1^{j+1} - T_1^j}{\Delta t} + k_c\left(T^{j+1}\right) \cdot \frac{T_1^{j+1} - T_2^{j+1}}{\Delta x} \quad \textbf{2.23}$$

$$\dot{q}''^{\,j+1}_{net_n} = \Delta x \cdot \rho_c\left(T^{j+1}\right) \cdot c_{p,c}\left(T^{j+1}\right) \cdot \frac{T_n^{j+1} - T_n^j}{\Delta t} + k_c\left(T^{j+1}\right) \cdot \frac{T_n^{j+1} - T_{n+1}^{j+1}}{\Delta x} \quad \textbf{2.24}$$

Here T_i^j and T_i^{j+1} are the temperatures of the node at the time steps *j* and *j+1*, respectively, $\frac{\Delta T}{\Delta t}\Big|_i^j$ and $\frac{\Delta T}{\Delta t}\Big|_i^{j+1}$ are the time variation of node *i* at time step *j* and *j+1*, and *Δt* is the time step.

In Eq. 2.25 the energy balance is rewritten (from Eq. 2.12), with respect to the known energy input from the burner ($\dot{Q}_{burner}$), but without the heat term from the SW core, as seen in Eq. 2.25. This provides a system for comparison across scales, and will be used as the method for analysing and comparing the results from the scaled compartment to those from the full scale compartment as it is dimensionless and versatile.

$$1 = \frac{\dot{Q}_{conv}^j}{\dot{Q}_{burner}^j} + \frac{\dot{Q}_{cond}^j}{\dot{Q}_{burner}^j} + \frac{\dot{Q}_{gas}^j}{\dot{Q}_{burner}^j} \qquad \textbf{2.25}$$

2.3.1 Temperature Dependent Conductivity

The conductivity of the cores at ambient conditions provided by the manufacturers was considered too coarse of an assumption to use for the heat transfer model as other authors reported significant increases [88]. The thermal conductivity increased by factors of 2.6 [87] and 6.5 [88] from 40 °C to 400 °C which is part of the expected temperature region for long periods of time for the compartment.

The in-depth thermocouples were used to determine the conductivity, *k(T)*, as seen in Eq. 2.26, as the sum of the conductivity at ambient conditions, k_0, and the temperature dependent conductivity, k_1, multiplied with the temperature measured, *T*. This function matches quite well with the model and the measurements found by Livkiss et al. [88] for a similar stone wool product.

$$k(T) = k_0 + k_1 \cdot T \qquad \textbf{2.26}$$

The heat transfer model included a best-fit optimization component which enabled the characterisation of any unknown material parameter, e.g. the specific heat capacity, conductivity or

density. The chosen optimisation method is a Levenberg-Marquardt least-square method [184] that compares the calculated temperature based on a range of values to the measured temperature to find the optimal value for the optimized parameter. The optimization model finds the local minima based on the provided initial values and the solution from the heat transfer model. The dominating internal boundary condition was measured directly by the mounted thermocouples, the density and specific heat capacity is considered fairly constant unless the core material changes significantly e.g. charring, pyrolysing or phase transitioning etc. during the experiments. The density and specific heat capacity for the cores were taken from the documentation from the supplier and literature and the density was verified through manual measurements. Even though the only parameter optimised is the temperature dependent conductivity term the algorithm finds local values which fits the model best. Ultimately this means the density, specific heat capacity and conductivity are lumped together as an effective parameter where many solutions could provide the same least-square value. The solutions are sensitive to the first two thermocouple measurements, and the boundary temperature will dominate the proposed solution. However, by having multiple measurement points the provided solutions become more robust as outliers are identifyiable.

3 Results and Discussion

The *Results and Discussion* section is split into three sections where Section 3.1 covers the three small scale experiments, namely, the STA/DSC, mass loss cone and gross calorific content. Section 3.2 presents observations from the compartment experiments Section 3.3 goes more in-depth with respect to the compartment experiments, which are analysed and discussed. The heat transfer results for the SW cored panels are also part of Section 3.3.

3.1 Small Scale Experiments

To get the intrinsic material properties a bomb calorimeter and a STA was used to determine the complete heat of combustion, ΔH_c, under oxygen rich conditions and the mass loss potential under oxygen lean and rich conditions, respectively. The core materials studied were originally covered by two steel sheets as they were from sandwich panels. All the three sandwich panel cores were studied in the bomb calorimeter as well as in the SGA. The PIR and SW were studied in both air and an inert atmosphere of nitrogen, whereas the PUR core was only studied in an inert nitrogen atmospheres.

3.1.1 Thermographic Analyses and Differential Scanning Calorimetry

The initial mass, m_0, mass loss (ML) and peak mass loss rate (pMLR) of the samples were measured initially and calculated, respectively, and the results are shown in Table 3.1. The experiments were conducted in an inert atmosphere of nitrogen to study the decomposition without oxygen readily available to prevent any flames from dominating the heating rate. However, as noted in Section 1.3.2 - *Polymeric Panels* the isocyanurate, isocyanurate rings and urethane all contain oxygen and can still react during the experiments. The mass as a function of temperature for the PIR and PUR cores showed similar initial behaviours. These products both have an initial mass loss around 100 °C which is most likely either water bound or absorbed from ambient conditions or allophanate bonds breaking up [95]. Another minor reaction was initiated around 185 °C, where the urethane bonds start to break, and peaked around 200 °C [185]. The results from the TGA show that the three polymeric core materials have many of the same reactions, including the breaking of the isocyanurate rings around 300 °C and long alcohol chains degrading around 400 °C [93], as seen in Figure 3.1. The breaking of the Isocyanurate rings, the primary component, is the dominant reaction in inert nitrogen atmosphere alongside the breaking of alcohol bonds, as identified by Garrido and

Front [185] for flexible foams. As the core materials were prepared in ambient conditions prior to the experiments, the influence of the blowing agent used during the manufacturing process to increase the thickness and decrease the density of the foam was not determined.

Table 3.1: Summary of the STA experiments for the three studied core samples conducted in atmospheres of air or nitrogen.

		Nitrogen (Figure 3.1 and Figure 3.2)				Air (Figure 3.3)			
		m_0 (mg)	ML_∞ (%)	pMLR (%/min)	T(pMLR) (°C)	m_0 (mg)	ML_∞ (%)	pMLR (%/min)	T(pMLR) (°C)
SW	1	11.674	3.21	-0.18	278	3.094	9.99	-1.11	505
SW	2	5.689	2.45	-0.22	264				
SW	3	5.457	2.61	-0.21	299				
PIR	1	1.252	62.19	-7.87	333	1.593	99.61	-5.79	575
PIR	2	1.457	63.31	-9.73	311				
PIR	3	1.769	67.65	-7.04	312				
PUR	1	1.771	75.01	-12.18	321				
PUR	2	1.404	73.54	-11.37	316				
PUR	3	1.573	75.46	-10.58	318				

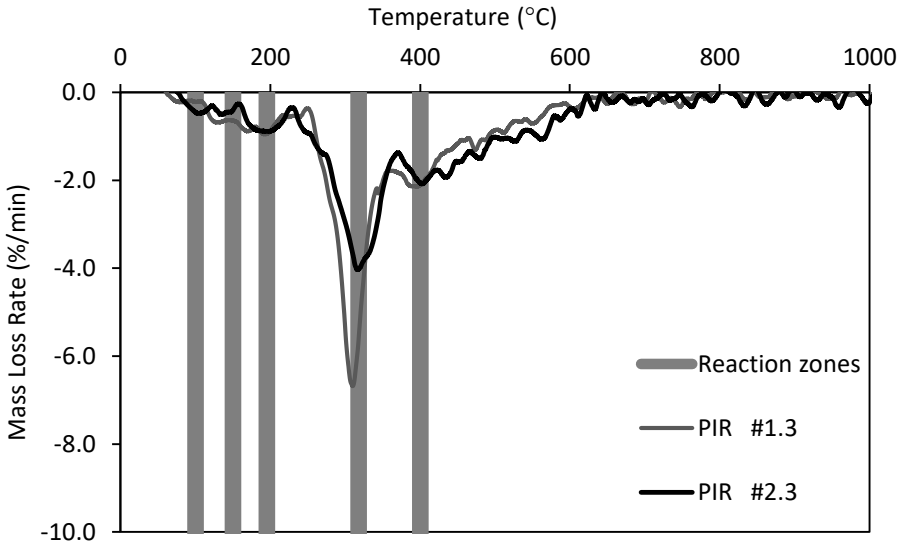

Figure 3.1: Mass loss rate for the three polymeric foams with hatched reaction regions studied in a pure nitrogen environment. The data has been smoothened.

A minor reaction peaks around 360 °C and along with the initiation of the breakdown of the isocyanurate rings around 280 °C for both the PIR and PUR cores suggest that their polyol is a polyester [93]. The PUR core generally showed additional reactions over the other cores with

multiple changes in the slope in the mass loss rate graph, as seen in Figure 3.1, and in*Appendix – Additional STA Graphs*.

The majority of the mass loss of the SW cores were initiated 250 °C with a peak around 300 °C, as seen in Figure 3.2.The mass lost during the SW experiments was, however, very limited, and its mass loss and derivatives are to be treated with care, because even small fluctuations can falsely appear to be a reaction.

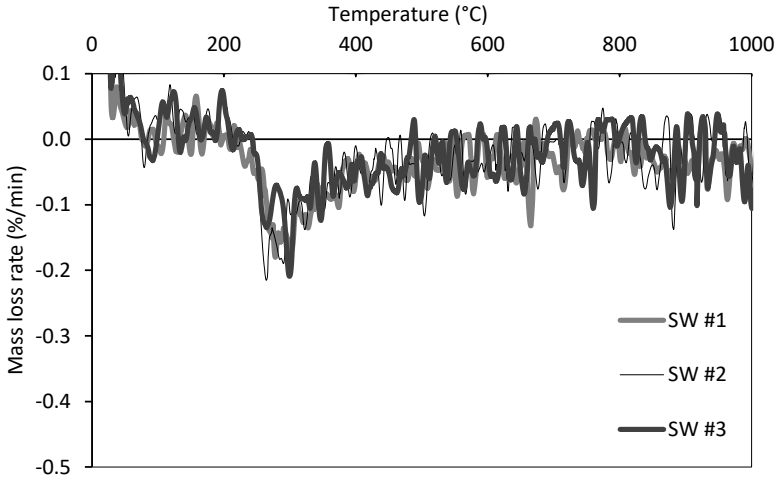

Figure 3.2: STA results for the SW core sample in a pure nitrogen environment.

The inert atmosphere allowed for identification of some of the reactions that occur in the core of the material as if the core protected due to an insulating upper layer of virgin-, charred material or the steel facing. Thermal expansion, delamination and buckling of the steel facings are, however, possible [186] and oxygen can potentially diffuse and change the combustion especially in or around the joints between the panels.

The five noticeable reactions for the PIR core in the nitrogen atmosphere were replaced by three major reactions when studied in an atmosphere of air, as seen in Figure 3.3, 1) starting at 75 °C with a longer plateau peaking around 190 °C, 2) initiating at 250 °C peaking at 320 °C both just like the reactions taking place in the nitrogen atmosphere, 3) initiating around 460 °C and peaking at 580 °C where the largest amount of mass was lost and the sample almost was completely pyrolysed, as seen in Figure 3.4. It should be noted that the decomposition of the PIR core in air also has several other reactions that can be identified by the change in the slope of the MLR. Those reactions will,

however, remain merely as a note, because they contributed either right before or after the other three major reactions.

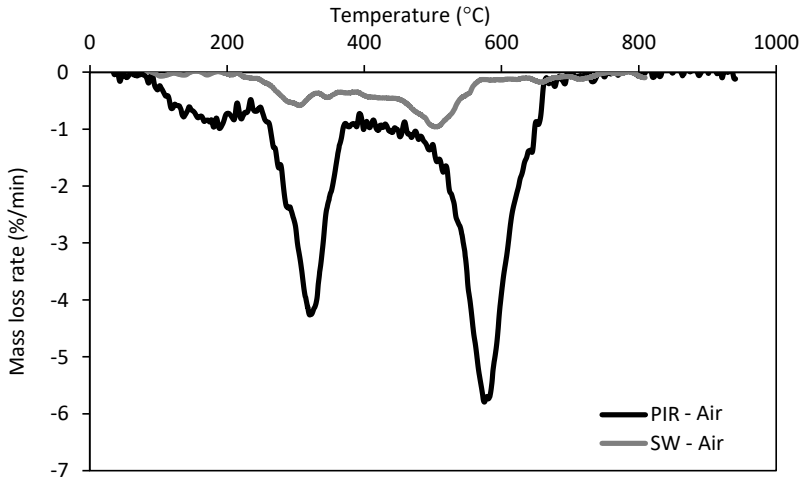

Figure 3.3: Mass loss rate for PIR and SW studied in air.

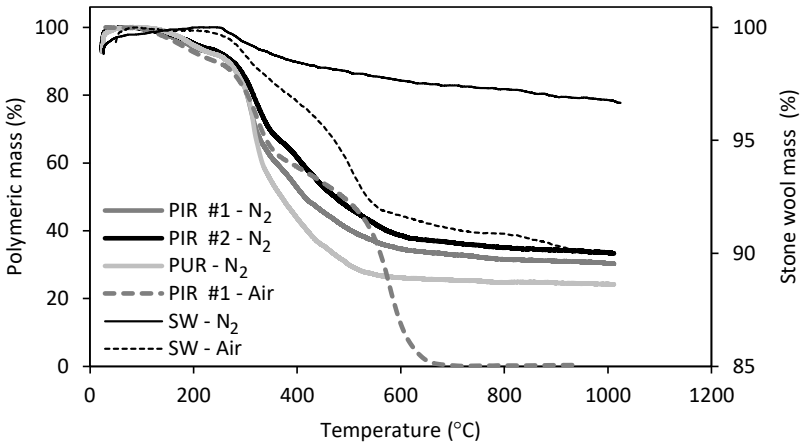

Figure 3.4: Mass loss for the cores studied under reactive air and inert nitrogen environments in the STA.

The STA analysis presents the data for the measured mass loss as a function of temperature for the three core types, PIR, PUR and SW and the MLR for the core materials in inert atmosphere peaked between 278 °C and 333 °C. When studied in a reactive atmosphere of air the SW and PIR cores were losing the most mass at 505 °C and 575 °C, respectively. The probability for a thermal runaway in a compartment is therefore greatest when the core material reaches one of those temperatures if the mass loss correlates to energy being released.

A Differential Scanning Calorimetry (DSC) analysis was performed for the samples studied under nitrogen atmosphere to provide a qualitative estimate of the minimum energy release of the core materials. The release of energy as a function of temperature, as seen in Figure 3.5, show how the DSC curve change significantly around 300 °C for the PUR matching the range where 40% of the mass of the sample was lost. The DSC results indicate that, on a component level, the polymeric cores release different amount of energy at different times. The PUR core release more energy after 280 °C than the PIR core, seen by the change in slope and that the PIR release more energy than the PUR after 750 °C also seen by the slope and dip. It is therefore expected at larger scales that the PUR will release more energy earlier on during the compartment experiments.

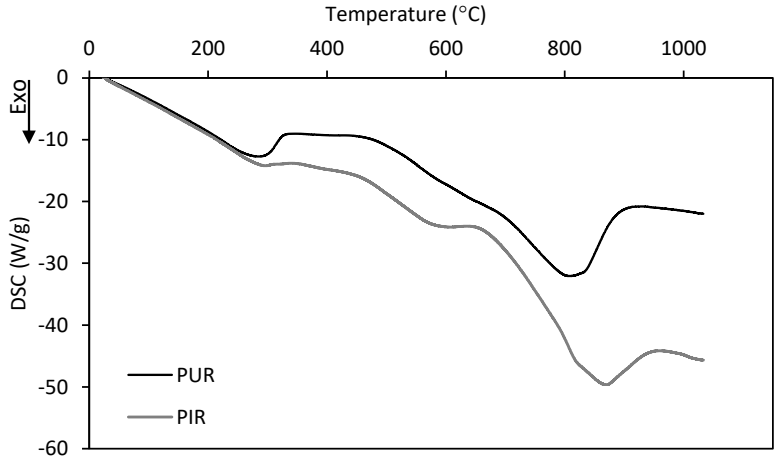

Figure 3.5: DSC curve for the two polymeric core materials studied in a pure nitrogen environment.

The STA and DSC provided information regarding the temperature ranges of concern indicated by large mass losses and energy release. The PIR will lose all of its mass if exposed to high temperatures if left unprotected in an atmosphere containing air and will maintain about 65% of its mass if the atmosphere is inert or if the formation of char is effective. When exposed to heat the PIR will react between 200 °C and 700 °C with the highest MLR at 300 °C and 400 °C in nitrogen and 300 °C and 600 °C in air. The probability of a thermal runaway in the compartment is increasing when the energy released into the CV exceeds the energy leaving. The contribution from the burners alone is not sufficient in causing a thermal runaway and as the PIR is reactive around the 300 °C the risk of a thermal runaway is therefore profound if the compartment reach that temperature. The thermal runaway could, however, also occur if less than the full surface area of the compartment reaches 300 °C provided a small surface area reaches 600 °C where, based on the data from the STA/DSC ,

even more mass and energy can to be lost and released, respectively, if air is available. A summary of the temperatures of interest is provided in Table 3.2

Table 3.2: Summary of temperatures of interest for the three core types when studied in the STA with nitrogen and air

	Nitrogen, initiation of losses			Air, peak values	
	PIR (°T)	PUR (°T)	SW (°T)	PIR (°T)	SW (°T)
1. reaction	100	100	250	185	300
2. reaction	185	185		360	500
3. reaction	300	300		580	
4. reaction	460	460			

3.1.2 Cone Calorimeter

Experiments were carried out with two types of sandwich panels: one with PIR, and one with the SW, with (w) and without (w/o) their respective steel faces in order to study the effect of the protective steel. The steel faces were removed by inserting a smooth 0.5 mm thick stainless steel disk under the steel face creating a lever. The face could hereby be removed with minimal impact on the underlying core surface. The spark plug was used for both series and of all the samples with protective steel only the SW samples exposed to 50 kW/m^2 and 70 kW/m^2 had a full surface ignition as the coating briefly ignited (< 4 s). All the SW samples maintained the same distance to the cone throughout the duration, which ensured a constant incident heat flux. The protected PIR samples expanded during the first 5 min of exposure, and it was visually estimated to be as much as 5 mm. during exposure to the heat the unprotected PIR samples initially expanded, and then later, predominantly at higher heat fluxes, shrunk back below their initial vertical surface location. The unprotected SW samples did not show this behaviour, which could be related to the minor mass loss, lack of expanding charring mechanisms. The SW could, however, be expected to shrink if mechanically loaded [187]. The samples and sample holder did not make a perfect fit allowing for the fitting of the thermocouples and as a consequence flames emerged between the interfaces around the top edges. All the protected PIR samples, except for the one exposed to 10 kW/m^2, ignited between 7.5 min and 20 s when exposed to 20 kW/m^2 and 70 kW/m^2, respectively. Applying these results to the incident heat flux from a radiative source for a thermally thick solid theory, as explained by Torero [188], the plotting of $\dot{q}''_{incident}$ as a function of $1/\sqrt{t_{ig}}$ suggests a critical heat flux (CHR) of approximately 10.5 kW/m^2 with a R^2 of 0.94. This can serve as a guide for PIR samples with steel. Without the steel to protect the core material from the radiation and to limit the

availability of oxygen, all the PIR samples ignited within a few seconds of exposure, with the exception of the one exposed to 10 kW/m^2, partially confirming the crude CHF estimate.

The PIR samples with and without the protective steel had lost between 4% and 17% and 7% and 34% after 1000 s of exposure of 10 kW/m^2 and 70 kW/m^2 , respectively. The SW samples with and without the protective steel behaved more unpredictable than the PIR samples and had lost between 1% to 5% and 3% and 9% also after 1000 s of exposure for 10 kW/m^2 and 70 kW/m^2 , respectively, as seen in Figure 3.6.

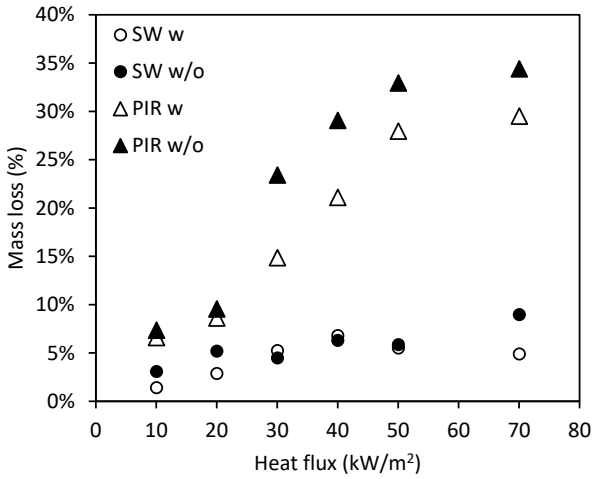

Figure 3.6: Mass loss relative to the initial mass for the SW and PIR samples studied with (w) and without (w/o) its protective steel.

The small mass loss from the SW samples meant that even small self-induced displacements in any of the thermocouples could influence the measurement of total mass. The mass loss of the SW and PIR samples, as seen in, Figure 3.7 and *Appendix – Additional Mass Loss Cone Graphs*, was, however, cleaned up for spikes that were unlikely to reflect the behaviour of the samples (e.g. a 10% momentarily drop). Despite igniting almost initially when subjected to the radiative heat source the unexposed PIR samples did not lose more than 34% of their mass over the duration of the experiments. This suggests an effective protective char formation, which was not seen in the small STA experiments.

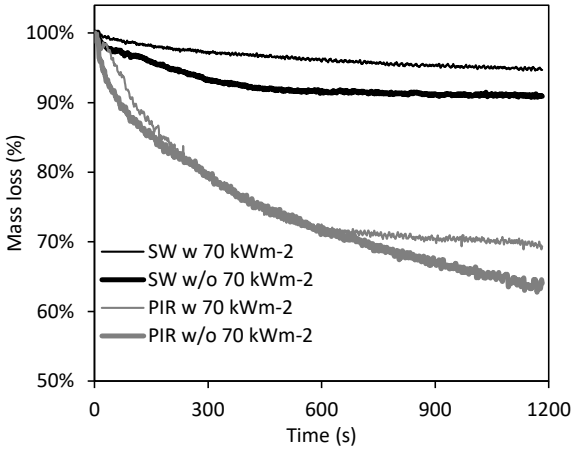

Figure 3.7: Mass loss for the SW and PIR samples studied with (w) and without (w/o) its protective steel while exposed to 70 kW/m².

The temperature measured 2 cm below the exposed surface in the protected PIR and SW samples reached steady state and quasi-steady state after 900 s for all incident heat fluxes, as seen in Figure 3.8 a) and b), respectively. The thermal equilibrium was reached faster for the PIR core than for the SW core despite the fact that the PIR has a lower thermal conductivity. The measured temperature throughout the thicknesses of both the PIR and SW samples for all the incident heat fluxes were similar in shapes to the representative curves 20 mm below the exposed surface, as shown in Figure 3.8 a) and b).

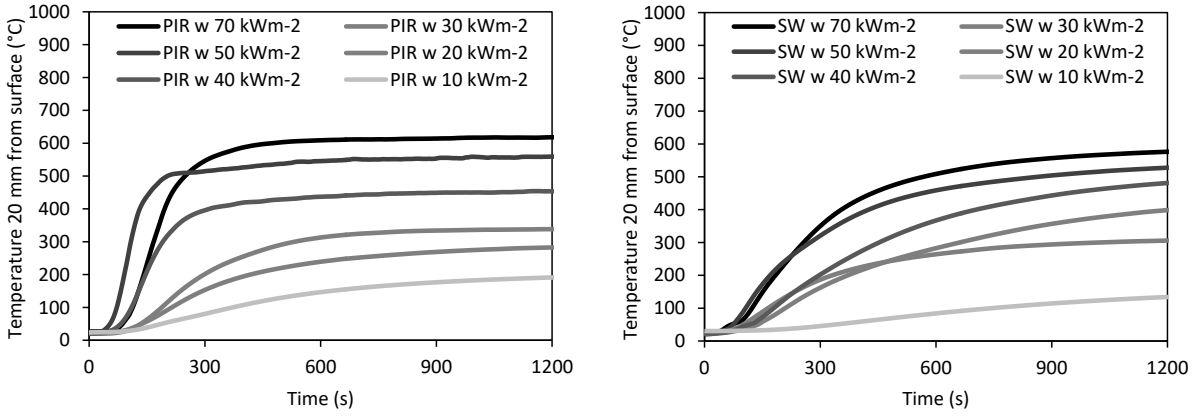

a) **b)**

Figure 3.8: Temperature measured 20 mm from the exposed surface for a) the PIR samples and b) for the SW samples.

The steady state temperatures 5 mm below the exposed surface ranged from 300 °C to 700 °C for 10 kW/m^2 to 70 kW/m^2, respectively. Following the STA results these temperatures could cause a mass

loss and a predicted exothermic reaction for both the SW and PIR cores. The measured temperature within the PIR samples did not reach steady state when unprotected and generally reached higher temperatures than the SW samples, as seen in Figure 3.9. For the SW cores the exothermic reactions were measured from 10 mm below the surface for 30 kW/m^2 to 70 kW/m^2, as seen in Figure 3.9 b). The exothermic reaction is recognizable by the slope of the curve changing from positive to negative, and thereby indicating the depletion of the binder, which was releasing the energy, and a transition towards steady state.

The unprotected SW and PIR samples showed the same behaviour as when protected by their respective steel faces for heat fluxes of 20 kW/m^2 and 10 kW/m^2, respectively, reaching their steady state equilibrium temperature. At heat fluxes of 20 kW/m^2 and higher the removal of the steel protection resulted in ignition, degradation and deformations for the PIR samples and steady state was not reached within 20 minutes. For unprotected SW samples exposed to heat fluxes of 30 kW/m^2 and higher, steady state only occurred much later (after the depletion of the binder), as seen in the *Appendix – Additional Mass Loss Cone Graphs*.

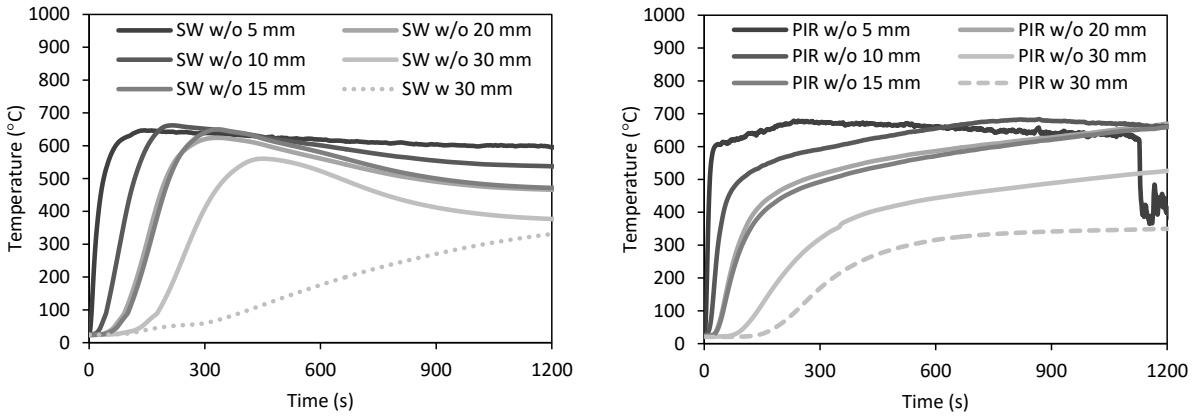

a) **b)**

Figure 3.9: Temperature measured for unprotected a) SW and b) PIR samples exposed to 40 kW/m² with the corresponding 30 mm measurement from the protected sample as reference.

When exposed to heat fluxes of 30 kW/m^2 and higher, both cores started to pyrolyze, though most noticeable for the PIR samples as they ignited. Steady state was reached 5 mm below the surface in the SW samples after being exposed for less than 200 s for all external heat fluxes. However, in-depth, the core heated up beyond the 5 mm steady state temperature, which was eventually

reached after 1200 s for the first 20 mm, while later for the measurements made at 30 mm from the surface, as seen in Figure 3.9 a) for 40 kW/m^2. The PIR sample, as seen in Figure 3.9 b), ignited after less than 1 min, and the thermocouple placed 5 mm from the surface detached from the core and the temperature dropped after approximately 1100 s. The PIR samples deformed quite significantly without their protective steel sheet and the distance to the heater was increased and the received heat flux decreased. However, as the sample ignited, additional heat flux was supplied by the flame, and the actual incident heat flux is therefore unknown. The displacement of the thermocouples due to shrinkage caused the temperature after 1200 s to be lower than the peak value for the thermocouples placed 5 mm in-depth, as seen in Figure 3.9 b), for the PIR core. The measured peak temperature for the unprotected SW samples were higher than their steady state temperature due to an exothermal reaction in the core. As the measurements at 15 mm and 20 mm in-depth were almost identical, as seen in Figure 3.9 a), the method for inserting the thermocouples could be improved as the exact location of the TCs were seemingly off by a few millimetres. The deformation of the polymeric cores without their protective steel-sheets were significant and the thermocouples were not at their intended depth as the height of the sample was reduced while exposed to the heat.

The thermal conductivity of the PIR material, and of polymeric insulation materials in general, is lower than the thermal conductivity of SW, and mineral wools in general, at least at ambient conditions while the integrity is not compromised. The final temperature reached after obtaining steady state or quasi-steady state in the PIR was, nevertheless, higher for 56% of the measurements when compared to the SW. This was after both 18 min and 20 min for the protected samples where the temperatures were within 7% of each, indicating a thermal penetration and steady state at a distance of 30 mm from the exposed surface. The steady state was obtained faster for the PIR samples compared to the SW samples. This was attributed to the lower thermal inertia rather than the conductivity as the bulk mass of the PIR was much less than the SW due to the different densities. By ignoring the effects associated with the thermal inertia, the lower conductivity of the PIR should otherwise have made the PIR cores reach steady state later than the SW cores. The thermal inertia is a concern for combustible wall coverings because it will lower the temperature required for a thermal runaway to occur, as reported by Poulsen and Jomaas [189] and Graham et al. [190]. This happens because the combination of the low thermal inertia and low conductivity results in the material requiring less energy to heat up and at the same time it conducts the heat away slowly. For a combustible material it means the temperature in the core increases fast at the

surface and with enough external energy ignition can occur. The core material is, however, not left unexposed when used as a wall panel and the internal steel face has a much higher thermal inertia and non-combustibility and as long as its integrity is maintained ignition should not be of concern.

The temperature development in the experiments with SW cores without steel showed a significant increase in temperature, caused by the core thus indicating a heat generation potential within the core that is initiated solely by the net heat flux penetrating from the surface. The difference of the measured temperature 30 mm from the surface between the samples with and without steel, as seen in Figure 3.9 a), corresponds to a quantity of energy required to heat up that specific mass of core.

The importance of the steel face with respect to the mass loss was found to be insignificant as only small amounts additional mass where lost when left unexposed. However, this is skewed as the unprotected samples shrank and the distance to the external heat source increased. The ignition of the PIR samples was significant when left unprotected and the cores ignited instantly at heat fluxes higher than 10 kW/m^2. The SW core showed as much as 10 % mass loss when left exposed and subjected to 70 kW/m^2 for 1200 s without igniting. Deflections were not seen at this scale but are expected in compartments as vertical and horizontal displacements are restricted leaving only the transversal axis for stress relief. If the thermal expansion is great enough, the steel face will buckle. Buckling behaviour will increase the accessibility of oxygen to the core and potentially increase the mass loss even further as the shielding effect is gone. Previously the SBI test (EN 13823-1) and the cone calorimeter [64] did, however, not provide an accurate prediction of the behaviour at full scale [40] and too much emphasis was not put on the micro and macro scale experiments. These experiments merely served as a way of studying the behaviour of the products under elevated temperatures and controlled conditions.

Table 3.3 provides an overview of the mass loss cone experiments with respect to the peak temperature and after 1200 s. Experiments where the maximum measured temperature was more than 4% higher than the temperature after 1200 s is marked with grey. This allows for a quick overview of which heat fluxes at which depths caused an exothermic reaction in the core.

Table 3.3: Summary of the mass loss cone experiments with respect to steady state temperature, peak temperature and mass loss as a function of incident heat flux and presence of steel-facing. The grey hatched cells indicate which experiments where an exothermal reaction was measured. This incude internal temperature increase and surface burning.

			T(max) / T(1200 s)						Mass	
Heat flux (kW/m^2)		Core type	0 (mm) (°C)	5 (mm) (°C)	10 (mm) (°C)	15 (mm) (°C)	20 (mm) (°C)	30 (mm) (°C)	m_0 (g)	ML (%)
10	w	SW	272 272	263 262	240 238	222 221	136 134	103 101	92.8	1%
20	w	SW	391 390	376 376	335 335	306 306	298 298	298 298	93.7	3%
30	w	SW	506 504	500 498	475 473	416 412	403 399	290 284	105.	5%
40	w	SW	585 581	571 571	535 533	499 495	485 481	338 331	99.9	7%
50	w	SW	602 601	600 600	554 553	529 528	508 507	508 507	83.4	6%
70	w	SW	714 714	696 696	641 640		578	576 473	471	5%
10	w/o	SW	338 334	331 330	329 328	296 295	224 223	166 164	81.4	3%
20	w/o	SW	472 461	468 461	424 420	380 379	365 364	282 282	85.1	5%
30	w/o	SW	568 546	556 532	542 492	520 450	499 432	398 336	82.6	4%
40	w/o	SW	647 604	647 595	662 537	624 466	650 472	561 377	86.0	6%
50	w/o	SW	690 670	701 662	709 594	676 539	675 529	627 424	88.7	6%
70	w/o	SW	788 748	771 745	760 696	746 635	736 624	674 472	85.0	9%
10	w	PIR	285 284	278 277	257 257	236 236	193 191	145 143	48.8	7%
20	w	PIR	381 376	376 372	336 336	293 292	283 283	196 196	53.5	9%
30	w	PIR		447 437	403 401	359 358	338 338	219 217	217	15%
40	w	PIR	530 530	554 544	492 491	454 454	439 439	439 439	36.6	21%
50	w	PIR	605 604	657 602	562 561	560 559	519 518	519 518	42.2	28%
70	w	PIR	734 734	704 703	693 692	639 638	619 618	515 514	44.5	30%
10	w/o	PIR	238 193	336 329	288 287	240 239	234 234	165 164	54.5	7%
20	w/o	PIR	624 401	523 481	511 508	492 488	460 459	301 298	48.8	7%
30	w/o	PIR	705 581	623 576	636 632	613 611	631 622	446 444	36.9	23%
40	w/o	PIR	800 508	679 414	684 661	674 669	662 660	532 526	41.1	29%
50	w/o	PIR	775 552	728 639	759 555	796 715	789 718	632 626	42.1	33%
70	w/o	PIR	824 548	842 571	829 643	837 791	826 788	611 596	38.8	34%

3.1.3 Gross Calorific Values

The gross calorific value provide an upper limit for the additional fuel load for a compartment constructed with these products and is presented for the sizes of compartments studied, as seen in Table 3.4. The uncertainty with respect to the total heat of combustion was around 5%. The polymeric cores were found to contain more than 10 times the energy content per unit mass as the SW. The density of the SW is, however, four times greater than the polymeric foam, the actual energy content difference is therefore less than five times greater per cubic meter, as seen in Table 3.4.

Table 3.4: The complete heat of combustion for the three studied core materials with the corresponding additional fuel load per floor area for various compartments with 0.10 m thick panels.

		PIR	PUR	SW
ΔH_c	(MJ/kg)	29.1 ±0.5	23.1 ±0.5	2.1 ±0.1
ΔH_c	(MJ/m^3)	1164 ±20	924 ±20	252 ±12
Q (2.4 m x 3.6 m x 2.4 m)	(MJ/m^2)	534	424	116
Q(1:2 scale)	(MJ/m^2)	565	448	122
Q(2:5 scale)	(MJ/m^2)	581	461	126
Q(1:5 scale)	(MJ/m^2)	663	527	144

From the Swedish study by Petersson et al. from the 1970s [191], two and three bedroom dwellings with a kitchen, offices, schools and hotels had fuel loads of 168 MJ/m^2, 149 MJ/m^2, 709 MJ/m^2, 96 MJ/m^2, 82 MJ/m^2, respectively. The data from literature is for compartment with assumed inert compartment boundaries and the addition of fuel from the panels is, theoretically, equivalent to that from the expected inventory present in 80% of the designs, as seen in Table 3.4. This means a fire safety engineer has to be aware of the potential for a different fire dynamic compared to traditional compartment fires. The walls and ceiling have the potential to contribute to the fire with additional fuel and thereby prolong the fire duration and thus increase the duration of the thermal attack on the enclosure, structure, occupants and increase the risk of injury to bystanders. The additional fuel in a compartment will get heated by the initial ignition source and can thereafter contribute with additional heat release and to the formation of a hot smoke layer accelerating the contribution from the enclosure boundaries back to all the fuels. Dwellings with panels with SW have a significant increase in their total fuel load while larger compartments have relatively less fuel load added. Furthermore, larger compartments such as warehouses and storage facilities, could have much higher fuel loads per floor area and the contribution from the walls would then be relatively smaller than presented in Table 3.4.

3.2 General Observations for the Compartment Experiments

At all scales, the compartments constructed with SW panels showed little or no sign of a thermal runaway with respect to HRR generated beyond that of the gas burner. Smoke from the interfaces between the ceiling and the corner situated directly above the burner was observed pouring out of the doorway for the 1:5, 1:2 and full scale, as seen in Figure 3.10 a) to c). During the 1:2 and full scale experiments with SW (E28 and E30) the gas burner malfunctioned releasing too much propane and losing pressure just after the initiation of the increase to the second burner step, respectively, as seen in Figure 3.10 a) and b), respectively. Minor exothermal reactions in a 1:5 scale experiment with SW core occurred just as the experiment had ended as seen under the cone for samples without steel protection exposed to 30 kW/m^2 or more. This was observed as a plateau in the temperature as a function of time measured 40mm and 20 mm from the internal boundary and seen in Figure 3.16.

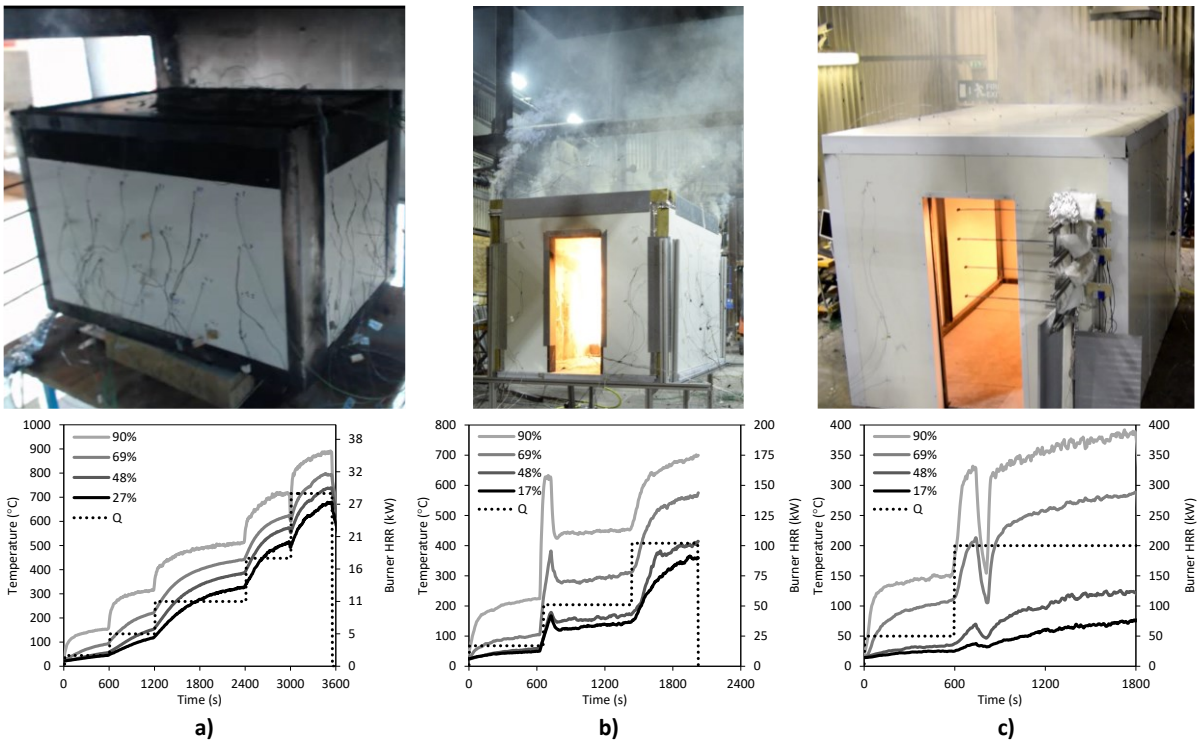

Figure 3.10: Smokeproduction and recorded temperatures at a distance from the ground of 90%, 69%, 48% and 27% of the height of the compartment for three compartment experiments with SW panels at a) 1:5 scale (E20), b) 1:2 scale(E28) and c) full scale (E30).

The PUR panel were classified as B-s3,d0, which translates to “limited contribution to flashover” while producing unlimited smoke unlike the PIR panels, which has a B-s1,d0 classification. The PUR product was only studied once, and at 1:5 scale, as it was deemed too dangerous for larger scale experiments due to the significant HRR and Smoke Production Rate (SPR) compared to the PIR and SW experiments, as seen in Figure 3.11 a) to d).

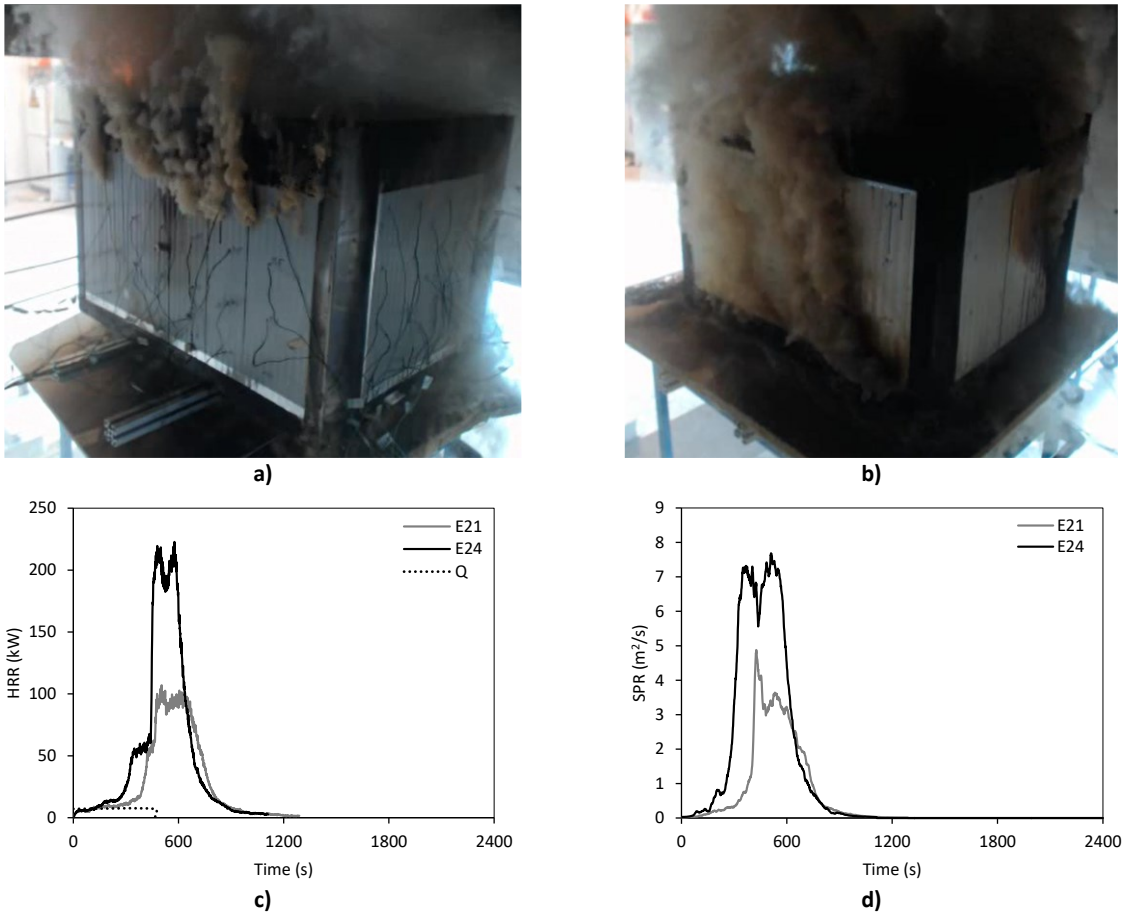

Figure 3.11: PIR (E21) and PUR (E24) 1:5 scale compartment experiments. Pictures of a) PIR at the time of SPR_{max}, b) PUR at the time of the second SPR peak, c) HRR measurements for E21 and E24, and d) SPR measurements for E21 and E24.

The two 1:2 scale PIR experiments conducted with 6 cm and 10 cm thick panels (E26 and E27, respectively) were subjected to two different fire scenarios and both failed with significant quantities of yellow and black smoke released prior to and after flashover and failure, as seen in Figure 3.12 a) and b), respectively. The full scale PIR compartment failed, as seen in Figure 3.12 c), shortly after the HRR of the gas burner was increased from the initial 100 kW to 300 kW.

a) b) c)

Figure 3.12: Photos from the PIR experiments as flames emerge from the doorway for a) E26 from the back, b) E27 from the front and c) E29 at full scale from the front.

3.3 Detailed Results for the Compartment Experiments

3.3.1 1:5 Scale

The steel-faced panels were delivered in standard sizes for construction (1.0 m x 3.6 m, 1.2 m x 3.0 m for the PIR and the SW, respectively) and were cut on site to fit the sizes of the respective compartments. Six 1:5 scale experiments (E3, E4, E7, E8, E11, E12) were conducted with joints in the mid-span and their seal of their joints were studied by comparing the compartment temperature and HRR to those from the compartments without mid-span joints (E1, E2, E5, E6, E9, E10). The external frame, as sketched in Figure 3.13 a), along with the aluminium tape and flashings along the ceiling edge were effective at confining the gases for these baseline experiments. The smoke emanating from other openings than the doorway was less noticeable for the SW experiments at 1:5 scale as compared to the other scales, although the smoke production rate (SPR) was generally very low during all the experiments with SW panels.

Prior to their flashover, all the experiments with polymeric cores were showing signs of integrity failures, with smoke coming out of other openings than the doorway. Most often that smoke came from the ceiling-to-wall interface at the back of the compartment. Leaks along the floor, as seen in Figure 3.13 b), were also observed, suggesting a combination of a non-perfect seal to begin with, integrity failure and deflections or rotation of the panels allowing for this flow of gases.

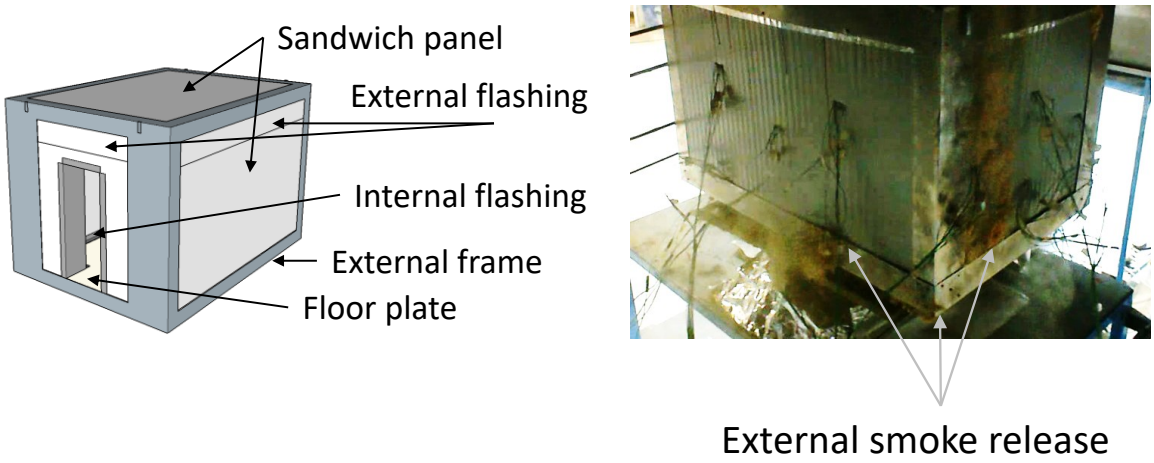

a) b)*

Figure 3.13: a) Sketch of the 1:5 scale frame and b) photo showing external smoke being released due to pressure differences (E10). *Brightness and contrast increased by 40%.

The external smoke production went through three distinguishable stages; 1) after each increase of the HRR of the burner white smoke would leak out of the compartment through other openings than, and as well as, the doorway, 2) just prior to the compartment flashing-over white and yellow smoke emanating from one or more leakages would fill the vicinity of the experimental-setup. The cool smoke, without buoyancy, would hang around and spread radially rather than vertically, and 3) when the compartment fire was fully developed the smoke would undergo a transition becoming gradually more brown, as seen in Figure 3.13 b), and eventually black and often igniting.

The first series of 1:5 scale compartment experiments were designed to study the thermal penetration through the core material and the ability of the joints and gaskets from the manufacturers to seal the compartment during the compartment fires. Additionally, the effect of the thermal conductivity on the temperature of the compartment was studied, because the thermal resistance of the 6 cm thick PIR core was relatively close to that of the SW, 0.035 $W/m^2 \cdot K$ and 0.038 $W/m^2 \cdot K$, respectively. This comparison assumes the core materials do not contribute to the temperature and maintain the same conductivity throughout the temperature range in the experiment. Furthermore, the contribution from the 10 cm thick and 6 cm thick PIR panels was of interest and if the additional 4 cm of core material would be shielded by the forming char.

The temperature measured near the ceiling in the SW(E1-E4) and PIR(E5-E8 [10 cm] and E9-E12 [6 cm]) compartments , as shown in Figure 3.14, followed the stepwise increase of the HRR from the burner for both the baseline and modified fire scenarios. After the first burner step the SW

compartments with joints were in average less than 6°C cooler than the SW compartments without joints and in average 4°C cooler than the 6 cm thick PIR compartments and less than 10 °C cooler than the rest of the compartments. Overall, the SW compartments were cooler on average than the PIR compartments prior to the third burner step, as seen in Table 3.5. The PIR compartments had various degrees of exothermic reactions compared to the SW, as seen by the increase in the temperature in the compartment in Figure 3.15. At the end of the second burner step the SW compartments with and without joints were 300 °C and 281 °C, respectively, which, according to the STA result, is high enough for the first reaction to take place. The temperature in the compartment did, however, not increase. Shortly after the initiation of the third burner step as a result of the contribution from the core materials the PIR compartments failed whereas the SW compartments continued to heat up in a similar way as for the previous two steps.

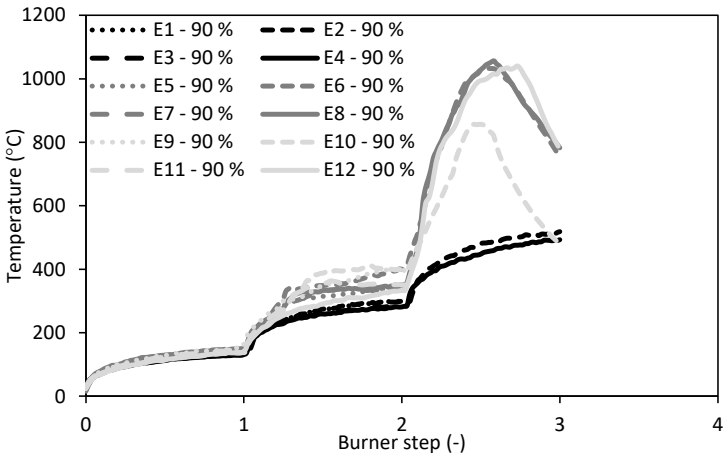

Figure 3.14: Temperatures measured 10% from the top of the compartment for E1-E4 (SW), E5-E8 (PIR, 6 cm) and E9-E12 (PIR 10 cm).

Table 3.5: Compartment temperatures after the first and second burner step.

	Step 1 (°C)	Step 2 (°C)
E1 - 90 % (SW)	140	302
E2 - 90 % (SW)	140	300
E3 - 90 % (SW)	133	286
E4 - 90 % (SW)	131	281
E5 - 90 % (PIR)	146	337
E6 - 90 % (PIR)	146	400
E7 - 90 % (PIR)	145	336
E8 - 90 % (PIR)	150	351
E9 - 90 % (PIR)	152	389
E10 - 90 % (PIR)	137	394
E11 - 90 % (PIR)	146	351
E12 - 90 % (PIR)	139	334

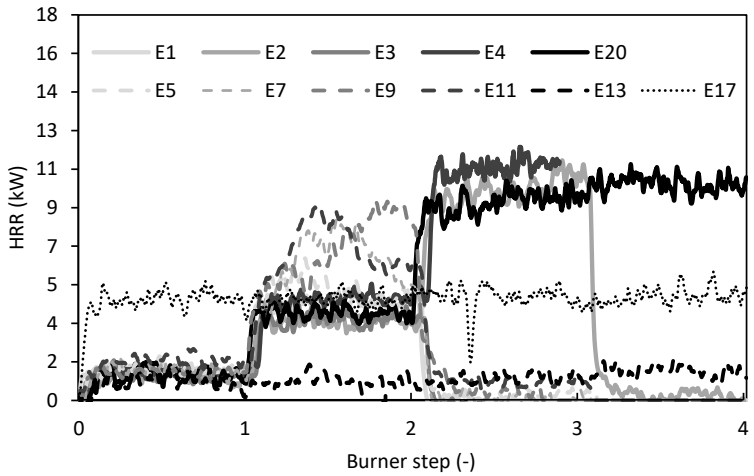

Figure 3.15: HRR measurements for the 1:5 scale compartments that did not fail (E1-E4 and E20 had SW cores, while E5 and E7-E17 had PIR cores).

The temperature developed a bit differently for E10 compared to the other failing compartments as a significant portion of the smoke from the panels leaked from the ceiling panel and therefore released its heat externally. The temperatures measured near the ceiling level in E6, E8 and E12, with and without joints, and with 6 cm and 10 cm thick panels were, however, similar throughout the duration of the experiments, as seen in Figure 3.14. When failure occurred, the flow of gas was turned off and the following decrease in the temperature of the compartments were a results of decreasing combustion processes. The effect of the difference between the thermal conductivity and thermal resistance of the SW and PIR panels was not conclusive as the temperature in the compartments with joints mid-span in 9 of the 12 experiments for the first two burning periods was lower and seems more dominant over the conductivity.

All the temperatures measured on the internal surface for E2, except for the cluster marked “B5” in Figure 2.13 a), which are shown in Figure 3.16, were below 300 °C for the first two burner steps, as seen in Figure 3.17. The rate of which the thermocouples heated up was slower in the compartment experiments compared to the samples studied under the incident heat flux suggesting an incident heat flux lower than 10 kW/m^2 in the compartment. It is, however, also possible that the thermocouples were not in contact with the internal surface as intended. The delay between increase of the burner and measured temperature is low, suggesting they were in fact, generally, touching the internal surface as intended. A few of the thermocouples measuring very low temperatures and the late registration of the termination of the gas burner suggests they were, however, not all placed correctly.

The thermocouples placed throughout the walls of the SW compartments identified the exothermic reaction, just as they did in the unprotected SW core when exposed to an incident heat flux higher than 20 kW/m^2 in the cone experiments. Upon turning off the gas after the third burner step (30 min), the in-depth thermocouple generally decreased immediately and so did the thermocouple placed at a depth of 80 mm. The temperature at 80 mm was, however, not decreasing as rapid as the internal temperature and steady state was observed in the temperature profile, as seen in Figure 3.16. The temperature in the core material on both sides of the thermocouple was lower and the temperature should be somewhere in between and, if the SW core was completely inert and only conducting the heat, not higher. With the STA in mind, two significant reactions were identified for the SW around 272 °C and 505 °C. The temperature was higher than both of those temperatures and an exothermal reaction could have occurred as indicated by the temperature profile. This occurred after the experiment was terminated and was not measured prior in any of the other experiments and is therefore not a concern for the validity of the heat transfer model.

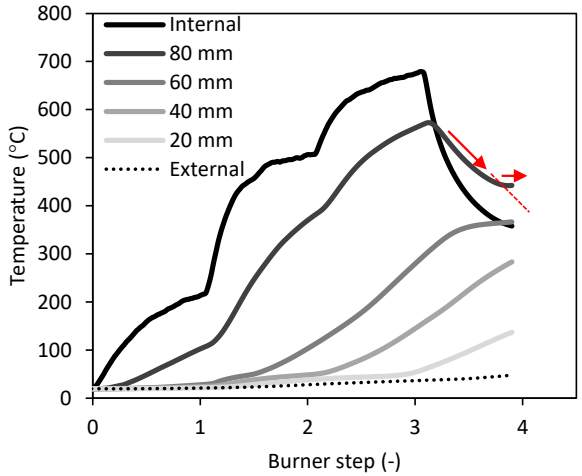

Figure 3.16: In-depth temperatures for cluster "B5", as seen in Figure 2.13 a), for E2 with a core of SW.

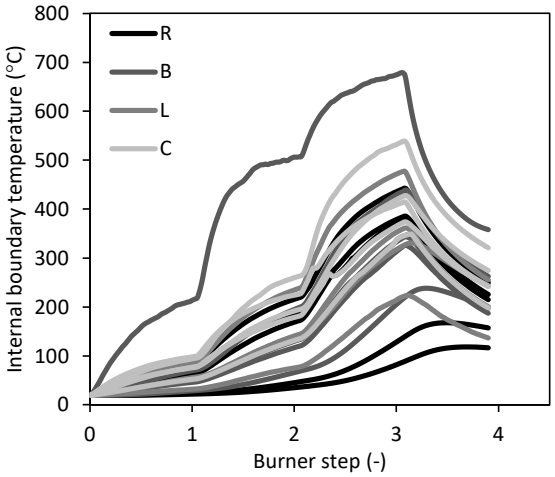

Figure 3.17: Internal surface temperatures from E2 with a core of SW. "R", "B", "L", "C" corresponds to thermocouples placed in the Right, Back, and Left walls and Ceiling, respectively.

The SW panels did not show any sign of contribution towards the temperature in the compartment but did show trends of an internal heating within the walls adjacent to the burner. The PIR compartments in E9 and E11 both reached pHRR values of 9 kW without causing a thermal runaway and showed signs of decreasing or stabilization, respectively, prior to the burner being turned off. The compartment with 10 cm thick PIR panels exposed to 5 kW (equivalent of 300 kW at full scale) for 40 min (E17) without causing a thermal runaway was an outlier as compartment subjected to

similar fire scenarios (E14 and E18), failed after 14 and 15 min of exposure to 5 kW, respectively. The behaviour of the compartment in E17 was attributed to an inaccurate placement of the gas burner. Opening the safety valve on the tube connecting the gas burner with the flow meter caused the burner to tilt away from the side of the wall. The importance of the impingement of the flames from burner onto the walls is recognized and considered a paramount feature of the experimental setup to ensure consistency and accurately maintaining a worst case scenario.

The mass and mass loss of the compartments were measured as a function of time in the 1:5 scale compartment experiments (except for E4, E14 and E20). The experimental setups consisting of the steel frame, a non-combustible floor, steel-faces with a few micrometres thick coating were all considered of negligible contribution and any mass loss measured was attributed to be the core material pyrolysing. This was in an effort to determine the effect of the char protecting the virgin material by maintaining as much of the initial mass as possible. The peak mass loss rate (pMLR) for the PIR compartments was fairly constant at 6.57 g/s ±0.46 g/s for the 13 compartments that failed. The pMLR for the PUR compartment was 11.03 g/s and almost 70% higher. Scaling the thickness of the wall meant a reduction in the burner duration, as presented in 2.1 - *Scaling Analysis*. Experiments with 6 cm thick panels have been plotted to match the burning periods of the 10 cm thick panels by the non-dimensional representation of the burner duration, as seen in Figure 3.18.

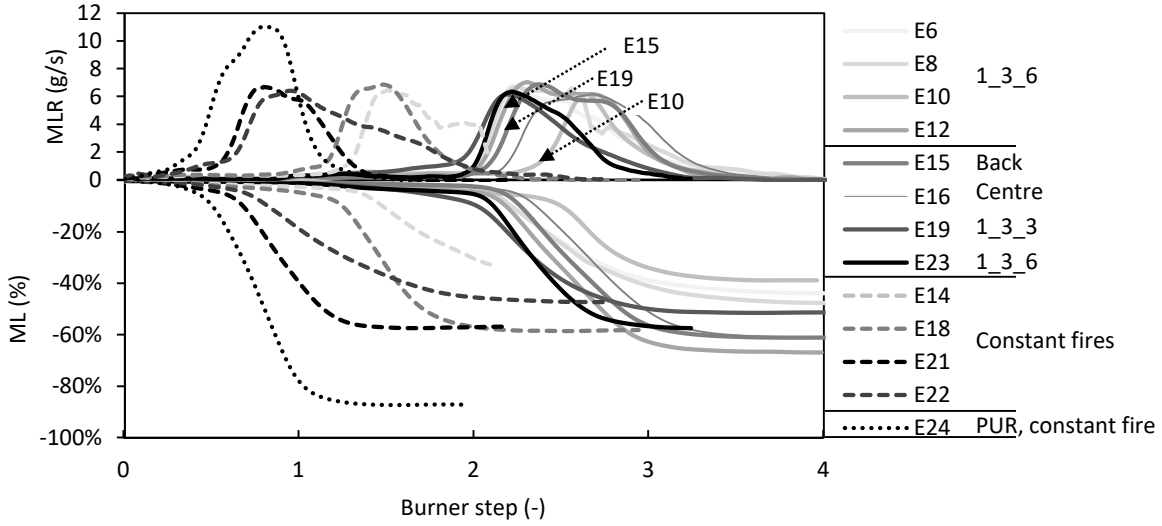

Figure 3.18: The ML (above the x-axis) and MLR (below the x-axis) for the 12 compartments with PIR cores and a single one with PUR all failing. The x-axis is non-dimensional with respect to burner steps. E14, E18, E21, E22 (all with PIR), are experiments with constant burner scenarios and are marked with dashed lines while E24 (with PUR) is also with a constant burner step and marked with dots. The burner step of the constant fires are scaled with respect to 600 s duration burner steps.

The PIR panels lost between 39 % and 67 % for E10 and E12, respectively, E10 was already identified as an outlier due to the large smoke released externally and lower compartment temperature fitting well with the reduced mass loss. The PUR panel lost 87 % of its initial mass which also matched the visual observations made during disassembly where the core material was burned through and left a seemingly ineffective light porous char. Many of the PIR panels had, however, still virgin core material along the corners or at the very least a solid char with some strength left unlike the PUR. Once the compartments failed and the fire was fully developed the pMLR and ML were the same for the constant and ramped up fire scenarios, as seen in Figure 3.18, where E18, E21 and E22 all lose approximately the same mass as E19 and E23. This was expected as the compartment fires were controlled by the fuel in the boundaries rather than the gas burner as well as the availability of oxygen restricted by the identical sized of the doorways.

The measured HRR corresponds very well with the MLR in terms of overall trend. Smoke that ignited when pouring out though the ceiling-to-wall joints, which converted the otherwise CO and soot rich smoke to varying degrees into CO_2 and H_2O, was releasing more energy. This meant that for the same pMLR the HRR could be higher, as seen for E14 and E18 or E19 and E23 between Figure 3.18 and Figure 3.19. Based on the steady state HRR measured for the experiments, the supply of oxygen through the doorway to the combustion zone was approximated to 4.6 g/s prior to any external ignition. Theoretically, for post-flashover fires, the flow of air through an opening can be determined as simply as $0.5 \cdot A_0 \cdot \sqrt{H_0}$ [145] in kg_{air}/s. The mass fraction of oxygen in air is 0.23 wt% and the theoretically oxygen supply is therefore 4.7 g_{ox}/s, equivalent of 61 kW, assuming complete combustion to CO_2 and H_2O matching the experimentally determined range.

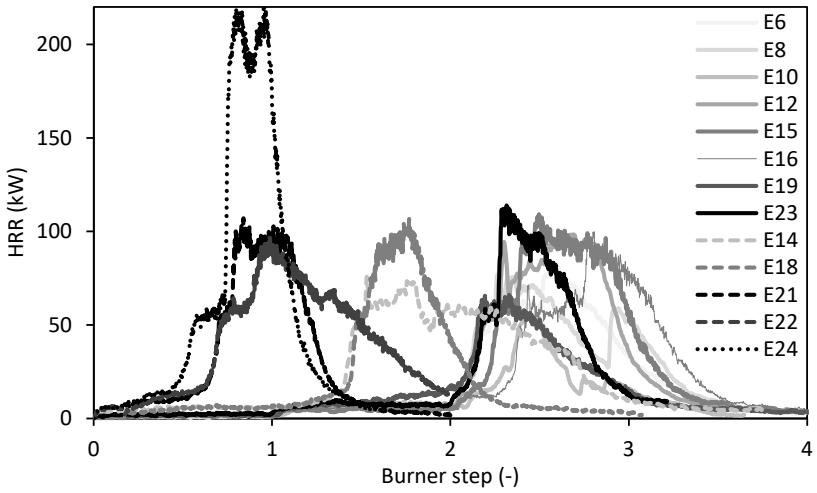

Figure 3.19: HRR measurements for the 13 1:5 scale compartments with polymeric cores with significant contribution. Solid lines denote modified fire scenarios of 2 kW, 5 kW, 10 kW, except for E19 which was 2 kW, 5 kW, 5 kW, dashed lines denote constant fires with E14 and E18 as 5 kW and E21, E22 and E24 (PUR) as 7 kW.

The mass loss was 0.5% for the experiments with SW cores (E1, E2, E3 (no mass was acquired for E4) that all withstood their respective fire scenario. The mass was lost with a constant rate for each of the three burner intensities, as seen in Figure 3.20 by the constant slopes. The four PIR experiments subjected to the baseline fire scenario all had an increase in mass loss rate after each of the two increases in gas burner intensities but never exceeded 1 g/s and shortly followed by a decreased with a total mass loss between 220 and 240 gram. The compartments subjected to constant fire scenarios with 2 kW(E13) and 5 kW(E17) lost 75 g and 300 g, respectively, and in average lost a constant of 0.03 g/s and 0.12 g/s, respectively, corresponding to 1 % and 7.5% total mass loss after 40 min, respectively, as seen in Figure 3.20.

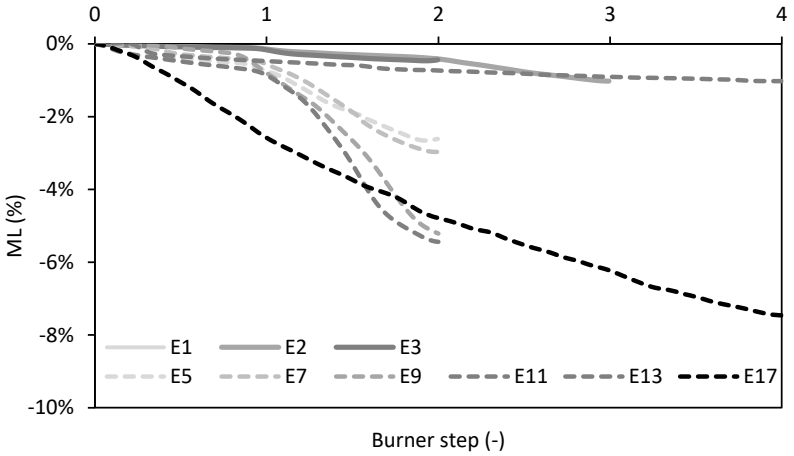

Figure 3.20: Mass loss measured for 1:5 scale experiments with negligable contribution for the three SW panels (E1-E3) and the six compartments with PIR panels (E5, E7, E13, E17 [10 cm] and E9 and E11 [6 cm]).

By conducting experiments with constant fire scenarios for the 6 cm and 10 cm thick panels the effect of the thickness was found to be insignificant with respect to the time of the thermal runaway. The increased thickness also meant an additional fuel load and the 10 cm thick panels generally released more energy, as seen in Figure 3.21, during E14 and E22 than the rest of the PIR experiments. The compartments in E6 and E8 were, however, also constructed with 10 cm thick panels and showed the same THR as the experiments conducted with the 6 cm thick panels and the relationship between THR and panel thickness was not conclusive. The average effective heat of combustion over the full duration of the experiments, ΔH_e, was 11.6 MJ/kg ±4 MJ/kg and 15 MJ/kg for the PIR and PUR, respectively. Prior to flashover, the combustion efficiency, χ, was found to be as low as 20% and post flashover increase up to 50% and all the way up to 80% in the decay phase. ΔH_e for both polymeric cores are significantly lower than the ΔH_c found in Section 2.2.1.3 *Gross calorific content* and χ was in average as low as 39% ±14% and 64% for the PIR and PUR cores, respectively.

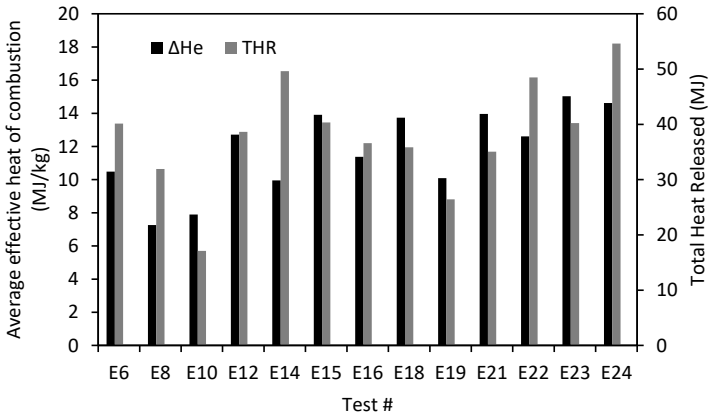

Figure 3.21: The average ΔHe and THR for the compartments with a thermal runaway at 1:5 scale experiments.

E12, E15 and E16 were all experiments with 6 cm thick PIR panels, but with the burner located in the corner, at the middle of the back wall and in the centre of their respective compartments, respectively. The time of failure had a strong correlations to the area impinged by the flames. E12 failed first followed by E15 and then by E16, which took the longest time to reach failure, as seen in Figure 3.22. The two experiments with the burners located in the corner and at back wall behaved similarly showing a rapid fire growth shortly after the initiation of the third burner step. For the compartment with the burner in the centre, the third burner step could be identified by the plateau prior to the occurrence of the thermal runaway.

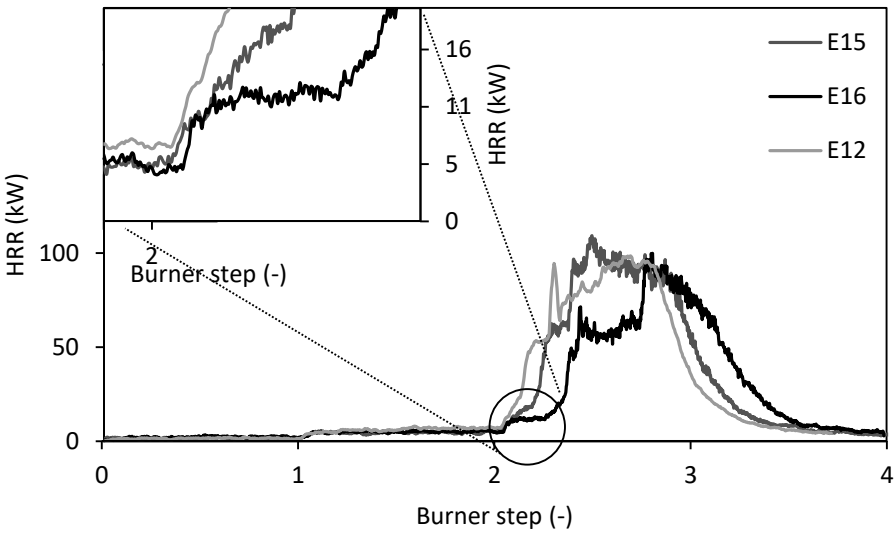

Figure 3.22: The HRR for E12, E15 and E16 which were constructed with PIR panels but the burner located in the corner, at the back wall and in the centre of the compartment, respectively.

3.3.2 2:5 Scale

The 2:5 scale experiment with a core of SW (E25) was subjected to the modified fire scenario with the aim of comparing the temperatures and net heat flux across scales. The compartment was constructed with panels covering the full length and width without mid-span joints, just as E1, E2 and E20. The temperature difference for compartments with joints at 1:5 scale showed no significant temperature difference and the lack of mid-span joints were not considered a requirement for cross-scale comparisons. The HRR measurement did not show a significant contribution from the SW core material as the measured HRR matched the HRR provided by the gas burner except for the very end where the flow to the burner was turned off and a “tail” of heat was measured, as seen in Figure 3.23.

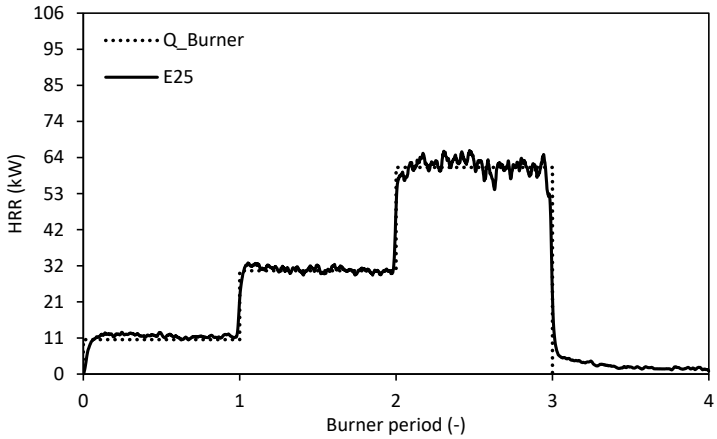

Figure 3.23: The HRR for E25 in solid line with the HRR of the gas burner marked with the dotted line.

The gas at the top of the compartment heated up rapidly after each burner step increase, as seen in Figure 3.24 a), whereas a lot of the wall temperatures increased beyond that. The highest, lowest and any inconsistent measurements made by the thermocouples in the right (R), back (B), left (L), ceiling (C) and front (F) walls are presented in Figure 3.24 b). The thermocouples in the walls close to the gas burner heated up the most, as expected, and some of the ceiling and left wall thermocouples heated up beyond that of the compartment gases, as seen in Figure 3.24 a).

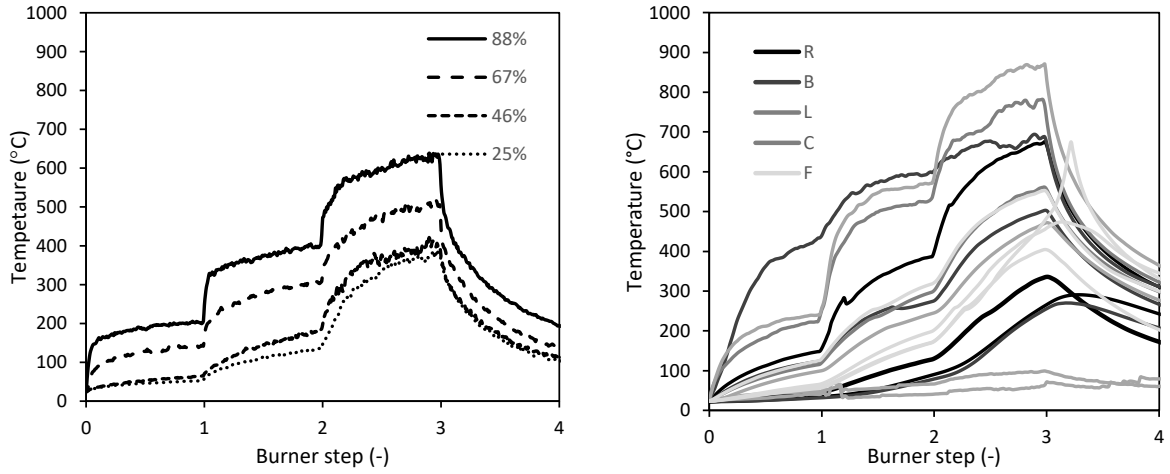

Figure 3.24: The temperature for E25 measured in a) within the volume of the compartment and b) the temperature of all the internal steel faces. "R", "B", "L", "F", "C" corresponds to thermocouples placed in the Right, Back, Left, and Front walls and Ceiling, respectively.

Two thermocouples broke shortly after the increase to the second burner step and a thermocouple in the front wall of the compartment increased unexpected after the gas was tuned off. Additionally,

two thermocouples placed in the backside and right wall, respectively, showed a dampened temperature increase suggesting they were not in contact with the internal steel-face, as intended.

The temperatures measured in the compartment ramped up faster as well as reached a higher temperature at the four measured location along the height after each increase of the HRR of the gas burner than in the 1:5 scale, as seen in Figure 3.25. The gas near the ceiling was 70 °C, 100 °C and 125 °C higher during the first, second and third burner step, respectively, corresponding to 34%, 26% and 20% higher temperatures for the 2:5 scale compared to the 1:5 scale. Besides the values, the time it took to reach the steady state or nearly steady state were very different between the 1:2 and 2:5 scaled compartments. The internal temperatures of the steel-face were also higher than those measured in the 1:5 scale experiments and the relative size of the fire from the burner did not match across the factor two in scales. The heat transfer in the compartments will be discussed below in Section 3.3.7 - *Heat Transfer Analysis* with the focus on the conductive and convective heat losses though the solid boundaries and the doorway, respectively.

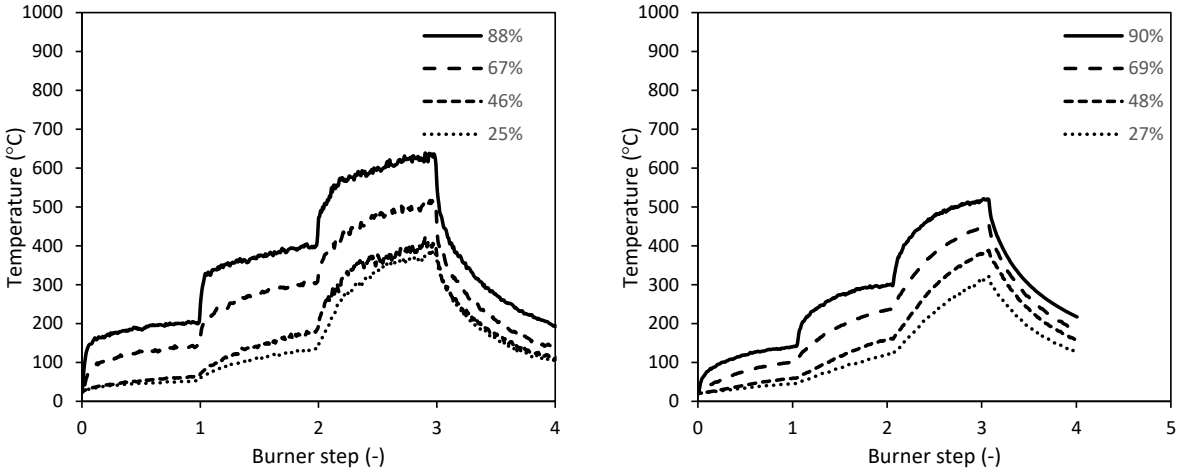

Figure 3.25: Temperature along the centre of the compartment for a) 2:5 scale (E25) and b) 1:5 scale (E2) experiment with SW panels.

3.3.3 1:2 Scale

The two 1:2 scale experiments conducted with PIR panels (E26, E27) and the one with SW panels (E28) were all constructed with joints. There were three focus areas for these experiments:

- Conduct an experiment with SW panels subjected to a modified fire scenario to compare with E2, E4, E20 and E25 (Burner scenario: "1_3_6", see Table 2.12)
- Conduct an experiment with PIR panels subjected to a constant HRR from the burner to compare to the time to failure from E18 and E21 (Burner scenario: "3_3" and "4_4", respectively, as seen in Table 2.12).
- Conduct a baseline experiment with PIR panels to compare with the temperature measurements from the first two burner steps from E19 (Burner scenario "1_3_3", see Table 2.12).

For the SW experiment the HRR provided by the gas burner was incorrectly ramped up when transitioning from the first to the second step resulting in an increased compartment temperature following the trend of the provided HRR, as seen in Figure 3.26 a) and b), respectively.

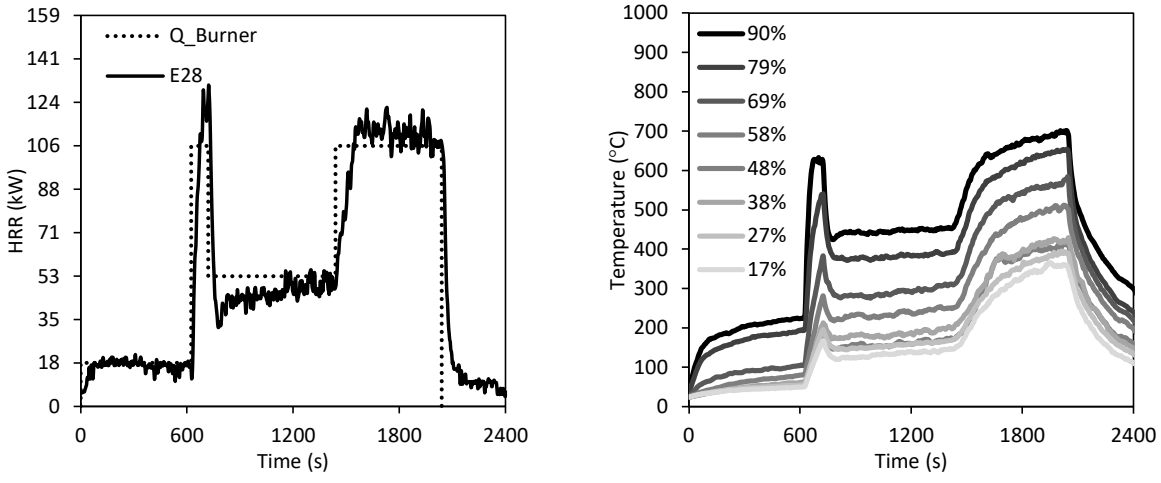

Figure 3.26: Results from E28 with SW panels with a) the measured HRR and burner input, and b) the temperature measured in the centre of the compartment at various distances from the floor. *The HRR correction can be found in *Appendix C*.

The measured HRR does not show any notable contribution from the SW core relative to the anticipated contribution from the burner. The unintended increase of the burner caused a rapid heating which caused the coating of the steel-sheets to flake prematurely and, as noted earlier, led

to significant smoke production. The HRR at the highest burner step also increased beyond that of the burners further supporting the contribution of the panels to the measured HRR. However, the fluctuations in the HRR measurements decrease its certainty regarding the magnitude of the contribution from the core. The accidental ramp up caused the gas temperatures to reach steady state immediately and once the HRR was decreased the temperature was sustained which was not seen for the other two steps where the compartment temperatures ramped up just as seen in the 1:5 scale experiments. The temperatures in the hot gas layer in the compartment were higher than measured at 1:5 scale suggesting a larger fire relative to the size of the compartment and not in line with the scaling theory. With the current data available this can suggests one of two possibilities; 1) the 1:5 scale is an inappropriate scale, or 2) the fire of the 1:2 scale experiment was, relative to its size, too big.

The similarity of the results at 1:5 scale between 10 cm and 6 cm thick PIR panels with respect to the HRR and compartment temperature was used as the justification for conducting two different fire scenarios in the 1:2 scale compartments. E27 was conducted with a constant HRR from the burner of 53 kW, equivalent to 300 kW at full scale ($\dot{Q}^*$=24), and compared with the two constant fire scenarios studied at 1:5 scale. Their dimensionless HRRs and actual HRR was 24 and 5.4 kW, and 32 and 7.1 kW for E18 and E21, respectively. The time for failure varied a great deal across the scales and fire scenarios. E21 with a $\dot{Q}^*$ of 32 compared to $\dot{Q}^*$ of 24 for E27 got the closest to matching the behaviour seen at 1:2 scale, but was still far off with respect to the HRR. The temperature in the 1:2 compartments showed a lower time to failure than in the two 1:5 scale experiments. The temperature near the ceiling for E21 was, however, matching that of E47, but levelled off for another 2 min before the thermal runaway of the compartment occurred, as seen in Figure 3.27 b). Shortly after the thermal runaway, the two 1:2 scale compartments with PIR were both extinguished by water, as suggested by their rapid drop in both HRR and temperature.

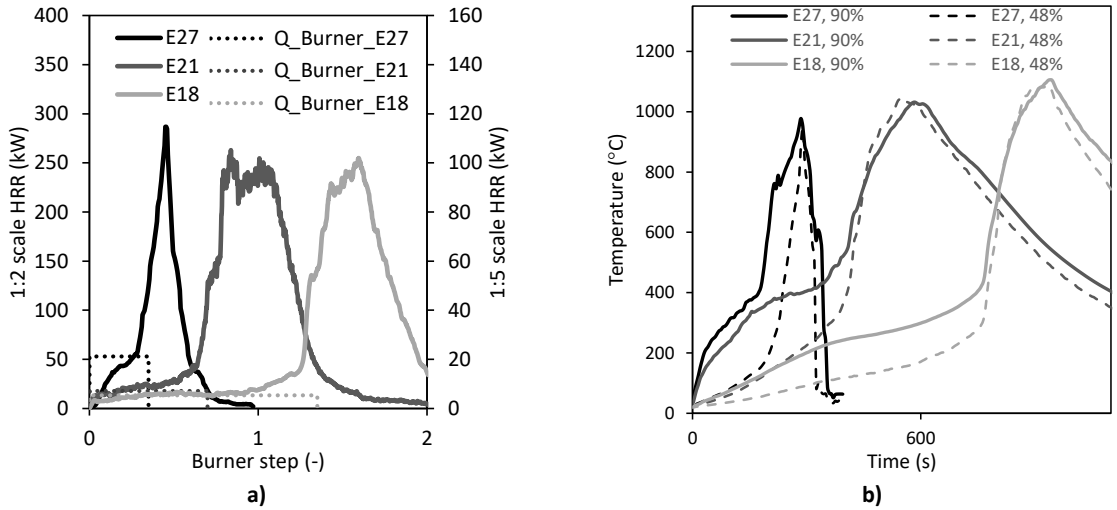

Figure 3.27: Results from three PIR experiments with constant fire scenarios for 1:2 (E27) and 1:5 scale (E18, E21) with a) the measured HRR and burner input and b) the measured temperature at the top and middle of the compartments (90% and 48%, respectively).

The scaling of the HRR from the burner for these scales were not able to capture the thermal runaway of the compartments and the times suggest the HRR at 1:5 scale is not enough as the failure occurs much later. Even as the temperatures near the ceiling for the first 250 s between E21 and E27 matched the temperature in the 1:5 scale compartment took longer to reach the point of thermal runaway. This leads to a new the hypothesis:

- The flashover at these two scales were not caused by the same mechanisms, which is a potential result of the scaling as even the $\dot{Q}^*$ =32 at 1:5 scale was not able to replicate the failure for the constant fire of $\dot{Q}^*$ =24 in a 1:2 scale compartment, which will be elaborated on in Section 3.3.5.1 below.

With the knowledge from the previous experiments with PIR and SW, the fire scenario for E26 with PIR was amended. Compartment with SW the hot gases near the ceiling was lower for the 1:5 scale compared to those measured at 2:5 and 1:2 scale. The time to thermal runaway for E18 compared to E27 (both with PIR panels) was longer. The second step for E26 was therefore lowered to match a scaled 200 kW instead of the intended baseline value of 300 kW as this burner output value was certain to cause a thermal runaway as seen in E27. During the first burning period for E26 steady-state was reached with temperatures of 231 °C and 306 °C in the hot gas layer measured at 79% and 90% of the compartments height, respectively, as seen in Figure 3.28 a). The thermal runaway occurred when the burner was increased from 17 kW to 34 kW and reached 240 kW before being

extinguished due to severe external smoke production. At 1:5 scale the compartment was able to withstand the second burner step with indications of minor contributions from the core by a spike in temperature near the ceiling, as seen in Figure 3.28 b). The thermal runaway for the 1:5 scale compartment was initiated by the third burner step after the temperature in the compartment had stabilised at 274 °C and 336 °C measured at 69% and 90% of the height of the compartment, respectively. This was higher than for the 1:2 scale and the increased compartment temperatures prior to failure supports the hypothesis that the failing mode for the 1:5 and 1:2 scale might be different.

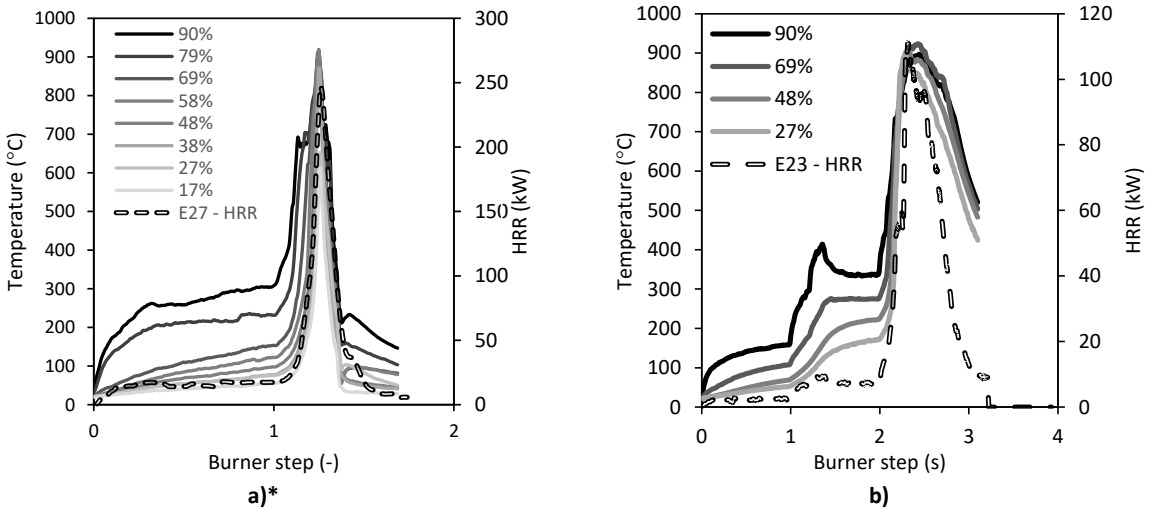

Figure 3.28: a) HRR and temperature at various heights from the floor in the compartment for E27 (PIR) and b) HRR and the temperature at various heights from the floor in the compartment for E23 (PIR). *HRR correction can be found in *Appendix C*.

3.3.4 Full Scale

The full scale experiments were conducted with an internal steel frame, as presented in Section 2.2.3, which prevented direct flame impingement along the edges and absorbed some of the energy from the fire. The fire scenario for these experiments was 100 kW and 300 kW being released in steps of 10 min and 20 min, respectively. The HRR based on the provided gas flow, was 50 kW and 200 kW for the compartment with SW panels, which resulted in a new fire scenario. The oxygen analyser failed to measure the first three min and the last two min of the 50 kW burner period and here after measured HRR of the second burner step of 200 kW, including the period where the burner system had to adjust for a depleted gas cylinder, as seen in Figure 3.29 a). The fire scenario for the compartment with PIR panels, according to the gas flow meter, was 100 kW for 540 s and 300 kW and as the compartment went into flashover 120 s into the second burner step the gas was

terminated for safety reasons, as seen in Figure 3.29 b). Figure 3.29 b) also shows how the measured HRR for experiment E29 with PIR is much higher than the input of the mass flow controller. Based on the bi-directional pressure probes, the energy flowing out of the compartment as convective energy was calculated as 100 kW after 540 s. This means that the mass flow controller was not providing the planned gas flow, as some energy would have been conducted through the boundaries. Based on the flow data from other experiments, the convective energy is, however, also unlikely to be as low as 50%, which is suggesting that the measured HRR was also incorrect. As seen in *Appendix – HRR Calculation, Analysis and Correction for E29* on page 169 the actual HRR was most likely 130 kW-133 kW for the first 540 s and not 100 kW or 200 kW as the mass flow meter and the gas analyser showed, respectively.

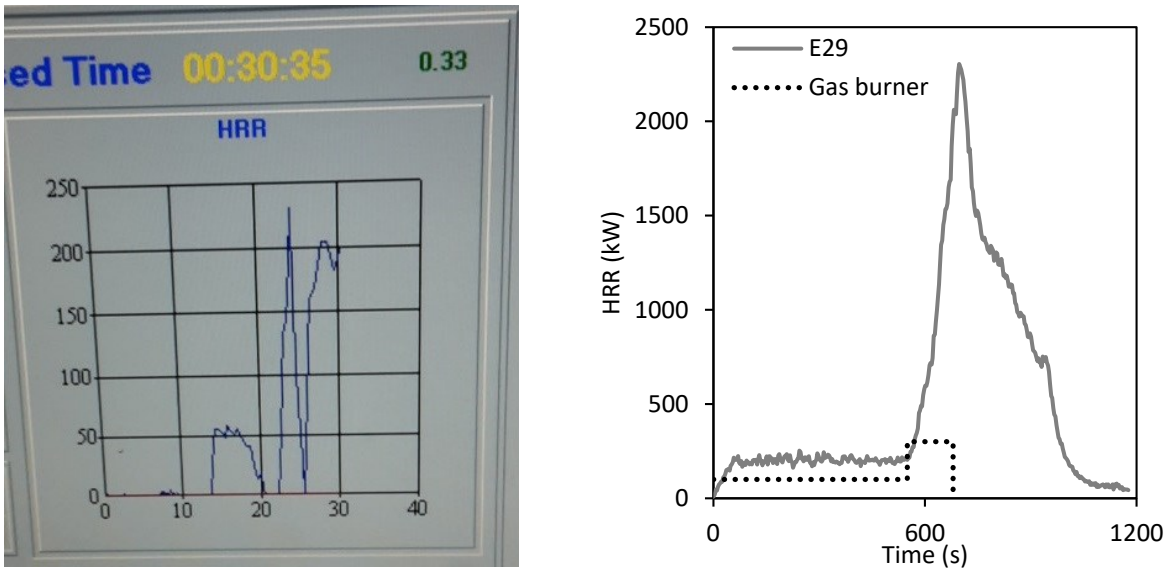

a) b)

Figure 3.29: HRR data the full scale experiments E29 and E30 with a) panels with a core of SW and b) panels with a core of PIR including the burner, respectively.

The temperatures in the compartment constructed with PIR panels reached steady state prior to the increase of the input of the burner to 300 kW where it failed. The temperature measured nearest the ceiling in the compartment was 270 °C and the lowest part of the smoke layer was 200 °C while for the compartment with SW panels the smoke layer was between 150 °C and 100 °C. Steady-state was never achieved for the compartment with SW panels after the increase to 200 kW and the shape of the temperature profile was similar to one from the 1:5 (E20) and not the 2:5 (E25) or 1:2 (E28) scale compartments, as seen in Figure 3.30 a). The temperature measured at 90% of the height of the compartment for the first 600 s (the first burner step) matched the temperatures measured at

similar relative height in the 1:5 scale compartment. The $\dot{Q}^*$ was 16 for the full scale compared to the 24 for the 1:5 scale during the second burner step the temperature was, however, higher for the full scale. The temperature in the PIR compartment during the first burner step matched the temperature measured in the 1:2 scale experiment (E27) and the second burner step in the 1:5 scale experiments (E12), as seen in Figure 3.30 b). Those failure temperatures fall within the range identified in Figure 3.1 and Figure 3.2 for ambient environments of nitrogen and air, respectively. This highlights that even the smallest scale experiments are important for identifying temperature ranges of concern.

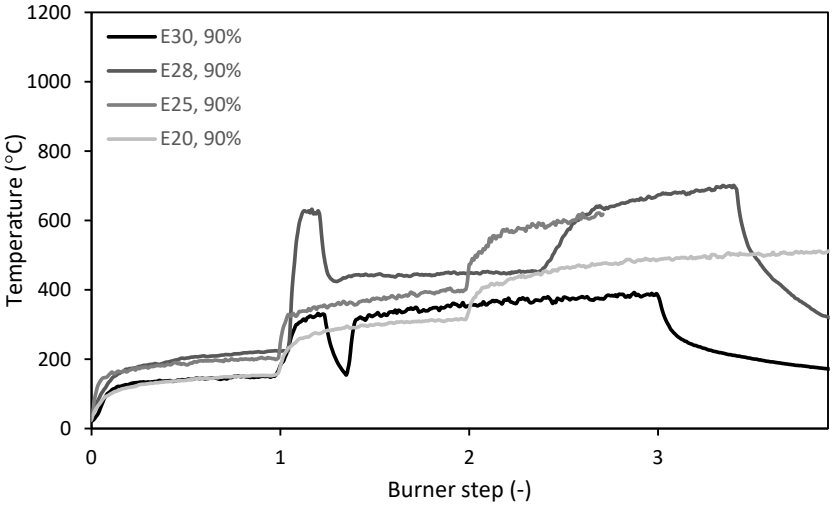

a)

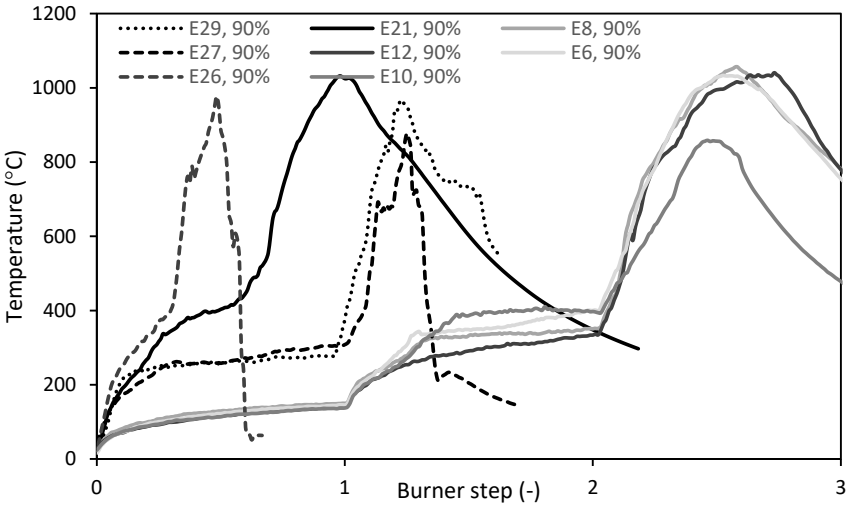

b)

Figure 3.30: Temperature measurements near the ceiling for a) compartments with SW panels at 1:5, 2:5, 1:2 and full scale (E20, E25, E28 and E30, respectively) and b) compartments with PIR panels at 1:5, 1:2 and full scale (E6-E21, E26-E27 and E29, respectively).

Additionally, data from an older set of experiments from literature [16] with similar panels (identical names, but different production years) with thermocouples located both in the volume of the compartment as well as inside the walls was used for comparisons [149, 133]. The fire scenarios for these experiments were intended as 100 kW, 300 kW and 600 kW for 10 min duration each for the compartment with PIR panels and with the 600 kW step prolonged for an additional 10 min for the compartment with SW panels. The HRR was determined by the use of doorway mounted flow and gas measurements instead of a hood collecting the combustion products meant and increased uncertainty regarding the HRR. The measured HRR regions were extracted from the work done by Hidalgo [16], as seen in Figure 3.31.

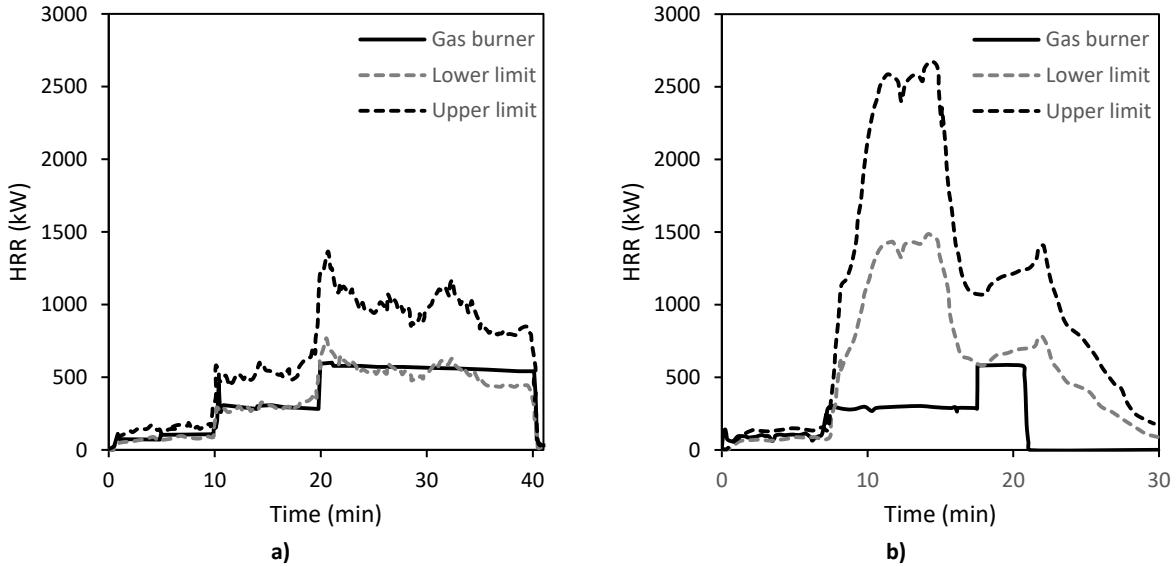

Figure 3.31: HRR data from literature [16] with full scale experiments with a) panels with a core of SW and b) panels with a core of PIR.

The gas burner for the experiments with PIR panels was accidentally increased after 7 min and not 10 min as planned and the final burner step of 600 kW was shortened. However, the thermal inertia of the gas is low and the temperatures in the compartment were stabilized prior to this increase and matched the temperatures in the compartment with SW panels reducing the implications of this premature increase, as seen in Figure 3.34.

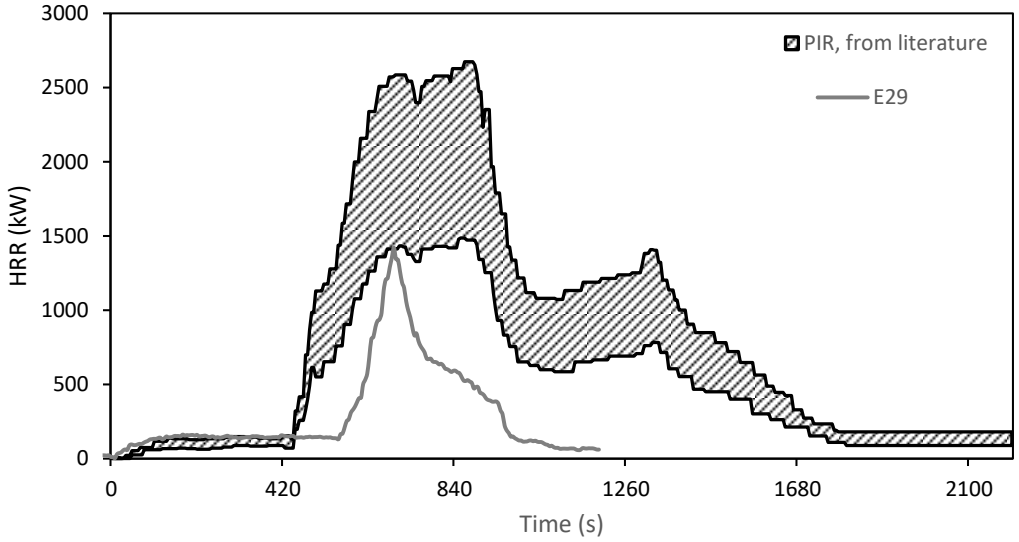

Figure 3.32: HRR for the two 1:1 scale compartments with PIR panels (E29 and from literature [16]).

The difference between the two full scale burner scenarios show how efficient the PIR panels are at limiting their heat release once the external heat source is removed. This behaviour was also seen at 1:5 scale, but not as efficient where between 40% and 60% of the mass was lost, which was significantly lower based on visual char depth analysis conducted during disassembly. The ceiling panels were all delaminated on the internal face while most wall panels were mostly unharmed in the lower half with significant char formation in the top half, as seen in Figure 3.36 (R2 and R3). The internal steel frame effectively protected the shielded panels behind, as seen by the virgin core material along the edges, as seen in Figure 3.33 (L1 and L4), and the panel directly adjacent to the gas burner (R1).

L1 **L4** **R1** **R2** **R3** **C1**

Figure 3.33: Char formation for six panels from E29 showing the various degrees of char formation from the compartment boundaries after the removal of the internal steel-face. "L", "R" and "C" refers to the left and right wall and ceiling, respectively, as seen in Figure 2.15.

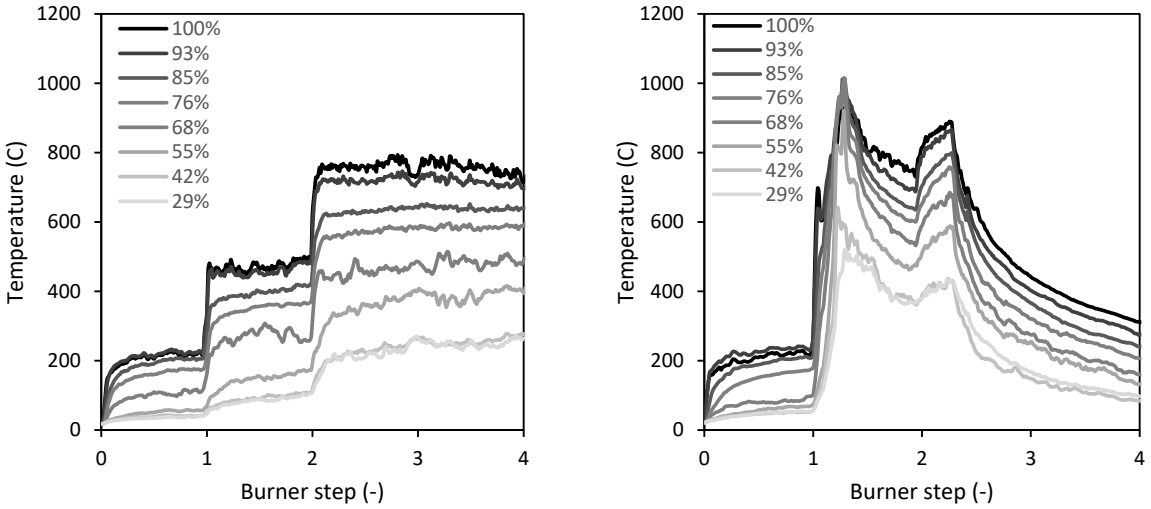

Figure 3.34: Temperature data from literature [16] with full scale experiments with a) panels with a core of SW and b) panels with a core of PIR.

As the full scale experiment with SW had complications the experiment with SW panels from literature was used as a reference for the modified fire scenario for neat heat transfer comparisons. The panels from literature were the same brand, type and thickness but with a red finish instead of the white herein. The full scale experiment with PIR panels from literature served as a duplicate as it also ignited within the first two burner steps. The PIR panels from literature were the same brand and type but differed with a grey finish on the outside instead of the white herein and a *flat* internal face whereas it is *mini box* herein.

3.3.5 Summary of the Compartment Experiments

The comparison of the temperatures in the hot gas layer across panel types and compartment sizes leads to the follow experimental relationships:

- The scaling of the fire scenario to 1:5 scale did not provide the same relative sized fire as seen by the lower compartment temperature and the time to failure was longer for the compartment with PIR panels.

- The gas temperature measured in the top 1/10th in the middle of the volume of the compartments the fire size of $\dot{Q}^*$ = 4 at 1:1 scale was nearly identical with the measurements taken at 1:5 scale for a $\dot{Q}^*$ = 8 for the compartments with SW. The quadruple

non-dimensional fire size $\dot{Q}^*$ = 16 caused a higher increase in temperatures at full scale than a $\dot{Q}^*$ = 24 at 1:5 scale, but lower than $\dot{Q}^*$ = 24 at 2:5 for E2 and E20, respectively. These results provide further support towards concluding that the scaling relationship is incapable of replicating the fire in compartments at this small scale.

- E27 and E29 with compartments of PIR panels with a fire scenario of $\dot{Q}^*$ = 8 for their first burning durations showed close to identical temperatures throughout the height of the compartment. At the initiation of the second burning step ($\dot{Q}^*$ = 16 and 24 for E27 and E29, respectively), the compartment fires transitioned to ventilated controlled dominated by the energy released by the panels over the burner and the compartment temperatures increasing at a similar rate. The fires were extinguished at different times and the burning duration is not possible or intended to be compared.

3.3.5.1 Hypothesis of Different Failure Mechanisms for the 1:5 Scale compared to Larger Scales

After the gas burner was turned off more than 90% of the internal thermocouples in the compartments with PIR panels at the 1:5 scale were able to maintain a temperature above 500 °C. At 1:2 and at full scale this was less than 40% and for much shorter duration, as seen in Figure 3.35, albeit influenced greatly by water being applied early. This does, however, show that after the onset of the thermal runaway in the compartments the fire dynamics are significant different as almost all thermocouples are measuring temperatures higher than 500 °C at 1:5 scale but less than 40% are at 1:2 and full scale. As a consequence of this, extrapolating the HRR based both on oxygen consumption or mass loss rate back up to 1:2 or 1:1 scale will be significantly overestimated.

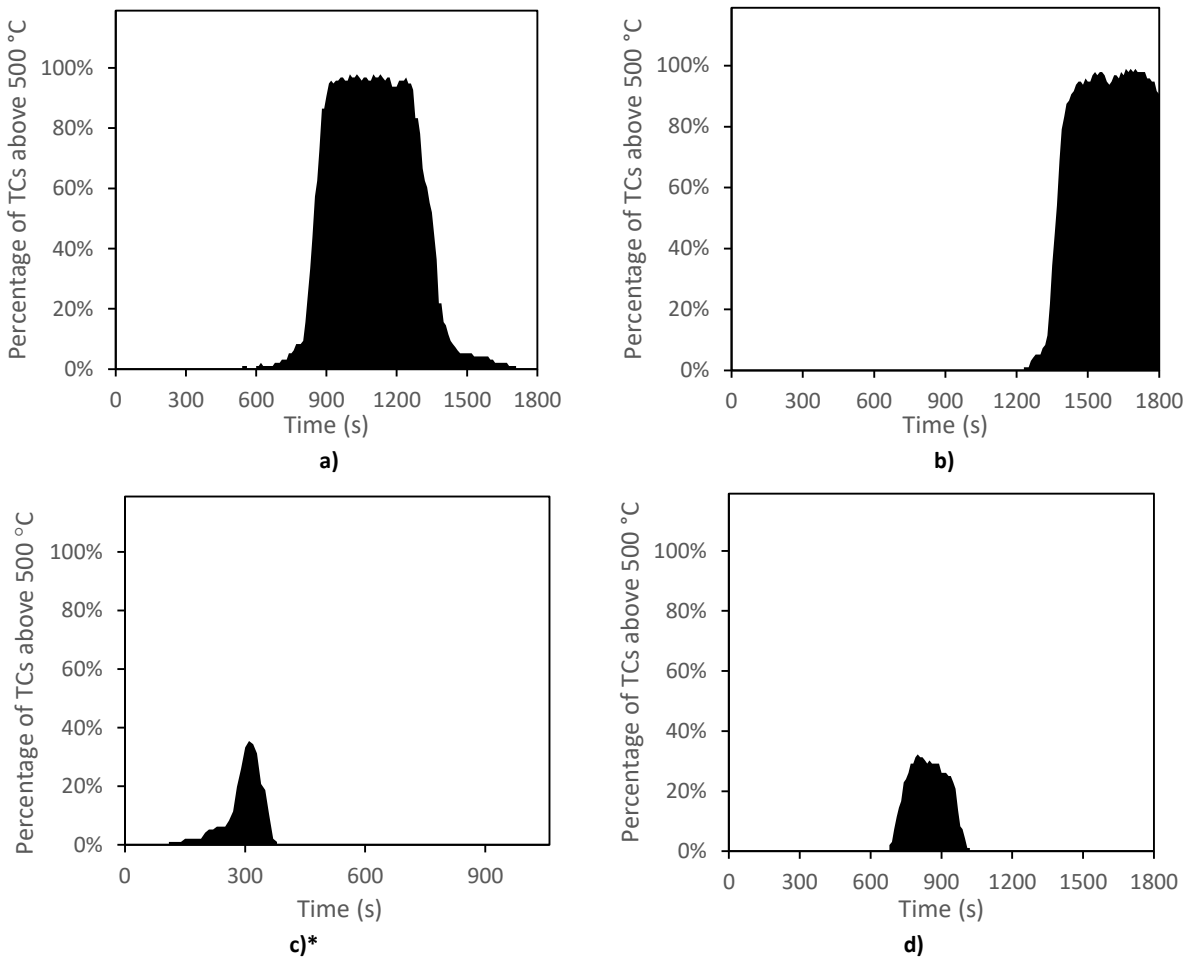

Figure 3.35: Distribution of thermocouples measuring more than 500 °C for a) E18, b) E23, c) E27 and d) E30, all compartments were with with PIR panels.
*** The compartment fire was put out with water shortly after it failed and the gas burner was turned off as well.**

3.3.6 Time to Failure and Critical HRR

The HRR required to cause a failure (critical HRR) and to cause a transition from a fuel- to ventilation controlled fire is given by Eq. 2.8 (repeated below for convenience). The fuel coefficient, C, is 1 and 1.7 for fuels burning in the middle and corner of a compartment, respectively. The expression was calculated for the 1:5 and 1:2 scale compartments with PIR panels, as seen in Figure 3.36 and Figure 3.37, respectively.

$$\dot{Q}_{FO} = C^{-3/2} \cdot 0.07 \cdot \sqrt{X^{9/4} \cdot h_k} \cdot \Delta T^{3/2} \qquad \textbf{2.8}$$

For the 1:5 scale experiments the best fit is with the coefficient of unity as the HRR for E21, E19 and E14 was in the early phase of transitioning towards becoming ventilations controlled. Furthermore, the 1.7 coefficient already has the compartments in a transition phase with just 3 kW and 2.6 kW after 300 s and 600 s, respectively, and with that correlation all non-constant HRR 1:5 scale experiments should have failed at the second burner step, not the third. E14, E12 and E23 all fail at a higher HRR than the empirical correlations predicts, but not by much. E21 and E19 with constant fire scenarios were both growing parabolic passing the predicted threshold value suggesting an increasing wall area contributing to the growth before the transition of the compartment to ventilation controlled burning conditions which caused a sudden increase in the HRR.

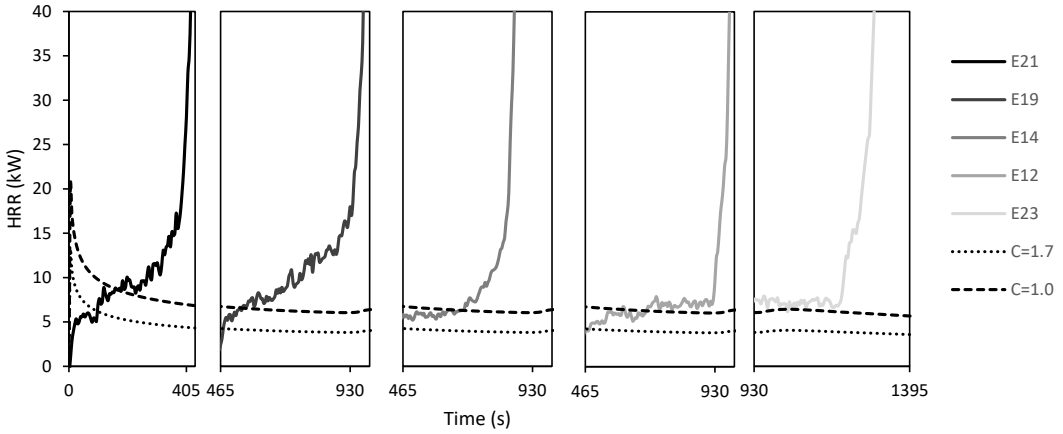

Figure 3.36: HRR for five 1:5 scale compartments with PIR panels combined and Eq. 2.8 with C equal to 1 and 1.7.

The 1:2 scale compartments correlated differently to the two coefficients compared to the 1:5 scale, and the location for the fuel in the corner (1.7) provides the best predictions. Both E27 and E26 were in the growing phase when passing the threshold. However, the 1.7 coefficient provided the lowest estimate of failure in the late growing phase, but still before the HRR spiked, as seen in Figure 3.37.

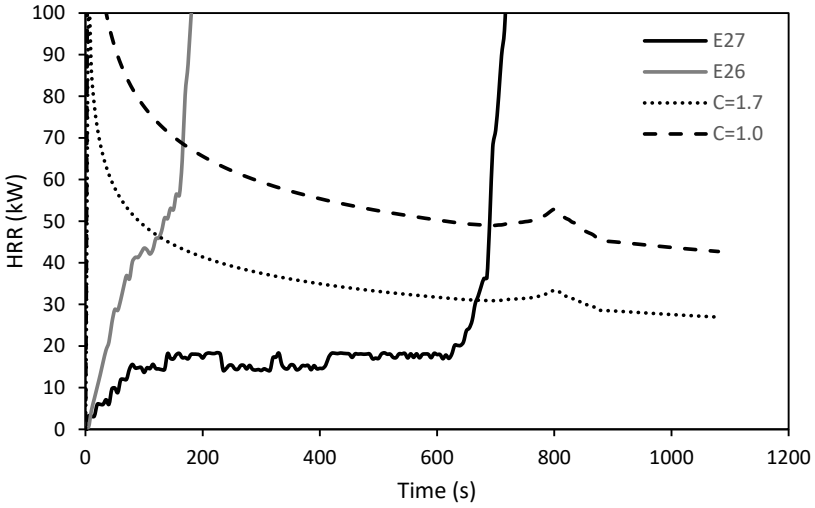

Figure 3.37: HRR for the two 1:2 scale compartments with PIR panels and Eq. 2.8 with C equal to 1 and 1.7.

For compartments with the geometry of the standard test room and the compartment experiments conducted inhere the critical HRR causing a flashover converges towards 150 kW and 220 kW for PIR and SW with a thermal inertia at ambient temperature of 1300 W^2s/m^4K^2 and 3800 W^2s/m^4K^2 respectively. The design fires used should therefore initiate a thermal runaway when the burner is increased from 100 kW to 300 kW 10 min after initiation of the experiments. The full scale compartments with PIR panels failed after 540 s and 480 s for E29 and the compartment from literature both shortly after the initiation of the second burner step to 300 kW, as seen in Figure 3.32. The burner was turned off for E29 shortly after the compartment failed and the HRR slowly decreased whereas in the literature the propane flow to the gas burner was sustained and eventually increased to 600 kW after 1052 s for 200 s explaining the difference in the two curves.

3.3.7 Heat Transfer Analysis

The heat transfer model is one-dimensional and based on zero energy generated within the CV. Energy within the CV is merely transported from hot to cold, unstable to stable and as such the validity range for temperatures for experiments with PIR panels is very narrow (< 300 °C), seen in section *3.1.1 Thermographic Analyses and Differential Scanning Calorimetry* as the first larger reaction. The heat transfer model is, therefore, only applied to compartments with SW panels as their limited mass loss and energy generation fit the limitations of the model. The in-depth temperature measurements for 26 thermocouple pairs from the full scale experiments with SW panels from literature exposed to the modified fire scenario [149] were used to determine the

thermal conductivity of the core material. In addition to those measurements, the 20 thermocouple clusters from both E1 and E3 were also used to determine k_1 for the core material, as seen in Eq. 2.26 (repeated below for convenience). A temperature dependent term was found for each of the thermocouple positions, as seen in Figure 3.38 and summarized in Table 3.6, and the median was used for further heat transfer analysis. The solution is sensitive to the location of the thermocouples and a scatter was expected and the conductive term from both the 1:5 scale and literature was found to be around 0.00020 W/m·K^2 with some peak values being four times as high and others negative.

$$k(T) = k_0 + k_1 \cdot T \qquad \textbf{2.26}$$

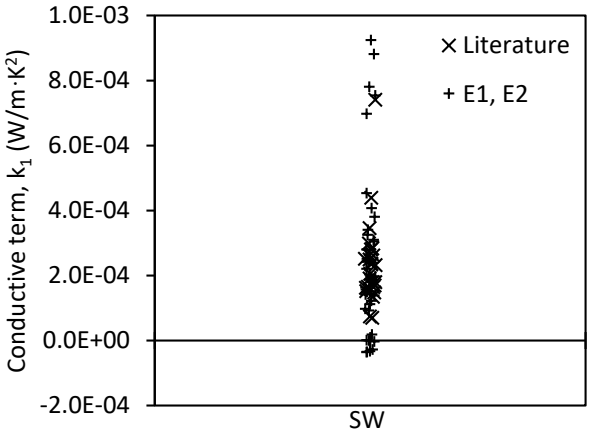

Figure 3.38: k_1 solutions for the SW panels from E1, E2 and literature based on the least square optimization algorithm.

Table 3.6: Summary of k_1 coefficients for the SW

k_0	(W/m·K)	3.8E-2
Median, k_1	(W/m·K^2)	2.0E-4

The one-directional heat transfer model was able to predict the thermal wave passing through the walls fairly well but by no means perfectly, as seen in Figure 3.39. The heat transferred was, however, still calculated to establish the net heat loss through the solid boundaries heat losses to compare it across scales. For the global heat loss analysis the calculated heat fluxes from the model are multiplied with the respective area the associated thermocouple corresponds to. The sum of all the heat conducted divided by the known HRR from the burner provides a versatile non-dimensional measure which is compared across scales, as seen in Eq. 3.1.

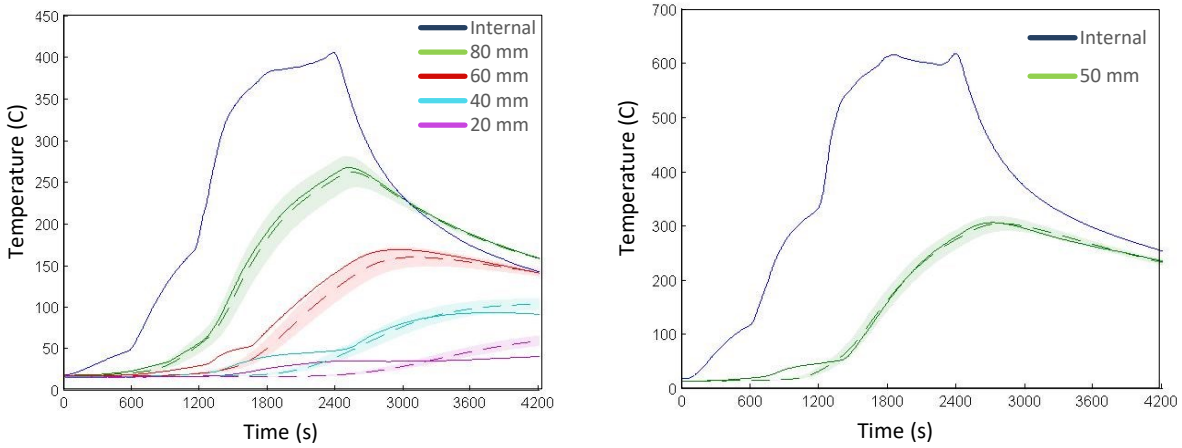

a) b)

Figure 3.39: The calculated in-depth temperature development marked with hatched marking a TC location ±3 mm from intended depth with the measured temperatures in solid lines for two wall measurements from the SW experiments from literature.

$$\chi_{cond}^{j} = \frac{1}{\dot{Q}_{cond}^{j}} \cdot \sum_{n=1}^{N} A_n \cdot \dot{q}_{cond,n}^{\prime\prime,j} \qquad 3.1$$

The compartment was not mounted with thermocouples along the boundary towards the floor and the exact conductive losses were not estimated. The Calcium Silicate plates used as the bottom boundary had a higher thermal conductivity than the walls, as seen in Table 3.7. The boundary was, however, subjected to lower temperatures than the panels due to the nature of buoyancy forces driving the hot gases upwards thus reducing the convective losses. The measurements from the thermocouples in the walls nearest the floor was assumed to conservatively reflect the magnitude of the internal surface temperature of the floor plates, seen in Figure 3.40 a). Based on this the heat transferred through the floor was calculated as less than 3% of the heat released from the burner for E20 (1:5 scale), as seen in Figure 3.40 b), equivalent of 0.04 kW, 0.11 kW and 0.27 kW after 600 s, 1200 s, 1800 s, respectively. As the magnitude of heat transferred was small the lack of thermocouples and undetermined heat transfer through the floor was considered negligible.

Table 3.7: Material properties for the floor plate [166].

	ρ (kg/m^3)	k_0 (W/m·K)	c_p (assumed) (J/kg·K)	t (m)	Reaction to fire (-)
FireFree ScandiBoard 850	250	0.0659	840	0.022	A1 (Non-combustible)

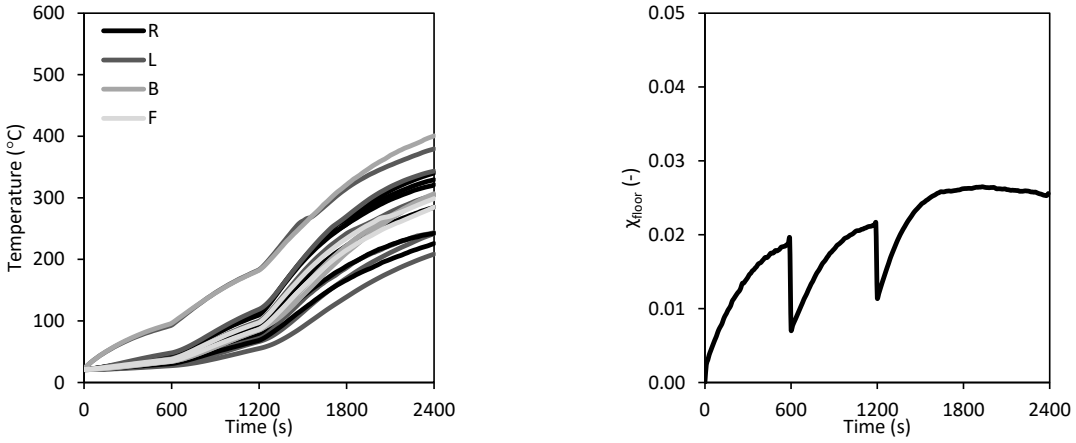

Figure 3.40: a) the measured temperature for the thermocouples closest to the floor from E20 (1:5) and b) the heat transmitted through the floor plate relative to the known heat output by the burner.

The bi-directional pressure probes mounted along the centre of the doorway was used to estimate the convective heat losses. Following traditional compartment fire dynamics, as explained by Karlsson and Quintiere [145], the flow can be calculated as a function of the pressure difference between inside and outside the compartment. The heat lost via convection through the doorway was determined on the basis of the measured velocities and temperature corresponded to a mass flow. By measuring the flow directly, the assumptions made regarding pressure difference being the dominating driving force from theory is avoided. This method accounts for the possibility of momentum driven flows caused by the deflection of hot gases by the ceiling. The convective heat losses were determined for four experiments at three different scales all with SW panels (E20, E25, E30 and literature), as seen in Eq. 3.2.

$$\dot{Q}_{conv} = C_d \cdot \dot{m}_g \cdot c_p \cdot \Delta T,$$

$$\dot{m}_g = C_d \cdot v \cdot A \cdot \rho_g = \int_{H_N}^{H_0} \int_0^W C_d \cdot v \cdot H \cdot x \cdot \rho_g \, dH dx = \quad \textbf{3.2}$$

$$C_d \cdot W \cdot \int_{H_N}^{H_0} v(H) \cdot H \cdot \rho_g(H) \, dH$$

Where $\dot{m}_g$ is the mass flow of the gas, C_d is the flow coefficient and assumed to be 0.7 [145], v is the velocity determined by the bi-directional pressure probes, W is the width of the door, H is the dynamic distance from the floor to the neutral plane, H_N, and H_0 is the height of the doorway. The

velocities along the height of the doorway for the experiments with SW panels at 1:5 scale and 2:5 scale peaked at 4.2 m/s and 4.0 m/s after 1800s, respectively, as seen in Figure 3.41 a) and b), respectively.

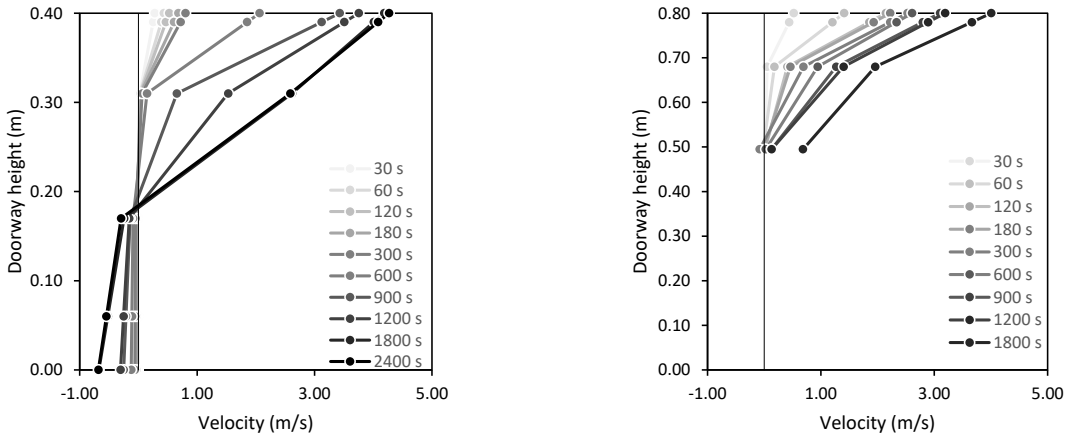

a) **b)**

Figure 3.41: a) the measured doorway velocities over the height of the door for various times during a) E20 (1:5) and b) E25 (2:5).

The weighted average of the temperature along the height of the smoke layer along with the assumption that the gases primarily consisted of air and acted ideal was used to determine the density of the gas as a function of time. Throughout the duration of the experiments small quantities of smoke, relative to the flow of gases from the doorway, was leaking from the compartments and was considered insignificant and was not accounted for. The fraction of heat lost through the doorway throughout the duration of the experiments compartment ranged from 0.20 to 0.80 where the first burner step for E20 was difficult to measure due to low velocities. At the initiation of the second burner step the fraction of heat lost via convection ranged from 0.40 to 0.60 and still with the 1:5 scale being in the lower end. The convective fraction of energy increased over time and, as seen in Figure 3.41, once the velocities in the doorway stabilized the energy loss also reached a constant quantity. The conductive energy initially peaked just after each increase in the HRR of the burner and as the temperature between the compartment volume and boundaries approximated each other the conductive losses approximated steady state. This was more correct for the full scale experiments than for the smaller scales, as seen in Figure 3.42.

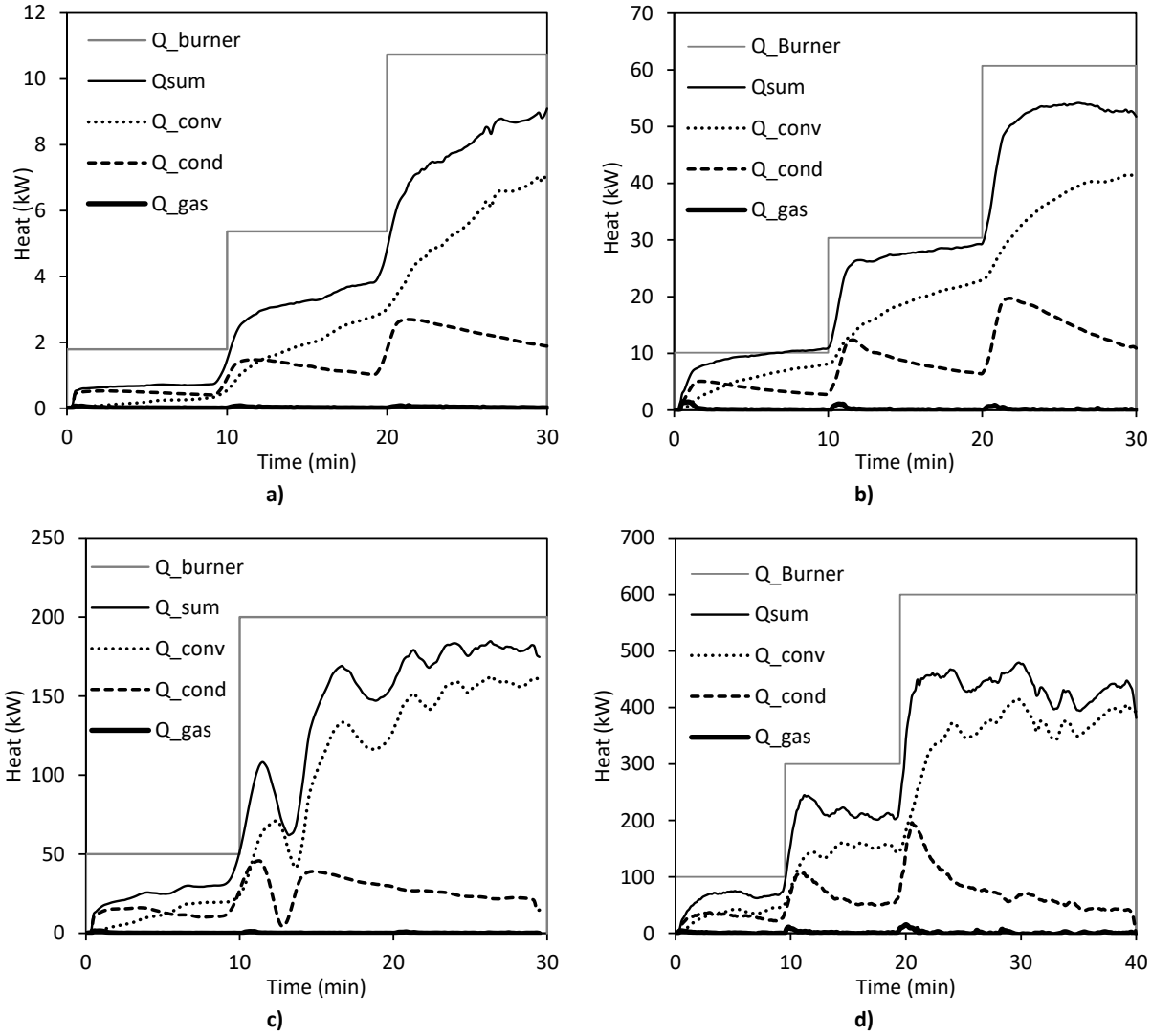

Figure 3.42: Heat for the experiments with SW panels separated as modes of transfer for a) E20 (1:5), b) E25 (2:5), c) E30 (1:1), and d) from literature (1:1).

Overall, the heat transfer across the three scales was in the same range with about 2/3 of the heat losses being convective regardless of the input of the burner, as seen in Figure 3.42. There are noticeable inconsistencies for the conductive fraction across the scales such as the 0.3, 0.5 and 0.3-0.4 initially for E20 (1:5), E25 (2:5), E30 (1:1) and literature (1:1), respectively, suggesting a discrepancy for the 2:5 scale experiment as it does not fit the 0.3 to 0.4 range. The distribution of heat in the 2:5 scale experiment is generally subjected to much more heat for both the conductive and convective fractions compared to the other experiments. A general trend across all scales is, however, the nearly-steady-state situation towards the end of the experiment where the calculated energy distribution accounts for 90% in three of the four experiments with the data from literature being about 15% lower.

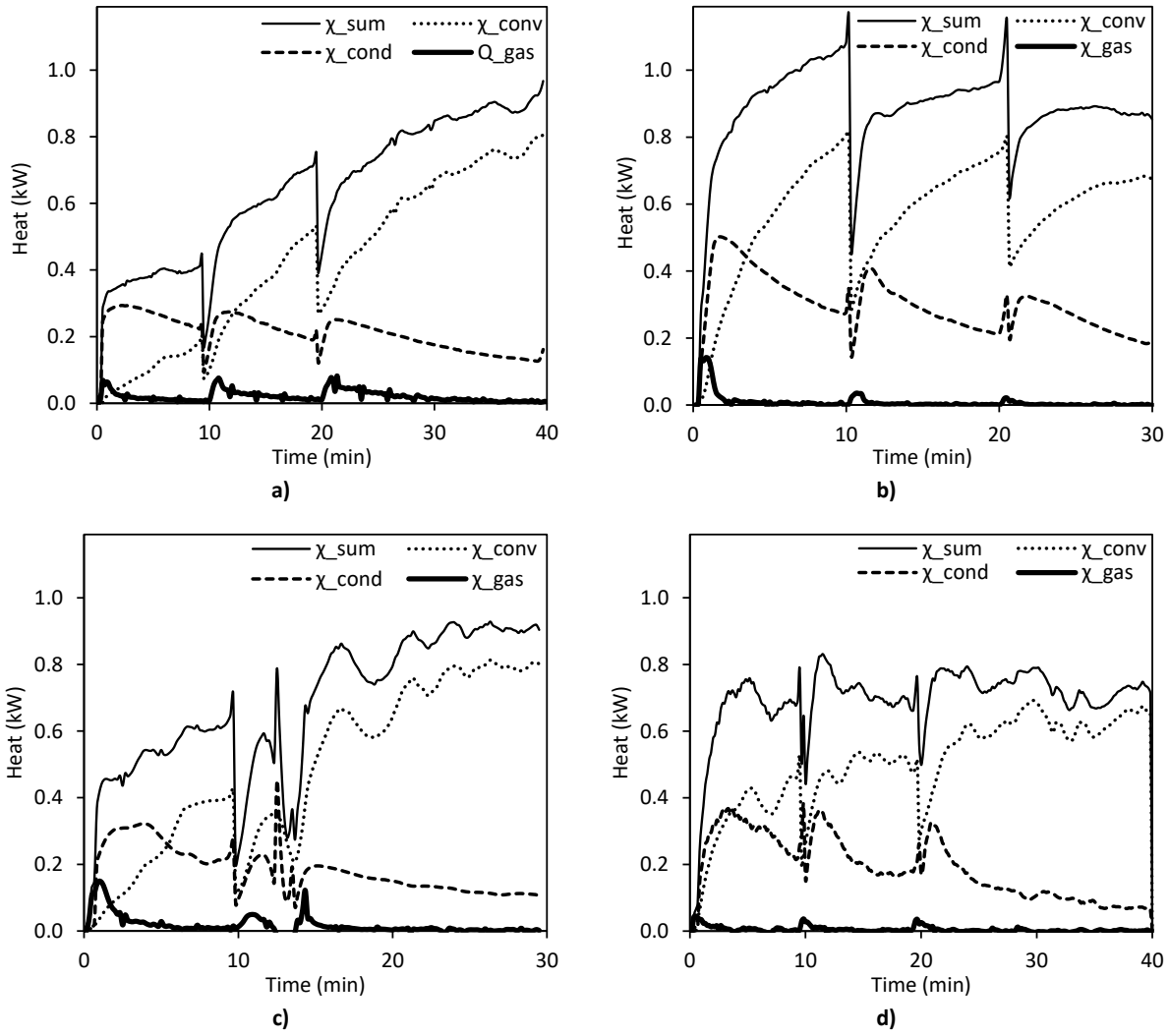

Figure 3.43: The distribution of heat for the experiments with SW panels for a) E20 (1:5), b) E25 (2:5), c) E30 (1:1), and d) from literature (1:1).

For compartments constructed with panels with an inert core material the satisfactory global heat transfer across the scales might be sufficient for some studies. The net heat flux penetrating the core material will, however, increase its temperature correspondingly as presented in Eq. 2.23 (repeated below for convenience) if solved for the temperature, T^{j+1}.

$$\dot{q}''^{\,j+1}_{net_1} = L_s \cdot \rho_s \cdot c_{p,s} \cdot \frac{T_1^{j+1} - T_1^{j}}{\Delta t} + \frac{\Delta x}{2} \cdot \rho_c\left(T^{j+1}\right) \cdot c_{p,c}\left(T^{j+1}\right) \cdot \frac{T_1^{j+1} - T_1^{j}}{\Delta t} + k_c\left(T^{j+1}\right) \cdot \frac{T_1^{j+1} - T_2^{j+1}}{\Delta x} \qquad \textbf{2.23}$$

To study the net heat flux transferred through the internal boundaries across four experiments and the four scales (E20 [1:5], E25 [2:5], E30 and from literature [1:1]) the calculated heat fluxes, as seen in Figure 3.44, were compared. The net heat flux peaks shortly after each increase in burner intensity as the increased HRR also caused the temperature of the enclosure and the temperature gradient between the gas phase and the steel-sheets to increase rapidly. This cause the net heat flux to increase temporarily followed by a slow decrease until steady state occurred. Conductive steady state or quasi-steady state was also identifiable in the global heat transfer analysis where E25, E30 as well as the SW experiment from literature decreased towards the end of their respective experiments.

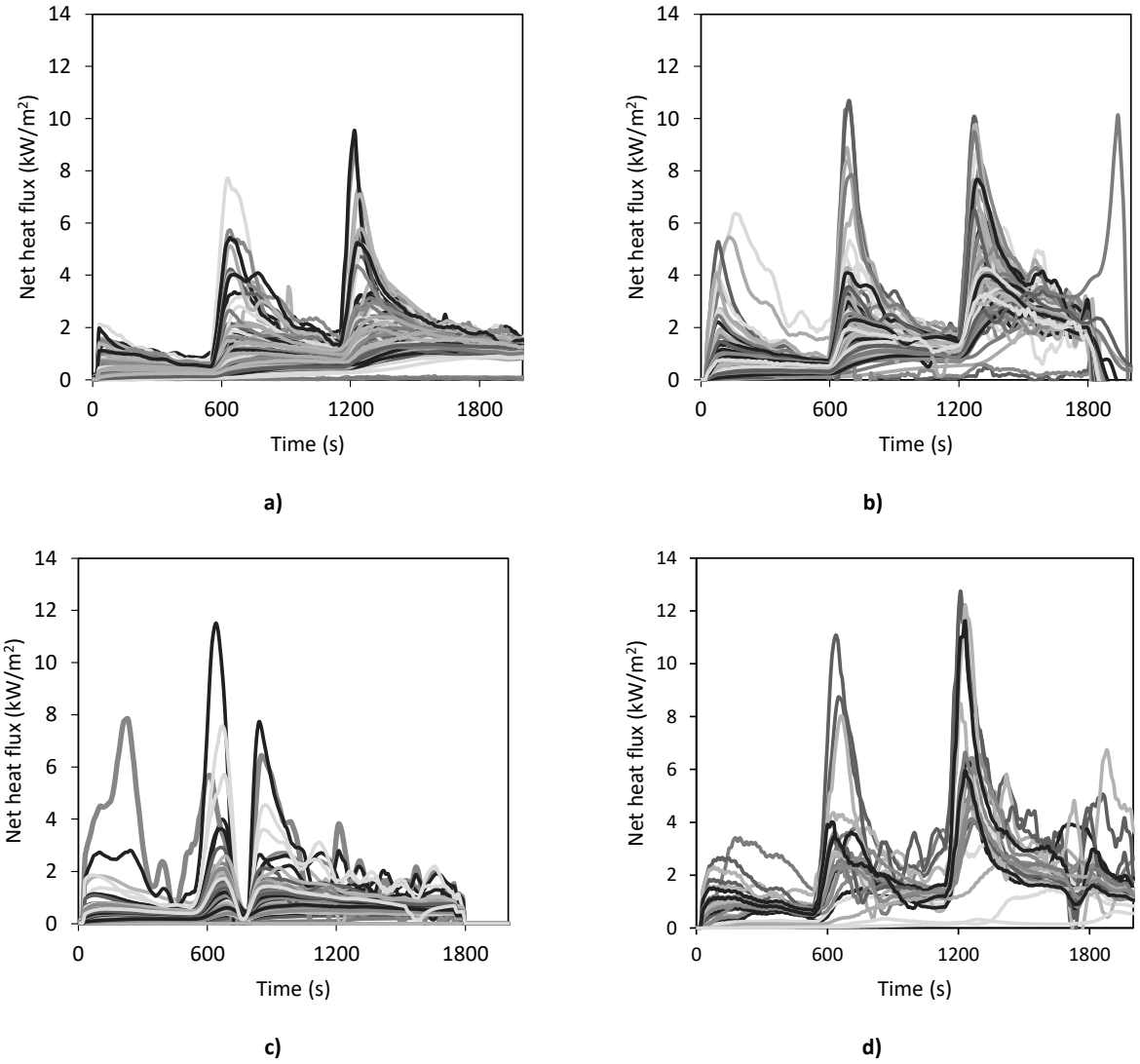

Figure 3.44: Net heat flux calculated for all the thermocouples in a) E2 (1:5), b) E25 (2:5), c) E30 (1:1) and d) literature (1:1).

To accommodate for the different measurement densities across the scales the number of measurement points were made relative to the number of thermocouples. This means that the net heat flux calculated for a compartment with 20 measurement points would be plotted with 5% distance on the x-axis whereas a representation of the results from a compartment with 100 thermocouples would be separated by just 1%. To compare the general distribution, and therefore also the applicability of the scaling method, the heat flux measured just prior and after each burner increase was ranked from lowest to highest to simplify the comparison, as seen in Figure 3.45. The net heat flux for the 2:5, 1:2 scale and from literature corresponded reasonable well for the initialisation of the experiment, as seen in Figure 3.45 a). The net heat flux for the full scale was higher for about 60% of the measurements. The net heat flux did, however, corresponded very well to the bottom and top 20% of thermocouples, as seen in Figure 3.45 b) and Figure 3.45 d), suggesting the surfaces closest and furthest away from the burner is heated the same. E2 and E30 matched very well at the end of the first and second burner step (500 s and 1100 s), as seen in Figure 3.45 c). This indicates that the scaling of the HRR of the burner in 1:5 scale is not correct as E30 only was 50 kW and not the 100 kW which E2 was scaled for. The second burner step in E28 was ramped up too high and was therefore not comparable with the equivalent steps for E25 and the literature. It was, however, comparable with their third respective burner increases which resulted in net heat fluxes in the same range albeit at different times, as seen in Figure 3.45 e). The full scale experiment from literature had greater heat fluxes compared to those from E25 at 2:5 scale, as seen in Figure 3.45 d), where the second step from E28 at 1:2 scale were the closest approximation. The quasi-steady state near the end of the scaled experiments the E25 matched the 25% larger E28 but were both greater than the full scale from literature, as seen in Figure 3.45 f). This goes for the whole range of measurements, except for the 10% of the wall areas represented by the thermocouples closest to the burner, where the net heat flux was much higher for the full scale from literature [16].

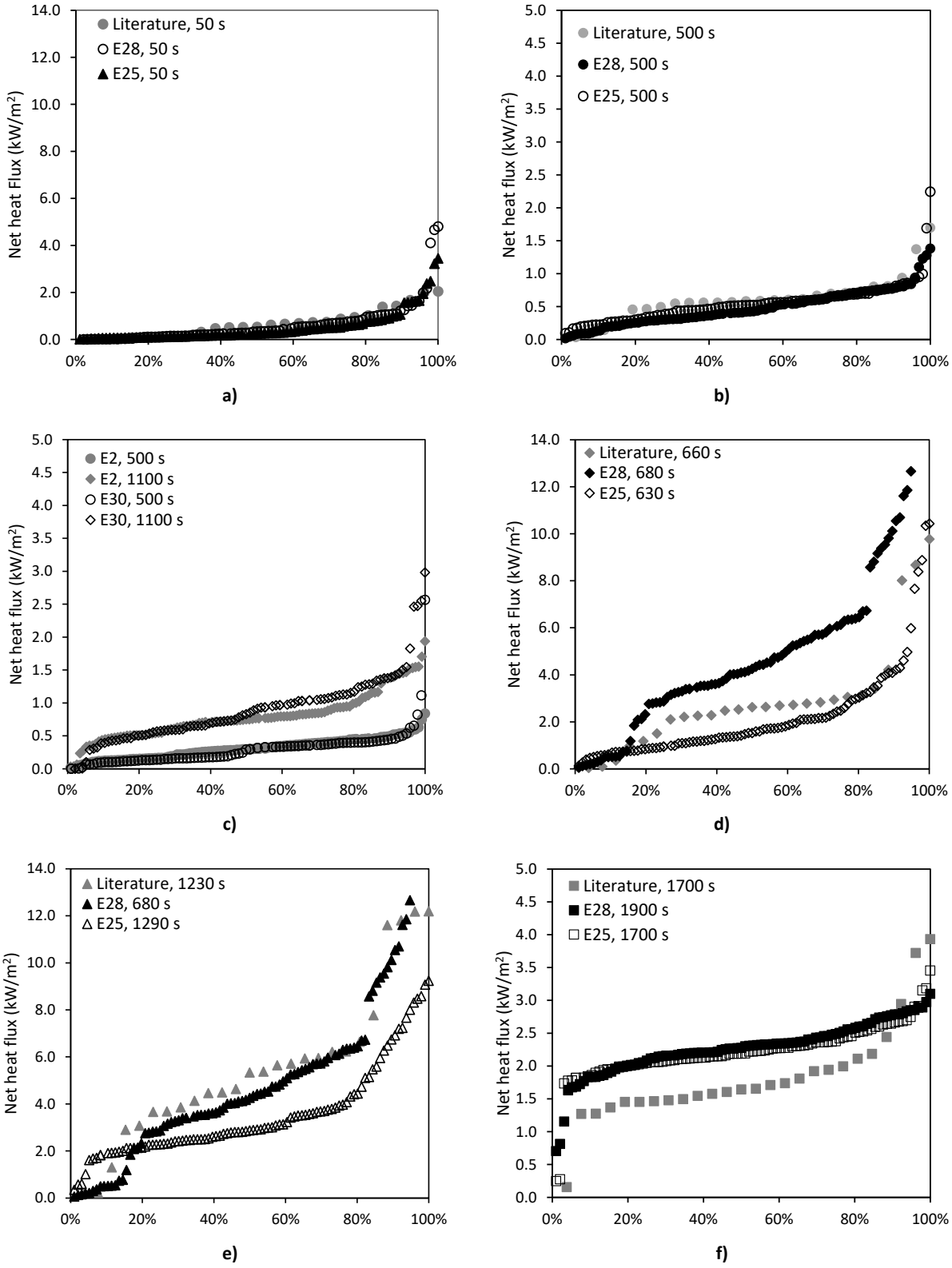

Figure 3.45: Net heat flux a) after the first burner step for E25 (2:5), E28 (1:2) and literature (1:1), b) just before the second burner step for E28 (1:2), E25 (2:5) and literature (1:1), c) before the two first burner increases for E2 (1:5) and E30 (1:1), d) the first burner step for E25 (2:5), E30 (1:1) and literature (1:1), e) after the second increase for E28 (1:2) and the third for E25 (2:5) and literature (1:1), and f) the quasi steady-state heat flux prior to the termination of the experiment for E28 (1:2) and E25 (2:5).

The comparison between the scales with respect to compartment temperature and for SW also the global heat transfer and net heat flux presented some differences but also some similarities, summarized as:

- Based on the compartment temperature, the reproducibility of the 1:5 scales for compartments with or SW was excellent if the placement of the gas burner was consistent.
- The net heat transfer across all 4 scales for the first 600 s were identical for a majority of the measurement with areas closest to the burner where the heat flux is the highest deviating.
- The quasi steady-state heat flux prior to the termination of the experiment for E28 (1:2) and E25 (2:5) was almost identical, suggesting a very similar fire compartment environment.
- The net heat flux just after burner increases were not as similar as the more steady and quasi-steady periods. The net heat flux at 1:2 scale after the first increase to $\dot{Q}^* = 24$ matched that of the full scale from literature, while the same increase at 2:5 scale was much lower.
- The steady state net heat transfer before the two burner increases in 1:5 scale and the full scale SW experiment matched quite well despite different $\dot{Q}^*$ suggesting a limit to the scaling of the net heat transfer.
- The first and second burner steps for E25 and the compartment from literature compared well on many parameters, such as compartment temperature, initially induced net heat flux and the top and bottom 20% heat flux for the first 1200 s.

3.3.7.1 Uncertainties

The heat transfer model was generally very good at accounting for the known heat released into the compartment by its simple one-dimensional heat transfer with a linear temperature adaptation for the conductivity of the SW core. A higher measurement density provides a better resolution of the temperature whether it being the compartment temperature or of the internal walls. The small scale experiments were, however, less instrumented along the height of both the volume of the compartment and the doorway whereas the walls in the data from the literature is less instrumented than the conducted experiments. Reducing the number of measurements points while correspondingly increasing the area or volume assigned to them provided a method for determining the influence of the reduced instrumentation density. The large scale experiment from literature with eight measurement point along the height was reduced to four while the volume each

thermocouple represented was doubled. The internal thermocouples from E2 and E20 were used to determine the difference in the conductive heat transfer for different measurement densities in the walls for similar fire scenarios with matching compartment temperatures. The full uncertainty analysis for the measurements can be found in *Appendix – Uncertainty Analysis of the Measurement Density* on page 173.

3.4 Results Highlights

- The three steel-faced insulation panels, all class B according to the European reaction to fire scheme, performed very differently when studied in a compartment framework in both small and large scale experiment.
    - The PUR panels released significant heat and had almost a complete loss of mass, which means that it did not perform like a class B product is intended and expected to do. The HRR was almost two times that measured in the PIR compartments, significant amounts of smoke was released externally due to integrity failure, and the HRR equalled four times the ventilation controlled limit for post flashover fires based on the geometry of the doorway.
    - The PIR panels performed much better than the PUR with significant less energy released but both at 1:5, 1:2 and at full scale the panels contributed with sufficient energy to cause a failure with external flaming throughout the doorway. The mass loss of the core in the 1:5 scale experiments ranged from 40% to 60% where the remaining core material towards the external boundary often was still virgin. The 1:2 and 1:1 scale experiments confirms that 300 kW (and its scaled equivalent) is beyond the limit of what the panels can mitigate matching with the data from literature.
    - In small scale experiments the SW were found to have the potential to release energy where an internal thermal runaway could occur. When mounted as boundaries of the enclosures the energy released was, however, insignificant and the mass loss was 1% after withstanding a modified fire scenario. At larger scales the smoke production was significantly increased localised around the ceiling area above the burner while the compartment temperatures showed no sign of additional energy being released internally.

- The flashover of the compartment was successfully replicated at 1:2 scale for the steel-faced panels with a PIR core using a stepwise fire scenario. Both compartments reached matching steady state temperature in the gas phase prior to the increase of the HRR from their respective burners, which immediately caused the thermal runaway.
- The time to flashover at 1:5 scale was not different for panels with 6 cm and 10 cm core thickness. This was attributed to the fire growth being a function of the increase in the surface temperature and increasing by the amount of heat conducted through. The increase in surface temperature activated an exothermal reactions within the time period where the contribution from the additional 4 cm closest to the external boundary was negligible.
- The burner placed in the 1:5 scale compartments was very sensitive to the angle of the burner where just a few millimetre caused the fire development to change radically. The location of the burner with respect to the placement in the corner, at the back wall or in the centre showed the corner is provide the most conservative results with respect to the time to failure.
- The global heat transfer across scales is maintained as approximately 60% - 80% convective and 20% - 30% conductive for compartments with boundaries providing negligible core contributions and without discussing any uncertainties. This is despite the fact that the heat flux results show that the heat flux was not scaled correctly for the 1:5 scale experiments. This makes this type of analysis less useful unless other parameters are also included.
- The temperature in the volume of the compartment as well as the net heat flux conducted through the enclosure boundaries was not successfully replicated at the 1:5 scale as compared to the 1:2 and full scale compartment experiments.
- For the PIR panels, the steady state temperatures in the compartment experiments just prior to failure matched those temperature ranges for the larger reactions found in the small scale STA study. These temperature ranges for which PIR in environments of either nitrogen or air can react can therefore be a good first indicator to determine if a product safely can be used for specific projects.
- The simple one-dimensional heat transfer model combined with the thermocouples within the volume of the compartment showed a strong correlation between the 2:5, 1:2 and full scale compartment experiments for the panels with SW core.
    - The net heat transfer during the first burner step both immediately after the ramp up and just prior to the second ramp up of the burner was matching

- After the increase to the second burner step the lowest 17% and highest 20% of the net heat transfer was identical with a higher net heat transfer for the remaining surfaces in favour of the full scale experiment compared to the 1:2 scale.
- The net heat flux prior to termination of the experiment was almost identical for the 2:5 and 1:2 scale experiments.

4 Conclusion

The study of the fire performance of steel-faced insulation panels in a compartment framework was conducted by small scale, scaled and full scale compartment experiments. The small scale experiments provided valuable data with respect to the potential increase in fuel load and the critical temperatures for mass loss, and the critical heat flux for ignition. The importance of the steel-face was identified in the mass loss calorimeter where an exothermal reaction within the unprotected SW core occurred. With the protective steel-face the samples subjected to the highest incident heat flux did not show the same reaction. This indicate a possibility of the occurrence of a smouldering fire penetrating from the core outwards if exposed to radiation directly while oxygen is free to diffuse into the core. In that case, the binder in the core and the glue binding the faces to the core can potentially ignite. Without the protective steel-face the PIR samples ignited instantly when exposed to 20 kW/m^2 or more. The ignition of the polymeric core was, however, successfully delayed when the steel was attached and only limited edge burning was observed. The small scale STA and DSC experiments are simple to conduct and repeat with little effort and provide easily interpretable data. The data provided can assist e.g. fire safety engineers in establishing threshold values for the smoke layer to reach before a significant risk for a thermal runaway and flashover can occur which requires significant resources to mitigate.

The compartments were experimented on in order to increase the quantity of experiments studying the fire performance of the panels in a compartment framework unlike the current test standard. Furthermore, the scaling of the entire compartment and not just a section was useful for understanding the effect of the heat feedback from a hot smoke layer. Continuous measurement of the mass, temperature, gas flow and HRR in the 1:5 scale compartment experiments provided data for the one-dimensional heat transfer model and for calculation of an effective heat of combustion. The difference between the measured complete heat of combustion and the calculated effective heat of combustion for the PIR was more than a factor two confirming either an under-ventilated fire, an effective fire retardant or both.

The compartments with PIR core panels failed at higher $\dot{Q}^*$ values in the 1:5 scale experiments than in the 1:2 and 1:1, which were also much more alike with respect to gas temperature and time to failure. The compartments in 1:5 scale withstood the first two burning steps, thus reaching a quasi-steady state compartment temperature exceeding the temperature near the ceiling compared to the 1:2 and full scale experiments. However, the ceiling temperature for all the experimental scales

was within the temperature ranges for the larger reactions identified in small scale STA experiments, thus proving the value of using even the smallest of scales to acquire fundamental material knowledge.

The heat transfer analysis and compartment temperature showed a poor correlation between the 1:5 scale compartments with SW cores compared with the larger 2:5, 1:2 and the 1:1 scale experiment from literature. The correlations were, however, better between the three larger scales, though only for the first two burner intensities. Complications during the larger scale experiments made a complete comparative analysis with own data difficult, but the 2:5 and 1:2 scale had the same steady state heat flux. A change in compartment dimensions from 2:5 to 1:2 scale is still a reduction of 25%, which reduces the size of the necessary exhaust hood to handle the gases for HRR measurements and 41% reduction in the HRR provided by the burner making the experiment safer to conduct. The success of the scaling was found to be limited to compartments larger or equal to a 2:5 scaling for the compartments constructed with SW panels and 1:2 for those with PIR panels. The full scale SW experiment had the same gas temperature in the compartment during the first burner step as the 1:5 scale experiments had. This was unexpected as the HRR of the gas burner in the full scale experiment was incorrectly made half of the intended. The successful scaling, however, of the larger scaled compartments with SW core was supported by the compartment temperatures as well as the net heat transfer model for the first two burner steps. Exothermic reaction(s) in the PIR core were not compatible with the assumptions of the heat transfer model rendering it too inaccurate and only the temperature of the compartments and time to failure were comparable and both matched for the 1:2 and full scale.

The measured and recorded temperatures, gas flows and HRR at larger and full scale SW experiments enabled the global heat transfer analysis which presented the distribution of heat exchange during the compartment fires across the scales. When the heat exchange within the volume of the compartment was transient and approaching a steady state the ratios between conductive and convective losses changed from 40% to 20% and 40% to 60%, respectively. It was, however, not possible to account for all the energy losses and the unaccounted heat lost conducted through the floor and radiated through the doorway are not to make up for this. This was the same for all the scales and not a scale specific issue.

The *Research Objectives* stated in Section 1.7 were met with respect to determining a successful experimental scale in which the execution of compartment fire experiments could be conducted at a

smaller than full scale. The heavy instrumentation of thermocouples in the compartments enabled analysis of the net heat flux conducted through the solid boundaries, which in turn revealed differences between the 1:5 scale and the other scales with the corresponding theoretical fire size. The partially scaling method preserving the Froude number proved to be robust enough for the relaxation of the dimensionless groups such as for radiation and the Reynolds number for the compartments with both SW and PIR which did not fail and which did fail for scales larger than 1:5, respectively.

The fact that the results from the experiments with the 1:2 scale compartments matched the results from the full scale experiments provides:

- Data for successfully conducting research on compartment fires at smaller scale, which greatly benefits intuitions with smaller laboratories.
- Classifying and regulatory bodies with data to argue in favour of smaller compartments tests, as the reduction allows for faster and safer testing.
- The manufactures with data showing how reduced scale experiments can predict large scale failures for research and development at a reduced expense.

At 1:5 scale the PIR and PUR panels produced two and four times the energy as otherwise ventilation controlled calculations would predict due to external flaming, respectively, while the SW panels remained practically inert and lost 1% of the mass of the core. At 1:2 scale and full scale the PIR panels failed and released abundant heat and black smoke while the heat contribution from the SW core was insignificant at 1:2 scale. Both at 1:2 and at full scale was white smoke release from the compartments with SW indicating a decomposition and combustion of either paint, glue or core material but not sufficiently exothermal to increase the compartment temperature to failure.

The importance of conducting experiments within the framework the products or the function of the materials were evident from this as the failure of the compartment with PIR was replicated at half scale while in the literature the SBI test was incapable of recognizing the failure of a sandwich panel with a combustible cores as pointed out by other authors. The ability to conduct additional experiments can be preferred over a single test as it can provide valuable quantitative parameters important to building fire safety such as the HRR, temperature or the heat flux to internal as well as external boundaries. By being able to conduct more tests in the same time adds robustness to product classifications e.g. by repeating tests for a measure of spread or various design fires to add certainty to the capability of a tested products to withstand multiple fire scenarios. It is also positive

from a design, research and development perspective as they can optimise and improve the design using less resources. The compartment experiments at 1:5 scale showed various fire scenarios at which the compartments with PIR would fail but from an up-scaling was of little importance as the measurements were not matching those from larger scales with the same up-scaled fire. The comparison between compartments with SW core at 2:5 1:2 and full scale showed promising results and were easier to analyse as the core was close to inert throughout the duration of all the experiments. The Froude scaling of the fire to reflect the size of the compartment was not successful across all scales or fire sizes which limits the generic physically based scaling method. However, as the Froude scaling is a partial scaling method it was expected to have boundaries of validity.

The fact that the three studied steel-faced sandwich panels with the same European classification performed so differently under the same conditions is a problem. The European classification is given under very specific conditions where the mounting, use of rivets and edges for the test set-up, where possible, are specified by the manufacturer or distributor ordering the testing. The same specifications were not followed in these experiments as the conditions under which they were conducted were different. As such, the implication of rivets along through the joints or sturdier fixation to internal or external frames are unknown. The current study showed that experiments can be carried out at a smaller scale, which allowed for more measurements and opened up for parametric studies of key attributes. As such, a more robust fire safety test should be possible to develop for sandwich panels.

4.1 Recommendations for Future Work

The data for the full scale experiments from literature in combination with the compartment experiments conducted in this study enables additional scaled experiments with different HRR using a more experimental approach focusing on a scaling correction factor. Constant and step-wise increasing fire scenarios at 1:5 scale with panels with PIR for fire scenarios with the goal of matching the results from both E27 and E29, respectively. The heat transfer analysis between E30 and E2 suggest that 50 kW at full scale is equivalent of 1.79 kW at 1:5 while the gas temperatures for E18, E21 and E27 suggest that 300 kW is slightly more than 5.37 and less than 7.19 kW at 1:5 scale. Conducting a 1:5 scale experiment with PIR panels subjected a fire scenario of 2_4½ to match the data from the 1_3 at full scale is of interest to determine a potential experimental coefficient or term to add to the scaling equation.

The fundamental behaviour of the core materials reported for small scale experiments is too different compared to compartment experiments. The nature and benefits of charring combustible core materials are not recognised at small scales as they are tested or studied either under conservative conditions such as very oxygen rich atmospheres or in sizes preventing the char formation. The solution to scaling the compartment lies in the details and the understanding of the buckling, delamination and pyrolysis are all essential. Additional scaling methods could be of interest such as pressure scaling which is a heavier laboratory demanding scaling method. Future experimental work to study the effect of rivet distance and fixation at larger scales are of interest. At 1:5 scale the compartment temperature did not change more than 10 °C in compartments with joints compared to those without for both PIR and SW compartments. Joints are unavoidable at larger scales and the fixation of steel faces to neighbouring panels could prevent larger openings caused by buckling whereby core materials are exposed directly to conductive and radiative heat transfer rather than conductive.

Alternatively, address the problem from a computational angle. There is now experimentally available data for making a CFD model to compare with. Setting up a model which is able to replicate the results already at hand and target in on a better HRR for the scaled experiments to match the full scale data is a way forward for the panels with SW. Once the model is able to replicate the data a new series of experiments are to be conducted, preferably at a scaled with no data available to blind test the models prediction with the experimentally obtainable data. If successful, research can be directed towards implementing a combustible core in the model.

Bibliography

[1] The Department of Economic and Social Affairs, “World Population Prospects The 2015 Revision - Key Findings and Advance Tables,” The United Nations Population Division, New York, 2015, https://esa.un.org/unpd/wpp/publications/files/key_findings_wpp_2015.pdf.

[2] T. E. Parliament, *DIRECTIVE 2010/31/EU OF THE EUROPEAN PARLIAMENT AND OF THE COUNCIL of 19 May 2010 on the energy performance of buildings,* Bruxelles, 2010; http://eur-lex.europa.eu/legal-content/EN/TXT/PDF/?uri=CELEX:32010L0031&from=en.

[3] WHO; UN Habitat, “Urban Global Report - Section 2: Plan Cities For People,” WHO, 2016, http://www.who.int/kobe_centre/measuring/urban-global-report/ugr_s2.pdf?ua=1.

[4] United Nations, “KYOTO PROTOCOL TO THE UNITED NATIONS FRAMEWORK CONVENTION ON CLIMATE CHANGE,” Kyoto, 1998.

[5] World Wildlife Fund, *Living Planet Report 2014 - Species and spaces, people and places,* Gland, Switzerland: World Wildlife Fund, 2014.

[6] United Nations, *Paris Accord,* Paris, FR: United Nations, 2017, http://unfccc.int/paris_agreement/items/9485.php.

[7] International Energy Agency, Experience Curves for Energy Technology Policy, Paris, Fr: International Energy Agency (IEA), 2000.

[8] E. Dominguez-Rosado, J. J. Liggat, C. E. Snape, B. Eling and J. Pichtel, “Thermal degradation of urethane modified polyisocyanurate foams based on aliphatic and aromatic polyester polyol,” *Polymer Degradation and Stability,* vol. 78, no. 1, pp. 1-5, 2002, doi: 10.1016/S0141-3910(02)00086-1.

[9] M. Modesti and A. Lorenzetti, “Recent Trends in Flame Retardancy of Polyurethan Foams,” in *Progress in Polymer Degradation and Stability Research*, New York, Nova Science Publishers, Inc, 2008, pp. 115-148.

[10] Buildings Performance Institute Europe, “Europe’s Buildings Under the Microscope - A country-by-country review of the energy performance of buildings,” Brussels, 2011, http://bpie.eu/wp-content/uploads/2015/10/HR_EU_B_under_microscope_study.pdf.

[11] K. G. PLC, “Annual Report & Financial Statements,” Kingspan, 2013.

[12] K. Dedecker, J. Deschaght and R. Kumar, “Sandwich Panels - Supporting Growth with an

Established and Proven Technology," PU Tech, Huntsman Polyurethanes, Belgium, 2008.

[13] European Insulation Manufactures Association, "The Critical Importance of Building Insulation for the Environment," EURIMA, Brussels, 2001, http://www.eurima.org/uploads/Modules/Mediacentre/brochure_en.pdf.

[14] A. Papadopoulos, "State of the Art in Thermal Insulation Materials and Aims for Future Developments," *Energy and Buildings,* vol. 37, no. 1, pp. 77-86, 2005, doi:10.1016/j.enbuild.2004.05.006.

[15] *SANDWICH PANELS,* Rautaruukki Corporation, accessed 2018, https://www.ruukki.com/gbr/b2b/products/sandwich-panels.

[16] J. P. Hidalgo, "Performance-Based Methodology for the Fire Safe Design of Insulation Materials in Energy Efficient Buildings," The University of Edinburgh, Phd thesis, 2015.

[17] Izopanel, *Sandwich panels - Technical catalogue,* Gdańsk, 2012, http://www.izopanel.org/files/Katalog_techniczny_ENG.pdf.

[18] Eurobond, *Firemaster - Internal wall and ceiling panel system,* 2017.

[19] EAE, "System loyalty pays off! - Why respecting the system is essential for quality, safety and long-term performance of External Thermal Insulation Composite Systems (ETICS).," European Association for External Thermal Insulation Composite Systems, Baden-Baden, http://etics.dk/media/20180/dk_brochure-system-loyality-pays-off.pdf [accessed 10(08/2017].

[20] SAND.CORe, "Best Practice Guide for Sandwich Structures in Marine Applications," Edited by NewRail, University of Newcastle upon Tyne, 2013, http://www.transport-research.info/sites/default/files/project/documents/20130201_105501_16344_RevisedBPGv1-00---Report-Format.pdf.

[21] C.-H. Wang and Y.-C. Huang, "Optimization Model For Construction Project Durations Using A Multistage Decision Process," *Engineering Optimization ,* vol. 30, no. 2, pp. 155-173, 1998, DOI: 10.1080/03052159808941242.

[22] Lego, *THE LEGO GROUP REACHES 100% RENEWABLE ENERGY TARGET THREE YEARS AHEAD OF SCHEDULE,* Billund, 2017, https://www.lego.com/en-us/aboutus/news-room/2017/may/100-percent-renewable-milestone.

[23] BRE, "The Green Guide to Specifications, Life Cycle Analysis," https://www.bre.co.uk/page.jsp?id=1578, 2016.

[24] A. D. D. Ferreira and F. B. Mainier, “Application of Life Cycle Assessment (LCA) in Construction Industry,” *International Journal of Civil & Environmental Engineering IJCEE-IJENS,* vol. 15, no. 5, pp. 1-5, 2015, http://ijens.org/Vol_15_I_05/150705-6868-IJCEE-IJENS.pdf.

[25] C. Falstrup, “Klimavenligt Byggeri - Med Moderne Byggematerialer,” in *Klimavenligt Byggeri Med Moderne Byggematerialer*, Copenhagen, 2015.

[26] C. Dossche, V. Boel and W. De Corte, “Use of Life Cycle Assessments in the Construction Sector: Critical Review,” *Procedia Engineering,* vol. 171, pp. 302-311, 2017, doi: 10.1016/j.proeng.2017.01.338.

[27] J. D. Silvestre, J. de Brito and M. D. Pinheiro , “Building’s External Walls in Life Cycle Assessment (LCA) Research Studies,” in *Portugal SB10 - Sustainable Building Affordable to All*, Algarve, P, 2010, https://www.irbnet.de/daten/iconda/CIB17437.pdf.

[28] R. Mateus, “Master thesis - Novas tecnologias construtivas com vista à sustentabilidade da construção,” Universidade do Minho, Braga, P, 2004.

[29] J. R. Booth, R. S. Graves and D. W. Yarbrough, “Effective Diffusion Coefficients for CFC-11 by Gravimetric Depletion from Thin Slices of PIR Foam,” in *Proceedings of the Twenty-Third International Thermal Conductivity Conference*, Tennessee, 1996.

[30] A. Schnipper, L. Smith-Hansen and E. Sonnich Thomsen, “Reduced combustion efficiency of chlorinated compounds, resulting in higher yields of carbon monoxide,” *Fire and Materials,* vol. 19, no. 2, pp. 61-64, 1995, doi: 10.1002/fam.810190203.

[31] D. B. Spalding, “Some Fundamentals of Combustion,” Butterworths, London, 1955.

[32] United Nations, *THE MONTREAL PROTOCOL ON SUBSTANCES THAT DEPLETE THE OZONE LAYER,* Montreal, Canada: United Nations Environment Programme - The Ozone Secretariat, 1987.

[33] S. N. Singh, *Optimizing Polyiso Blowing Agents,* Texas, USA: Huntsman Advanced Technology Center.

[34] L. Ross, “A blowing agent update - Learn why the change to pentane was made and what it means for polyiso,” *Professional Roofing,* Feb 2005, http://www.professionalroofing.net/Articles/A-blowing-agent-update--02-01-2005/590.

[35] Dentons US, LLP, “Emission Reduction Measurement and Monitoring Methodology for the Conversion of Foam Blowing Agents from High-GWP Materials to Low-GWP Materials,”

American Carbon Registry, 2014.

[36] Department for Environment, Food & Rural Affairs, *Bans on F gas in new equipment,* 2014, URL: https://www.gov.uk/guidance/bans-on-f-gas-in-new-equipment.

[37] L. Anthony Cox Jr, "What's Wrong with Risk Matrices," *Risk Analysis,* vol. 28, no. 2, pp. 497-512, 2008.

[38] *EN 13823:2010 - The Single Burning Item Test,* B-1000 Brussels: European Committeee for Standarisation, 2010.

[39] *EN 13501-1 + A1:2009, Fire classification of construction products and building elements - Part 1: Classification using data from reaction tests,* B-1000 Brussels: European Committeee for Standarisation, 2009.

[40] B. Messerschmidt, "The Capabilities and Limitations of the Single Burning Item (SBI) Test," in *Fire and Building Safety in the Single European Market. Does CE Compliance Ensure Fire Safety?*, Edinburgh, 2008.

[41] D. Gayle, "The Guardian," 24 02 2017. [Online]. Available: https://www.theguardian.com/uk-news/2017/feb/24/southwark-council-admits-safety-failings-tower-block-lakanal-house-blaze. [Accessed 16 08 2017].

[42] UC Davis Health, "UC Davis Health," 07 02 2012. [Online]. Available: https://www.ucdmc.ucdavis.edu/publish/news/newsroom/6199. [Accessed 16 08 2017].

[43] G. Will, "BBC News," 05 06 2014. [Online]. Available: http://www.bbc.com/news/world-latin-america-27684358. [Accessed 08 08 2017].

[44] The Human Rights Watch, "The Human Rights Watch," 14 11 2013. [Online]. Available: https://www.hrw.org/news/2013/11/14/bangladesh-factory-deaths-could-have-been-prevented. [Accessed 16 08 2017].

[45] L. Pasha-Robinson, "The Independent," 08 08 2017. [Online]. Available: http://www.independent.co.uk/news/uk/home-news/grenfell-tower-fire-victims-numbers-death-met-police-identify-remains-bodies-a7882246.html. [Accessed 16 08 2017].

[46] *Grenfell Tower - How Did It Happen?,* Passiv House +, Aug, 2017, https://passivehouseplus.ie/magazine/dispatches/grenfell-tower-how-did-it-happen.

[47] *ISO 13784-1:2014 Reaction to Fire Tests for Sandwich Panel Building Systems - Part 1: Small Room Test,* Genéve: International Organization for Standardization, 2014.

[48] *ISO 834 - Fire Resistance Tests Elements of Building Construction,* Genéve: International

Organization for Standardization, 1975.

[49] T. Z. Haramathy and T. T. Lie, “Fire Test Standard in the Light of Fire Research,” *Fire Test Performance: Symposium Presented at the Winter Meeting ASTM,* pp. 85-97, 1969, doi: 10.1520/STP44713S.

[50] HM Government, *Approved Document B,* HM Government, 2010, https://www.gov.uk/government/uploads/system/uploads/attachment_data/file/485420/BR_PDF_AD_B1_2013.pdf.

[51] Building Control Alliance, *BCA Technical Guidance Note 18 - Use of Combustible Cladding Materials on Buildings Exceeding 18m in Height,* BCA, 2015, https://www.labc.co.uk/sites/default/files/BCA%20GN%2018%20-Use%20of%20combustible%20cladding%20materials%20-%20Rev%201%20-%20Jun%2015.pdf.

[52] *Fire safety: Approved Document B,* GMGovernment, 2006 incorporating the 2010 and 2013 amendments.

[53] *NFPA 204 - Standard for Smoke and Heat Venting,* 2015.

[54] Nordtest, “UPHOLSTERED FURNITURE: BURNING BEHAVIOUR - FULL SCALE TEST,” Nordtest, Esbo, Findland, 1991, ISSN 0283-7188.

[55] B. Sundström, “Upholstered furniture. Another Application of the new technology,” 1986.

[56] B. Sundström, “A New Generation of Large Scale Fire Test Methods (Report SE-LUTVDG/TVBB-33054),” Swedish National Testing Institute, Borås, 1990, publikationer.extweb.sp.se/ViewDocument.aspx?RapportId=136.

[57] H. L. de Witte, “Impression tests upholstered furniture and mattresses,” Arnhem: Institute For Safety., Arnhem, 2017, .

[58] S. Mehta, “Upholstered Furniture Full Scale Chair Tests – Open Flame Ignition Results and Analysis,” United States Consumer Product Safety Commission, BETHESDA, MD 20814, 2012, https://www.cpsc.gov/s3fs-public/openflame.pdf.

[59] SP Technical Research Institute of Sweden, “Smoke and Heat Emission during fire resistance test of sandwich panel walls - Draft,” SP, Borås, 2013.

[60] *ISO 5660-1:2015 Reaction-to-fire tests -- Heat release, smoke production and mass loss rate -- Part 1: Heat release rate (cone calorimeter method),* Genève: International Organization for Standardization, 2015 .

[61] *BS 476-15 : Fire Tests on Building Materials and Structures Part 15: Method of Measuring the Rate of Heat Release of Products,* British Standard, 1993.

[62] S. Rabe and B. Schartel, "The rapid mass calorimeter: Understanding reduced-scale fire test results," *Polymer Testing,* vol. 57, pp. 165-174, 2017, 10.1016/j.polymertesting.2016.11.027.

[63] A. B. Morgan and E. Toubia, "Cone calorimeter and room corner fire testing of balsa wood core/phenolic composite skin sandwich panels," *Journal of Fire Science,* vol. 32, no. 4, pp. 328-345, 2014.

[64] H. Yoshioka, Y. Tanaka, Y. Nishio, X. Zhao, M. Tamura, Y. Tanaike, T. Noguchi, K. Kobayashi, Y. Ohmiya, M. Kanematsu and M. Yoshida, "Intermediate-Scale Free-Standing Box test for Fire Performance of Sandwich Panels," *Fire Science and Technology,* vol. 33, no. 2, pp. 47-58, 2014.

[65] P. Johansson and P. Van Hees, "Development of a Test Procedure for Sandwich Panels Using ISO 9705 Philosophy - Nordtest Project nr 1432-99," SP, Borås, 2000.

[66] J. Axelsson and P. V. Hees, "New Data for Sandwich Panels on the Correlation Between SBI Test Method and the Room Corner Reference Scenario," *Fire and Materials,* vol. 29, no. 1, pp. 53-59, 2004.

[67] H. Yoshioka, . Y. Tanaka, N. Yuhei, T. Noguchi, K. Kobayashi, . Y. Ohmiya, M. Kanematsu, . T. Ando, T. Naruse, . K. Kagiya and T. Hayakawa, "Self-standing Compartment Fire Tests on Sandwich Panels," *Fire Science and Technology,* vol. 35, no. 1, pp. 19-83, 2014, https://www.jstage.jst.go.jp/article/fst/35/1/35_19/_pdf/-char/en.

[68] A. I. Bartlett, R. M. Hadden, J. P. Hidalgo, S. Santamaria, F. Wiesner, L. A. Bisby, S. Deeny and B. Lane, "Auto-extinction of engineered timber: Application to compartment fires with exposed timber surfaces," *Fire Safety Journal, IAFSS 12th Symposium 2017,* vol. 91, pp. 407-413, 2017, http://dx.doi.org/10.1016/j.firesaf.2017.03.050.

[69] R. Emberley, C. G. Putynska, A. Bolanos, A. Lucherini, A. Solarte, D. Soriguer, M. G. Gonzalez, H. Humphreys, J. P. Hidalgo, C. Maluk, A. Law and J. L. Torero, "Description of small and large-scale cross laminated timber fire tests," *Fire Safety Journal,* vol. 91, pp. 327-335, 2017, DOI: 10.1016/j.firesaf.2017.03.024.

[70] T. R. Hull, A. Wotkowski and L. Hollimhbery, "Fire retardant action of mineral fillers," *Polymer Degradation and Stability,* vol. 96, no. 8, pp. 1462-1469, 2011, doi: 10.1016/j.polymdegradstab.2011.05.006.

[71] S. Molyneux, A. A. Stec and T. R. Hull, “The effect of gas phase flame retardants on fire effluent toxicity,” *Polymer Degradation and Stability,* vol. 106, pp. 36-46, 2014, doi: 10.1016/j.polymdegradstab.2013.09.013.

[72] *ASTM E2102 − 14 Standard Test Method for Measurement of Mass Loss and Ignitability for Screening Purposes Using a Conical Radiant Heater,* 2014, doi: 10.1520/E2102-14.

[73] FM Global, *FM 4882 - Approval Standard for Class 1 Interior Wall and Ceiling Materials or Systems for Smoke Sensitive Occupancies,* 2010.

[74] *NFPA 286 - Standard Methods for Fire Tests for Evaluating Contribution of Wall and Ceiling Interior Finish to Grrom Fire Growth,* Quincy, MA, 2015.

[75] Rockwool International, *From waste to resource - utilising more residue materials from other industries in the Rockwool process.*

[76] A. Dunster, “Characterisation of Mineral Wastes, Resources and Processing technologies – Integrated waste management for the production of construction material,” BRE, 2007.

[77] Eurobond, “Contemporary external wall panel system,” 2017.

[78] Rockwool International, “Technical Data Sheet: Rockwool Duraflex, Pressure-resistant Stone Wool Mat,” 2011.

[79] “DIN 4102-17. Fire behaviour of building materials and elements. Determination of melting point of mineral fibre insulating materials. Concepts, requirements and testing,” 2016.

[80] M. Bomberg and S. Klarsfeld, “Semi-Empirical Model of Heat Transfer in Dry Mineral Fibre Insulation,” *Journal of Building Physics,* vol. 6, no. 3, pp. 156-173, 1983, doi: 10.1177/109719638300600304.

[81] S. Klarsfeld, “La conductivite des isolants fibreux en fonction de leur structure,” *Cahiers du Centre Scientifique et Technique du Batiment,* vol. 213, pp. 38-50, 1980.

[82] C. Bankvall, “Heat Transfer in Fibrous Materials,” *Journal of Testing and Evaluation,* vol. Vol. 1, no. No. 3, pp. 235-243, 1973, doi: 10.1520/JTE10010J.

[83] D. Fournier and S. Klarsfeld, *Some Recent Experimental Data on Glass Fiber Insulating Materials and Their Use for a Reliable Design of Insulations at Low Temperatures,* 1974, doi: 10.1520/STP34781S.

[84] S. Klarsfeld, “La conductivite thermique des isolants fibreux en relation avec leur structure,” *Compte rendus scientifiques, Groupement Universitaire de Thermique,* 1976.

[85] S. Dyrbøl, “Heat transfer in Rockwool modelling and method of measurement,” *Phd thesis,*

Technical University of Denmark, Denmark, 1998, http://orbit.dtu.dk/files/5285904/Dyrb%C3%B8l1.pdf.

[86] S. R. Piñeiro, M. d. R. Merino and C. P. García, "New Plaster Composite with Mineral Wool Fibres from CDW Recycling," *Advances in Materials Science and Engineering,* 2015, doi: 10.1155/2015/854192.

[87] F. de Dianous, F. Pincemin, B. Pascal and G. Jeandel, "MODELING AND EXPERIMENTAL EVALUATION OF THE THERMAL INSULATION PROPERTIES OF MINERAL WOOL PRODUCTS AT HIGH TEMPERATURE," *Insulation Materials: Testing and Applications, ASTM STP 1320,* vol. 3, 1997, doi: 10.1520/STP12278S.

[88] K. Livkiss, B. Andres, N. Johansson and P. v. Hees, "Uncertainties in modelling heat transfer in fire resistance tests: A case study of stone wool sandwich panels," *Fire and Materials,* 2017.

[89] *EN 14509:2013 - Self-supporting double skin metal faced insulating panels – Factory made products – Specifications,* B-1000 Brussels: European Committeee for Standarisation, 2013.

[90] "ASTM E119-16a, Standard Test Methods for Fire Tests of Building Construction and Materials," ASTM International, West Conshohocken, PA, 2016, doi: 10.1520/E0119-16A.

[91] FM Global, *Approval Standard 4880 for fire performance.*

[92] G. Avar, W. Meier, H. Casselmann and D. Achten, "Polyurethanes," *Polymer Science: A Comprehensive Reference,* vol. 10, pp. 411-441, 2012, doi: 10.1016/B978-0-444-53349-4.00275-2.

[93] S. T. McKenna and R. T. Hull, "The fire toxicity of polyurethane foams," *Fire Science Reviews,* vol. 5, no. 3, 2016, doi: 10.1186/s40038-016-0012-3.

[94] B. D. Kaushiva, *Structure-Property Relationships Of Flexible Polyurethane Foams,* Phd Thesis: Virginia Polytechnic Institute and State University, 1996.

[95] A. Z. Gharehbagh A, "Chapter 6: Polyurethane Flexible Foam Fire," in *Polyurethane*, E. S. Fahima Z, Ed., 2012, doi: 10.5772/47965, pp. 102-120.

[96] B. Czupryński, J. Liszkowska and J. Paciorek-Sadowska, "Modyfication of the Rigid Polyurethane-Polyisocyanurate Foams," *Journal of Chemistry,* pp. 1-12, 2014, doi: 10.1155/2014/130823.

[97] S. N. Singh, J. S. Fife, S. Dubs and P. D. Coleman, *Effect of Formulation Parameters on Performance of Polyisocyanurate Laminate Boardstock Insulation,* Huntsman Advanced Technology Center, 2006.

[98] IAL Consultants, “Rigid Metal-Faced Insulated Panel Production and Products,” IAL Consultants, London, 2015.

[99] Kingspan Ltd, *Architectural Wall Panel Range KS600-1000 CW, CX, EB, FL, FL-S, LV, MM, MR, PL, TL, WV, Product Data Sheet,* 2017, https://www.kingspan.com/gb/en-gb/products/insulated-panel-systems/downloads/kingspan-architectural-wall-panel-datasheet.

[100] Lindab, “Sandwich Wall Panels - Technical Facts,” accessed: 04.04.2018, https://itsolution.lindab.com/LindabWebProductsDoc/PDF/Documentation/BuildingProducts/Lindab/Technical/Sandwichpanel.pdf.

[101] Metecno Group, *Sandwich wall element with polyurethane hard foam and concealed fastening - SUPERWALL ML,* Provided 2017.

[102] “Contemporary External Wall Panel System,” Europanels, accessed: 04.04.2018, http://www.eurobond.co.uk/media/25677/europanel_brochure_lr.pdf.

[103] Europerfill, *Facade Sandwich Panel - ETNA Advance 600,* 2017, http://www.archiexpo.com/prod/europerfil/product-50760-1684060.html.

[104] Kingspan, “Kingspan_Architectural Wall Panel_Horizontal_CAD_DWG,” 2017, https://www.kingspan.com/gb/en-gb/products/insulated-panel-systems/wall-panel-systems/architectural-wall-ks1000-awp-en.

[105] Isolparma Rigid foam;, *Isolparma Rigid Foam Technical Data Sheet RF3,* Due Carrare, IT: Isolparma Srl, 2007, http://www.bel-mat.be/Pirisol/RF3.pdf.

[106] REACT, *Thermal insulation materials Polyurethane (PUR) and Polyisocyanurate (PIR) foam,* Eisenstadt, AUT: REACT: Renewable Energy and Efficiency Action, 2013, http://www.react-ite.eu/uploads/tx_mddownloadbox/PP02_Thermal_insulation_materials_-_PP02_20130715.pdf.

[107] Rockwool, *Technical Insulation Data Sheet Pipes,* Sofia, BG: SIPER-BULGARIA Ltd, 2004, http://www.siper-bg.com/files/products/pic136_1_en.pdf.

[108] Chemical Products, *Technical Datasheet of Mineral Stone Wool Lamella MAT ISOLLAM,* Yambol, BG: Chemical Products Insulation Solutions, http://www.chemprod.eu/headers/567c2c6abbaa4c6afa1c3a182bf84eb15f5e4e65.pdf.

[109] *EN 1363 - Fire resistance tests,* B-1000 Brussels: European Committeee for Standarisation, 1999.

[110] *BS 8414-1 Fire performance of external cladding systems. Test methods for non-loadbearing external cladding systems applied to the face of a building,* British Standard Institution, 2015.

[111] *BS 8414-2:2005 Fire performance of external cladding systems. Test method for non-loadbearing external cladding systems fixed to and supported by a structural steel frame,* British Standards Institution, 2015.

[112] *SP Fire 105 - External wall assemblies and facade claddings - Reaction to fire,* Boräs: SP Technical Research Institute of Sweden, 1994.

[113] *FM 4881 - Approval Standard for Class 1 Exterior Wall Systems,* 2007.

[114] *EN ISO 1182:2010 Reaction to fire tests for products – Non-combustibility test,* B-1000 Brussels: European Committeee for Standarisation, 2010.

[115] *EN ISO 1716:2010 - Reaction to fire tests for products – Determination of the gross heat of combustion (calorific value),* B-1000 Brussels: European Committeee for Standarisation, 2010.

[116] VTT, “EUROCLASS System,” [Online]. Available: http://virtual.vtt.fi/virtual/innofirewood/stateoftheart/database/euroclass/euroclass.html#classescriteria. [Accessed 21 07 2017].

[117] *EN ISO 11925-2:2010, Reaction to fire tests - Ignitability of building products subjected to direct impingement of flame - Part 2: Single-flame source test.,* B-1000 Brussels: European Committeee for Standarisation, 2010.

[118] *ISO 9705-1:2016 Reaction to fire tests – Room corner test for wall and ceiling lining products – Part 1: Test method for a small room configuration,* Genève: International Organization for Standardization, 2016.

[119] “Series of fire growth tests for LPCB approval and listing of construction product systems, Part one: Requirements and tests for built up cladding and sandwich panel systems for use as the external envelope of buildings,” BRE Global Ltd, 2014, https://www.redbooklive.com/download/pdf/LPS1181part1.pdf.

[120] Minstry of Transport, Building and Housing, “"Nu bliver det nemmere at bygge i Danmark (It will now be easier to build in Denmark)",” Copenhagen K, 2016, https://www.trm.dk/da/ministeriet/nu-bliver-det-nemmere-at-bygge-i-danmark, accessed 11.11.2017.

[121] S. McKenna, R. Birtles, K. Dickens, R. Walker, M. Spearpoint, A. A. Stec and T. R. Hull, “Flame

retardants in UK furniture increase smoke toxicity more than they reduce fire growth rate," *Chemosphere,* p. In Press, 2017, DOI: 10.1016/j.chemosphere.2017.12.017.

[122] S. Olsson, "Calibration of Fire Resistance Furnaces with Plate Thermometers," Commission of the European Communities bcr information, 1993, https://publications.europa.eu/da/publication-detail/-/publication/d140018f-029f-4f18-aa6f-195227ce9c48.

[123] DBI - Dansk Brand og sikrings Institut, "Brandtests bliver billigere med DBI's nye miniovn," *Brand & Sikring,* no. 2, pp. 4-5, 2017.

[124] P. v. Hees and P. Johansson, "The need for full-scale testing of sandwich panels - comparison of full scale test and intermediate scale tests," *Interflam,* pp. 495-503, 2001.

[125] S. H. Clarke, "Twenty Five Million Pounds Go Up In Smoke," Fire Research Notes 286, 1956, http://www.iafss.org/publications/frn/286/-1/view/frn_286.pdf.

[126] B. Bøhm, "Fire resistance tests and differentiated design procedures — The Building Code: Aims and means," *Fire Technology,* vol. 14, no. 3, pp. 239-246, 1978, doi: 10.1007/BF01983058.

[127] C. H. Maluk Zedán, "Development and Application of a Novel Test Method for Studying the Fire Behaviour of CFRP Prestressed Concrete Structural Elements, PhD. Thesis," The University of Edinburgh, 2014.

[128] D. M. Marquis, M. Pavageau and E. Guillaume, "Multi-scale simulations of fire growth on a sandwich composite structure," *Journal of Fire Science,* vol. 31, no. 1, pp. 3-34, 2012.

[129] S. E. Magnusson and S. Thelandersson, "Temperature-time curves of complete process of fire development : theoretical study of wood fuel fires in enclosed spaces," Royal Swedish Academy of Engineering Sciences, Stockholm, 1970.

[130] O. Pettersson, S. E. Magnusson and J. Thor, "Fire Engineering Design of Steel Structures, Swedish Institute of Steel Construction, Publication No. 50," Swedish Institute of Steel Construction, Stockholm, 1976, http://portal.research.lu.se/portal/files/5989339/1245743.pdf.

[131] P. v. Hees, "Only large-scale tests can properly evaluate the fire behavior of sandwich panels," *Brandposten,* no. 33, Published by SP, 2005.

[132] T. Z. Haramathy, "A new look at compartment fires," *Fire Technology,* vol. 8, no. 3, pp. 196-217, 1972, doi:10.1007/BF02590544.

[133] M. X. Sørensen, J. M. Hidalgo, M. Mclaggan, R. J. Crewe, S. Molyneux, A. Sønderskov, G. Jomaas, S. Welch, J. L. Torero, R. T. Hull and A. A. Stec, “Fire performance of sandwich panels in a modified ISO room test,” *Materiały Budowlane,* no. 10, pp. 58-61, 2014.

[134] R. C. Corlett and A. Luketa-Hanlin, “Pressure Scaling of Fire Dynamics,” in *Saito K. (eds) Progress in Scale Modeling*, Dordrecht, Springer, 2008, DOI: 10.1007/978-1-4020-8682-3_7, pp. 85-97.

[135] Y. Z. Li and H. Ingason, “Scaling of wood pallet fires,” *Fire Safety Journal,* vol. 88, pp. 96-103, 2017.

[136] G. Heskestad, “Modeling of Enclosure Fires,” in *Proceedings of the Fourteenth Symposium (International) on Combustion*, The Pennsylvania State University, USA, 1972.

[137] J. Quintiere, “Application of scale fire modeling,” *Fire Safety Journal,* vol. 15, pp. 3-29, 1989.

[138] D. Drysdale, *An Introduction to Fire Dynamics,* Wiley, 2011.

[139] F. A. Williams, “Scaling Mass Fires,” *Fire Research Abstracts and Reviews,* vol. 11, 1969.

[140] G. Hestestad, “Physical Modeling of Fire,” *Journal of Fire and Flammability,* vol. 6, no. 3, pp. 253-273, 1975.

[141] J. G. Quintiere, Fundamentals of Fire Phenomena, John Wiley & Sons, Inc, 2006.

[142] B. J. McCaffrey, “Purely Buoyant Diffusion Flames: Some Experimental Results, NBSIR 79-1910,” National Bureau of Standards (NIST), 1979.

[143] G. Heskestad, “Fire Plumes, Flame Height, and Air Entrainment,” in *SFPE Handbook for fire Safety Engineering*, Springer, 2016, DOI: 10.1007/978-1-4939-2565-0, pp. 396-428.

[144] B. J. McCaffrey, J. G. Quintiere and M. F. and Harkleroad, “Estimating Room Fire Temperatures and the Likelihood of Flashover Using Fire Test Data Correlations,” *Fire technology,* vol. 17, no. 2, pp. 98-119, 1981, DOI: 10.1007/BF02993495.

[145] B. Karlsson and J. G. Quintiere, Enclosure Fire Dynamics, CRC Press, 1999.

[146] *ISO 11358-1:2014, Thermogravimetric (TG) of Polymers – Part 1: General principles,* Genève: International Organization for Standardization, 2014.

[147] NETZSCH, “STA 449 F3 Jupiter,” Selb, 2017, https://www.netzsch-thermal-analysis.com/en/products-solutions/simultaneous-thermogravimetry-differential-scanning-calorimetry/sta-449-f3-jupiter/.

[148] M. M. HIRSCHLER, “Thermal decomposition (STA and DSC) of PVC compounds under a

variety of atmospheres and heating rates," *European Polymer Journal,* vol. 22, no. 2, pp. 153-160, 1986, DOI: 10.1016/0014-3057(86)90111-4.

[149] R. R. Leisted, M. X. Sørensen and G. Jomaas, "Experimental study on the influence of different thermal insulation materials on the fire dynamics in a reduced-scale enclosure," *Fire Safety Journal,* vol. 93, pp. 114-125, 2017, https://doi.org/10.1016/j.firesaf.2017.09.004.

[150] M. X. Sørensen, "Small and medium scale fire experiments with different insulation materials," *Department of civil engineering,* vol. Thesis, p. Technical University of Denmark, 2014.

[151] Perkin Elmer, "STA 6000 - Simultaneous Thermal Analyzer," Perkin Elmer, Waltham, MA, 2008, https://www.perkinelmer.com/Content/RelatedMaterials/Brochures/BRO_STA-6000.pdf.

[152] NFPA, "NPFA 271 - Standard Method of Test for Heat and Visible Smoke Release Rates for Materials and Products Using an Oxygen Consumption Calorimeter," National Fire Protection Association, Quincy Maryland, 2009.

[153] A. E1354-17, "ASTM - Standard Test Method for Heat and Visible Smoke Release Rates for Materials and Products Using an Oxygen Consumption Calorimeter," ASTM International, West Conshohocken, PA, 2017, 2017.

[154] S. Chernyy, S. Ullah, G. Jomaas, P. A. Mindykowsky, R. R. Leisted, J. B. Ravnsbæk, S. W. Tordrup and K. Almdal, "Modification of poly(styrene-block-butadiene-block-styrene) [SBS] with phosphorus containing fire retardants," *European Polymer Journal,* vol. 70, pp. 136-146, 2015.

[155] M. Försth and A. Roos, "Absorptivity and its Dependence on Heat Source Temperature and Degree of Thermal Breakdown," *Fire and Materials,* vol. 25, p. 285–301, 2011. DOI: 10.1002/fam.1053.

[156] P. Patel, T. R. Hull, A. A. Stec and R. E. Lyon, "Influence of physical properties on polymer flammability in the cone calorimeter," *Polymers for Advanced Technologies,* vol. 22, p. 1100–1107, 2011. DOI: 10.1002/pat.1943.

[157] P. A. Beaulieu and N. A. and Dembsey, "Flammability Characteristics at Applied Heat Flux Levels up to 200 kW m-2," *Fire and Materials,* pp. 61-86, 2008. DOI: 10.1002/fam.948.

[158] Fire Testing Technology, *Mass Loss Calorimeter,* Grinstead, England: http://www.fire-testing.com/mass-loss-calorimeter, 2017.

[159] V. Babrauskas, “Development of the cone calorimeter -- a bench-scale heat release rate apparatus based on oxygen consumption,” National Bureau of Standards Center for Fire Research, NBSIR 82-2611, Washington, DC, 1982.

[160] V. Babrauskas, “Development of the cone calorimeter – a bench scale heat release rate apparatus based on oxygen consumption,” *Fire and Materials,* vol. 8, no. 2, pp. 81-95, 1984, DO: 10.1002/fam.810080206.

[161] IKA, *C 200 Data sheet,* IKA® Werke Staufen/Germany 2017, 2017.

[162] P. H. Thomas, “Behavior of fires in enclosure - Some recent progress,” *Symposium (International) on Combustion,* vol. 14, no. 1, pp. 1007-1020, 1973, doi: 10.1016/S0082-0784(73)80091-8.

[163] *ISO 13784-2:2002 Reaction to Fire Tests for Sandwich Panel Building Systems - Part 2: Test method ofr large roomds,* Genéve: International Organization for Standardization, 2002.

[164] P. Thomas, A. J. Heselden and M. Law, “Fully-developed compartment fires -two kinds of behaviour,” *Fire Research Technical Paper, HMSO, London,* no. No. 18, 1967.

[165] T. M. Harmathy, “Design of Buildings for Fire Safety - Part I,” *Fire Technology,* pp. 95-108, 1975; .

[166] “FireFree® ScandiBoard 850 - Declaration of Performance,” Scandi Supply a/s, 2017.

[167] Kosangas, *Safety Data Sheet,* 2013.

[168] W. H. Seaton and B. K. Harrison, “A new general method for estimation of heats of combustion forhazard evaluation,” *Journal of Loss Prevention in the Process Industries,* vol. 3, no. 3, pp. 311-320, 1990, doi:10.1016/0950-4230(90)80025-6.

[169] M. Janssens, “Measuring Rate of Heat Release by Oxygen Consumption,” *Fire Technology,* pp. 234-249, 1991.

[170] W. Thornton, “The Relation of Oxygen to the Heat of Combustion of Organic Compunds,” *Philosophical Magazine and Journal of Science,* vol. 33, 1917.

[171] C. Hugget, “Estimation of rate of heat release by means of oxygen consumption measurements,” *Fire and Materials,* vol. 4, no. 2, pp. 61-65, 1980, DOI: 10.1002/fam.810040202.

[172] B. J. McCaffrey and G. Heskestad, “A Robust Bidirectional Low-Velocity Probe for flame and Fire Application,” *Combustion and Flame,* vol. 26, pp. 125-127, 1976.

[173] B. Hägglund, “Simulating Fires in Natural and Forced Ventilated Enclosures,” *FOA Rapport C*

20637-2.4, no. National Defense Research Institute, 1986.

[174] J. M. Hidalgo, C. Maluk, A. Cowlard, C. Abecassis-Empis, M. Krajcovic and J. L. Torero, "A Thin Skin Calorimeter (TSC) for quantifying irradiation during large-scale fire testing," *International Journal of Thermal Sciences,* vol. 112, p. 383–394, 2016.

[175] H. Ingason and U. Wickström, "Measuring incident radiant heat flux using the plate thermometer," *Fire Safety Journal,* vol. 42, no. 2, p. 161–166, 2007.

[176] *EN 1993-1-2:2005 - Eurocode 3. Design of steel structures. Part 1-2: General Rules - Structural Fire Design,* B-1000 Brussels: European Committeee for Standarisation, 2005.

[177] P. Veloo and J. G. Quintiere, "Convective heat transfer coefficient in compartment fires," *Journal of Fire Sciences,* pp. 1-14, 2013, doi: 10.1177/0734904113479001.

[178] INCO The International Nickel Company, "Mechanical and physical properties of the austenitic chromium-nickel stainless steels at elevated temperatures," 1968.

[179] B. Raveendran Nair, *Kinetics and mechanism of urea - formaldehyde and related reactions,* University of Cochin, India, 1981, http://dyuthi.cusat.ac.in/purl/3619.

[180] S. Kowatsch, "Chapter 10 - Mineral Wool Insulation Binders," in *Phenolic Resins: A Century of Progress*, New York, Springer , 2010, doi: 10.1007/978-3-642-04714-5, pp. 209-242.

[181] Y. Yue, M. Korsgaard and L. F. Kirkegaard, "Formation of a Nanocrystalline Layer on the Surface of Stone Wool Fibers," *Journal of the American Ceramic Society,* vol. 92, no. 1, pp. 62-67, 2009.

[182] H. Olsen, J. Sjöström, Jansson, Robert and J. Anderson, "Thermal Properties of Heated Thermal Insulation Materials," *Interflam,* pp. 1049-1060, 2013.

[183] J. Crank and P. Nicolson, "A practical method for numerical evaluation of solutions of partial differential equations of the heat conduction type," *Mathematical Proceedings of the Cambridge Philosophical Society,* vol. 43, no. 1, pp. 50-67, 1947.

[184] K. Madsen, H. B. Nielsen and O. Tingleff, "The Levenberg-Marquardt Method," in *Methods for Non-Linear Least Squares Problems*, Lyngby, Informatics and Mathematical Modelling Technical University of Denmark, 2004, http://www2.imm.dtu.dk/pubdb/views/edoc_download.php/3215/pdf/imm3215.pdf, pp. 24-28.

[185] M. A. Garrido and R. Font, "Pyrolysis and combustion study of flexible polyurethane foam," *Journal of Analytical and Applied pyrolysis 113,* vol. 113, p. 202–215, 2015,

DOI:10.1016/j.jaap.2014.12.017.

[186] G. Cooke, “Stability of lightweight structural sandwich panels exposed to fire,” *Fire and Materials,* vol. 28, no. 2-4, pp. 299-308, 2004.

[187] A. W. Giunta d'Albani, d. K. L. L, A. C. J. de Korte, R. A. P. van Herpen, R. Weewer and H. J. H. Brouwers, “Mass loss and flammability of insulation materials used in sandwich panels during the pre-flashover phase of fire,” *Fire and Materials,* vol. 41, no. 6, pp. 779-796, 2017, DOI: 10.1002/fam.2418.

[188] J. Torero, “Flaming Ignition of Solid Fuels - Chapter 21,” in *SFPE Handbook of Fire Protection Engineering, Vol 5*, New York, Springer, 2016, pp. 633-661.

[189] A. Poulsen and G. Jomaas, “Experimental Study on the Burning Behavior of Pool Fires in Rooms with Different Wall Linings,” *Fire Technology,* vol. 48, no. 2, pp. 419-439, 2011, DOI: 10.1007/s10694-011-0230-0.

[190] T. L. Graham, G. M. Makhviladze and J. P. Roberts, “The effect of the thermal inertia of the walls upon flashover development,” *Fire Safety Journal,* vol. 32, no. 1, pp. 35-60, 1999, DOI:10.1016/S0379-7112(98)00022-8.

[191] O. Pettersson, S. E. Magnusson and J. Thor, “Fire Engineering Design of Steel Structures,” Bulletin of Division of Structural Mechanics and Concrete Construction, Bulletin 52; Vol. Bulletin 52, Lund Institute of Technology, 1976, http://portal.research.lu.se/portal/files/5989339/1245743.pdf .

[192] *ASTM E2058-1 - Standard Test Methods for Measurement of Synthetic Polymer Material Flammability Using a Fire Propagation Apparatus (FPA),* 2002, doi: 10.1520/E2058-01.

[193] *ISO 12136:2011 - Reaction to fire tests — Measurement of material properties using a fire propagation apparatus,* Genève: International Organization for Standardization, 2011.

A. Appendix – Supplementary Standard Tests Relevant for Sandwich Panels

1. EN ISO 11925-2:2010

The EN ISO 11925-2:2010 - Reaction to fire tests – Ignitibility products subjected to direct impingement of flame – Part 2: Single-flame source test is required for materials to obtain a B, C, D and E classification. The single flame source is impinging on the surface or edge of the product with a 45° angle, as seen in Appendix Figure A.1, for 15 s or 30 s for class E and B, C and D, respectively. The Flame spread (F_s) is not allowed to propagate beyond 150 mm within 20 s or 60 s for class E and B, C and D, respectively, for any of the three required repetitions. If the tested element is thicker than 6 cm it should be reduced in thickness and the cut side should not be exposed to the flame. A piece of paper is placed below the setup to monitor if dripping occurs and if so to what extent to determine if d0, d1 or d2 is the appropriate sub classification. For all multilayer products thicker than 10 mm the burner is moved so the flame is impinging the centre of the width of the bottom edge.

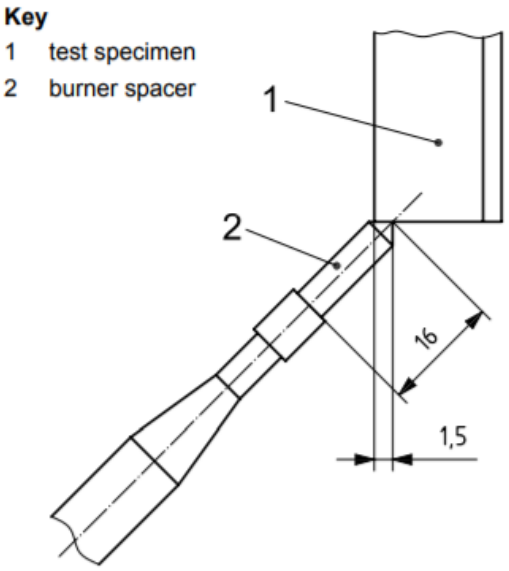

Appendix Figure A.1: Side view of the single flame test setup. The test specimen is placed in the holder marked with *1* in the figure, from [117] with modifications.

2. FM 4880 and FM 4881

The FM 4880 [91] compose of four individual tests each products wanting approval needs to pass: A sample measuring 10 cm by 10 cm by a maximum of 10 cm in width, length and height, respectively, is tested under a 50 kW/m^2 heat flux to characterize the flammability of the product in the Fire Propagation Apparatus (FPA) following the same methodology as proposed in the ASTM E2058-03 [192] and ISO 12136:2011 [193]. Second, a 25 ft. (7.6 m) tall corner mock-up of the product with a corner located wood crib burning for 15 minutes to test the flame spread. Third, a 50 ft. (15.2 m) also a corner mock-up with the product with a corner located wood crib burning for 15 minutes to test the flame spread, both corner tests can be seen in Appendix Figure A.2 a) and b), respectively, where the propensity of fire spread is evaluated. Fourth, a compartment fire where the product is mounted internally in an enclosure measuring approximately 2.4 x 3.6 x 2.4 m in width, length and heights, respectively, enclosure following one of three standard fire scenarios to test the fire growth. These three tests are the National Fire Protection Association (NFPA) 285:2012, the NFPA 286:2015 and the ISO 9705-1:2016 test. These three possible enclosure tests vary in burner duration, intensity and burner size. The two NFPA tests dictate a burner effect of 40 kW for 5 min followed by 160 kW by 10 min from a 0.305 m by 0.305 m burner and ISO test is 100 kW for 10 min followed by 300 kW for 10 min from a 0.17 m by 0.17 m burner. Of the three types of compartment tests required by the FM 4880 test two are applicable to sandwich panels and they have different fire scenarios, yet both are equally valid from a classification perspective.

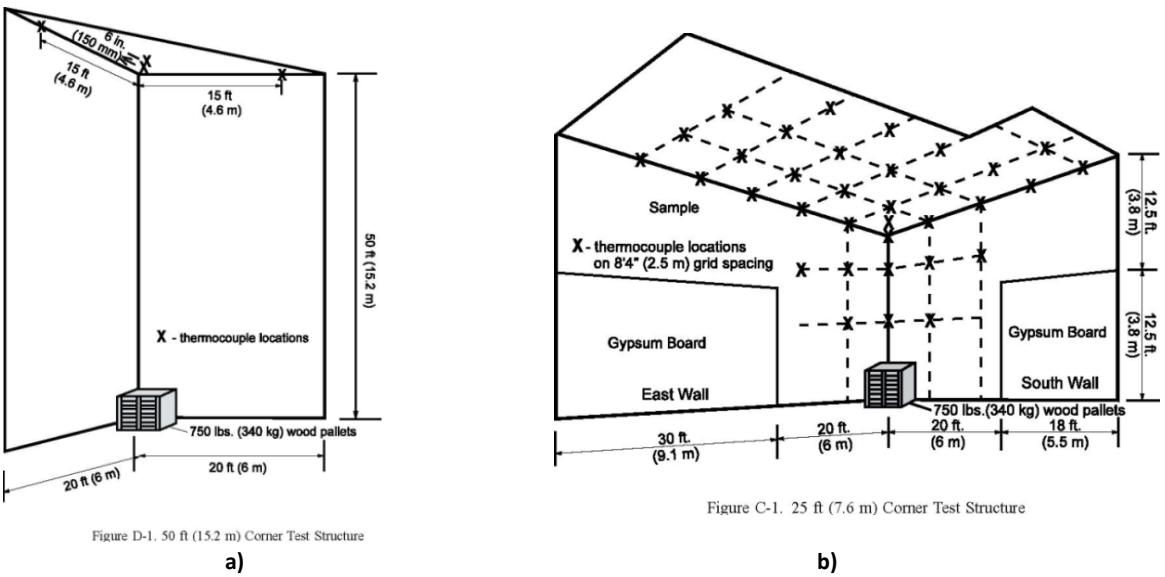

a) **b)**

Appendix Figure A.2: Fire test setup for the 50 ft. and 25 ft. setup in a) and b), respectively, from [91].

The FM 4881 – Approval Standard for Class 1 Exterior Wall Systems is, unlike the EN 13501 and FM 4880, focusing on the external spread of fires. The previously presented European classifications focus solely on a fire scenario where a fire is growing within an enclosure whereas the test of the insurance industry, namely the FM 4881, is a holistic classification with many aspects such as wind, hails and fire resistance. The fire test specified is the FM 4880 with a requirement of limited flame spread and unlimited, 50 ft. or 30 ft. height restriction, from a fire classification perspective the FM 4881 and the FM 4880 are identical.

3. Loss Prevention Standard 1181

The Loss Prevention Standard 1181 Series of fire growth tests for LPCB approval and listing of construction product systems; Part one: Requirements and tests for built up cladding and sandwich panel systems for use as the external envelope of buildings [119], is a standard which focus on property protection rather than life safety of occupants. The compartment is 4.5 m x 10 m x 3 m in width, length and height, respectively, with a 10 m x 2.25 m in width and height opening at one end. Opposite the opening, 1 m from the long wall and 0.5 m from the short wall is the centre base of a 34 kg ±1 kg wood crib placed 0.76 m above the floor. The test lasts 30 min and can be extinguished after the 30 min has passed. The sandwich panel product is classified based on damage to the core. Other materials with combustible surfaces are also classified based on the damage to the surface lining and metal faced sandwich panels are exempt of this criterion.

4. Appendix – Additional STA Graphs

Additional STA curves related to Section 3.1.1 - Thermographic Analyses on page 77.

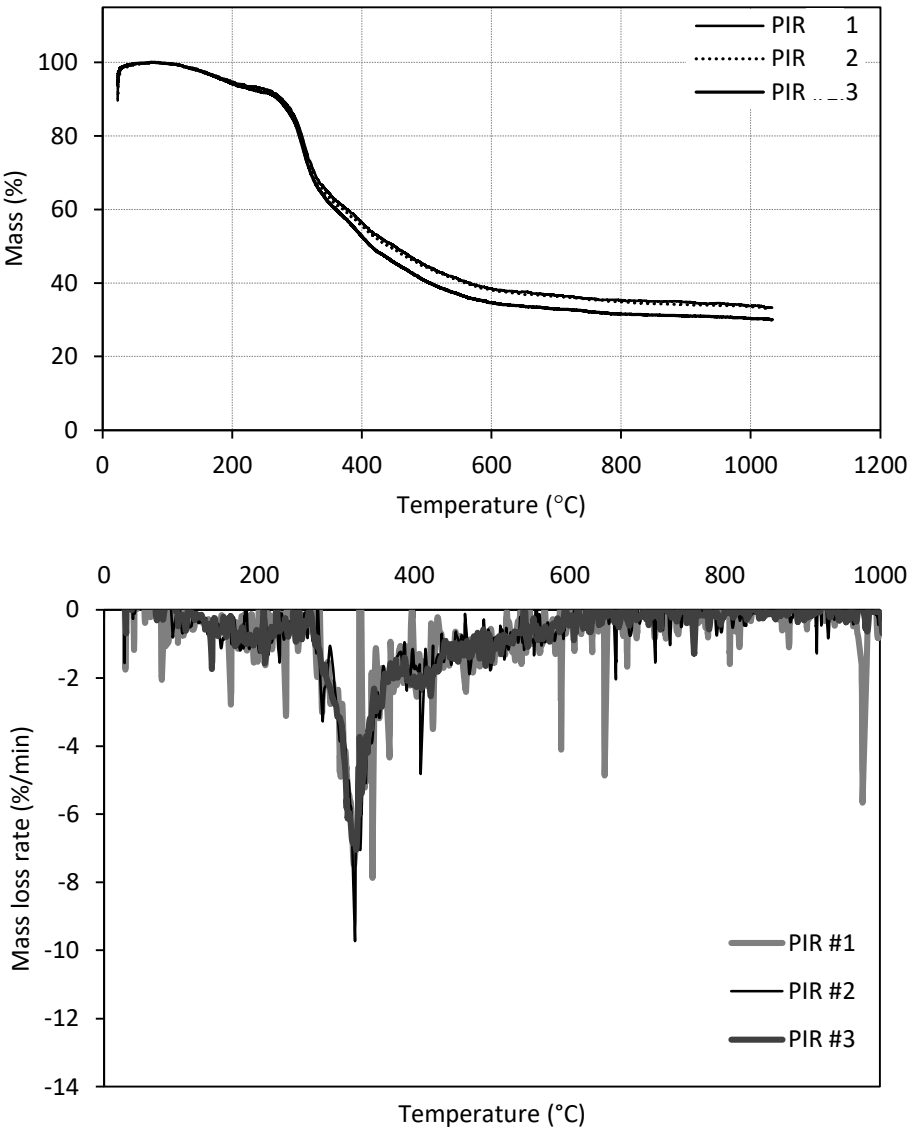

Appendix Figure A.3: Mass and mass loss rate curves from the three PIR samples studied in the STA in a pure nitrogen environment.

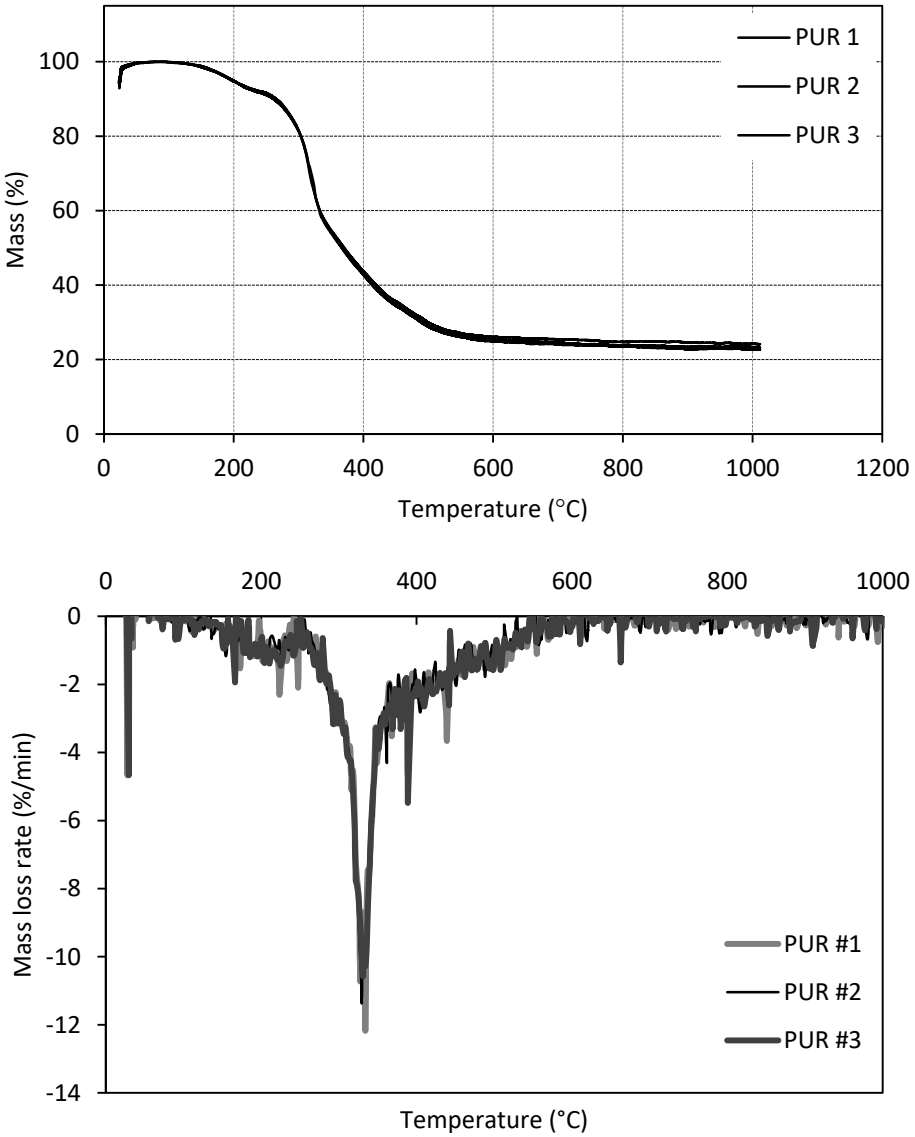

Appendix Figure A.4: Mass and mass loss rate curves from the three PUR samples studied in the STA in a pure nitrogen environment.

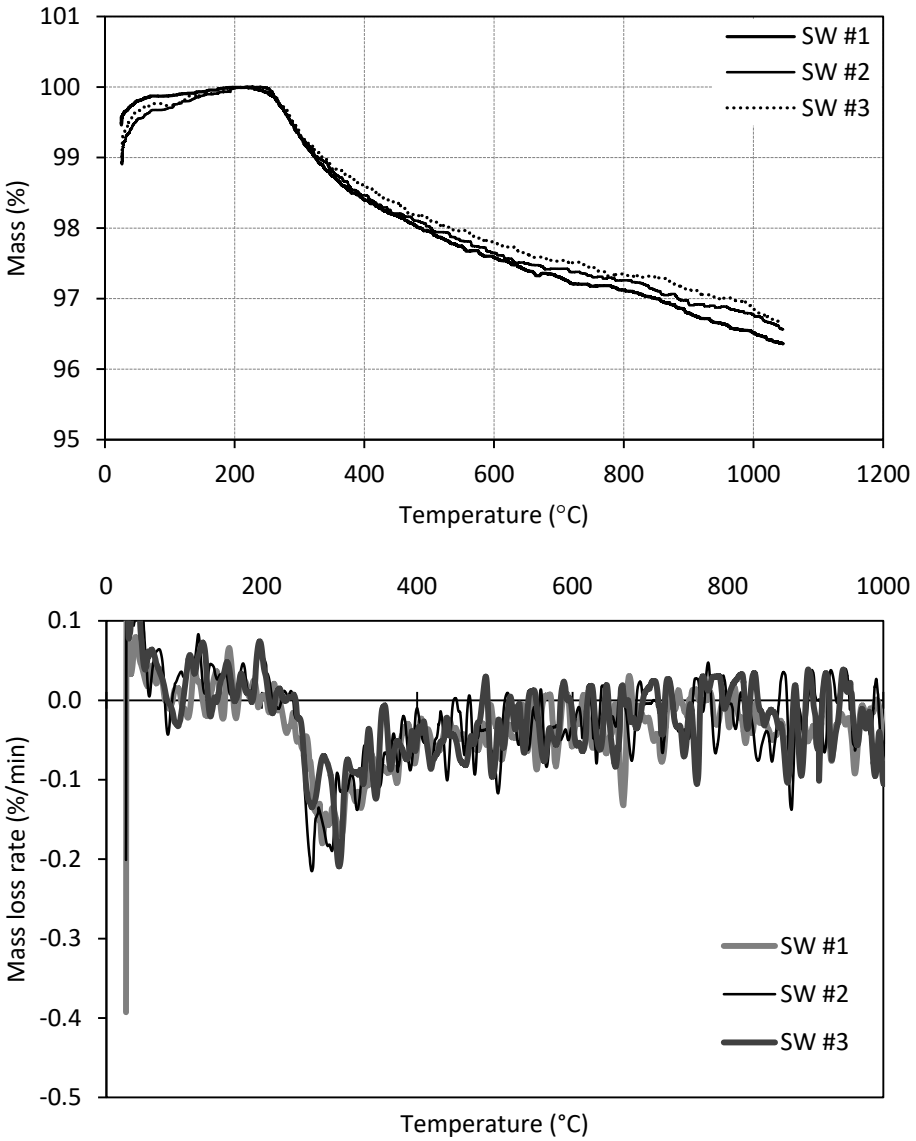

Appendix Figure A.5: Mass and mass loss rate curves from the three SW samples studied in the STA in a pure nitrogen environment.

B. Appendix – Additional Mass Loss Cone Graphs

Additional mass loss curves related to Section 3.1.2 - *Cone Calorimeter* on page 82.

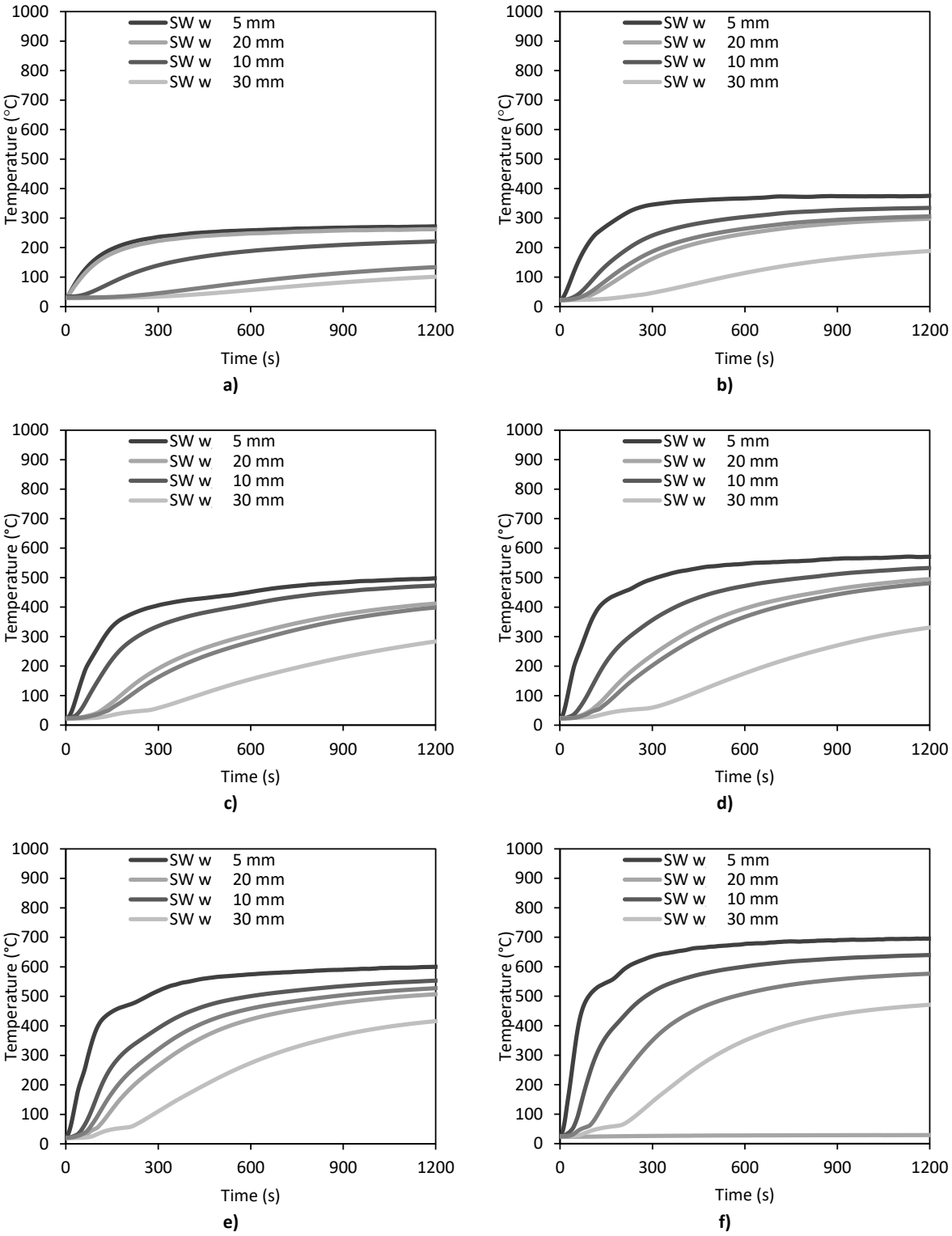

Appendix Figure B.1: In-depth temperature measurements for SW exposed to a) 10 kW/m² b) 20 kW/m² c) 30 kW/m² d) 40 kW/m² e) 50 kW/m² f) 70 kW/m² with their steel faces.

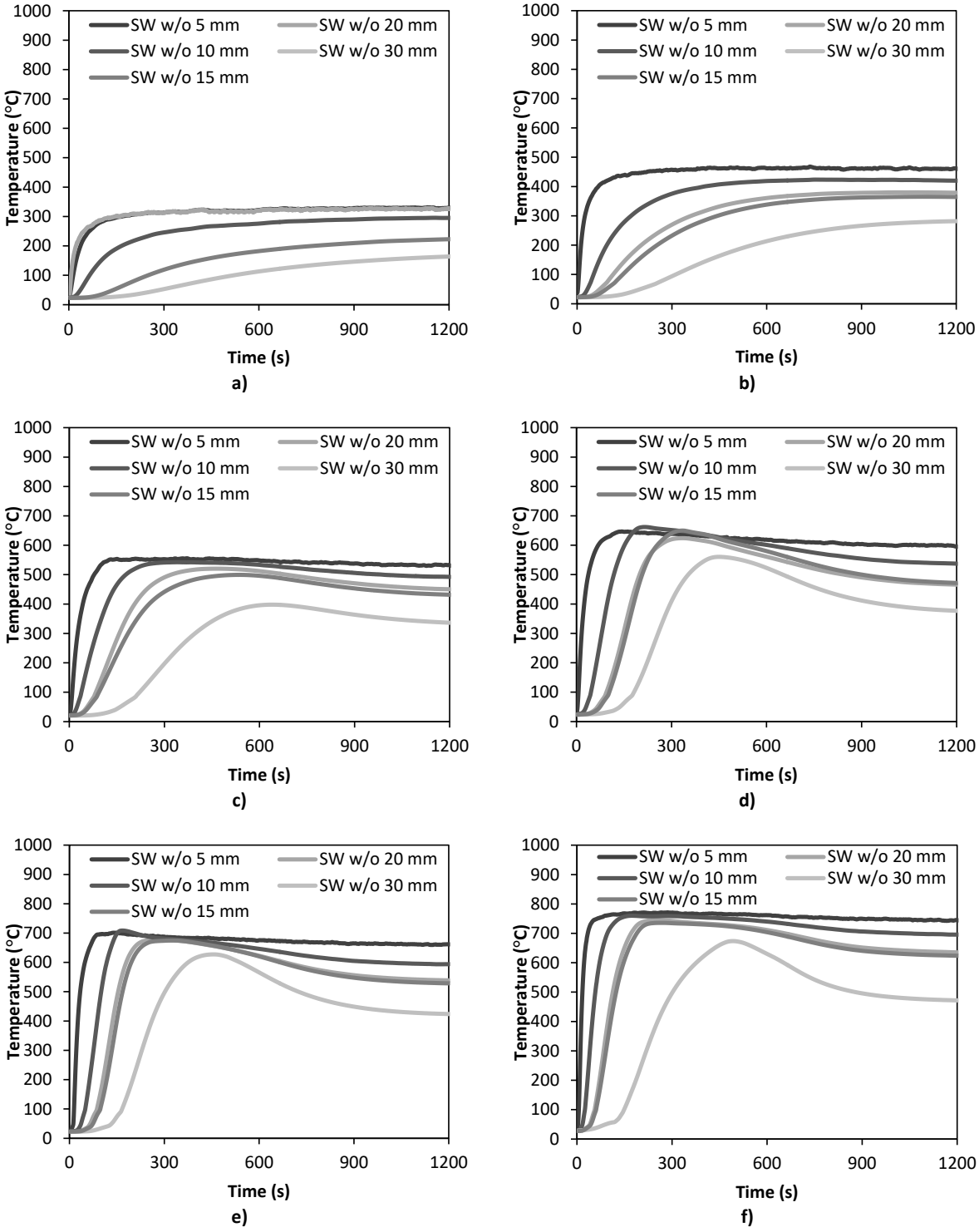

Appendix Figure B.2: In-depth temperature measurements for SW exposed to a) 10 kW/m² b) 20 kW/m², c) 30 kW/m² d) 40 kW/m² e) 50 kW/m² f) 70 kW/m² without their steel faces.

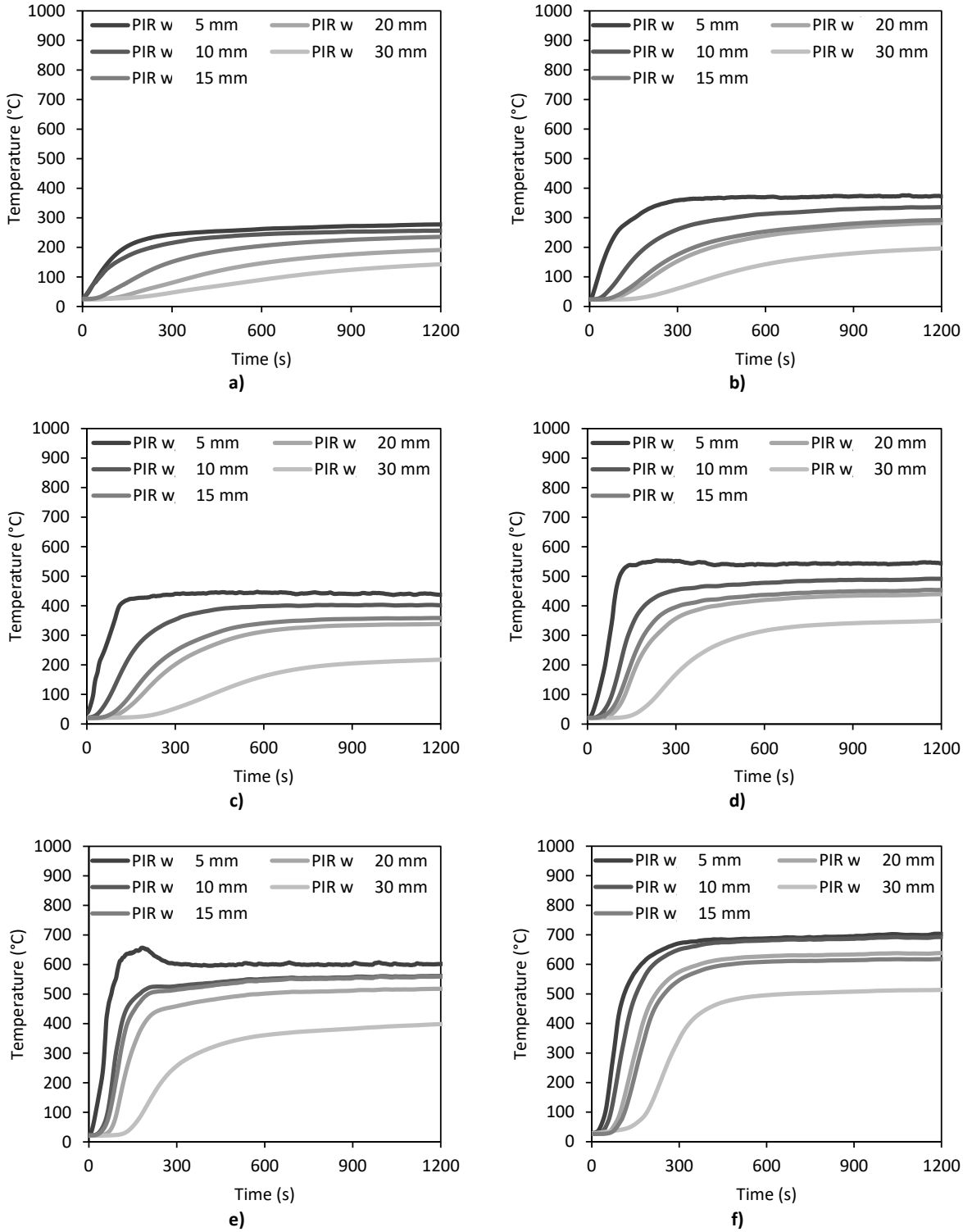

Appendix Figure B.3: In-depth temperature measurements for PIR samples exposed to a) 10 kW/m², b) 20 kW/m², c) 30 kW/m², d) 40 kW/m², e) 50 kW/m², and f) 70 kW/m² with their respective steel faces.

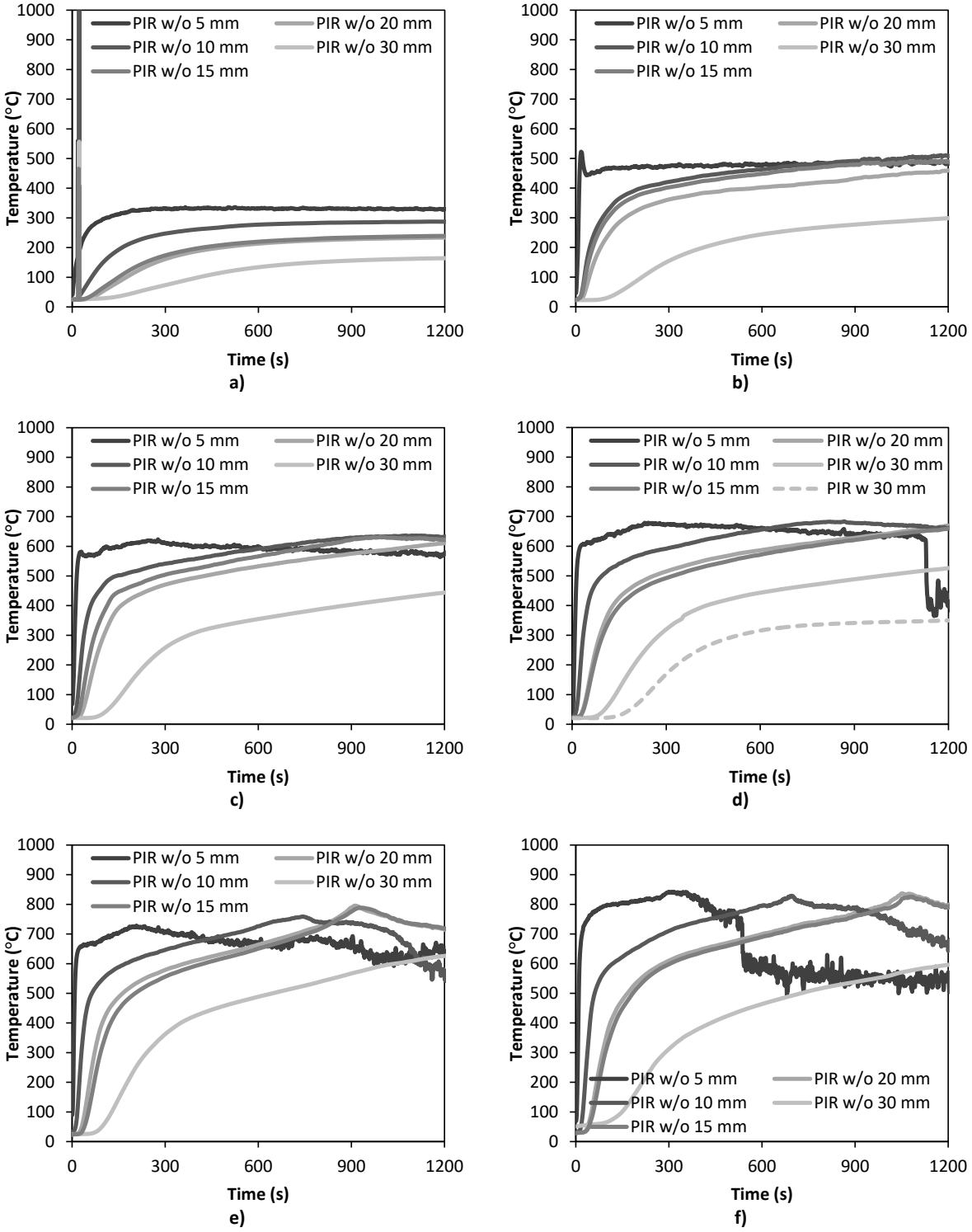

Appendix Figure B.4: In-depth temperature measurements for PIR samples exposed to a) 10 kW/m², b) 20 kW/m², c) 30 kW/m², d) 40 kW/m², e) 50 kW/m², and f) 70 kW/m² without their respective steel faces.

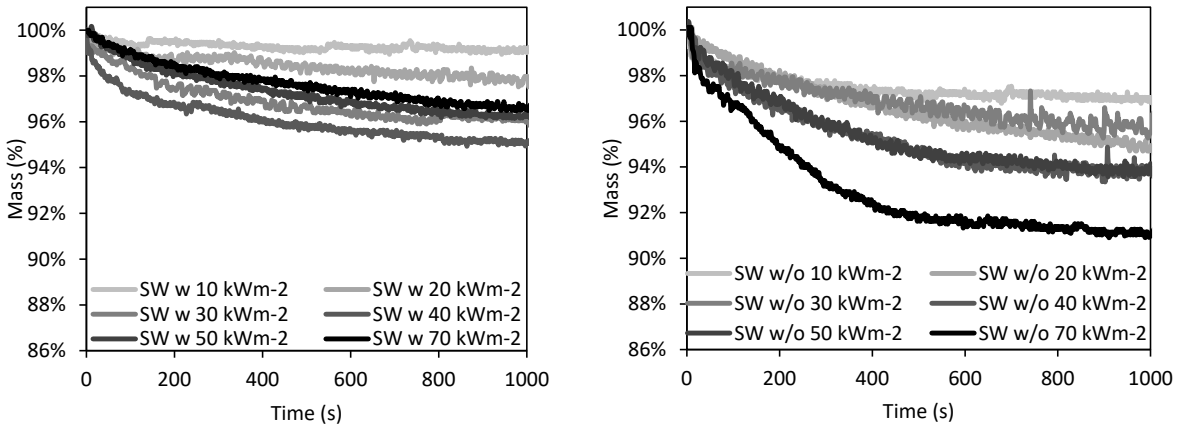

Appendix Figure B.5: Mass loss measurements for SW samples a) with and b) without their steel faces.

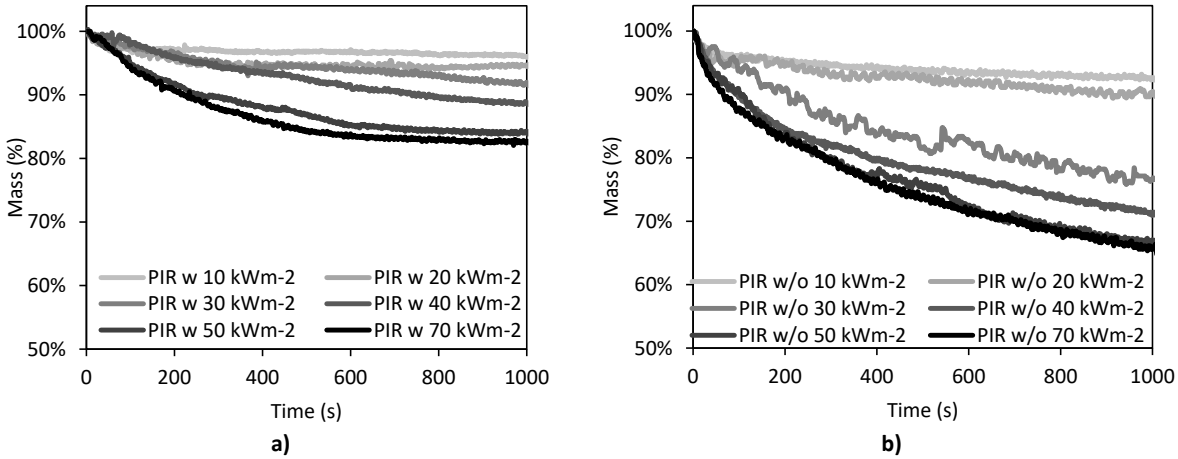

Appendix Figure B.6: Mass loss measurements for PIR samples a) with and b) without their steel faces.

C. Appendix – HRR Calculations, Analysis and Correction of E26-E28

The measured HRR for this series of experiments were significantly higher than expected based on the known propane gas flow. The relationship between the two ($\dot{Q}_{calc}$ and $\dot{Q}_{C_3H_8}$ was determined by dividing them with each other, as seen in the top of Appendix Figure C.1 a). The HRR measurement was greater by a factor 3 averaged over the duration of the experiment. This assumes the HRR from the SW core was of negligible magnitude, which, based on the 1:5 and full scale experiments, E20 and E30, respectively, it was considered a fair assumption. The drift in the oxygen unit was corrected by inversely calculating the O_2 concentration based on the relationship between O2 consumed and CO2 produced for the 1:5 and 2:5 scale experiments with SW panels (E1-E4, E20). This resulted in a change of the energy released after the gas burner was turned off but otherwise not much, as seen in Appendix Figure C.1 b).

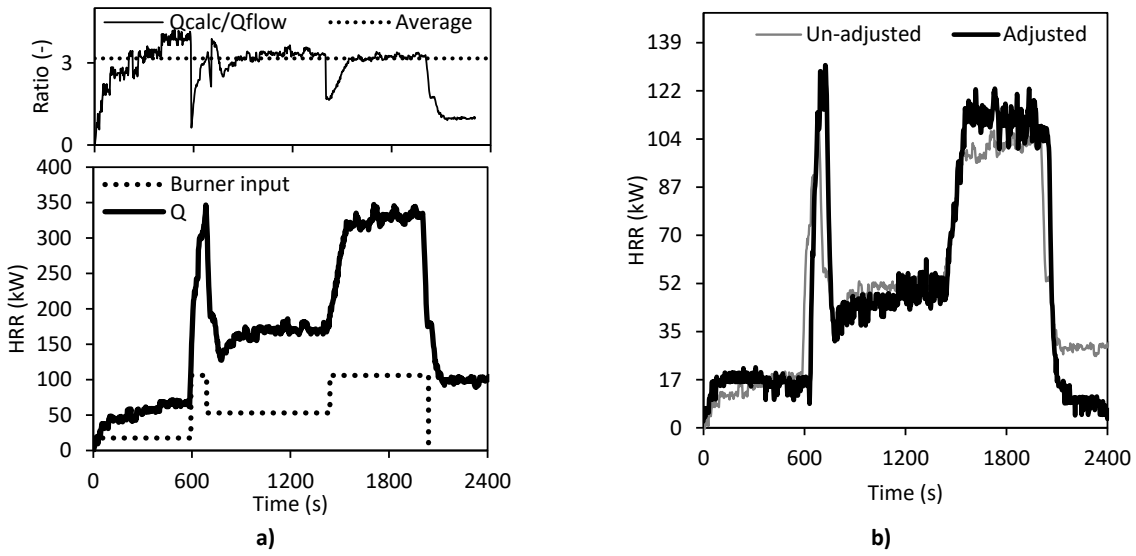

Appendix Figure C.1: E28 with SW panels at 1:2 scale with a) corrected HRR and b) adjusted for the drifting of the O_2 analyser.

The correction factor of 3 was extended to the two PIR compartments, as their initial HRR measurements also yielded much higher energy than expected. Based on a post-flashover compartment, as suggested both visually and by the HRR, the generic equation for the pHRR is determined for the compartments, as seen in Eq. C.1, as 610 kW.

$$\dot{Q}_{FO} = 0.5 \cdot A_0 \cdot \sqrt{H_0} \cdot X_{O_2} \cdot \mathrm{E}_{\mathrm{O}_2} = 0.5 \cdot (1 \cdot 0.4) \cdot \sqrt{(1)} \cdot 0.233 \cdot 13.1 = 610\ kW \quad \textbf{C.1}$$

The un-corrected HRRs are 804 kW and 909 kW for E26 and E27, respectively, which are higher than the theoretical limit by 32% and 40% without flames emanating other places than the door further suggests the correction is correct, also for these experiments.

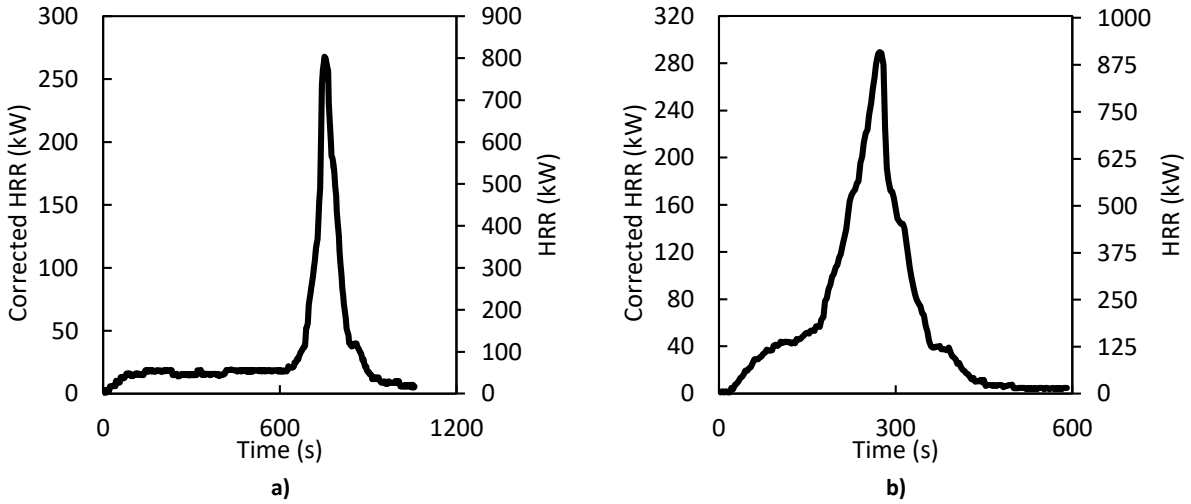

Appendix Figure C.2: HRR data and corrected data for a) E26 and b) E27, both experiments with panels with PIR cores.

D. Appendix – HRR Calculation, Analysis and Correction for E29

The mass flow meter controlling the HRR of the gas burner was set for 100 kW and after 10 min should be increased to 300 kW for another 10 min before being terminated. As Figure 3.29 (presented again for ease) below shows was the measured HRR did not correspond to the output of the gas burner. The compartment temperature near the ceiling in the two full scale experiments (E29 and E30) as well as in the full scale experiments from literature (SW: 1_3_6, 1:1, from literature and SW: 1_3_6, 1:1, from literature) were compared. The input in the experiments from literature were 100 kW, 300 kW and 600 kW and the same exact size which enables a comparison to E29.

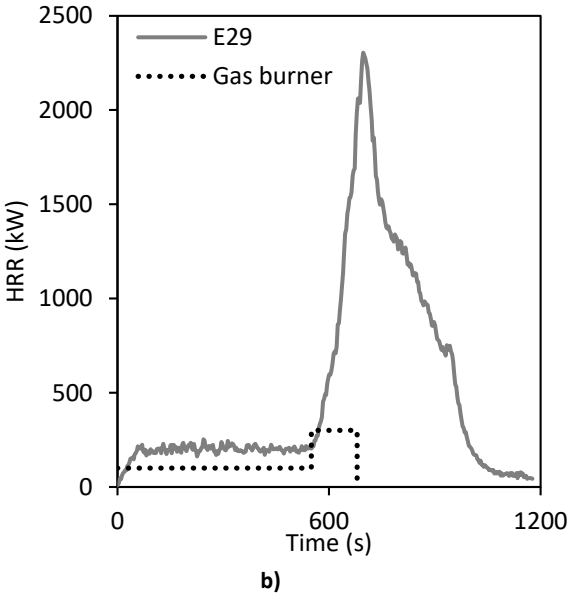

b)

Figure 3.29 b) panels with a core of PIR including the burner, respectively.

The experiments from literature combined with E30 provides temperatures as a function of HRRs of 50 kW, 100 kW, 200 kW and 300 kW, as seen in Appendix Figure D.1 where a power and 2nd order polynomial trend lines have been added. The estimated HRR based on the steady state temperature for the other experiments is 130 kW and 133 kW for the power and polynomial trend lines, respectively. This means the mass flow meter was providing approximately 30% too much gas and the oxygen analyser was measuring 35% more than it should rather than one being 100% wrong.

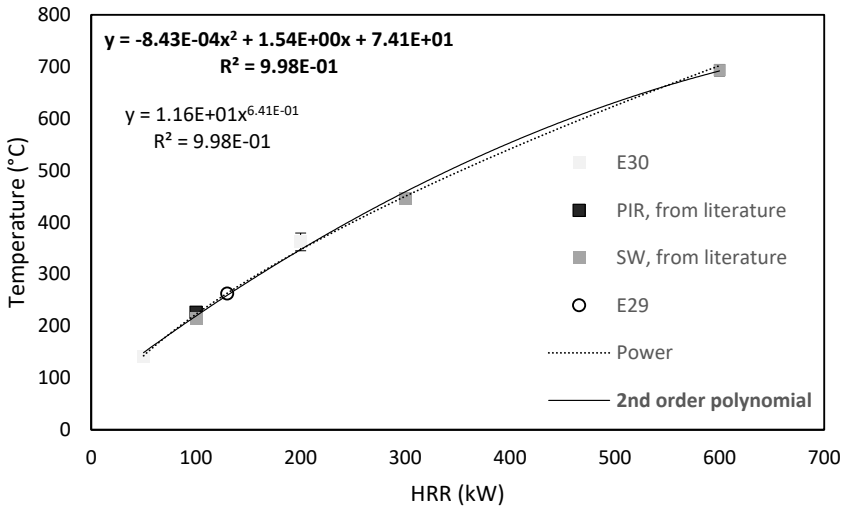

Appendix Figure D.1: Smokelayer temperature near the ceiling as a function of the HRR of the gas burner with a power trendline and a 2nd order polynomial.

The hot gases leaving the compartment as convective energy from the PIR compartment from literature is compared with E29 and the new HRR to analyse the validity of the estimate for the new HRR of approximately 130 kW. The energy released from the compartment from literature and from E29, as seen in Appendix Figure D.2 a) and b), respectively, are not significantly different. The convective energy released, presented in Eq. 3.2 in Section 3.3.7 on page 116, relative to the release from the gas burner in E29 is very similar to that from literature for the first 200 s hereafter the experiment from literature experiences a small drop while E29 continues to increase, as seen in Appendix Figure D.2 c). The ratio in the experiment from literature increase back up again and reach 0.62 just prior to the increase in HRR from the gas burner whereas E29 reach 0.86 before its increase in burner intensity. The difference between ratios are however difficult to conclude upon as the behaviour in the literature changed and had it continued to grow could perhaps have reached the same ratio estimated for E29.

- Based on these two methods of analysing and comparing the HRR is it not unlikely that the mass flow meter and the gas analyser were 30% and 35% wrong with respect to the actual energy released by the gas burner.

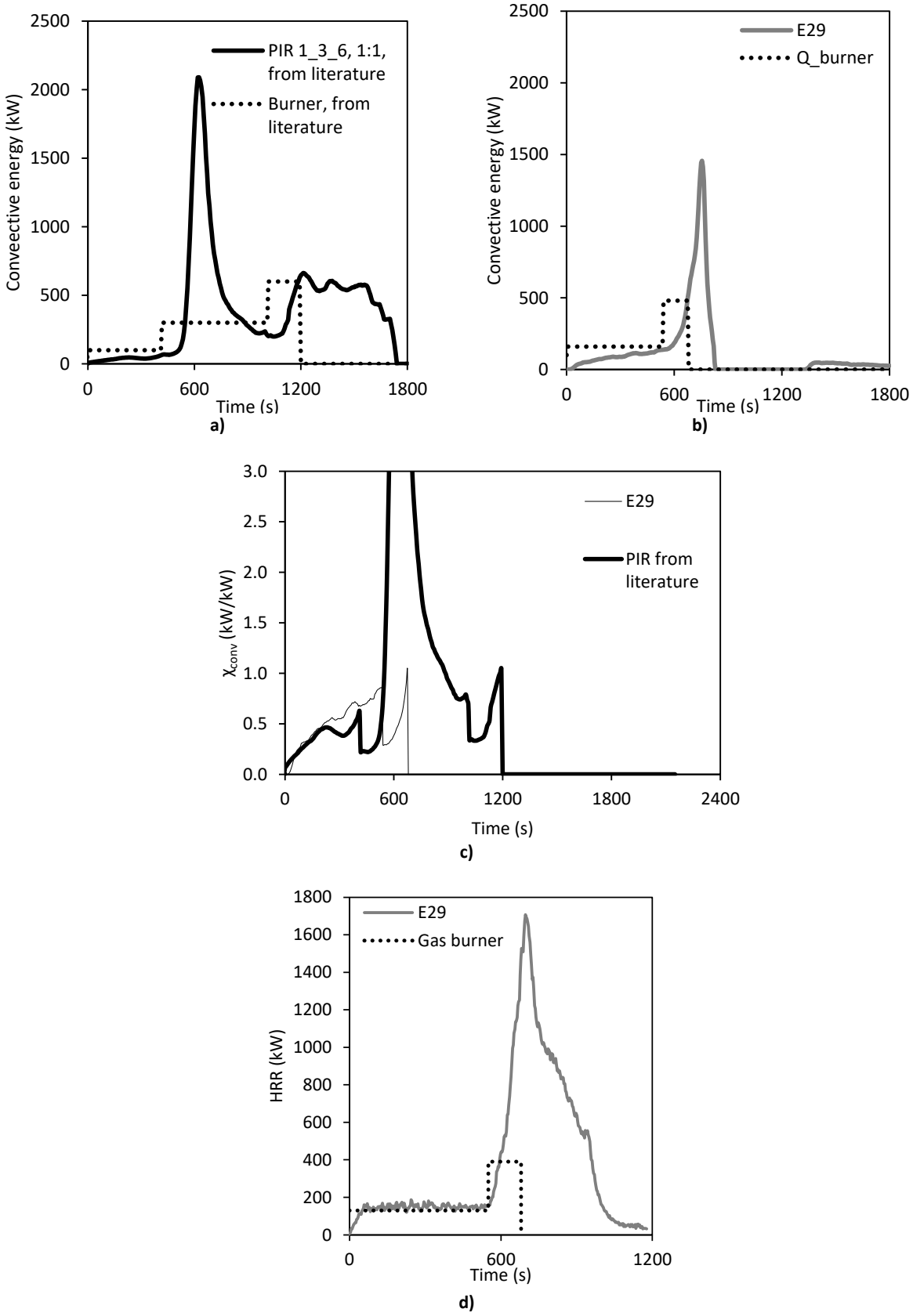

Appendix Figure D.2: Convective energy released for a) PIR compartment from literature, b) from E29, c) with their convective energy divided by the HRR of their respective gas burners and d) the corrected HRR for E29 with PIR

E. Appendix – Uncertainty Analysis of the Measurement Density

Using only four of the eight thermocouples evenly distributed along the vertical axis used for determining the change in stored energy in the CV was used to determine the effect of a higher density of measurement points. The same goes for using only two of the pressure transducers at the top and bottom instead of all four and reducing the number of used thermocouples in the walls while increasing their corresponding areas by a factor four. The uncertainties will be determined as the difference between the respective fractions, as seen in Eq. E.1.

$$\varepsilon_w^j = \left| \frac{\dot{q}_{w,high}^j}{\dot{Q}_{burner}^j} - \frac{\dot{q}_{w,low}^j}{\dot{Q}_{burner}^j} \right| \qquad \textbf{E.1}$$

Where ε is the difference between the densely and less densely instrumented calculations, *j* is the time step and *w* is the specific mode of heat transfer. This method of calculating the error will give low values as they reflect the overall contribution in percent points rather than percent and was considered easier to interpret.

The uncertainties for the three modes of heat transfer was dominated by the conductive term where a difference between the high and the lower resolution was 0.14, as seen in Appendix Figure E.1, equivalent of a 35% uncertainty at its highest. Small changes in the location of the top pressure probes resulted in a large difference in the results. For the 1:5 scaled experiments a change from 40 cm to 39 cm in the location of the top probe resulted in χ_{conv} changing by 0.10 and the importance of accurate placement of the measuring instrumentation was noted as a key focus. The fraction of energy that was used to heat up the CV was minor and the uncertainty related to the density of the thermocouples was close to zero. The fraction of convective energy leaving the compartment was very sensitive to the number of probes as they were directly used in determining the thickness of the smoke layer. More measurement points and a dynamic smoke layer made it easier with more than two measurement points to get credible smoke layer thicknesses. The uncertainties related to measurement density are highest during the first 10 min and gradually decrease and reach 5% at quasi-steady state after 30 min.

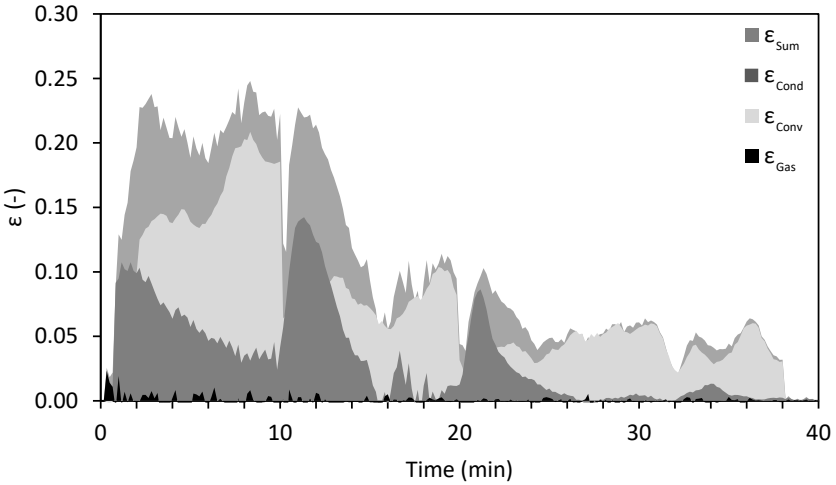

Appendix Figure E.1: Estimated error as a function of the low and high measurement densities for the heat transferred by conduction and convection and the energy stored in the gas phase.

The measurement density was not always in the advantage of one of the scales, which means the small-scale experiments have the uncertainty for the convective and gas energies whereas the full scale has the uncertainties associated to the conductive. Fewer thermocouples and larger areas for the conductive fraction meant a higher calculated fraction and the same was the case for the convective part where two pressure probes estimated more energy leaving the compartment. The largest uncertainty was related to the fraction of convective energy but overall the uncertainty related to the measurement density was less than 25% of the total energy and much less towards the end of the experiments as a quasi-steady state was obtained.

The heat transfer and fire dynamics of enclosure fires in compartments made from steel-faced sandwich panels were studied experimentally to assess the feasibility of down-scaling the ISO 13784-1 test compartment. The results showed that, when scaling the compartment geometrically by a factor of two, both the temperature and the time to flashover was satisfactory replicated across the scales. Furthermore, the temperature required for initiation of flashovers across half and full scale matched very with the results found in the small scale experiments.

DTU Civil Engineering
Technical University of Denmark

Brovej, Building 118
2800 Kongens Lyngby

www.byg.dtu.dk

ISBN 9788778774880
ISSN 1601-2917